Initial State Radiative Corrections to Z^0 Pair Production in e^+e^- Annihilation – The Semi-Analytical Approach –

D i s s e r t a t i o n

zur Erlangung des akademischen Grades

doctor rerum naturalium
(Dr. rer. nat.)

eingereicht an der
Mathematisch-Naturwissenschaftlichen Fakultät I
der Humboldt-Universität zu Berlin

von
Diplom-Physiker Dietrich Lehner
geb. am 2. November 1967 in München

Präsidentin der Humboldt-Universität zu Berlin:
Prof. Dr. M. Dürkop

Dekan der Mathematisch-Naturwissenschaftlichen Fakultät I:
Prof. Dr. M. v. Ortenberg

Gutachter:
1. Prof. Dr. F. Jegerlehner
2. Prof. Dr. M. Müller-Preußker
3. Prof. Dr. P. Söding

Tag der mündlichen Prüfung: 7. Dezember 1995

Vollständiger Abdruck der von der Mathematisch-Naturwissenschaftlichen Fakultät I der Humboldt-Universität zu Berlin genehmigten Dissertation unter Verbesserung zweier orthographischer Fehler.

Abstract

A total and differential cross-section calculation for the Electroweak Standard Model reaction $e^+e^- \to (Z^0Z^0) \to f_1\bar{f}_1f_2\bar{f}_2(\gamma)$ including the effects of the finite Z^0 width and, for the first time, all QED initial state radiative corrections (ISR) is presented. A semi-analytical technique is used: All angular phase space integrations, five for the tree level process, seven if ISR is included, are carried out analytically. The remaining phase space variables are the invariant masses of the two decaying Z^0 bosons for tree level plus the reduced center of mass energy squared in the ISR case. Invariant masses are submitted to high precision numerical integration. Semi-analytical and numerical results for e^+e^- center of mass energies between $\sqrt{s} = 130$ GeV and 1 TeV are reported. It is shown that the radiatively corrected cross-section splits into a universal, leading logarithm part with the tree level cross-section factorizing on one hand and a non-universal contribution on the other hand. A generalization to the case of Standard Model neutral boson pair production, $e^+e^- \to (Z^0Z^0, Z^0\gamma, \gamma\gamma) \to f_1\bar{f}_1f_2\bar{f}_2(\gamma)$, is worked out in detail. The relevance of the presented calculation for the phenomenology of e^+e^- collider physics is discussed, especially for W and Higgs physics both of which will be important topics in the near future. All significant technical details of the calculation are explained.

Zusammenfassung

Im Rahmen des Standardmodells elektroschwacher Wechselwirkungen wird eine Berechnung totaler und differentieller Wirkungsquerschnitte für die Reaktion $e^+e^- \to (Z^0Z^0) \to f_1\bar{f}_1f_2\bar{f}_2(\gamma)$ vorgestellt. Dabei werden die Effekte der endlichen Bosonlebensdauer und erstmalig die vollständigen Eingangszustands-QED-Strahlungskorrekturen (ISR) berücksichtigt. Es wird eine semianalytische Technik angewandt: Sämtliche Winkelvariablen des Phasenraums, fünf für die Born-Approximation, sieben im ISR-Fall, werden analytisch integriert. Die verbleibenden Phasenraumvariablen sind invariante Massen, nämlich die invarianten Massen der zerfallenden Z^0-Bosonen und im ISR-Fall zusätzlich die reduzierte Schwerpunktsenergie. Über die invarianten Massen wird mit einem sehr präzisen numerischen Algorithmus integriert. Es wird über semianalytische und numerische Ergebnisse für e^+e^--Schwerpunktsenergien zwischen $\sqrt{s} = 130$ GeV und 1 TeV berichtet. Dabei wird gezeigt, daß der Wirkungsquerschnitt mit ISR in einen universellen Anteil führender Logarithmen mit dem Born-Wirkungsquerschnitt als Faktor einerseits und einen nichtuniversellen Beitrag andererseits zerlegt werden kann. Eine Verallgemeinerung der Resultate auf die Standardmodell-Paarproduktion neutraler Bosonen, $e^+e^- \to (Z^0Z^0, Z^0\gamma, \gamma\gamma) \to f_1\bar{f}_1f_2\bar{f}_2(\gamma)$ wird detailliert ausgearbeitet. Die phänomenologische Bedeutung der vorgestellten Rechnungen für die e^+e^- Beschleunigerphysik wird diskutiert, insbesondere die Bedeutung für die in naher Zukunft wichtigen Themen der W- und der Higgs-Physik. Alle wesentlichen technischen Einzelheiten der Rechnung sind erläutert.

Contents

List of Figures

List of Tables

Chapter 1

Introduction

It is the goal of modern physics to achieve reduction of nature's complexity to as few as possible fundamental principles. The method is increasing abstraction, the tool mathematics, the result unification of, up to that date, distinct phenomena. An important success pointing in that direction was Maxwell's formulation of the theory of electromagnetism in 1864 [1]. The electromagnetic theory was not only the origin of the theory of relativity [2], but it could also be cast into a Lorentz-covariant form. In the late twenties, originating from Dirac's work [3], electromagnetism continued its career as a quantum field theory [4] which was shown to be U(1) gauge invariant by Weyl [5]. Quantum Electrodynamics (QED) was born, when Schwinger reformulated the electromagnetic quantum field theory in a Lorentz-covariant way [6]. Shortly thereafter the well-known Feynman diagrams were introduced [7], and it only took another year to establish the mathematical foundations of Feynman's theory [8]. Today, QED is one of the best-tested theories we know. A manifestation of this success is the prediction of the anomalous magnetic moment a_e of the electron up to $\delta a_e/a_e = 2.4 \times 10^{-8}$ from perturbative QED [9] in agreement with experiment [10]. Other QED predictions matching high precision experiments are the anomalous magnetic moment a_μ of the muon [11] and the Lamb shift of the hydrogen atom [9, 12]. This list could be continued. The successes of QED are clear evidence for the quantum corrections as obtained from relativistic quantum field theory. Perturbative QED is a very important ingredient of the Standard Model of Electroweak Interactions (SM).

The second main ingredient of the Standard Model are the weak interactions which entered history in 1896 when Becquerel discovered radioactivity in the form of nuclear β-decay [13]. In 1934 Fermi developed a "theory of weak interactions" for β-decay which was constructed along the lines of QED [14]. The structure of weak interactions was further clarified with the theoretical consideration of parity violation by Lee and Yang [15]. Soon thereafter, parity violation was experimentally confirmed in the famous Wu experiment [16]. This was when Fermi's original pure vector currents were replaced by a (V–A) structure which is maintained until today [17]. Although very successful, Fermi's theory of weak interactions is not renormalizable and runs into a unitarity problem at center of mass energies around 600 GeV. This problem was cured by the introduction of gauge bosons that mediate the weak interaction. The short range of weak interactions requires massive gauge bosons via the Yukawa theory [18]. However, for the sake of gauge

symmetry, bosons are not allowed to have explicit mass terms within the framework of a Yang-Mills field theory [19]. A remedy to this mass prohibition was found with the Higgs(-Kibble) mechanism of spontaneous symmetry breaking which "generates" gauge boson masses that are proportional to the non-vanishing vacuum expectation value of a newly introduced scalar field [20]. In addition, the Higgs mechanism enables the gauge invariant introduction of chiral fermion masses into a Yang-Mills theory. In 1971, it could be proven that Yang-Mills theories with gauge boson masses generated by spontaneous symmetry breaking are renormalizable [21].

It has been a milestone of modern physics when, in parallel to the development of the Higgs mechanism in the sixties, a renormalizable, non-abelian $SU(2)_L \times U(1)_Y$ gauge field theory for the unified description of weak interactions and QED could be found [22] which is today called the Standard Model of Electroweak Interactions. The groups $SU(2)_L$ and $U(1)_Y$ are associated with the weak isospin and the weak hypercharge symmetries. Via the Higgs mechanism three of the four gauge bosons of the model, namely the $W^{\pm}$ and the Z^0 are endowed with masses, whereas the photon as the mediator of the electromagnetic force stays massless as required by the infinite range of QED forces. In the framework of the Standard Model, the Higgs mechanism entails the introduction of one scalar boson, the so-called Higgs boson. The photon has a pure vector coupling to electromagnetically charged particles, $W^{\pm}$ bosons have maximally parity violating (V–A) coupling structure, and the Z^0 bosons comprise both (V–A) and (V+A) couplings. In the 1950s and 1960s many weak decays of hadrons were experimentally studied. With respect to these observations it is a crucial feature of the Standard Model that it is able to naturally incorporate the hadronic constituents, the quarks [23], via the Glashow-Iliopoulos-Maiani mechanism [24]. This incorporation was based on the idea of a unitary transformation of the quark flavor mass eigenstates into weak eigenstates which is today known as the Cabibbo-Kobayashi-Maskawa matrix [25]. The present version of the Standard Model is made anomaly-free by the introduction of color [26], a concept originating from Quantum Chromodynamics [27].

The experimental confirmation of the Standard Model started in 1973 with the discovery of the predicted neutral current interactions in the Gargamelle bubble chamber at the CERN proton synchrotron, where $\overset{(-)}{\nu}_{\mu}$ scattering on electrons and nucleons was investigated [28]. Soon the Standard Model was further supported by the discovery of the weak isospin partner of the strange quark, which was called "charm" [29]. The breakthrough came with the direct observation of the gauge bosons $W^{\pm}$ and Z^0 by the UA1 and UA2 experiments at the CERN $Sp\bar{p}S$ [30]. With the advent of the SLC and LEP e^+e^- colliders for resonance production of Z^0 bosons in e^+e^- annihilation, the Standard Model entered its precision test era. From LEP and SLC, the mass M_Z and the width Γ_Z of the Z^0 as well as the Weinberg mixing angle $\sin^2\theta^{lept}_{eff}$ are very accurately known [31]:

$$\begin{aligned} M_Z &= (91.1887 \pm 0.0022)\ \text{GeV} \\ \Gamma_Z &= (\ 2.4971 \pm 0.0032)\ \text{GeV} \\ \sin^2\theta^{lept}_{eff} &= 0.2315 \pm 0.0004\ . \end{aligned}$$

These impressive numbers, however, are only the peak of an iceberg of electroweak precision measurements all of which agree with the Standard Model. The measurements at

LEP have reached a level of precision which enables to test radiative corrections not only in the QED sector of the theory. Also the truly electroweak radiative corrections and thus the quantum corrections of the Standard Model are now established [32]. The renormalizability of the Standard Model ensures the sensibility of the perturbation expansion of these quantum effects. The latest success in the confirmation of the Standard Model is the discovery of the last missing fermion of the Model, the top quark, by the CDF and D0 collaborations at the Fermilab "Tevatron" $p\bar{p}$ collider [33][†]. It is very noteworthy that the direct measurements of the top quark mass are in good agreement with indirect mass determinations obtained from precision experiments at the Z^0 pole [31, 33]. Precision measurements can also severely constrain new physics beyond the Standard Model, and it is discussed, whether they can put limits on the Higgs mass, if the precision of top quark mass measurements is further improved.

An upgraded version of LEP, commonly referred to as LEP2, will pass the threshold for the pair production of heavy gauge bosons in the very near future and operate at center of mass energies between 175 and 206 GeV [34]. This opens the opportunity to study the properties of the W boson in W pair and single W production processes. Furthermore, the non-abelian coupling structure of the electroweak theory will be investigated directly for the first time through the observation of trilinear γW^+W^- and $Z^0W^+W^-$ interactions. Recently, the different non-standard trilinear boson couplings have been subject of several studies [35][‡]. If LEP2 does not yield the discovery of the Higgs boson, it will at least increase the lower Higgs mass limit to approximately the machine energy minus 100 GeV, i.e. $\sqrt{s} - 100$ GeV [37, 38]. The above-mentioned physics tasks at LEP2 involve the analysis of four-fermion final states. At present, the latter are heavily studied, and several experimental analyses were already carried out at LEP1 [39, 40]. This thesis is a contribution to the clarification of the physics of four-fermion final states in e^+e^- annihilation. A study of the process

$$e^+e^- \to (Z^0Z^0) \to f_1\bar{f}_1f_2\bar{f}_2(\gamma) \;, \qquad f_1 \neq f_2 \;, \quad f_i \neq e^\pm, \nu_e \tag{1.1}$$

will be presented, including the first complete treatment of initial state radiation in first order perturbation theory [41]. Process (1.1) is not only observable at LEP2, but also interesting at planned higher energy e^+e^- colliders. Process (1.1) yields a higher order test of the Standard Model and can easily be extended to nonstandard neutral current physics with additional neutral bosons replacing the Z^0's. Another strong motivation for this study is the importance of process (1.1) for W pair physics and for Higgs searches at LEP2. The relevance to W pair physics is twofold. Process (1.1) does not only constitute a double resonance background to some decay channels in W pair production, but it was also important to confirm the generality of properties found for W pair production in the framework of the "current splitting technique" [42, 43]. As far as Higgs searches at LEP2 are concerned the Z^0 pair double resonance background to four-fermion final

[†]Since the determination of the number of light neutrino generations as $N_\nu = 2.987 \pm 0.016$ [31], there is reason to believe that only three generations of quarks and leptons exist. Thus, in the framework of the Standard Model, the observation of the top quark together with the indirect evidence for the τ neutrino justifies the statement that the last missing fermion has been discovered.

[‡]It should be mentioned that non-standard trilinear boson couplings are heavily constrained by unitarity requirements [36].

states with a b quark pair *must* be taken into account. This thesis presents sufficiently precise results for studies of the Z^0 pair double resonance background to Higgs searches. Further importance of the presented results on process (1.1) lies in their straightforward generalizability to include new heavy neutral bosons. It should be investigated in how far Z^0Z' pair production in e^+e^- annihilation can put competitive limits on the mass and/or couplings of a new boson Z'. On-shell Z^0 pair production has been discussed long ago [44]. Numerical calculations including all $\mathcal{O}(\alpha)$ electroweak corrections[†] except hard photon bremsstrahlung were reported in [45] for on-shell and in [46] for off-shell Z^0 bosons. In this thesis, initial state radiation (ISR) to Z^0 pair production will be treated completely, including hard bremsstrahlung corrections. Contrary to the more common approaches to process (1.1) and other neutral current processes with Monte Carlo phase space integration [47, 48, 49], this thesis follows a "semi-analytical" approach where all angular phase space variables are integrated analytically and the remaining invariant masses are subjected to a high precision numerical integration. Thus the precision of the cross-section calculation is physics dominated, meaning that the error on the computed cross-section essentially originates from theoretical systematic errors such as the disregard of other radiative corrections or the small final state mass approximation. Another advantage of semi-analytical calculations is their transparency, i.e. the fact that, at tree level, they yield very compact expressions for cross-sections and invariant mass distributions. Even with initial state radiation included, semi-analytical cross-section formulae allow to identify physically interesting properties. Having in mind that, using the semi-analytical method, it is difficult to implement experimental cuts on all relevant angular variables it is clear that semi-analytical and Monte Carlo calculations of four-fermion final states complement each other. However, it should be born in mind that experimental cuts on invariant masses and the boson scattering angle can be easily implemented in semi-analytical calculations, and it is also possible to obtain semi-analytical distributions in many interesting variables [50].

Despite its stunning successes, the Standard Model has conceptual drawbacks, and it is expected that there will be new physics at higher energies. Firstly, and more philosophically, the Standard Model relies on "too many" arbitrary assumptions and parameters. This fostered the hope to find an underlying theory that can e.g. explain the origin of mass, of electric charge, or color. Secondly, one would like to find a quantum field theory that unifies the electroweak with the other known interactions, namely the strong interaction described by Quantum Chromodynamics (QCD) and gravitation. Thirdly, the fact that the Standard Model is not asymptotically free suggests that it is a kind of "low energy" effective theory of a more fundamental one [51]. In addition it is known that, within the framework of the Standard Model, the scattering of longitudinally polarized W bosons violates the Froissart limit for the proper high energy behavior of cross-sections. Finally, there is the well-known fine-tuning or naturalness problem of the Standard Model which is related to a quadratic divergence in the radiative corrections to the Higgs mass. This problem necessitates new phenomena at a scale of $\mathcal{O}(1\text{ TeV})$ [51]. A candidate to solve the fine-tuning problem is Supersymmetry which introduces a fundamental symmetry between bosons and fermions and thus, via the relative minus sign in fermion loops compared to boson loops and via supersymmetric relations between masses and couplings, cancels

[†]That is the electroweak corrections of first order in the fine structure constant $\alpha = e^2/(4\pi)$.

the problematic quadratic divergence. Supersymmetric theories are free of quadratic divergences [51, 52]. A further interesting class of theories beyond the Standard Model are String Theories. In spite of their mathematical difficulties, String Theories are attractive, because they are finite to all orders of perturbation theory and ultraviolet divergence free, because they rely on few free parameters, because they may be able to explain mass hierarchies, and because they yield coupling constant unification. In addition, String Theories comprise gravitation, possibly solve the problem of the non-vanishing cosmological constant [53], and they may also be on their way to reach phenomenological predictability [54]. As a final remark it must, however, be stressed that so far no experimental evidence for physics beyond the Standard Model exists.

This thesis is organized as follows. In Chapter 2, the tree level results for process (1.1) will be discussed, followed by the presentation of QED initial state radiation (ISR) results in chapter 3. In chapter 4, results from preceding chapters are generalized to include s-channel exchange photons. Following this body of the thesis a set of appendices contains notations, definitions, and technical details of the presented calculations. Appendix A gives the metric for this thesis and appendix B introduces the Standard Model Lagrangian, the Feynman rules, and the renormalization that were used. Appendix C contains the definitions of polylogarithms and in appendix D the $2\to4$ and $2\to5$ particle phase space parametrizations needed for the evaluation of cross-sections at tree level and with ISR are given. In appendix E, all important details of the calculation of the tree level and ISR cross-sections are collected. Appendix F presents techniques for the evaluation of loop integrals as encountered in the virtual initial state QED corrections to process (1.1) and appendix G contains all analytical integrals required for the angular phase space integrations to be carried out in the cross-section calculation for process (1.1).

Chapter 2

The Z^0 Pair Born Cross-Section

At Born or tree level and for a center of mass energy $\sqrt{s}$, process (1.1) is described by the two Feynman diagrams depicted in figure 2.1. The corresponding cross-section is derived in appendix E.1. It can be written as a simple double convolution formula

$$\sigma^B(s) = \int_{4m_1^2}^{(\sqrt{s}-2m_2)^2} ds_{12}\,\rho_Z(s_{12}) \int_{4m_2^2}^{(\sqrt{s}-\sqrt{s_{12}})^2} ds_{34}\,\rho_Z(s_{34}) \times 2 \cdot BR(1) \cdot BR(2) \times \times \sigma_4^B(s; s_{12}, s_{34}) \tag{2.1}$$

with branching ratios $BR(1)$ and $BR(2)^\dagger$ of the Z^0 boson into the fermion-antifermion pairs $f_1\bar{f}_1$ and $f_2\bar{f}_2$ respectively, with invariant fermion pair masses s_{12} and s_{34}, and with the Z^0 boson Breit-Wigner densities

$$\rho_Z(s_{ij}) = \frac{1}{\pi} \frac{\sqrt{s_{ij}}\,\Gamma_Z(s_{ij})}{|s_{ij} - M_Z^2 + i\sqrt{s_{ij}}\,\Gamma_Z(s_{ij})|^2} \xrightarrow[\Gamma_Z \to 0]{} \delta(s_{ij} - M_Z^2) \ . \tag{2.2}$$

In the limit of on-shell Z^0 bosons their widths vanish and the Breit-Wigner densities are replaced by Dirac δ distributions. The Z^0 width is given by

$$\Gamma_Z(s_{ij}) = \frac{G_\mu\, M_Z^2}{24\pi\sqrt{2}} \sqrt{s_{ij}} \cdot \sum_f \left({g^V_{f\bar{f}Z}}^2 + {g^A_{f\bar{f}Z}}^2 \right) \cdot N_c(f) \ , \tag{2.3}$$

where M_Z represents the Z^0 mass, G_μ is the Fermi coupling constant, and $g^V_{f\bar{f}Z}$ and $g^A_{f\bar{f}Z}$ are the vector and axial vector couplings of a fermion-antifermion pair $f\bar{f}$ to the Z^0 boson (see appendix B.2). The color factor $N_c(f)$ is unity for leptons and three for quarks. Using left- and right-handed couplings as introduced in equation (E.3),

$$L_{e^+e^-Z} = -\frac{e}{4\,\sin\theta_w\,\cos\theta_w} \cdot \left(1 - 2\,\sin^2\theta_w\right) \equiv \left[\frac{G_\mu M_Z^2}{2\sqrt{2}}\right]^{\frac{1}{2}} \cdot L_e$$

$$R_{e^+e^-Z} = \frac{e}{4\,\sin\theta_w\,\cos\theta_w} \cdot 2\,\sin^2\theta_w \equiv \left[\frac{G_\mu M_Z^2}{2\sqrt{2}}\right]^{\frac{1}{2}} \cdot R_e \ ,$$

†The factor 2 conventionally introduced with the branching ratios, simplifies comparisons with on-shell Z^0 pair production. This is seen from equation (2.7) and was explained in some detail in reference [41].

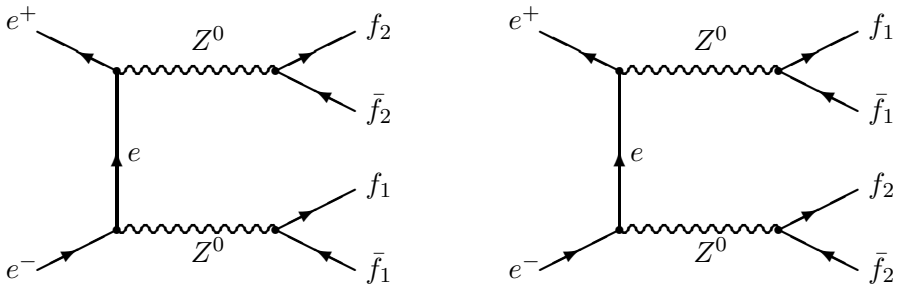

Figure 2.1: *The Born level Feynman diagrams for off-shell Z^0 pair production, the so-called 'Conversion' (or 'Crab') diagrams. Left: t-channel. Right: u-channel.*

$\sigma_4^B(s; s_{12}, s_{34})$ is obtained after fivefold analytical integration over the angular degrees of freedom of the $2 \to 4$ particle phase space (see appendix D.1),

$$\sigma_4^B(s; s_{12}, s_{34}) \;=\; \frac{\sqrt{\lambda}}{\pi\, s^2}\, \frac{\left(G_\mu M_Z^2\right)^2}{8} \left(L_e^4 + R_e^4\right) \cdot \mathcal{G}_4^{t+u}(s; s_{12}, s_{34}) \quad , \tag{2.4}$$

with the sub-index 4 indicating that the underlying matrix element contains four resonant Z^0 propagators. In σ_4^B, final state fermion masses are neglected. The factor in front of $\mathcal{G}_4^{t+u}$ comprises phase space factors and couplings to the initial state current. The kinematical function $\mathcal{G}_4^{t+u}(s; s_{12}, s_{34})$ for the summed contributions from the t-channel, the u-channel, and the t-u interference is given by

$$\mathcal{G}_4^{t+u}(s; s_{12}, s_{34}) \;=\; \frac{s^2 + (s_{12} + s_{34})^2}{s - s_{12} - s_{34}}\, \mathcal{L}_B - 2 \quad , \tag{2.5}$$

with

$$\begin{aligned} \mathcal{L}_B \;&=\; \mathcal{L}(s; s_{12}, s_{34}) \;=\; \frac{1}{\sqrt{\lambda}} \ln \frac{s - s_{12} - s_{34} + \sqrt{\lambda}}{s - s_{12} - s_{34} - \sqrt{\lambda}} \quad , \\ \lambda \;&=\; \lambda(s, s_{12}, s_{34}) \quad , \\ \lambda(a,b,c) \;&\equiv\; a^2 + b^2 + c^2 - 2ab - 2ac - 2bc \quad . \end{aligned}$$

$\mathcal{G}_4^{t+u}$ was rederived and fully agrees with earlier results [44, 55]. As is shown in reference [41], the on-shell limit of equation (2.5) recovers the result given in [44]. $\mathcal{G}_4^{t+u}$ is also known in the context of $\mathcal{O}(\alpha^2)$ corrections to e^+e^- annihilation into fermion pairs [56]. $\mathcal{G}_4^{t+u}$ separartes into contributions from the t- and u-channels and a t-u interference contribution (compare equation (E.12)):

$$\begin{aligned} \mathcal{G}_4^{t+u}(s; s_{12}, s_{34}) \;&=\; \mathcal{G}_4^t + \mathcal{G}_4^u + \mathcal{G}_4^{tu} \\ \\ \mathcal{G}_4^t \;=\; \mathcal{G}_4^u \;&=\; \frac{1}{8\, s_{12} s_{34}} \left[\frac{\lambda}{6} + 2s(s_{12}+s_{34}) - 8 s_{12} s_{34} + 4 s_{12} s_{34} (s - s_{12} - s_{34}) \mathcal{L}_B \right] \\ \mathcal{G}_4^{tu} \;&=\; -\frac{1}{8\, s_{12} s_{34}} \left[\frac{\lambda}{3} + 4s(s_{12}+s_{34}) + 16\, s\, s_{12} s_{34} \left(1 - \frac{s}{s - s_{12} - s_{34}}\right) \mathcal{L}_B \right] \quad . \end{aligned} \tag{2.6}$$

If considered separately, the contributions $\mathcal{G}_4^t$ from the t-channel, $\mathcal{G}_4^u$ from the u-channel, and $\mathcal{G}_4^{tu}$ from the t-u interference violate unitarity. As can be seen from equations (2.4) and (2.6), every contribution yields a total cross-section behavior proportional to s as $s \to \infty$. Thus each single contribution violates the Froissart limit [57], and only summation of the contributions $\mathcal{G}_4^t$, $\mathcal{G}_4^u$, and $\mathcal{G}_4^{tu}$, corresponding to the gauge invariant set of Feynman diagrams shown in figure 2.1, delivers a reasonable result with proper high energy behavior. This is a standard result of Yang-Mills theories [58]. It is noteworthy that, adding the three contributions from t-channel, u-channel, and t-u-interference, the factors $1/(s_{12}s_{34})$ contained in the individual kinematical functions given in equation (2.6) cancel. Consequently, the presence of the overall damping factor $(s_{12}s_{34})/s^2$ in $d^2\sigma^B/(ds_{12}ds_{34})$ should be considered a result of the gauge cancellations ensuring the unitarity of σ^B.

A graphical representation of $\sqrt{\lambda}/s \cdot \mathcal{G}_4^{t+u}$ is given in plots a) and b) of figure 2.2 for two different ranges of the variables $1 - s_{12}/s$ and $1 - s_{34}/s$. As $\sqrt{\lambda}/s \cdot \mathcal{G}_4^{t+u}$ is a dimensionless quantity, it only depends on s_{12}/s and s_{34}/s. From plot c) of figure 2.2 one can see how the double-resonance behavior entering the cross-section via the product $\rho_Z(s_{12})\,\rho_Z(s_{34})$ of Breit-Wigner densities dominates the character of the twofold differential cross-section $d^2\sigma^B/(ds_{12}\,ds_{34})$: Two intersecting resonances are seen in plot c) whereas the behavior of $\mathcal{G}_4^{t+u}$ in dependence on s_{12} and s_{34} is rather suppressed. Final cross-section results are obtained from equation (2.1) by twofold numerical integration[†].

To be able to compare the on-shell with the off-shell case, a "total" cross-section is introduced via

$$\sigma_{tot}^B(s) \;\equiv\; \frac{\sigma^B(s)}{2 \cdot BR(1) \cdot BR(2)} \quad , \tag{2.7}$$

which, in the narrow width limit, corresponds to the on-shell Z^0 pair cross-section. The effect of the finite Z^0 width on the total cross-section (2.7) is illustrated in figure 2.3. The off-shellness of the Z^0 bosons causes the characteristic smearing of the excitation curve with a dumped peak and stretched tails. The change in the cross-section induced by the finite width is of the order Γ_Z/M_Z and ranges from -7% at the cross-section peak to $+5\%$ at 1 TeV. The peak is shifted by approximately +4.5 GeV. Using a constant width, i.e. $\sqrt{s}\,\Gamma_Z(s) \to M_Z\Gamma_Z$, corresponds to a redefinition of the Z^0 boson mass [60]: $M_Z \to \bar{M}_Z = M_Z + \frac{1}{2}\Gamma_Z^2/M_Z$, resulting in $\bar{M}_Z \approx M_Z + 34$ MeV.

In the case of W pair production, gauge violating imaginary parts from the introduction of the finite width are only properly cancelled by imaginary parts from the trilinear vertex correction [61, 62]. Such gauge invariance problems due to the naive introduction of the finite boson width into the propagators are not present in Z^0 pair production. Possible gauge violations from the introduction of the Z^0 width as an s-dependent or s-independent quantity are phenomenologically irrelevant and may be trivially resolved by adjusting the definition of the width. The absence of the more serious gauge violations in off-shell Z^0 pair production is understood from the fact that gauge cancellations already happen at the level of σ_4^B because of the identical coupling structure of the t- and the u-channel contributions.

[†]All numerical programs for this thesis were written in FORTRAN. The author is grateful to D. Bardin for providing the integration routines `SIMP` and `FDSIMP` together with routines for the evaluation of Dilogarithm and Trilogarithm functions.

Figure 2.2: *Plots a) & b): Behavior of the dimensionless kinematical function* $\sqrt{\lambda}/s \cdot \mathcal{G}_4^{t+u}$ *for the two different ranges* $0 \leq 1\text{–}s_{ij}/s < 1\text{–}s_{ij,min}/s$ *and* $0.15 \leq 1\text{–}s_{ij}/s \leq 0.995$. *The variables* $1\text{–}s_{12}/s$ *and* $1\text{–}s_{34}/s$ *were chosen for the sake of clearer graphical presentation. Note that the used graphics package PAW [59] has problems at the lower edges of phase space because of the very steep gradient of the plotted function. The flat region in the foreground represents zero level and lies outside the phase space. The edge of phase space is clearly seen from plot b). Plot c): Multiplication of* $\sqrt{\lambda}/s \cdot \mathcal{G}_4^{t+u}$ *with* $s \cdot \rho_Z(s_{12})\rho_Z(s_{34})$ *at* $\sqrt{s} = 200$ *GeV emphasizes the dominance of the double-resonance character of process (1.1).*

Figure 2.3: *The total Z^0 pair production cross-section $\sigma^B_{tot}(s)$ for process (1.1) and the effect of the finite Z^0 width. The numerical input for the Z^0 pair production figures is:* $G_\mu = 1.16639 \times 10^{-5}\ GeV^{-2}$, $M_Z = 91.173\ GeV$, $\Gamma_Z(M_Z) = 2.487\ GeV$, $\sin^2\theta_w = 0.2325$. *Final state fermion masses are neglected. The numerical precision is estimated to be better than 0.01‰.*

Chapter 3

$\mathcal{O}(\alpha)$ Initial State Radiation

In e^+e^- annihilation, initial state radiation (ISR) is known to represent the bulk of the radiative corrections. The $\mathcal{O}(\alpha)$ 'amputated' Feynman diagrams for initial state bremsstrahlung to process (1.1) are shown in figure 3.1, the corresponding virtual initial state correction diagrams are given in figure 3.2. External leg self energies are absorbed into on-shell renormalization. For both the t- and the u-channel, Z^0 bosons have to be attached to the two unconnected vertices of each 'amputated' Feynman diagram.

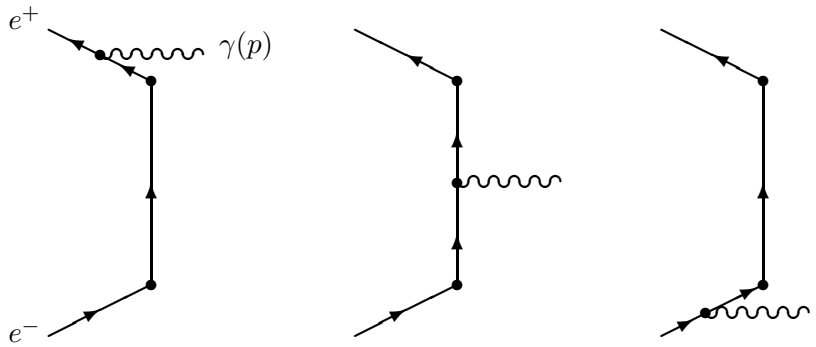

Figure 3.1: *The amputated initial state bremsstrahlung diagrams for Z^0 pair production.*

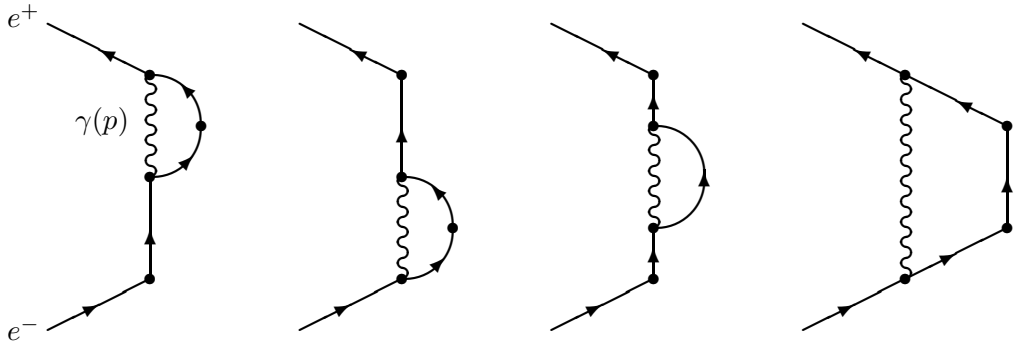

Figure 3.2: *The amputated virtual initial state correction diagrams for Z^0 pair production.*

The computation of the virtual $\mathcal{O}(\alpha)$ cross-section starts from the $2 \to 4$ particle phase space given in equation (D.1), appendix D.1. A cross-section differential in s_{12} and s_{34} is obtained by fivefold analytical angular integration of the interference between the Born and the virtual matrix elements over the boson scattering angle and over the fermion decay azimuthal and polar angles in the corresponding boson rest frames. The computation of $\mathcal{O}(\alpha)$ initial state bremsstrahlung starts from the $2 \to 5$ particle phase space given in equation (D.7), appendix D.2. Then, a sevenfold analytical angular integration of the bremsstrahlung matrix element squared is carried out over the photon scattering angle, the boson scattering azimuthal and polar angles in the two boson rest frame, and over the fermion decay azimuthal and polar angles in the corresponding boson rest frames. After these five- and sevenfold angular integrations, the differential cross-section for the Z^0 pair production process (1.1) including $\mathcal{O}(\alpha)$ ISR with soft photon exponentiation is given by

$$\frac{d^2\sigma^{ISR}}{ds_{12}\,ds_{34}} \;=\; \int\limits_{(\sqrt{s_{12}}+\sqrt{s_{34}})^2}^{s} \frac{ds'}{s}\; \rho_Z(s_{12})\; \rho_Z(s_{34}) \cdot 2BR(1)BR(2) \cdot \Big[\beta_e v^{\beta_e - 1}\mathcal{S} + \mathcal{H}\Big] \qquad (3.1)$$

with $\beta_e = 2\alpha/\pi\,[\ln(s/m_e^2) - 1]$ and $v = 1 - s'/s$. This is exactly the result derived in appendix E.5 and finally given in equation (E.68), except that the sequence of integration has been changed to match the $2 \to 5$ phase space parametrization described in equation (D.9), appendix D.2. The soft+virtual and hard photonic parts $\mathcal{S}$ and $\mathcal{H}$ in equation (3.1) were calculated analytically. Both $\mathcal{S}$ and $\mathcal{H}$ separate into a universal part with the Born cross-section at the reduced center of mass energy squared s' factorizing and a non-universal part:

$$\begin{aligned}
\mathcal{S}(s, s'; s_{12}, s_{34}) &= \Big[1 + \bar{S}_1(s)\Big] \cdot \sigma_4^B(s'; s_{12}, s_{34}) \;+\; \sigma_{\hat{S}}(s'; s_{12}, s_{34}) \quad , \\
\mathcal{H}(s, s'; s_{12}, s_{34}) &= \underbrace{\bar{H}_1(s, s') \cdot \sigma_4^B(s'; s_{12}, s_{34})}_{\text{Universal Part}} \;+\; \underbrace{\sigma_{\hat{H}}(s, s'; s_{12}, s_{34})}_{\text{Non-universal Part}} \quad . \qquad (3.2)
\end{aligned}$$

The $\mathcal{O}(\alpha)$ radiators $\bar{S}_1$ and $\bar{H}_1$ were explicitly derived in the full calculation. They emerged from the virtual and bremsstrahlung matrix elements after five- and sevenfold angular integration. Their derivation is outlined in appendix E.5:

$$\begin{aligned}
\bar{S}_1 &= \frac{\alpha}{\pi}\left[\frac{\pi^2}{3} - \frac{1}{2}\right] \;+\; \frac{3}{4}\,\beta_e \quad , \\
\bar{H}_1 &= -\frac{1}{2}\left[1 + \frac{s'}{s}\right] \cdot \beta_e \quad . \qquad (3.3)
\end{aligned}$$

$\mathcal{O}(\alpha^2)$ corrections may be taken into account in the universal corrections by adding the radiators $\bar{S}_2$ and $\bar{H}_2$ to $\bar{S}_1$ and $\bar{H}_1$ respectively. $\bar{S}_2$ and $\bar{H}_2$ are e.g. found in reference [63]. The factorizing parts of the cross-sections $\mathcal{S}$ and $\mathcal{H}$ are called "universal", because they are independent of the process topology, and especially of the initial state topology of the radiation process[†]. In fact, the universal radiators $\bar{S}_1$ and $\bar{H}_1$ are also found in the literature on fermion pair production in e^+e^- annihilation, e.g. in reference [63]. It must be stressed that, although it was expected to find a separation of the cross-section into

[†]In this statement it is implicitly assumed that the considered initial state topologies have unit charge initial state fermion lines connecting the initial state e^+ and e^-.

universal and non-universal contributions, the working out of the separation was a technically difficult task, especially for the t-u interference contribution. The virtual+soft and hard, non-universal, non-factorizable contributions in equation (3.2) are given by

$$\begin{aligned}\sigma_{\hat{S}}(s';s_{12},s_{34}) &= \frac{\alpha}{\pi}\cdot\frac{\left(G_\mu M_Z^2\right)^2}{8\pi s'}\left(L_e^4+R_e^4\right)\cdot\sigma^V_{4,nonuni}(s';s_{12},s_{34})\\ \sigma_{\hat{H}}(s,s';s_{12},s_{34}) &= \frac{\alpha}{\pi}\cdot\frac{\left(G_\mu M_Z^2\right)^2}{8\pi s}\left(L_e^4+R_e^4\right)\cdot\sigma^R_{4,nonuni}(s,s';s_{12},s_{34})\end{aligned}\tag{3.4}$$

with $\sigma^V_{4,nonuni}$ and $\sigma^R_{4,nonuni}$ as derived in appendix E. The full expressions are given in equation (E.20), appendix E.2 and in equation (E.32), appendix E.3. Equations (E.20) and (E.32) represent a main result of this thesis, but will not be rewritten here because of their considerable length. The result (3.4) is new even in its limit for the case of on-shell Z^0 bosons. It is seen from equations (E.20) and (E.32) that the non-universal contributions contain many dilogarithm and trilogarithm functions and are rather involved. One should note that, in equation (3.4), the virtual+soft non-universal contribution is evaluated at s' instead of s. The reason for this treatment is to avoid an unphysical, δ distribution-like concentration of non-universal virtual+soft ISR corrections at zero radiative energy loss. One of the reasons for the appearance of non-universal ISR contributions is the angular dependence of t- and u-channel propagators. For both virtual and bremsstrahlung corrections the angular behavior of t- and u-channel propagators is much more complicated than the angular behavior of s-channel propagators (see appendices D.2, E.2, and E.3 for details). Total cross-sections are computed from equation (3.1) by threefold numerical integration over s', s_{34}, and s_{12}.

Several other remarkable properties of equation (3.2) are worth mention. The leading ISR corrections to the cross-section with the mass singularities β_e factorize and are contained in the universal cross-section contributions. This is true not only for the overall cross-section, but also for the individual contributions from the t- and the u-channel and from their interference. As one would expect, non-universal contributions do not contain the mass singularity β_e. As a consequence, non-universal ISR corrections are suppressed with respect to the universal ones. The numerical influence of universal and complete ISR corrections on the cross-section for process (1.1) is presented in figure 3.3. Some discussion of the results presented in figure 3.3 is in order. Around threshold, in the energy range of LEP2, universal ISR peaks at large negative contributions with a relative correction of almost –30% at the Z^0 pair threshold itself. Below $\sqrt{s}$=280 GeV, ISR radiatively reduces the Z^0 pair cross-section. At higher energies ISR corrections are positive and develop a radiative tail increasing the Born off-shell cross-section by +14% at $\sqrt{s}$=1 TeV. These patterns are familiar from the Z^0 pole, which is not surprising, because single Z^0 production is a resonant process too, and because the radiators $\bar{S}_1$ and $\bar{H}_1$ describe the complete $\mathcal{O}(\alpha)$ ISR at the Z^0 pole [64]. The radiative tail, already present in universal ISR, is further pronounced by non-universal ISR, whereas non-universal corrections are hardly noticeable around threshold and therefore irrelevant in the LEP2 energy regime. The explanation for the radiative tail in the universal corrections is that radiative reduction of s to s' increases the relevant Born cross-section $\sigma_4^B(s',s_{12}s_{34})$ (see equations (2.4) and (3.2)) in the region of negative slope of σ_4^B. The additional corrections due to non-universal contributions range from 0.3% below threshold up to 2.5% at 1 TeV. In the

Figure 3.3: *The total off-shell Z^0 pair production cross-section $\sigma_{tot}(s)$. The solid line represents the Born cross-section $\sigma^B_{tot}(s)$ as in figure 2.3. The dash-dotted line gives the cross-section with universal ISR corrections only, i.e. $\sigma_{\hat{S}}$ and $\sigma_{\hat{H}}$ are set to zero. The dotted line gives the cross-section with complete ISR from eq. (3.1). In the inset, the relative deviations of the universally and completely ISR corrected cross-sections from the off-shell Born cross-section $\sigma^B_{tot}(s)$ are given. The numerical input for the ISR corrections is: $\alpha = 1/137.0359895$, $m_e = 0.51099906\ MeV$. The numerical precision is around 0.1‰.*

energy range of LEP2, non-universal corrections do not exceed 0.4%. Comparison of figures 2.3 and 3.3 shows that the high energy tail due to ISR is much more pronounced than the one due to the off-shellness of the Z^0 bosons. It should also be realized that ISR shifts the cross-section maximum by 9 GeV from $\sqrt{s}$=211 GeV to $\sqrt{s}$=220 GeV.

$\sqrt{s}$ [GeV]	σ_{tot}^{B} [pb]	$\sigma_{tot}^{ISR,uni}$ [pb]	$\sigma_{tot}^{ISR,compl.}$ [pb]
130.0	0.0015	0.0013	0.0013
150.0	0.0067	0.0055	0.0056
165.0	0.0215	0.0175	0.0176
180.0	0.1657	0.1227	0.1231
190.0	0.8971	0.6995	0.7021
200.0	1.1397	0.9641	0.9678
212.0	1.1898	1.0629	1.0671
230.0	1.1316	1.0611	1.0657
260.0	0.9799	0.9613	0.9663
300.0	0.8099	0.8211	0.8264
400.0	0.5503	0.5811	0.5866
500.0	0.4074	0.4399	0.4454
600.0	0.3171	0.3481	0.3534
800.0	0.2111	0.2374	0.2422
1000.0	0.1524	0.1744	0.1787

Table 3.1: *Numerical values for the off-shell Z^0 pair production cross-section at tree level, with universal ISR, and with complete ISR as obtained from equations (2.1) and (3.1) by numerical integration.*

Investigating the unitarity for the ISR corrected cross-section, one observes from equations (3.1) to (3.3) that the $1/s$ behavior observed in the Born cross-section is altered by factors $\ln(s/m_e^2)$ originating from the mass singularity β_e. Therefore the unitary behavior due to the gauge cancellations discussed in chapter 2 is carried through to the universal part of the ISR corrections. For $s \to \infty$, the universally ISR corrected cross-section behaves better than $(\ln^3 s)/s$ and thus approaches zero. As is seen from table 3.1, the absolute value of the non-universal corrections reaches a maximum around $\sqrt{s}$=450 GeV and then decreases with increasing $\sqrt{s}$. This already hints at the unitary behavior of the non-universal ISR corrections which is ensured by the overall damping factor already discussed in chapter 2. However, an important difference between the appearance of the factor $(s_{12}s_{34})/s^2$ in the tree level and in the non-universally ISR corrected cross-section exists: All ISR cross-section contributions, namely the ISR t-channel, the ISR u-channel, and the ISR t-u interference contributions, contain this *screening* factor, whereas at tree level its appearance is only a result of the gauge cancellations. Thus the screening factor appears separately in all the following non-universal cross-section parts,

$$\rho(s_{12})\,\rho(s_{34}) \cdot \sigma_{\hat{S},\hat{H}}^{t,u,tu} \;\sim\; \frac{s_{12}\,s_{34}}{s^2} \quad , \tag{3.5}$$

and it ensures the unitary behavior, i.e. the smallness of non-universal ISR corrections, at the level of individual contributions. This is more than one could expect, because cross-section unitarity only requires a unitarity-conserving mechanism for the sum of all contributions.

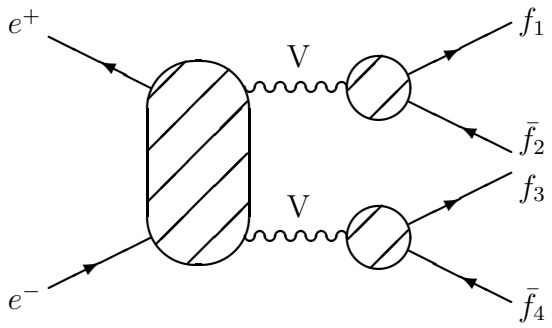

Figure 3.4: *The generic two-boson production and decay Feynman diagram for e^+e^- annihilation. V stands for any vector boson, the $f_i,\ i = 1, 2, 3, 4$ represent the decay fermions.*

To summarize this chapter, the previously unknown full initial state QED corrections to Z^0 pair production were calculated and separated into a universal leading logarithm and a non-universal part. It was illustrated how high energy unitarity is conserved for the radiatively corrected cross-section. Complementary results for W^+W^- pair production were reported in [42] where, instead of a u-channel amplitude two s-channel amplitudes containing the $W^+W^-Z^0$ and $W^+W^-\gamma$ vertices are present. Taking these results into account, one can claim knowledge of all initial state QED corrections for the whole class of four-fermion production via two-boson production processes in e^+e^- annihilation. The corresponding generic two-boson production and decay Feynman diagram is shown in figure 3.4.

Chapter 4

Generalization to Neutral Current Pair Production

Four-fermion production via massive boson pairs is easily accessible through experimental cuts on fermion pair invariant masses. But still one would like to know not only the four-fermion cross-section proceeding via Z^0 pair production, but the full four-fermion generalization

$$e^+e^- \to f_1\bar{f}_1 f_2\bar{f}_2 \ , \qquad f_1 \neq f_2 \ , \quad f_i \neq e^{\pm}, \overset{(-)}{\nu}_e \tag{4.1}$$

of process (1.1). Process (4.1) is described by 24 electroweak Feynman diagrams [65]. If f_1 and f_2 are quarks, QCD contributions from 8 gluon exchange diagrams must be taken into account [66], and if massive fermions are produced, associated Higgs production must not be forgotten. In the electroweak case, if f_1 and f_2 belong to the same isospin doublet, both charged current (CC) and neutral current (NC) processes contribute to reaction (4.1). The various aspects of the CC reactions have been studied by many authors [42, 43, 67, 68, 69, 70, 71]. Interferences between CC and NC contributions should be small due to different invariant masses favored by the production of fermion pairs via boson decays. Born level semi-analytical calculations for the NC case are available, and the inclusion of initial state radiation (ISR) in a leading logarithm approximation is unproblematic [47, 65]. In figure 4.1, all NC Feynman diagrams of the so-called *Conversion* type are depicted. As is seen from table 4.1, the *Conversion* Feynman diagrams strongly dominate the cross-

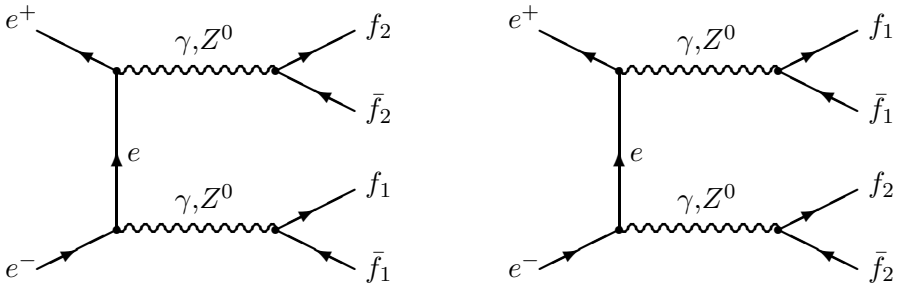

Figure 4.1: *The Born level Feynman diagrams for neutral current pair production. Left: t-channel. Right: u-channel.*

$\sqrt{s}$ [GeV]	$\sigma_{NC}^{\mu^+\mu^- b\bar{b}}$ [fb] All NC diagrams	$\sigma_{Conv}^{\mu^+\mu^- b\bar{b}}$ [fb] NC Conversion diagrams
91.0	613.832	278.080
141.0	94.469	94.477
191.0	53.252	53.231
241.0	38.610	38.613
291.0	28.396	28.422
341.0	22.128	22.161
391.0	17.930	17.970
441.0	14.946	14.982
491.0	12.713	12.742
591.0	9.620	9.570
691.0	7.551	7.603
791.0	5.935	6.187
891.0	5.166	5.165
991.0	4.237	4.382

Table 4.1: *Neutral current (NC) $\mu^+\mu^- b\bar{b}$ production cross-sections. By "NC" it is emphasized that only amplitudes containing intermediate Z^0 bosons or photons are accounted for. Feynman diagrams containing the Higgs boson are excluded. No cuts are applied. The author is grateful to A. Leike for supplying the* FORTRAN *code* `4fAN` *[65] for the production of the results in this table.*

section at energies above the Z^0 mass. Interferences between *Conversion* type and other NC diagrams are small and negative. Therefore it is interesting to investigate the process

$$e^+e^- \to (Z^0Z^0, Z^0\gamma, \gamma\gamma) \to f_1\bar{f}_1 f_2\bar{f}_2(\gamma) \;, \qquad f_1 \neq f_2 \;, \quad f_i \neq e^\pm, \overset{(-)}{\nu}_e \tag{4.2}$$

with full ISR, proceeding via the tree level diagrams shown in figure 4.1. The exchange photons to be taken into account have no resonance behavior. Consequently, contrary to the double-resonance case treated in chapter 2, it is not advantageous to express initial state couplings and boson propagators in terms of Breit-Wigner densities as given in equation (2.2). Since process (4.2) can be described by several sets of t-channel, u-channel and t-u interference contributions, it is appropriate to replace equation (2.1) by

$$\sigma_{Conv}^B(s) \;=\; \int\limits_{4m_1^2}^{(\sqrt{s}-2m_2)^2} ds_{12} \int\limits_{4m_2^2}^{(\sqrt{s}-\sqrt{s_{12}})^2} ds_{34}\, \frac{d^2\sigma_{Conv}^B(s;s_{12},s_{34})}{ds_{12}\,ds_{34}} \tag{4.3}$$

with the twofold differential cross-section factorizing into a phase space factor, a function $\mathcal{C}$ of couplings and propagators, and the kinematical function $\mathcal{G}_4^{t+u}$ already known from equation (2.5),

$$\frac{d^2\sigma_{Conv}^B\,(s;s_{12},s_{34})}{ds_{12}\,ds_{34}} \;=\; \frac{\sqrt{\lambda}}{\pi\, s^2}\cdot \mathcal{C}(f_1,s_{12};f_2,s_{34})\,\mathcal{G}_4^{t+u}(s;s_{12},s_{34}) \;\; . \tag{4.4}$$

As $\mathcal{G}_4^{t+u}$ is, in the language of Feynman diagrams, related to a pair of t- and u-channel diagrams, the function $\mathcal{C}$ is obtained by summing over all 16 such pairs that can be formed from the eight diagrams of figure 4.1. This results in

$$\begin{aligned}
\mathcal{C}(f_1, s_{12}; f_2, s_{34}) &= \frac{2\, s_{12}\, s_{34}}{(6\pi^2)^2} \times \\
&\Re\mathrm{e}\left\{ \sum_{B_i, B_j, B_k, B_l = \gamma, Z} \frac{1}{D_{B_i}(s_{12})} \frac{1}{D_{B_j}(s_{34})} \frac{1}{D^*_{B_k}(s_{12})} \frac{1}{D^*_{B_l}(s_{34})} \times \right. \\
&\quad \Big[L_{e^+e^-B_i}\, L_{e^+e^-B_k}\, L_{e^+e^-B_j}\, L_{e^+e^-B_l} \;+\; R_{e^+e^-B_i}\, R_{e^+e^-B_k}\, R_{e^+e^-B_j}\, R_{e^+e^-B_l} \Big] \times \\
&\quad \Big[L_{f_1\bar{f}_1 B_i}\, L_{f_1\bar{f}_1 B_k} \;+\; R_{f_1\bar{f}_1 B_i}\, R_{f_1\bar{f}_1 B_k} \Big] \cdot N_c(f_1)\, N_p(B_i, B_k, m_1, s_{12}) \times \\
&\quad \left. \Big[L_{f_2\bar{f}_2 B_j}\, L_{f_2\bar{f}_2 B_l} \;+\; R_{f_2\bar{f}_2 B_j}\, R_{f_2\bar{f}_2 B_l} \Big] \cdot N_c(f_2)\, N_p(B_j, B_l, m_2, s_{34}) \right\} \qquad (4.5)
\end{aligned}$$

where left- and right-handed couplings are used as defined in equations (B.27) and (B.28). The propagator denominators are given by

$$D_B(s_{ij}) \;=\; s_{ij} - M_B^2 + i\sqrt{s_{ij}}\,\Gamma_B(s_{ij}) \qquad (4.6)$$

with their complex conjugates D^*_B. $M_\gamma = \Gamma_\gamma = 0$ for the photon and $\Gamma_Z(s_{ij}) = \sqrt{s_{ij}}\,\Gamma_Z/M_Z$ which is a good approximation around the Z^0 peak and above. The color factor $N_c(f)$ is unity for leptons and three for quarks. The phase space factor

$$N_p(B_i, B_k, m, s) \;=\; \begin{cases} 1 & \text{for} \quad B_i \neq \gamma \;\text{ or }\; B_k \neq \gamma \\ \sqrt{1 - 4m^2/s} \cdot (1 + 2m^2/s) & \text{for} \quad B_i = B_k = \gamma \end{cases} \qquad (4.7)$$

correctly takes into account that fermion masses may be neglected if the corresponding fermion pair couples to a Z^0 resonance but may not if it only couples to a photon. In the latter case, finite cross-section contributions arise from close to the lower boundary of the invariant masses s_{ij}. It is readily verified that the above generalization of the Z^0 pair results from chapter 2 is formally carried out through the replacement

$$\rho_Z(s_{12})\,\rho_Z(s_{34}) \cdot 2BR(1)BR(2) \cdot \frac{\left(G_\mu M_Z^2\right)^2}{8} \left(L_e^4 + R_e^4\right) \;\longrightarrow\; \mathcal{C}(f_1, s_{12}; f_2, s_{34})\;. \qquad (4.8)$$

The input for numerical calculations was chosen as $G_\mu = 1.16639 \cdot 10^{-5}$ GeV^{-2}, $M_Z = 91.173$ GeV, $\Gamma_Z = 2.4971$ GeV, $M_W = 80.22$ GeV, and $m_e = 0.51099906$ MeV. For the electroweak mixing angle, the effective value $\sin^2\theta_w = 0.2325$ was chosen. The input for the left- and right-handed couplings was $Q_e = -1$, $\mathcal{T}^{(3)}_{W,e} = -\frac{1}{2}$, and $e = \sqrt{4\pi\alpha}$ with $\alpha = \sqrt{2} M_W^2 \sin^2\theta_w\, G_\mu/\pi$. For the QED corrections, because they are mainly due to soft photons, the Thomson limit $\alpha = 1/137.0359895$ [10] was used. These parameter choices enabled straightforward comparisons with the results in reference [65]. For several center of mass energies in the range of LEP2 and above and for different final state fermion pair combinations, tree level results for the full set of *Conversion* diagrams were compared to the appropriate contribution as obtained from the FORTRAN code `4fAN` used in reference [65]. Agreement was found to be at the level of the numerical precision of the integration routine.

Taking ISR into account, means to implement the replacement (4.8) into formula (3.1), resulting in

$$\frac{d^2\sigma^{ISR}_{Conv}}{ds_{12}\,ds_{34}} \;=\; \int\limits_{(\sqrt{s_{12}}+\sqrt{s_{34}})^2}^{s} \frac{ds'}{s}\,\mathcal{C}(f_1,s_{12};f_2,s_{34})\cdot\Big[\,\beta_e v^{\beta_e-1}\,\mathcal{S}_{Conv}\;+\;\mathcal{H}_{Conv}\,\Big] \tag{4.9}$$

for the twofold differential $\mathcal{O}(\alpha)$ ISR corrected cross-section with soft photon exponentiation for the NC pair production process (4.2). Recalling that the factor $(G_\mu M_Z^2)^2/8\cdot(L_e^4+R_e^4)$ is now absorbed in $\mathcal{C}$ and defining

$$\sigma^0_{Conv}(s;s_{12},s_{34}) \;\equiv\; \frac{\sqrt{\lambda}}{\pi\,s^2}\,\mathcal{G}_4^{t+u}(s;s_{12},s_{34}) \tag{4.10}$$

one finds from equation (2.4) and in analogy to equations (3.2) and (3.4)

$$\begin{aligned}
\mathcal{S}_{Conv}(s,s';s_{12},s_{34}) &= \Big[1+\bar{S}_1(s)\Big]\cdot\sigma^0_{Conv}(s';s_{12},s_{34}) \;+\; \sigma_{\hat{S},Conv}(s';s_{12},s_{34})\;,\\
\mathcal{H}_{Conv}(s,s';s_{12},s_{34}) &= \underbrace{\bar{H}_1(s,s')\cdot\sigma^0_{Conv}(s';s_{12},s_{34})}_{\text{Universal Part}} \;+\; \underbrace{\sigma_{\hat{H},Conv}(s,s';s_{12},s_{34})}_{\text{Non-universal Part}}
\end{aligned} \tag{4.11}$$

with the radiators $\bar{S}_1$ and $\bar{H}_1$ given in equation (3.3) and

$$\begin{aligned}
\sigma_{\hat{S},Conv}(s';s_{12},s_{34}) &= \frac{\alpha}{\pi}\cdot\frac{\sigma^V_{4,nonuni}(s';s_{12},s_{34})}{\pi s'}\quad,\\
\sigma_{\hat{H},Conv}(s,s';s_{12},s_{34}) &= \frac{\alpha}{\pi}\cdot\frac{\sigma^R_{4,nonuni}(s,s';s_{12},s_{34})}{\pi s}\quad.
\end{aligned} \tag{4.12}$$

$\sigma^V_{4,nonuni}$ and $\sigma^R_{4,nonuni}$ are found in equations (E.20) and (E.32) respectively.

As it yields a final state of experimental importance for Higgs searches and as it is also representative for semi-leptonic final states, the following presentation of results will focus on the reaction

$$e^+e^- \;\to\; (Z^0Z^0, Z^0\gamma, \gamma\gamma) \;\to\; \mu^+\mu^-\,b\bar{b} \tag{4.13}$$

which has already received considerable attention in the literature [49, 75, 65]. In figure 4.2, cross-sections for reaction (4.13) as obtained from equations (4.3) and (4.9) are presented. The cross-section correction due to universal ISR is approximately 12% at $\sqrt{s}$=130 GeV, increases to 18% below the Z^0 pair threshold, decreases to 13% in the region of the Z^0 pair-induced cross-section "bump" and then steadily increases to 21% at 600 GeV. The additional relative correction from non-universal ISR corrections increases from 9‰ at 130 GeV to 4.2% at 600 GeV. These numbers can be extracted from table 4.2 where numerical values for the cross-sections presented in figure 4.2 are given. The numerical precision of the values in table 4.2 is around 0.1‰[†]. With respect to Z^0 pair production the relative corrections of both universal and non-universal ISR are enhanced.

[†]In the following, numerical precisions will not be quoted any more. They are around 0.1‰ or better throughout this thesis.

Figure 4.2: *The NC pair production cross-section for process (4.13). The solid line represents the Born cross-section, the dash-dotted line includes universal, and the dotted line includes all ISR corrections. In the inset the full NC pair cross-section is compared to the contributions from Z^0 and photon pair production. The muon and b quark masses were taken as m_μ=0.105658389 GeV and m_b=4.3 GeV [10].*

Figure 4.3: *The effect of cuts of $2{\cdot}\Gamma_Z$ and $5{\cdot}\Gamma_Z$ around the Z^0 mass M_Z on the NC pair ('All Graphs') and Z^0 pair ('ZZ Graphs') cross-sections. $\Gamma_Z = 2.4971$ GeV. The cuts were applied to both fermion pair invariant masses. All curves show cross-sections for reaction (4.13) with universal ISR corrections.*

$\sqrt{s}$ [GeV]	$\sigma^{B}_{\mu^+\mu^- b\bar{b}}$ [fb]	$\sigma^{ISR,uni}_{\mu^+\mu^- b\bar{b}}$ [fb]	$\sigma^{ISR,compl.}_{\mu^+\mu^- b\bar{b}}$ [fb]	$\sigma^{ISR,uni}_{\mu^+\mu^- b\bar{b}}$ [fb] $s'/s \geq 0.9$	$\sigma^{ISR,compl.}_{\mu^+\mu^- b\bar{b}}$ [fb] $s'/s \geq 0.9$
130.0	131.4968	147.4554	148.7304	111.5411	112.2462
150.0	84.3863	97.9860	99.2177	71.1558	71.7510
165.0	65.8298	77.5651	78.7483	55.3251	55.8606
180.0	55.0144	64.8390	65.9749	45.9486	46.4371
190.0	56.4100	63.8071	64.9309	46.6443	47.1260
200.0	54.0441	60.9149	62.0168	44.9442	45.4106
212.0	49.8441	56.4425	57.5120	41.5066	41.9482
230.0	43.7651	49.9910	51.0124	36.4290	36.8391
260.0	35.7550	41.3205	42.2653	29.7064	30.0696
300.0	28.3717	33.1358	33.9928	23.5131	23.8300
400.0	18.1597	21.5427	–	14.9760	–
500.0	12.9578	15.5310	16.1086	10.6475	10.8406
600.0	9.8428	11.8958	12.3895	8.0646	8.2251
800.0	6.3587	7.7901	–	5.1868	–
1000.0	4.5111	5.5883	–	3.6671	–

Table 4.2: *Numerical values for the cross-section of process (4.13) at tree level, with universal ISR, and with complete ISR as obtained from equations (4.3) to (4.12). The last two columns give ISR corrected cross-section values after cutting on s' as indicated.*

Contrary to Z^0 pair production, ISR corrections are always positive which is easily explained by the negative slope of the cross-section curve for all center of mass energies $\sqrt{s}$. Thus a radiative reduction of s to s' enhances the cross-section in a way very similar to the radiative tail in Z^0 pair production. It must be stressed that the absolute value of the non-universal corrections to reaction (4.13) steadily decreases with energy, which is expected as an effect of the screening property. It is seen from figure 4.2 that, as expected, ISR smears out the Z^0 pair threshold behavior. In the inset of figure 4.2, the full NC pair production is compared to the contributions due to Z^0 and photon pair production for the universally ISR corrected case. Clearly, the main part of the cross-section is due to contributions which contain both Z^0 bosons and photons.

Figure 4.3 shows how the Z^0 pair production cross-section is restored from the full set of *Conversion* diagrams through invariant mass cuts on s_{12} and s_{34}. Also seen is the influence of the applied cuts on the Z^0 pair cross-section.

In figure 4.4 it is shown how the cross-section for reaction (4.13) evolves when invariant mass cuts on the $\mu^+\mu^-$ and the $b\bar{b}$ pairs are tightened. Already cuts of 50 GeV on both invariant pair masses yield an s-dependence of the cross-section very much resembling the double-resonant excitation curve for Z^0 pair production. The cuts $|M_{\mu^+\mu^-} - M_Z| \leq 5\Gamma_Z$ and $M_{b\bar{b}} \geq 60$ GeV represented by the dash-dotted line in the figure are of interest for Higgs searches, as the current Higgs mass limit lies around 60 GeV [38]. In these searches,

Figure 4.4: *Evolution of the cross-section for reaction (4.13) for different cuts on the* $\mu^+\mu^-$ *and* $b\bar{b}$ *invariant pair masses. All curves show cross-sections with universal ISR corrections.*

associated Higgs production is used with the $b\bar{b}$ pair coupling to the Higgs boson.

From figure 4.5 one can see how cross-sections behave if cuts are applied to the reduced center of mass energy squared s', i. e. to the invariant mass squared of the four-fermion system. In experimental analyses such cuts are very commonly used to reduce backgrounds. Numerical values after cuts on s' are given in table 4.2. Both plots of figure 4.5 show cross-sections for the final state $\mu^+\mu^- b\bar{b}(\gamma)$. The upper plot is for the Z^0 pair reaction (1.1), the lower one for process (4.13). The main windows present the development of universally ISR corrected cross-sections when the s' cut is tightened. The insets, where the ratio of the cross-section with complete over the cross-section with universal ISR is plotted, give the additional relative cross-section contribution from non-universal ISR correction. From the upper plot for $e^+e^- \to (Z^0Z^0) \to \mu^+\mu^- b\bar{b}$ one can make three observations. First of all, one notices that the cross-section with ISR is dominated by rather soft radiation. Secondly, hard photon ISR[†] is strongly suppressed below the double-resonance peak. Only above the peak, such hard photon events represent a significant cross-sec-

[†]By hard photon radiation the author denotes the radiation of photons strongly reducing s. This "strong reduction" may be several per cent or more than 10%, depending on the context.

Figure 4.5: *Effect of s' cuts on the $\mu^+\mu^- b\bar{b}\,(\gamma)$ cross-section for final state production via process (1.1) (upper plot) and process (4.13) (lower plot). The main windows present universally ISR corrected cross-sections, the insets show ratios of completely over universally corrected cross-sections. No cuts are applied to s_{12} and s_{34}.*

tion contribution. Both these results are analogous to similar ones at the single Z^0 peak at LEP1 [64]. This is, because both processes, single and double Z^0 production, are resonant processes with Breit-Wigner factors

$$\frac{\sqrt{s}\,\Gamma_Z(s)}{|s - M_Z^2 + i\sqrt{s}\,\Gamma_Z(s)|^2}$$

limiting hard radiation in the peak region. In addition, both calculations use the same $\mathcal{O}(\alpha)$ radiators $\bar{S}_1$ and $\bar{H}_1$. The third observation, made from the inset of the upper plot, is that non-universal ISR tends to be harder than universal ISR so that the ratio of the cross-section corrected with complete ISR over the universally corrected cross-section decreases with a cut on s'. In other words, the non-universal ISR corrections in per cent decrease with a cut on s'. This may be understood as follows: $\mathcal{O}(\alpha)$ non-universal corrections are infrared finite, whereas the infrared divergent universal corrections underwent a resummation, namely the soft photon exponentiation. Thus the universal corrections contain important soft resummed parts, and the non-universal corrections don't. The opening angle between the two curves in the inset reflects the increasing importance of hard radiation at higher energies. Around the double Z^0 peak and below however, the ratio of the completely over the universally corrected cross-section is unaffected by the s' cut. This means that, below $\sqrt{s} \approx 200$ GeV, no considerable excess of hard photon radiation due to non-universal corrections exists. As for universal ISR, where deviations of the cross-section with the cut $s'/s \geq 0.9$ from the cross-section without cut are only seen above $\sqrt{s} \approx 200$ GeV too, harder radiation is disfavored by the steep rise of the tree level cross-section around threshold.

Turning to the lower plot of figure 4.5 which is for reaction (4.13), patterns similar to the upper plot of the figure are encountered. There is, however, no disincentive for hard radiation due to a steep rise of the cross-section. Therefore, the ISR corrected cross-sections in the main window are lowered throughout the presented energy region by all cuts on s'. The approach between the curves for no cut and for $s'/s \geq 0.5$ around 150 GeV must be attributed to the inhibition of a reduction of s' below the threshold for single-resonant $Z^0\gamma \to \mu^+\mu^- b\bar{b}$ production. From the inset of the lower plot of figure 4.5 one may draw the same conclusions as for the inset of the upper plot, except that there is no disturbance of hard radiation due to the rise of the cross-section in the double Z^0 resonance region.

To conclude the discussion of figure 4.5, it is mentioned that the integration of the involved non-universal cross-section contributions is very CPU time consuming. This means that, contrary to what would be desirable, it is not possible to mass-produce results with non-universal ISR and all kinds of cuts. Still, a more thorough analysis including an investigation of the spectrum of radiated photons is under way [72].

Figure 4.6 shows cross-sections for process (4.2) with different final states. The upper plot of the figure shows final states containing $b\bar{b}$ pairs, the lower plot the smaller cross-sections for final states with $\mu^+\mu^-$ pairs. Cuts were applied to require $\sqrt{s_{12}} \geq 5$ GeV and $\sqrt{s_{34}} \geq 20$ GeV. Comparing the final states $u\bar{u}b\bar{b}$ and $d\bar{d}b\bar{b}$, it is interesting to observe how the different u and d quark electric charges affect the cross-section below threshold: There, the $d\bar{d}b\bar{b}$ cross-section is much smaller than the $u\bar{u}b\bar{b}$ cross-section . Similarly interesting is the comparison between $\mu^+\mu^- b\bar{b}$ and $\nu_\mu\bar{\nu}_\mu b\bar{b}$. The $\nu_\mu\bar{\nu}_\mu b\bar{b}$ cross-section has a shape very

Figure 4.6: *Universally ISR corrected cross-sections from process (4.2) for different four-fermion final states containing $b\bar{b}$ pairs (upper plot) or $\mu^+\mu^-$ pairs (lower plot).*

Fermion	ν_μ	μ	τ	u	d	c	b
Mass [GeV]	0	0.105658389	1.7771	0.005	0.01	1.3	4.3

Table 4.3: *The fermion masses for the numerical computations presented in the figures.*

much like the Z^0 pair excitation curve due to the cuts and the weak coupling of b quarks to photons. The $\mu^+\mu^- b\bar{b}$ cross-section on the other hand receives significant contributions below the Z^0 pair threshold due to the muon's electric charge. Also rather interesting, but straightforwardly explained by the cuts and the photonic and weak couplings, are comparisons between the final states $\mu^+\mu^- b\bar{b}$ versus $\mu^+\mu^- c\bar{c}$ and $\mu^+\mu^- \nu_\mu \bar{\nu}_\mu$ versus $\mu^+\mu^- \tau^+\tau^-$. The fermion masses for all numerical computations were taken from reference [10] and are listed in table 4.3.

To conclude the chapter, figure 4.7 presents the influence of final state fermion masses as taken into account in the semi-analytical approach. It is recalled that final state fermion masses are only taken into account through the factors $N_p(B_i, B_k, m, s)$. Figure 4.7 shows, in the main window, the two cross-sections of reaction (4.2) into the final states $\mu^+\mu^- d\bar{d}$ and $\mu^+\mu^- b\bar{b}$ which do not differ in couplings, but only in final state quark masses (see table 4.3). The $\mu^+\mu^- d\bar{d}$ cross-section is larger because of its larger phase space due to $m_d < m_b$. If now the invariant $d\bar{d}$ mass is cut at exactly two times the b quark mass, the phase spaces for the two final states have equal volume. However, a difference remains due to the factors N_p for the quarks. While for the final state $\mu^+\mu^- d\bar{d}$

$$N_p(\gamma, \gamma, m_d, s_{34}) \;=\; \sqrt{1 - 4m_d^2/s_{34}} \cdot (1 + 2m_d^2/s_{34}) \;\approx\; 1$$

throughout the phase space cut at $\sqrt{s_{34}} = 2\,m_b$, because of the, compared to the cut, small d quark mass, this is different for the final state $\mu^+\mu^- b\bar{b}$. $N_p(\gamma, \gamma, m_b, s_{34})$ is zero at the phase space boundary $\sqrt{s_{34}} = 2\,m_b$ and approaches its limiting value 1 to a precision of $1\,‰$ only around $\sqrt{s_{34}} = 38$ GeV. Thus the cross-section for the final state $\mu^+\mu^- b\bar{b}$ is slightly smaller than the one for $\mu^+\mu^- d\bar{d}$ cut at $\sqrt{s_{34}} = 2\,m_b$. This is seen from the inset of figure 4.7 where the ratio of $\sigma_{\mu^+\mu^- d\bar{d}}$ with the cut $\sqrt{s_{34}} \geq 2\,m_b$ over $\sigma_{\mu^+\mu^- b\bar{b}}$ is given.

Figure 4.7: *The effects of masses in the cross-sections for* $\mu^+\mu^- d\bar{d}$ *and* $\mu^+\mu^- b\bar{b}$ *production according to reaction (4.2). The main window shows the cross-section enhancement due to the larger phase space for the production of lighter fermion pairs. The inset shows the small effect of the factors* $N_p(\gamma, \gamma, m, s)$*, if phase spaces are made equally large by applying a cut of* $\sqrt{s_{34}} = 2\, m_b$ *to the invariant* $d\bar{d}$ *pair mass. A small bump is seen around the* Z^0 *pair threshold. All curves are with universal ISR.*

Chapter 5

Summary, Conclusions, and Outlook

Even around the Z^0 pole, four-fermion production is an interesting topic, relevant not only for Higgs boson searches [38] but also for higher order corrections to the Z^0 line shape [56, 63, 73]. Above the production thresholds for resonant gauge boson pair production, e^+e^- annihilation into four fermions is one of the most significant Standard Model processes. Thus, double-resonance production plays a very important rôle at LEP2 and other future e^+e^- colliders, and the study of four-fermion final states will provide further understanding of gauge boson properties and may be the key to the mechanism of electroweak symmetry breaking via investigations of associated Higgs boson production.

In the preceding chapters, the first complete calculation of initial state QED corrections (ISR) for neutral current double-resonance production in e^+e^- annihilation was presented. A semi-analytical method was used to compute cross-sections and invariant mass distributions for Z^0 and neutral current (NC) pair production processes (1.1) and (4.2)[†]. These processes are interesting by themselves and also as background to W^+W^- physics and Higgs searches. All angular degrees of freedom were integrated analytically. After the angular integrations, only two fermion pair invariant masses were left for numerical integration with a straightforward self-adaptive Simpson algorithm. In the case of ISR, also the four-fermion invariant mass had to be integrated numerically. It was shown that boson off-shellness and ISR both yield considerable corrections to the cross-section, each of $\mathcal{O}(10\%)$ and up to $\mathcal{O}(20\%)$ for neutral current pair production. ISR corrections separate into universal parts with the Born cross-section factorizing and non-universal parts. Contrary to non-universal contributions, universal ISR parts contain the large logarithm $\ln(s/m_e^2)$ as a result of collinear photon radiation from the initial state electrons. Thus universal ISR is enhanced with respect to non-universal ISR. Invariant mass cuts can be easily implemented to isolate the Z^0 pair signal from the full NC process. Such cuts do not only suppress NC pair production, but also irreducible backgrounds of the annihilation type. Two examples of annihilation type background Feynman diagrams are given in figure 5.1 (compare reference [65]).

The systematic errors of the presented calculation are physics dominated, because of the numerical integration's excellent precision. Errors arise via

[†]A similar calculation for W^+W^- pair production had to face ambiguities of the definition of initial state radiation due to the charge transfer from the initial to the final state in the t-channel W^+W^- production amplitude [42].

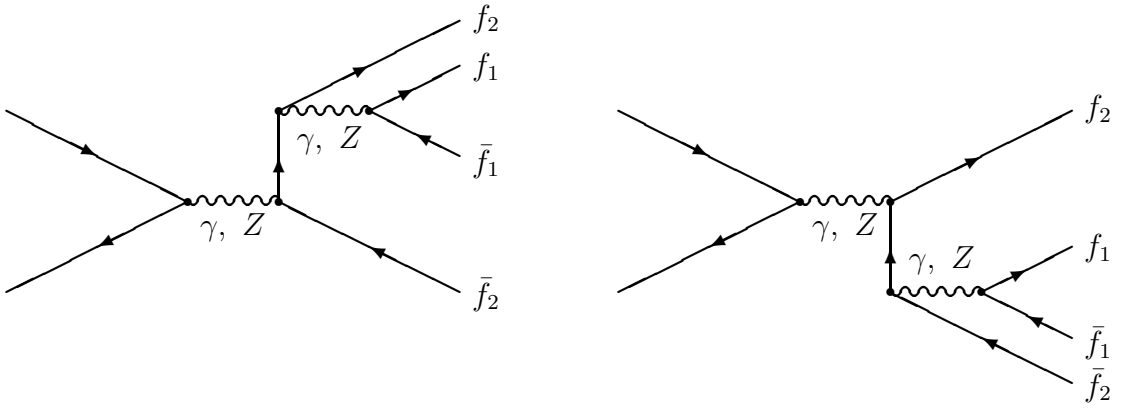

Figure 5.1: *Two examples of annihilation type Feynman diagrams for singly resonant electroweak background to reaction (4.2).*

- The use of the ultrarelativistic approximation (URA) with neglect of terms of $\mathcal{O}(m_e^2/s)$ and $\mathcal{O}(m_e^2/s_{ij})$. Errors due to the URA are very small. This is evidently true for Z^0 pair production. As all used fermion masses are at least one order of magnitude larger than the electron mass, and as lower invariant mass cuts of several GeV are quite commonly applied, the URA is a valid approximation also for the NC pair production process (4.2).

- Neglect of final state fermion masses in the matrix elements. For light fermions, the effect on the total cross-section is small. In the NC pair case with exchange photons, all important mass effects are properly taken into account by the factors N_p given in equation (4.7). Mass effects are removed by even moderate invariant mass cuts. For some cases, such cuts are also desirable with respect to non-perturbative threshold effects.

- Neglect of final state QED corrections. Compared to ISR, final state QED (FSR) is known to be suppressed, but may become important at very high energies beyond the TeV level. Interference effects between ISR and FSR were found to be suppressed by $\mathcal{O}(\Gamma_B/M_B)$ in resonant pair production of bosons B [74].

- Neglect of true electroweak corrections. For on-shell Z^0 pair production true electroweak effects were found to yield corrections around 1% to 2% [45]. This estimate may have to be increased to accommodate off-shell boson pair production, but no full calculation of electroweak one loop corrections for process (1.1) is available at present. In reference [45], a strong dependence of electroweak corrections on the Z^0 scattering angle was found for center of mass energies above 500 GeV.

- Theoretical and experimental uncertainties of the parameters entered into the numerical calculation.

In the following, it will be shown how the investigations presented in this thesis are embedded in the environment of four-fermion final state physics and in the framework of semi-analytical calculations dealing with four-fermion production in charged current and neutral current processes [41, 50, 42, 43, 75, 65, 72]. The semi-analytical method yields compact formulae for total and differential cross-sections at tree level and with leading initial state QED corrections. At present, semi-analytical cross-sections are available which are differential in the two boson invariant mass and the boson scattering angle [50]. These are easily numerically integrated to yield singly differential or total cross-sections. In this thesis, the semi-analytical method was used to present non-leading initial state QED corrections [41, 43]. The screening property was found in these non-leading corrections. A complete initial state QED calculation for a double-resonant four-fermion production is documented in detail for the first time.

In the presented calculation, some non-resonant annihilation type background contributions, see figure 5.1, to process (4.1),

$$e^+e^- \to f_1\bar{f}_1 f_2\bar{f}_2 \ , \qquad f_1 \neq f_2 \ , \quad f_i \neq e^{\pm}, \overset{(-)}{\nu}_e \quad ,$$

are not taken into account. But already for moderate cuts, the results given in this thesis represent the dominant contribution to process (4.1). Process (4.1) was completely and semi-analytically calculated in references [50, 75, 65], but only at tree level. However, as background contributions are small at LEP2 energies and above and as the leading universal ISR corrections may be straightforwardly implemented by multiplication of the tree level cross-section with the radiators $\bar{S}_1$ and $\bar{H}_1$ (see equation (3.3)), sufficiently precise results are available for process (4.1). This is still true if associated Higgs production is considered, because interferences of the Higgs Feynman diagram are negligible and because $\bar{S}_1$ and $\bar{H}_1$ describe the Higgs diagram's complete ISR corrections[†]. Thus, for the leptonic[‡] and the important semi-leptonic channels of process (4.1), the description obtained from this thesis and references [50, 75, 65] is sufficient in view of future e^+e^- collider data. The treatment of four-quark final states requires the consideration of eight additional Feynman diagrams of the annihilation type with decaying gluons radiated from the final state quarks. Two examples of such diagrams are given in figure 5.2. These diagrams were taken into account in semi-analytical [65] and in Monte Carlo calculations [66, 76]. The annihilation type QCD background diagrams are described by the same semi-analytical kinematical functions as the electroweak annihilation type background diagrams. The differences lie in coupling constants and color factors. Going a little further one realizes that hadron jets stemming from light quarks or gluons are experimentally not really distinguishable so that one must incoherently add several contributions to obtain a prediction for an experimental signature. This means that new contributions with the virtual gluon from figure 5.2 decaying into two gluons instead of two quarks must be taken into account.

[†]Generally, for Feynman diagrams of the *Annihilation* type with only one vertex in the initial state electron current (like the diagrams in figure 5.1) the radiators $\bar{S}_1$ and $\bar{H}_1$ describe the complete $\mathcal{O}(\alpha)$ ISR. As soon as *Conversion* type Feynman diagrams (like the diagrams in figure 4.1) are involved, non-universal ISR contributions are present.

[‡]It should be noted that final states with μ- and τ-neutrinos can be calculated semi-analytically, but are not experimentally observable individually, because the signature from final states with electron neutrinos is identical.

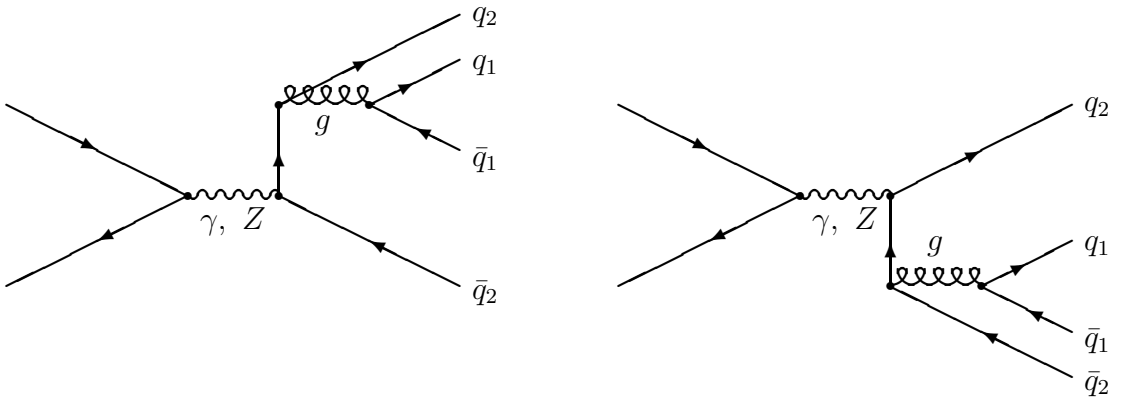

Figure 5.2: *Two examples of annihilation type Feynman diagrams for singly resonant QCD background to reaction (4.2). The curled lines represent gluons.*

Recently, the reaction $e^+e^- \to b\bar{b} + 2\,Jets$ was evaluated [76]. Another problem of the four-quark final states is related to so-called color reconnection effects which are mainly of interest for W^+W^- pair production and the W mass measurement [77].

It is, at this point, interesting to compare the results for Z^0 pair production with those of W^+W^- pair production. Both calculations are fundamentally different in two regards. Firstly, the contributing amplitudes differ: t- and u-channel amplitudes for Z^0 pairs, but t- and s-channel amplitudes for W^+W^- pairs (see e.g. reference [43]). Secondly, trilinear boson couplings contribute to Standard Model W^+W^- pair production, but not to Standard Model Z^0 pair production. On the other hand there are, of course, patterns that are common to W^+W^- and Z^0 pair production, such as the double-resonance behavior and the screening property. For four-fermion final states containing fermion-antifermion pairs from the same weak isospin doublet, double-resonant contributions arise from W^+W^- as well as Z^0 pair production, not to mention the many background contributions to both. The individual charged current and neutral current contributions to such final states have already been semi-analytically calculated. The interferences between CC and NC contributions, though small, require special treatment. This is due to different particle pairings from the decays of charged and neutral bosons which invalidates the unique assignment of the invariant masses s_{12} and s_{34} to fermion pairs. This problem is illustrated in equation (5.1) for the double-resonant signals yielding a $U\bar{U}D\bar{D}$ final state, where U and D denote generic particles with third weak isospin component $+\frac{1}{2}$ and $-\frac{1}{2}$ respectively:

$$\begin{aligned}
&\text{CC}: \quad e^+e^- \to W^+W^- \;\begin{cases} \to \bar{U}D & (\text{inv. mass } s_{12}) \\ \to U\bar{D} & (\text{inv. mass } s_{34}) \end{cases} \\
&\text{NC}: \quad e^+e^- \to Z^0Z^0 \;\begin{cases} \to \bar{U}U & (\text{inv. mass } s_{12}) \\ \to D\bar{D} & (\text{inv. mass } s_{34}) \end{cases} \quad .
\end{aligned} \tag{5.1}$$

	$\bar{d}d$	$\bar{u}u$	$\bar{e}e$	$\bar{\mu}\mu$	$\bar{\nu}_e\nu_e$	$\bar{\nu}_\mu\nu_\mu$
$\bar{d}d$	4·16	*43*	48	**24**	21	**10**
$\bar{s}s$	**32**	*43*	48	**24**	21	**10**
$\bar{u}u$	*43*	4·16	48	**24**	21	**10**
$\bar{e}e$	48	48	4·36	48	*56*	20
$\bar{\mu}\mu$	**24**	**24**	48	4·12	19	*19*
$\bar{\tau}\tau$	**24**	**24**	48	**24**	19	**10**
$\bar{\nu}_e\nu_e$	21	21	*56*	19	4·9	12
$\bar{\nu}_\mu\nu_\mu$	**10**	**10**	20	*19*	12	4·3
$\bar{\nu}_\tau\nu_\tau$	**10**	**10**	20	**10**	12	**6**

Table 5.1: *Number of tree level Feynman diagrams contributing to the production of four-fermion final states via neutral bosons.*

The complete process $e^+e^- \to U\bar{U}D\bar{D}$ including the small CC-NC interferences is, at present, only calculated by Monte Carlo programs (see e.g. [47]). Similarly four-fermion final states containing electrons or electron neutrinos in the final state have not yet been calculated semi-analytically, but constitute no problem to Monte Carlo programs [78, 79]. The additional complexity of final states with electrons or electron neutrinos is due to their additional amplitudes with t-channel boson propagators. In table 5.1, the number of Feynman diagrams contributing to four-fermion production via neutral boson exchange, i.e. the final states this thesis is concerned with, are listed. The simplest case (numbers in **boldface**) does not contain identical particles, electrons, electron neutrinos or particles from the same isospin doublet. Those final states were calculated semi-analytically and the calculations presented in this thesis describe the corresponding dominant contributions for energies above the Z^0 pole. For pairs of identical fermions, antisymmetrization of the final state as needed to satisfy the Pauli principle increases the number of Feynman diagrams (given in `typewriter`). Numbers in roman are for final states with electrons or electron neutrinos, and numbers in *italics* correspond to final states with particles from the same isospin doublet. Numerous Monte Carlo approaches [47, 48, 49, 66, 73, 78, 79, 80] treat four-fermion production in e^+e^- annihilation. The scopes of the two independent approaches represented by the semi-analytical and the Monte Carlo method are different. The semi-analytical method provides formulae to strongly promote the understanding of four-fermion production processes. Monte Carlo programs on the other hand aim at complete sets of Feynman diagrams and are needed by experimentalists to produce input for their detector simulations and to apply all experimental cuts. Semi-analytical programs can only be run with quasi-experimental cuts. Unfortunately, Monte Carlo programs are often "black boxes" to the experimentalist. It becomes clear that semi-analytical and Monte Carlo calculations are nicely complementary. Keeping in mind that four-fermion final states are much richer in structure, much more interesting and much more complicated than fermion pair final states, the ultimate goal of semi-analytical calculations is rather obvious, namely to describe four-fermionic complexity by as much simplicity as possible. The semi-analytical method has been very successful in this respect, because a

	$e^+e^- \to \mu^+\mu^- b\bar{b}$	$e^+e^- \to u\bar{d}\mu^-\bar{\nu}_\mu$	$e^+e^- \to (Z^0Z^0, Z^0\gamma, \gamma\gamma) \to f_1\bar{f}_1 f_2\bar{f}_2(\gamma)$
N_{diag}	25	10	8 (+56)
N_{inter}	325	55	36 (+532)
$N_{\mathcal{G}}$	4	8	1 (+2)
Refs.	[75, 65]	[42, 81]	This thesis

Table 5.2: *Examples for the number* N_{diag} *of Feynman diagrams contributing to the production of four-fermion final states in* e^+e^- *annihilation. Also given are the numbers of interferences between Feynman diagrams* (N_{inter}) *and the numbers of kinematical functions* $N_{\mathcal{G}}$ *needed to semi-analytically describe the process. The numbers in parentheses in the last column give the additional diagrams, interferences, and kinematical functions due to non-universal ISR as described in this thesis.*

description of many Feynman diagrams and their interferences by few kinematical functions (such as $\mathcal{G}_4^{t+u}$, see equation (2.4)) was achieved for several interesting four-fermion final states. Table 5.2 gives some examples.

It is of fundamental theoretical interest to continue the systematic semi-analytical treatment of e^+e^- annihilation into four fermions. For the future it is planned to extend the work of this thesis to include a non-standard, heavy new neutral boson Z' and to evaluate the corresponding discovery limits at future e^+e^- colliders. Further a full calculation for process (4.1) with all ISR corrections and semi-analytical calculations of four-fermion final states with electrons and electron neutrinos are very desirable. It could also be interesting to extend the presented results to accommodate anomalous couplings between three neutral gauge bosons. Such couplings are not present in the Standard Model. Their inclusion would require to take into account an additional Feynman diagram with s-channel e^+e^- annihilation into *one* neutral gauge boson which then decays into two neutral bosons that finally decay into the four final state fermions[†]. It is worth mentioning that all initial state QED corrections for such an inclusion are known from references [41, 42] and from this thesis. Anomalous trilinear neutral gauge bosons couplings are discussed in reference [82], but no deviations from the Standard Model were experimentally found so far [83]. Finally, it should be realized that the results presented in this thesis can be validated for proton-proton collisions at the Large Hadron Collider (LHC) by folding in parton distributions, changing coupling constants and introducing color factors.

[†]Depending on cuts, one may also have to account for annihilation type background diagrams.

Appendix A

Metric and Conventions

Every calculation in four-dimensional space-time requires the choice of a metric which is uniquely defined by a metric tensor $g_{\mu\nu}$. For this thesis,

$$g_{\mu\nu} \;=\; \begin{pmatrix} -1 & 0 & 0 & 0 \\ 0 & 1 & 0 & 0 \\ 0 & 0 & 1 & 0 \\ 0 & 0 & 0 & 1 \end{pmatrix} \;, \qquad \mu,\nu = 0,1,2,3 \tag{A.1}$$

is chosen as metric tensor. This is just the negative of the Bjorken-Drell metric tensor [90]. A contravariant 4-vector is defined by

$$v^\mu \;\equiv\; \left(v^0, \vec{v}\right) \;=\; \left(v^0, v^1, v^2, v^3\right) \tag{A.2}$$

with time-like component v^0 and space-like components $\vec{v}$. The corresponding covariant vector is given by

$$v_\mu \;=\; g_{\mu\nu}\, v^\nu = \left(-v^0, \vec{v}\right) \;, \tag{A.3}$$

where the convention to sum over repeated indices is adopted. The summation convention is used throughout this thesis unless stated otherwise. The scalar product of two 4-vectors is defined as the contraction with the metric tensor:

$$v{\cdot}w \;\equiv\; v_\mu w^\mu \;=\; v^\mu u_\mu \;=\; v^\mu\, g_{\mu\nu}\, w^\nu \;. \tag{A.4}$$

It should be noticed that, with the above convention, time-like four-vectors have negative and space-like four-vectors have positive metric. The choice of metric also entails that the invariant mass squared $M^2_{\mathcal{K}}$ of a system $\mathcal{K}$ with 4-vector k is given by

$$M^2_{\mathcal{K}} \;=\; (k^0)^2 - \vec{k}^2 \;=\; -k{\cdot}k \;\;. \tag{A.5}$$

The Dirac algebra is defined by

$$\begin{aligned} \left[\gamma_\mu, \gamma_\nu\right]_+ \;&=\; 2\, g_{\mu\nu} \\ \gamma_5 \;&=\; -\,\mathrm{i}\,\gamma_0\gamma_1\gamma_2\gamma_3 \;\;. \end{aligned} \tag{A.6}$$

Finally, it should be mentioned that natural units $c = \hbar = 1$ are used throughout this thesis.

Appendix B

The Standard Model of Electroweak Interactions

B.1 The Standard Model Lagrangian

Phenomenologically, the Standard Model is based on the empirical fermion content of nature given in table B.1, on the existence of the four vector bosons γ, W^+, W^-, and Z^0 that mediate the electroweak force, and on the Gell-Mann-Nishijima relation [84]

$$Q_f \;=\; \mathcal{T}_W^{(3)} + \frac{Y_W}{2} \quad . \tag{B.1}$$

These empirical facts can be embedded into a theoretical description which is characterized by a Lagrangian that is invariant under $SU(2)_L \times U(1)_{Y_W}$ gauge transformations,

$$\mathcal{L}_{SM} \;=\; \mathcal{L}_G + \mathcal{L}_H + \mathcal{L}_F + \mathcal{L}_{Yukawa} \quad . \tag{B.2}$$

The Gauge Field Lagrangian
The pure gauge field part $\mathcal{L}_G$ is given in terms of the massless gauge fields W_μ^a ($a = 1,2,3$) and B_μ. The isotriplet W_μ^a corresponds to the three generators $\mathcal{T}_a$ of the isospin group $SU(2)_L$, belongs to the adjoint representation of $SU(2)$, and couples to the left-handed doublets only. B_μ corresponds to the generator $-Y_W/2$ of the $U(1)$ subgroup of gauge transformations and couples to hypercharge. Adopting the conventions from appendix A one finds

$$\mathcal{L}_G = -\frac{1}{4}\, W_{\mu\nu}^a W^{a,\mu\nu} - \frac{1}{4}\, B_{\mu\nu} B^{\mu\nu} \quad . \tag{B.3}$$

Summation is also assumed over a, and the field strength tensors are given by

$$\begin{aligned} W^{a,\mu\nu} &= \partial^\mu W^{a,\nu} - \partial^\nu W^{a,\mu} + g_2 \epsilon_{abc} W^{b,\mu} W^{c,\nu} \quad , \\ B^{\mu\nu} &= \partial^\mu B^\nu - \partial^\nu B^\mu \quad , \end{aligned} \tag{B.4}$$

where ϵ_{abc} are the $SU(2)$ structure constants and g_1, g_2 denote the $U(1)$ and $SU(2)$ coupling constants. The non-abelian structure of the gauge group manifests itself in the trilinear and quartic gauge boson self couplings obtained from $\mathcal{L}_G$.

	Families			Q_f	$\mathcal{T}_W^{(3)}$	Y_W
	1	2	3			
Leptons	$\begin{pmatrix} \nu_e \\ e \end{pmatrix}_L$	$\begin{pmatrix} \nu_\mu \\ \mu \end{pmatrix}_L$	$\begin{pmatrix} \nu_\tau \\ \tau \end{pmatrix}_L$	0 -1	$+\frac{1}{2}$ $-\frac{1}{2}$	-1 -1
	e_R	μ_R	τ_R	-1	0	-2
Quarks	$\begin{pmatrix} u \\ d' \end{pmatrix}_L$	$\begin{pmatrix} c \\ s' \end{pmatrix}_L$	$\begin{pmatrix} t \\ b' \end{pmatrix}_L$	$+\frac{2}{3}$ $-\frac{1}{3}$	$+\frac{1}{2}$ $-\frac{1}{2}$	$+\frac{1}{3}$ $+\frac{1}{3}$
	u_R	c_R	t_R	$+\frac{2}{3}$	0	$+\frac{4}{3}$
	d'_R	s'_R	b'_R	$-\frac{1}{3}$	0	$-\frac{2}{3}$

Table B.1: *The classification of fermions into three families of weak isospin multiplets. The quantum numbers are the fermion charge Q_f, the third component of the weak isospin $\mathcal{T}_W^{(3)}$, and the weak hypercharge Y_W. The weak eigenstates (d', s', b') are obtained from the mass eigenstates (d, s, b) by Cabibbo-Kobayashi-Maskawa rotation. For each particle state, an antiparticle state which is obtained by charge conjugation exists.*

The Higgs Field and Higgs - Gauge Field Lagrangian

It is a well-known fact that mass terms of the kind $M^2 B_\mu B^\mu/2$ violate gauge invariance (see e.g. [85]) and are therefore forbidden. To have the carriers W^+, W^-, and Z^0 massive as is required by experimental observations, the $SU(2)_L \times U(1)_{Y_W}$ symmetry is spontaneously broken via the Higgs mechanism [20], leaving behind an unbroken $U(1)$ to be interpreted as the electromagnetic gauge subgroup $U(1)_{em}$. The minimal Higgs mechanism introduces a complex scalar isodoublet field with $Y_W = 1$

$$\Phi(x) = \begin{pmatrix} \phi^+(x) \\ \phi^0(x) \end{pmatrix} \tag{B.5}$$

at the space-time point x. Its self-interaction and coupling to gauge bosons is described by

$$\mathcal{L}_H \;=\; -\left(\mathcal{D}_\mu \Phi\right)^\dagger \left(\mathcal{D}^\mu \Phi\right) - V(\Phi) \tag{B.6}$$

with the covariant derivative

$$\mathcal{D}^\mu \;=\; \partial^\mu \,-\, \mathrm{i} g_2 \mathcal{T}_a W^{\mu,a} \,+\, \mathrm{i} g_1 \frac{Y_W}{2} B^\mu \tag{B.7}$$

and the Higgs potential

$$V(\Phi) \;=\; -\mu^2 \left(\Phi^\dagger \Phi\right) + \frac{\lambda}{4} \left(\Phi^\dagger \Phi\right)^2 \quad . \tag{B.8}$$

The ground state of the quantum system with Higgs field is obtained by minimizing the potential $V(\Phi)$. In the ground state, the Higgs field has a non-vanishing vacuum expectation value which can be chosen as

$$\langle\Phi\rangle_0 \equiv \begin{pmatrix} 0 \\ \frac{v}{\sqrt{2}} \end{pmatrix} = \begin{pmatrix} 0 \\ \frac{2\mu}{\sqrt{2\lambda}} \end{pmatrix} . \tag{B.9}$$

This reduces the manifest $SU(2)$ symmetry to $U(1)_{em}$. The Higgs field can now be written as

$$\Phi(x) = \begin{pmatrix} \phi^+(x) \\ \left(v + H(x) + \mathrm{i}\chi(x)\right)/\sqrt{2} \end{pmatrix} . \tag{B.10}$$

The fields ϕ^+ and χ, however, can be gauged away and therefore do not have any physical meaning. The remaining real part $H(x)$ of ϕ^0 can thus be interpreted as a new scalar particle with its mass acquired via the quartic self coupling of the Higgs field:

$$M_H = \sqrt{2}\mu . \tag{B.11}$$

The kinetic part of the Higgs Lagrangian, eq. (B.6), gives rise to mass terms for the gauge fields. Since $Y_W = 1$ for the Higgs field, the gauge boson mass terms can be written as

$$-\frac{v^2}{8}\left(W^1_\mu, W^2_\mu, W^3_\mu, B_\mu\right) \begin{pmatrix} g_2^2 & 0 & 0 & 0 \\ 0 & g_2^2 & 0 & 0 \\ 0 & 0 & g_2^2 & g_1 g_2 \\ 0 & 0 & g_1 g_2 & g_1^2 \end{pmatrix} \begin{pmatrix} W^{\mu,1} \\ W^{\mu,2} \\ W^{\mu,3} \\ B^\mu \end{pmatrix} . \tag{B.12}$$

The physical parameters and fields are obtained from determination of the mass eigenvalues and eigenvectors of equation (B.12). For the gauge boson mass part of $\mathcal{L}_H$ one thus finds

$$-M_W^2\, W^+_\mu W^{\mu,-} - \frac{1}{2}\left(A_\mu, Z_\mu\right) \begin{pmatrix} 0 & 0 \\ 0 & M_Z^2 \end{pmatrix} \begin{pmatrix} A^\mu \\ Z^\mu \end{pmatrix} \tag{B.13}$$

with the physical fields

$$\begin{aligned} W^{\mu\pm} &= \frac{1}{\sqrt{2}}\left(W^{\mu,1} \mp \mathrm{i}\, W^{\mu,2}\right) \\ Z^\mu &= \cos\theta_w\, W^{\mu,3} + \sin\theta_w\, B^\mu \\ A^\mu &= -\sin\theta_w\, W^{\mu,3} + \cos\theta_w\, B^\mu , \end{aligned} \tag{B.14}$$

the masses

$$\begin{aligned} M_W &= \frac{v}{2} g_2 \\ M_Z &= \frac{v}{2}\sqrt{g_1^2 + g_2^2} \\ M_\gamma &= 0 , \end{aligned} \tag{B.15}$$

and the electroweak mixing angle defined by

$$\cos\theta_w = \frac{g_2}{\sqrt{g_1^2 + g_2^2}} = \frac{M_W}{M_Z} . \tag{B.16}$$

Identification of A_μ with the photon field coupling to the electric charge e yields an expression for e (compare equation (B.14)):

$$e \;=\; \frac{g_1 g_2}{\sqrt{g_1^2 + g_2^2}} \;=\; g_2 \sin\theta_w \;=\; g_1 \cos\theta_w \quad . \tag{B.17}$$

The Fermion - Gauge Field Lagrangian

As is seen from table B.1, fermions are grouped in left-handed doublets with field operators

$$\psi_j^L \;=\; \begin{pmatrix} \psi_{j+}^L \\ \psi_{j-}^L \end{pmatrix} \tag{B.18}$$

and right-handed singlets with field operators

$$\psi_j^R \;=\; \psi_{j,\sigma}^R \tag{B.19}$$

with the family index $j = 1, 2, 3$ and the isospin index $\sigma = \pm$. For the left-handed $SU(2)$ doublets σ is the sign of the third isospin component, and for the right-handed $U(1)$ singlets it denotes the corresponding particle type. The color index of quarks is suppressed. The Lagrangian for the fermion - gauge field interaction can be written in terms of the covariant derivative (see equation (B.7))

$$\mathcal{L}_F \;=\; -\sum_j \bar{\psi}_j^L \gamma^\mu \mathcal{D}_\mu \psi_j^L \;-\; \sum_{j,\sigma} \bar{\psi}_{j,\sigma}^R \gamma^\mu \mathcal{D}_\mu \psi_{j,\sigma}^R \tag{B.20}$$

with

$$\begin{aligned} \psi_{j,\sigma}^{(L_R^L)} \;&\equiv\; \frac{1}{2}\left(1 \pm \gamma_5\right) \psi_{j,\sigma} \\ \bar{\psi} \;&\equiv\; \psi^\dagger \, \mathrm{i}\gamma^0 \quad . \end{aligned}$$

The latter definition ensures that $\bar{\psi}$ is identical to the commonly used one.

The Yukawa Interaction

Because of the different gauge transformation behavior of left- and right-handed fermion fields, mass terms of the kind $m\bar{\psi}\psi$ are forbidden. Fermion masses can, however, be dynamically generated via the gauge invariant Yukawa Interaction

$$\mathcal{L}_{Yukawa} \;=\; -\sum_j \left\{ \left[g_{j-} \, \bar{\psi}_j^L \, \Phi \, \psi_{j-}^R \;+\; g_{j+} \, \bar{\psi}_{j+}^R \, \Phi^\dagger \, \tau_1 \psi_j^L \right] \;+\; h.c. \right\} \quad . \tag{B.21}$$

Here, we have used the Pauli matrix

$$\tau_1 = \begin{pmatrix} 0 & 1 \\ 1 & 0 \end{pmatrix} \quad . \tag{B.22}$$

The fermion masses are derived from the Yukawa coupling constants $g_{j\sigma}$ and the non-vanishing vacuum expectation value of the Higgs field operator. The Yukawa Interaction takes on a very simple form in the unitary gauge where the unphysical degrees of freedom of the Higgs field are gauged away [26],

$$\mathcal{L}_{Yukawa} \;=\; -\sum_f m_f \bar{\psi}_f \psi_f \;-\; \sum_f \frac{m_f}{v} \bar{\psi}_f \psi_f H \quad , \tag{B.23}$$

where the sum runs over all fermions. Note, however, that this is a description in a specific gauge and not a gauge-invariant Lagrangian density.

Quantization of the Lagrangian, Gauge Fixing and Ghosts
In general, to be able to quantize the Lagrangian described above, it is necessary to apply a gauge fixing procedure. Simultaneously, a compensation of the unphysical content of the gauge fixing Lagrangian $\mathcal{L}_{GF}$ is needed. This compensation is provided by the introduction of a Faddeev-Popov ghost term $\mathcal{L}_{FP}$. Details of the procedure can be found in references [26, 86] or in standard textbooks [57, 87]. As this thesis is worked out in the unitary gauge, no additional gauge fixing and ghost terms are needed, no unphysical particles appear in the actual calculation. As only QED corrections are treated, the subtleties connected with unitarity and renormalizability of the unitary gauge do not play any rôle.

B.2 Feynman Rules

One can express the Lagrangian as exposed in appendix B.1 in terms of physical parameters and derive the Feynman rules for the Standard Model. Below, Feynman rules relevant for this thesis are presented. Complete lists of Feynman rules are found in the literature [88, 89, 90] and in the unconventional, but excellent textbook by Veltman [91].

Rule 1: External Lines
External fermions with momentum p and helicity index r, external gauge bosons with momentum k and polarization index λ.

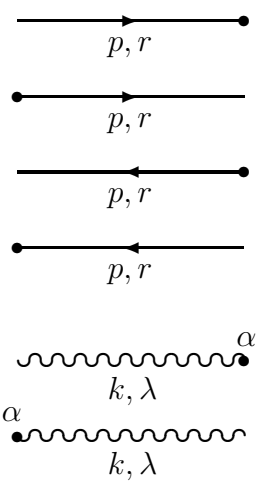

incoming fermion : $u^r(p,m)$

outgoing fermion : $\bar{u}^r(p,m)$

incoming antifermion : $\bar{u}^r(-p,m)$

outgoing antifermion : $u^r(-p,m)$

incoming / outgoing gauge boson: $\varepsilon^{\lambda,\alpha}(k)$

The fermion spin and vector boson polarization summation conventions are given by

$$\begin{aligned} \sum_r u^r(p,m)\,\bar{u}^r(p,m) &= -\mathrm{i}\left(\not{p} + \mathrm{i}m\right) \quad , \\ \sum_\lambda \varepsilon^{\lambda,\alpha}(k)\,\varepsilon^{\lambda,\beta}(k) &= g^{\alpha\beta} + \frac{k^\alpha\,k^\beta}{M_V^2} \quad . \end{aligned} \tag{B.24}$$

Rule 2: Propagators

Propagators with momenta p for fermions, k for photons, and q for bosons. The imaginary parts $-\mathrm{i}\varepsilon$ ensure proper causal behavior. Define $\not{p} \equiv \gamma^\mu p_\mu$.

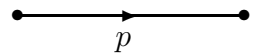

fermion : $$-\frac{\not{p} + \mathrm{i}m}{p^2 + m^2 - \mathrm{i}\varepsilon}$$

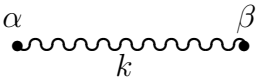

photon : $$-\frac{\mathrm{i}\, g_{\alpha\beta}}{k^2 - \mathrm{i}\varepsilon}$$

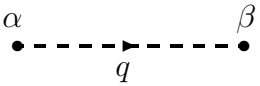

massive gauge boson V: $$-\frac{\mathrm{i}\,(g_{\alpha\beta} + q_\alpha q_\beta / M_V^2)}{q^2 + M_V^2 - \mathrm{i}\varepsilon}$$

Rule 3: Vertices

In this thesis, only neutral current vertices are needed. They can be cast into a simple generic form:

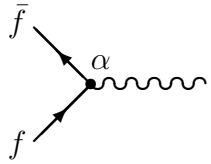

$B = \gamma,\, Z^0$ $$-\, g_B\, g_2 \cdot \gamma^\alpha \left(g^V_{f\bar{f}B} + g^A_{f\bar{f}B}\, \gamma_5 \right) \quad .$$

For the couplings g_B, $g^V_{f\bar{f}B}$, and $g^A_{f\bar{f}B}$ of the fermion f to the photon and the Z^0 the relations

$$g_2 \;=\; \frac{e}{\sin\theta_w}$$

$$\begin{aligned} g_\gamma \;&=\; 1 & \qquad g_Z \;&=\; \frac{1}{4 \cdot \cos\theta_w} \\ g^V_{f\bar{f}\gamma} \;&=\; \sin\theta_w\, Q_f & \qquad g^V_{f\bar{f}Z} \;&=\; 2\mathcal{T}^{(3)}_{W,f} - 4 \cdot \sin^2\theta_w\, Q_f \\ g^A_{f\bar{f}\gamma} \;&=\; 0 & \qquad g^A_{f\bar{f}Z} \;&=\; 2\mathcal{T}^{(3)}_{W,f} \end{aligned} \tag{B.25}$$

hold, with the fermion's electric charge Q_f in units of the positron charge e and the fermion's weak isospin third component $\mathcal{T}^{(3)}_{W,f}$. It is often desirable to write the vertices in terms of left- and right-handed couplings,

$$-\; g_B\, g_2 \cdot \gamma^\alpha \left(g^V_{f\bar{f}B} + g^A_{f\bar{f}B}\gamma_5 \right) \;=\; -\,\gamma^\alpha \left(L_{f\bar{f}B} \cdot (1+\gamma_5) + R_{f\bar{f}B} \cdot (1-\gamma_5) \right) \tag{B.26}$$

with

$$L_{f\bar{f}B} \;\equiv\; \frac{g_B\, g_2}{2} \left(g^V_{f\bar{f}B} + g^A_{f\bar{f}B} \right) \qquad R_{f\bar{f}B} \;\equiv\; \frac{g_B\, g_2}{2} \left(g^V_{f\bar{f}B} - g^A_{f\bar{f}B} \right) \quad . \tag{B.27}$$

For the above neutral current vertices one obtains

$$\begin{aligned} L_{f\bar{f}\gamma} \;&=\; \frac{e\, Q_f}{2} & \qquad L_{f\bar{f}Z} \;&=\; \frac{e}{2\, \sin\theta_w\, \cos\theta_w} \left(\mathcal{T}^{(3)}_{W,f} - \sin^2\theta_w\, Q_f \right) \\ R_{f\bar{f}\gamma} \;&=\; \frac{e\, Q_f}{2} & \qquad R_{f\bar{f}Z} \;&=\; -\frac{e}{2\, \sin\theta_w\, \cos\theta_w}\, \sin^2\theta_w\, Q_f \quad . \end{aligned} \tag{B.28}$$

Rule 4: Ordering
The spinor factors (γ-matrices, propagators, 4-spinors) for each fermion line are ordered from right to left while following the line in its arrow sense. Multiply the expression by a phase factor +1 (–1), if an even (odd) permutation is required to write the fermion operators in the correct normal order.

Rule 5: Four-Momentum Conservation
The four-momenta of lines meeting at a vertex satisfy four-momentum conservation. For each four-momentum q which is not fixed by four-momentum conservation, carry out the integration $\frac{1}{(2\pi)^4}\int d^4q$.

Rule 6: Fermion Loops
For each closed fermion loop take the trace and multiply by –1.

Rule 7: Symmetrization
Introduce a relative sign +1 (–1) for diagrams that are obtained by an even (odd) number of permutations of identical final state fermions. Obtain the matrix element by adding all diagrams.

Rule 8: Differential 2 →n Cross-Section
$\mathcal{M}_{if}$ be the matrix element for the scattering of a two-particle initial state $i = \{1, 2\}$ to an n-particle final state $f = \{3, 4, ..., n+2\}$. Then obtain the differential cross-section by

$$\begin{aligned} d\sigma &= \frac{1}{4\sqrt{(p_1\cdot p_2)^2 - m_1^2 m_2^2}} \frac{|\mathcal{M}_{if}|^2}{S} (2\pi)^4 \, \delta^{(4)}(P_i - P_f) \, d\tilde{p}_3 \cdots d\tilde{p}_{n+2} \\ P_i &= p_1 + p_2 \qquad\qquad P_f = \sum_{k=3}^{n+2} p_k \quad . \end{aligned} \tag{B.29}$$

S yields the symmetry factor, if there are l sets with k_l identical particles,

$$S = \prod_l k_l! \quad .$$

With p^0 representing the particle energy, $p^0 = \sqrt{\vec{p}^{\,2} + m^2}$, the Lorentz invariant phase space element is given by

$$d\tilde{p} = \frac{d^3p}{(2\pi)^3 \, 2p^0} \quad .$$

In case of unobserved polarization degrees of freedom, the average over initial state and the sum over final state polarizations has to be taken. The factors $2m$ left out in equation (B.29) compared to common textbooks like [57] is cancelled by the normalization chosen for the fermion spinors $u(p, m)$.

B.3 Renormalization

In higher order perturbation theory, the relations between the parameters of the Standard Model Lagrangian (B.2) and the physical observables differ from tree level. At loop level, the "bare" parameters of the tree level Lagrangian have no more physical meaning, and a redefinition of parameters and fields is required to recover physical meaning. The procedure of redefinition is called renormalization and properly removes divergences appearing in loop diagrams. For a mathematically consistent treatment of divergences, the theory must be regularized which is most commonly done with dimensional regularization. The "renormalizability" of the Standard Model assures that a finite number of so-called renormalization constants suffices to redefine physical quantities in all orders of perturbation theory [21]†. Renormalization schemes differ in the choice of input parameters and renormalization conditions. As physical results must be scheme independent, the observables calculated in different renormalization schemes are identical in infinite order perturbation theory. Results from n^{th} order perturbation theory obtained in different schemes, deviate from each other in higher order contributions [92]. The accuracy of the finite order approximation is influenced by the choice of input parameters. Among the various renormalization schemes found in the literature, the most prominent ones are

- The "modified minimal subtraction" ($\overline{\text{MS}}$) scheme [93, 94], where the rôle of the electroweak mixing angle is emphasized. Renormalization constants are fixed by a simple subtraction of the singular parts

  $$\frac{1}{n-4} + \frac{\gamma_E}{2} - \ln(2\sqrt{\pi})$$

  from the two- and three-point functions calculated in dimensional regularization (see appendix F). The common input parameters for the $\overline{\text{MS}}$ scheme are

  $$\alpha,\ M_W,\ M_Z,\ M_H, \quad \text{and the fermion masses } m_f.$$

  An advantage of the $\overline{\text{MS}}$ scheme is that theoretical uncertainties due to quark induced self-energy effects are much reduced [94].

- The * scheme [95] which emphasizes vector boson propagator effects and running parameters [96]. The * scheme is not very commonly used today [97].

- The G_μ scheme [92, 96] uses the input parameters

  $$G_\mu,\ M_W,\ M_Z,\ M_H, \quad \text{and the fermion masses } m_f.$$

  It is important that G_μ does not run from low energies up to the vector boson mass scale. The fine structure constant α and the Fermi coupling constant G_μ are related via Δr, the non-QED correction to μ-decay.

†In "unrenormalizable" theories, additional renormalization constants are needed for each new perturbation order.

- The on-shell scheme [26, 98] which was used for this thesis and will now be described in some detail.

In the on-shell renormalization scheme, to recover physical meaning at loop level, so-called multiplicative renormalization of bare fields ϕ_0 and bare couplings g_0 is applied,

$$\phi_0 \;=\; Z_\phi^{1/2}\phi \qquad\qquad g_0 \;=\; Z_g g \;\; . \tag{B.30}$$

The renormalized parameters g are finite and fixed by renormalization conditions. Field renormalization ensures finite Green functions [26]. Using the expansions $Z_i = 1+\delta Z_i$, the bare Lagrangian is split into a renormalized part and a counterterm part,

$$\mathcal{L}(\phi_0, g_0) = \mathcal{L}(Z_\phi^{1/2}\phi, Z_g g) = \mathcal{L}(\phi, g) + \delta\mathcal{L}(\phi, g, \delta Z_\phi, \delta g) \;\; . \tag{B.31}$$

The renormalized Lagrangian can be expressed in terms of the chosen set of physical parameters, and from $\delta\mathcal{L}$ one derives counterterm Feynman rules in accordance with the on-shell renormalization conditions. Renormalization conditions fix the renormalization constants and thus give meaning to the theory. Counterterms properly remove ultraviolet divergences arising from loop diagrams. Infrared divergences from loop diagrams are cancelled by real bremsstrahlung radiative corrections. In the on-shell scheme, renormalization conditions are chosen to have propagator poles at the physical particle masses with residue $= 1$ and to recover the classical Thomson limit for the $ee\gamma$-vertex. The common set of input parameters for the on-shell renormalization scheme is

$$e,\; M_W,\; M_Z,\; M_H, \;\text{ and the fermion masses } m_f. \tag{B.32}$$

It is a vital property of the on-shell scheme that tree level relations between masses, couplings and the electroweak mixing angle θ_W remain intact also at loop level. Thus one may easily switch between input parameters. In particular

$$\sin^2\theta_w = 1 - \frac{M_W^2}{M_Z^2} \tag{B.33}$$

can be retained in the on-shell renormalization. For the renormalized Fermi coupling constant G_μ which is an attractive input parameter, because it is experimentally known with high precision, the following relation holds [96]:

$$\sqrt{2}\, G_\mu \;=\; \frac{\pi\alpha}{M_W^2\, \sin^2\theta_w\, (1-\Delta r)} \;\; . \tag{B.34}$$

Thus, in the case of pure QED loop corrections to a process, even G_μ retains its tree level relation to the other parameters.

As this thesis is concerned with QED corrections, the on-shell renormalization for QED will be worked out in some detail below. After choosing a set of input parameters, one starts from the tree level QED Lagrangian

$$\begin{aligned} \mathcal{L}_0^{QED} \;&=\; -\frac{1}{4}\, F_{0,\mu\nu} F_0^{\mu\nu} \;-\; \bar\psi_0\, \gamma^\mu \partial_\mu\, \psi_0 \;-\; m_0\, \bar\psi_0 \psi_0 \;+\; \mathrm{i} e_0 Q_f\, \bar\psi_0\, \gamma^\mu\, \psi_0\, A_{0,\mu} \\ F_0^{\mu\nu} \;&\equiv\; \partial^\mu A_0^\nu - \partial^\nu A_0^\mu \end{aligned} \tag{B.35}$$

with the photon field A_0^μ and introduces multiplicative renormalization constants:

$$\begin{aligned} \psi_0 &= \sqrt{Z_\psi}\cdot\psi & A_0^\mu &= \sqrt{Z_A}\cdot A^\mu \\ m_0 &= \frac{Z_m}{Z_\psi}\cdot m & e_0 &= \frac{Z_e}{Z_\psi\sqrt{Z_A}}\cdot e \quad . \end{aligned} \tag{B.36}$$

Therefore, expanding $Z_i = 1+\delta Z_i$, the QED Lagrangian is given by

$$\mathcal{L}^{QED} = -\frac{1}{4}F_{\mu\nu}F^{\mu\nu} - \bar\psi\,\gamma^\mu\partial_\mu\,\psi - m\,\bar\psi\psi + \mathrm{i}eQ_f\,\bar\psi\,\gamma^\mu\,\psi\,A_\mu + \delta\mathcal{L} \tag{B.37}$$

with the counterterm Lagrangian

$$\delta\mathcal{L} = -\frac{\delta Z_A}{4}\cdot F_{\mu\nu}F^{\mu\nu} - \delta Z_\psi\cdot\bar\psi\,\gamma^\mu\partial_\mu\,\psi - \delta Z_m\cdot m\,\bar\psi\psi + \delta Z_e\cdot\mathrm{i}eQ_f\,\bar\psi\,\gamma^\mu\,\psi\,A_\mu \quad . \tag{B.38}$$

From the requirement of gauge invariance one concludes that the counterterms δZ_e and δZ_ψ are equal which is nothing but the QED Ward identity in the language of renormalization constants [88]. In the next step, counterterm Feynman rules are derived from $\delta\mathcal{L}$. Counterterms are then added to physical 1-loop amplitudes and finally fixed by the on-shell renormalization conditions. The QED counterterm Feynman rules are given on page 50 after explicit expressions for the counterterms have been derived.

The photon field counterterm δZ_A

Renormalization of the photon propagator means to add an ultraviolet divergent vacuum polarization diagram and a counterterm diagram as given in figure B.1 to the photon propagator derived from the renormalized Lagrangian $\mathcal{L}$ in equation (B.37). From the three diagrams in figure B.1, the 1-loop expression for the photon propagator is derived as

$$D_\gamma^{\mu\nu} = \frac{-\mathrm{i}g^{\mu\nu}\,(1-\delta Z_A)}{k^2-\mathrm{i}\varepsilon} + \frac{-\mathrm{i}g^{\mu\alpha}}{k^2-\mathrm{i}\varepsilon}\,\mathrm{i}\Pi_{\alpha\beta}\frac{-\mathrm{i}g^{\beta\nu}}{k^2-\mathrm{i}\varepsilon} \tag{B.39}$$

with the vacuum polarization given by (see e.g. [99])

$$\begin{aligned} \mathrm{i}\Pi_{\alpha\beta} &= -\,(eQ_f)^2\;\mu^{(4-n)}\int\frac{d^np}{(2\pi)^n}\;\frac{\mathrm{Tr}\left[\gamma_\alpha\,(\not p+\mathrm{i}m)\,\gamma_\beta\,(\not p-\not k+\mathrm{i}m)\right]}{\left[p^2+m^2-\mathrm{i}\varepsilon\right]\left[(p-k)^2+m^2-\mathrm{i}\varepsilon\right]}\;\Bigg|_{\mu=m_e} \\ &= \frac{4\mathrm{i}\,(eQ_f)^2}{16\,\pi^2}\left[\frac{2}{3}\left(k^2g_{\alpha\beta}-k_\alpha k_\beta\right)\,\mathrm{P} + 2\left(k^2g_{\alpha\beta}-k_\alpha k_\beta\right)\,\mathcal{I}(k^2,m^2,m^2)\right] \\ &\equiv \mathrm{i}\,g_{\alpha\beta}\,\Pi^\gamma(k^2) + \mathrm{i}\,k_\alpha k_\beta\,\Pi^{(2)}(k^2) \quad , \end{aligned} \tag{B.40}$$

$$\mathcal{I}(k^2,m^2,m^2) = \int_0^1 dx\;x(1-x)\cdot\ln\left[x(1-x)\frac{k^2}{m_e^2}+\frac{m^2}{m_e^2}\right] \quad . \tag{B.41}$$

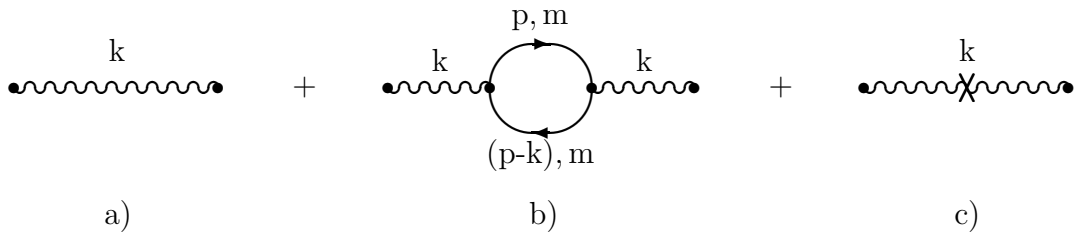

Figure B.1: *Feynman diagrams for the photon propagator renormalization. a) Renormalized photon propagator, b) Vacuum polarization, and c) Photon propagator counterterm.*

The dimensionally regularized ultraviolet divergence P is defined in equation (G.7). It follows from current conservation that, in equation (B.40), the term proportional to the photon momentum k yields vanishing contributions [88]. Therefore one finds

$$D_\gamma^{\mu\nu} \;=\; \frac{-\mathrm{i}g^{\mu\nu}}{k^2-\mathrm{i}\varepsilon}\left(1+\frac{\Pi^\gamma \;-\; k^2\,\delta Z_A}{k^2-\mathrm{i}\varepsilon}\right) \quad . \tag{B.42}$$

Introducing the renormalized vacuum polarization $\hat{\Pi}^\gamma = \Pi^\gamma \;-\; k^2\,\delta Z_A$ which is a "small" quantity, one can rewrite equation (B.42):

$$\begin{aligned} D_\gamma^{\mu\nu} \;&=\; \frac{-\mathrm{i}g^{\mu\nu}}{k^2-\mathrm{i}\varepsilon}\cdot\frac{1}{1-\frac{\hat{\Pi}^\gamma}{k^2-\mathrm{i}\varepsilon}} \quad + \quad \text{higher orders} \\ &=\; \frac{-\mathrm{i}g^{\mu\nu}}{k^2-\mathrm{i}\varepsilon-\hat{\Pi}^\gamma} \quad + \quad \text{higher orders} \quad . \end{aligned} \tag{B.43}$$

It is seen from equation (B.43) that the photon propagator has a pole strictly at $k^2=0$, if $\hat{\Pi}^\gamma = k^2 d\hat{\Pi}^\gamma/dk^2|_{k^2=0} + \mathcal{O}(k^4)$. Then, the photon does not acquire a mass term through higher order effects and hence there is no photon mass renormalization. The on-shell renormalization condition requires the photon propagator (B.42) to have residue $=1$, i.e to retain its tree level form in the limit $k^2=0$. Thus $\hat{\Pi}^\gamma/k^2|_{k^2=0}=0$ and therefore

$$\delta Z_A \;=\; \left.\frac{\Pi^\gamma(k^2)}{k^2}\right|_{k^2=0} \quad , \tag{B.44}$$

which is readily evaluated from equation (B.41), yielding

$$\delta Z_A \;=\; \frac{(eQ_f)^2}{16\,\pi^2}\cdot\frac{4}{3}\left(2\mathrm{P}\;+\;\ln\frac{m^2}{m_e^2}\right) \quad . \tag{B.45}$$

For non-vanishing k^2, $\hat{\Pi}^\gamma$ yields the charge renormalization familiar from many textbooks [57, 88, 100].

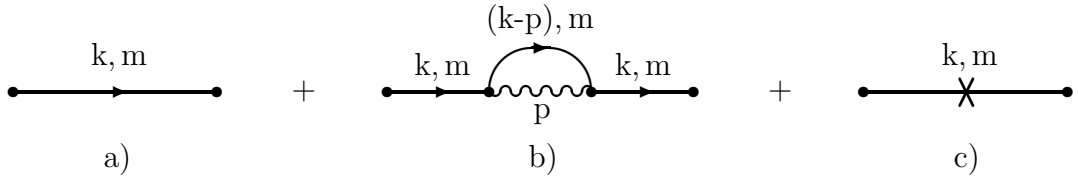

Figure B.2: *Feynman diagrams for the fermion propagator renormalization. a) Renormalized fermion propagator, b) Fermion self energy, and c) Fermion propagator counterterm.*

The fermion field and mass counterterms δZ_ψ, δZ_m, and δm.

The Feynman diagrams for the renormalized fermion propagator are shown in figure B.2. Decomposing the fermionic terms from the counterterm Lagrangian,

$$\begin{aligned} \not{k}\,\delta Z_\psi \;-\; \mathrm{i}m\,\delta Z_m \;&\equiv\; (\not{k} \;-\mathrm{i}m)\,\delta Z_\psi - \mathrm{i}\,\delta m \\ \delta m \;&=\; m\,(\delta Z_m - \delta Z_\psi) \quad , \end{aligned} \tag{B.46}$$

the 1-loop expression for the fermion propagator corresponding to the three diagrams is

$$S^f \;=\; -\frac{1}{\not{k}-\mathrm{i}m-\mathrm{i}\varepsilon}\left(1-\delta Z_\psi+\frac{\mathrm{i}\,\delta m}{\not{k}\;-\mathrm{i}m}\right) \;-\; \frac{1}{\not{k}-\mathrm{i}m-\mathrm{i}\varepsilon}\cdot\Sigma^f\cdot\frac{1}{\not{k}-\mathrm{i}m-\mathrm{i}\varepsilon} \tag{B.47}$$

with the fermion self energy given by

$$\begin{aligned} \Sigma^f(k) \;&=\; -\mathrm{i}\,(eQ_f)^2\;\;\mu^{(4-n)}\int\frac{d^np}{(2\pi)^n}\;\frac{\gamma^\mu\,(\not{k}\;-\not{p}\;+\mathrm{i}m)\,\gamma_\mu}{\Big[(k-p)^2+m^2-\mathrm{i}\varepsilon\Big]\Big[p^2-\mathrm{i}\varepsilon\Big]}\;\Bigg|_{\mu=m_e} \\ &=\; \Sigma^f(\mathrm{i}m) \;+\; B^f\;\Big(\not{k}\;-\mathrm{i}m\Big) \;+\; \mathcal{O}\Big[\,(\not{k}\;-\mathrm{i}m)^2\Big] \end{aligned}$$

$$\begin{aligned} \Sigma^f(\mathrm{i}m) \;&=\; -\frac{(eQ_f)^2}{16\,\pi^2}\;\mathrm{i}m\left(6\mathrm{P}-4+3\;\ln\frac{m^2}{m_e^2}\right) \\ B^f \;&=\; \frac{(eQ_f)^2}{16\,\pi^2}\;\left(2\mathrm{P}+4\mathrm{P}^{\mathrm{IR}}-4+3\;\ln\frac{m^2}{m_e^2}\right) \quad . \end{aligned} \tag{B.48}$$

The dimensionally regularized infrared singularity P^{IR} is defined in equation (G.8). Using the fermion self energy decomposition from equation (B.48), the renormalized fermion propagator S^f can be written as

$$S^f \;=\; -\frac{1}{\not{k}-\mathrm{i}m-\mathrm{i}\varepsilon}\left(1-\delta Z_\psi+B^f\;+\;\mathcal{O}\,(\not{k}\;-\mathrm{i}m)\;+\;\frac{\mathrm{i}\,\delta m+\Sigma^f(\mathrm{i}m)}{\not{k}\;-\mathrm{i}m}\right) \tag{B.49}$$

$$S^f \;=\; -\frac{1}{(\not{k}-\mathrm{i}m)\Big[1+\delta Z_\psi-B^f\;-\;\mathcal{O}(\not{k}-\mathrm{i}m)\Big]-\mathrm{i}\,\delta m-\Sigma^f(\mathrm{i}m)}\;+\;\text{higher orders}\,. \tag{B.50}$$

Imposing the on-shell condition, i.e. requiring S^f in equation (B.50) to have a pole at $\not{k} = \mathrm{i}m$, the result for the fermion mass counterterm reads

$$\delta m \;=\; -\frac{\Sigma^f(\mathrm{i}m)}{\mathrm{i}} \;=\; m\,\frac{(eQ_f)^2}{16\,\pi^2}\left(6\mathrm{P}-4+3\,\ln\frac{m^2}{m_e^2}\right) \quad . \tag{B.51}$$

In addition, as the pole of the 1-loop fermion propagator is required to have residue $=1$, the second fermion propagator renormalization condition reads

$$\delta Z_\psi \;=\; B^f \;=\; \frac{(eQ_f)^2}{16\,\pi^2}\left(2\mathrm{P}+4\mathrm{P}^{\mathrm{IR}}-4+3\,\ln\frac{m^2}{m_e^2}\right) \quad . \tag{B.52}$$

With the renormalization conditions (B.51) and (B.52) it is ensured that external on-shell fermion lines in Feynman diagrams do not receive any QED loop corrections. The mass counterterm δZ_m is now easily derived by introducing the results (B.51) and (B.52) into equation (B.46):

$$\delta Z_m \;=\; \delta Z_\psi + \frac{\delta m}{m} \;=\; \frac{(eQ_f)^2}{16\,\pi^2}\left(8\mathrm{P}+4\mathrm{P}^{\mathrm{IR}}-8+6\,\ln\frac{m^2}{m_e^2}\right) \quad . \tag{B.53}$$

The vertex counterterm δZ_e

The renormalized 1-loop electromagnetic vertex consists of the three Feynman diagrams depicted in figure B.3. For on-shell external fermions it is given by

$$-\,eQ_f\hat{\Gamma}^\lambda \;=\; -\,eQ_f\gamma^\lambda\,(1+\delta Z_e) \;-\; eQ_f\,\Gamma^\lambda \tag{B.54}$$

with the vertex correction

$$\begin{aligned}
\Gamma^\lambda \;&=\; -\mathrm{i}(eQ_f)^2\,\mu^{(4-n)}\int\frac{d^np}{(2\pi)^n}\,\frac{\gamma^\mu\,(\not{k}_2-\not{p}+\mathrm{i}m)\,\gamma^\lambda\,(\not{k}_1-\not{p}+\mathrm{i}m)\,\gamma_\mu}{\Big[(k_1-p)^2+m^2-\mathrm{i}\varepsilon\Big]\Big[(k_2-p)^2+m^2-\mathrm{i}\varepsilon\Big]\Big[p^2-\mathrm{i}\varepsilon\Big]}\,\Bigg|_{\mu=m_e} \\
&=\; \frac{(eQ_f)^2}{16\,\pi^2}\Bigg\{\;\gamma^\lambda\Bigg[-2\mathrm{P}-2\left(q^2+2m^2\right)\mathcal{J}(q^2,m^2,m^2)\,\mathrm{P}^{\mathrm{IR}}-\ln\frac{m^2}{m_e^2}+ \\
&\qquad\qquad \left(3q^2/2+4m^2\right)\mathcal{J}(q^2,m^2,m^2)-\left(q^2+2m^2\right)\mathcal{K}(q^2,m^2,m^2)\Bigg] \\
&\qquad +\frac{\mathrm{i}m}{2}\left(\gamma^\lambda\not{q}-\not{q}\gamma^\lambda\right)\mathcal{J}(q^2,m^2,m^2) \qquad\qquad\Bigg\} \\
&\equiv\; \gamma^\lambda\cdot F_1(q^2,m^2,m^2) \;+\; \left(\gamma^\lambda\not{q}-\not{q}\gamma^\lambda\right)\cdot F_2(q^2,m^2,m^2)
\end{aligned} \tag{B.55}$$

where

$$\begin{aligned}
\mathcal{J}(q^2,m^2,m^2) \;&=\; \int_0^1\frac{dx}{x(1-x)q^2+m^2} \;\overset{q^2=0}{=}\; \frac{1}{m^2} \quad , \\
\mathcal{K}(q^2,m^2,m^2) \;&=\; \int_0^1\frac{dx}{x(1-x)q^2+m^2}\cdot\ln\frac{x(1-x)q^2+m^2}{m_e^2} \;\overset{q^2=0}{=}\; \frac{1}{m^2}\cdot\ln\frac{m^2}{m_e^2} \quad .
\end{aligned} \tag{B.56}$$

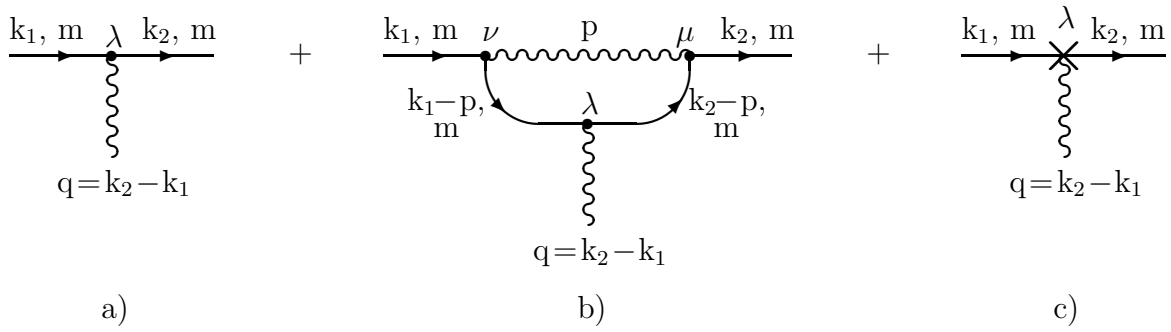

Figure B.3: *Feynman diagrams for the electromagnetic vertex renormalization. a) Vertex, b) Vertex correction, and c) Vertex counterterm.*

From equation (B.55), the Dirac form factor F_1 and the Pauli form factor F_2 can easily be read off. The on-shell renormalization condition requires the renormalized vertex $\hat{\Gamma}^\lambda$ to recover γ^λ in the Thomson limit $q \to 0$,

$$\hat{\Gamma}^\lambda(q=0, m^2, m^2) \;=\; \gamma^\lambda \quad . \tag{B.57}$$

Equivalently one may require

$$F_1(q^2=0, m^2, m^2) \;=\; -\delta Z_e \tag{B.58}$$

for the Dirac form factor. Introducing condition (B.57) or (B.58) into equation (B.54) and using the result for Γ^λ from equation (B.55) with the proper limits $\mathcal{J}(q^2=0, m^2, m^2)$ and $\mathcal{K}(q^2=0, m^2, m^2)$, one obtains

$$\delta Z_e \cdot \gamma^\lambda \;=\; -\,\Gamma^\lambda(0, m^2, m^2) \;=\; \frac{(eQ_f)^2}{16\,\pi^2}\left(2\mathrm{P} + 4\mathrm{P}^{\mathrm{IR}} - 4 + 3\ln\frac{m^2}{m_e^2}\right)\cdot\gamma^\lambda \tag{B.59}$$

for the vertex counterterm. It is therefore seen that δZ_ψ and δZ_e are equal and thus indeed fulfill the QED Ward identity.

It should be mentioned that the vertex counterterm derived above is also valid for the QED renormalized $f\bar{f}Z^0$ vertex. Briefly, one could argue that the term $\left(g^V_{f\bar{f}Z} + g^A_{f\bar{f}Z}\,\gamma_5\right)$ from the replacement

$$-\;eQ_f\,\gamma^\lambda \;\longrightarrow\; -\,g_Z\,g_2\cdot\gamma^\lambda\left(g^V_{f\bar{f}Z} + g^A_{f\bar{f}Z}\,\gamma_5\right)$$

is exactly pulled through to the end of the vertex correction,

$$\Gamma^\lambda_{f\bar{f}Z} \;=\; -\,g_Z\,g_2\cdot\Gamma^\lambda\cdot\left(g^V_{f\bar{f}Z} + g^A_{f\bar{f}Z}\,\gamma_5\right) \;=\; \frac{-\,e}{4\,\sin\theta_w\,\cos\theta_w}\cdot\Gamma^\lambda\cdot\left(g^V_{f\bar{f}Z} + g^A_{f\bar{f}Z}\,\gamma_5\right) \quad . \tag{B.60}$$

Therefore, as the weak mixing angle is not affected by the on-shell QED renormalization,

$$\hat{\Gamma}^\lambda_{f\bar{f}Z} \;=\; \frac{-\,e}{4\,\sin\theta_w\,\cos\theta_w}\cdot\hat{\Gamma}^\lambda\cdot\left(g^V_{f\bar{f}Z} + g^A_{f\bar{f}Z}\,\gamma_5\right) \quad . \tag{B.61}$$

Thus the renormalization condition (B.57) and its solution (B.59) yield the same multiplicative counterterm for the $f\bar{f}Z^0$ and the $f\bar{f}\gamma$ vertex.

The same result may be obtained from equation (58) of reference [101] or from equation (4.21) of reference [102] by neglecting the counterterms that do not belong to the on-shell QED renormalization.

Counterterm Feynman rules

With the above results, namely equations (B.45), (B.51), (B.52), and (B.59), the counterterms as needed in the 1-loop QED counterterm Feynman rules are fixed. The QED counterterm Feynman rules are listed below and must be used together with the set of rules given in section B.2. Subsequently the abbreviation c.t. will be used for "counterterm".

Rule 9: Renormalized external lines

Do not add loop contributions nor counterterms to on-shell external particle lines.

Rule 10: QED Counterterms

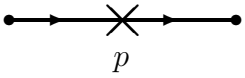

fermion c.t. : $$\frac{-1}{\not{p}-\mathrm{i}m-\mathrm{i}\varepsilon}\cdot\Big[\,(\not{p}-\mathrm{i}m)\,\delta Z_\psi-\mathrm{i}\delta m\Big]\cdot\frac{-1}{\not{p}-\mathrm{i}m-\mathrm{i}\varepsilon}$$

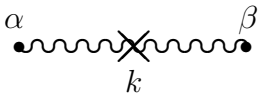

photon c.t. : $$\frac{-\,\mathrm{i}g^{\mu\alpha}}{k^2-\mathrm{i}\varepsilon}\cdot\Big(-\,\mathrm{i}g_{\alpha\beta}\,k^2\,\delta Z_A\Big)\,\frac{-\,\mathrm{i}g^{\beta\nu}}{k^2-\mathrm{i}\varepsilon}$$

$$= \frac{-\,\mathrm{i}g^{\mu\nu}}{k^2-\mathrm{i}\varepsilon}\cdot\Big(-\,\delta Z_A\Big)$$

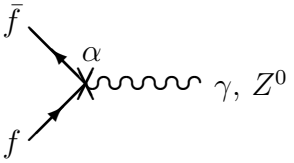

vertex c.t. : $$-\,g_B\,g_2\cdot\gamma^\alpha\left(g^V_{f\bar{f}B}+g^A_{f\bar{f}B}\,\gamma_5\right)\cdot\delta Z_e$$

From the above counterterm Feynman rules, several observations are made:

- In case of electron lines, the logarithms $\ln(m^2/m_e^2)$ vanish in all counterterms. Initially, these logarithms arose due to the choice of the electron mass as the scale for dimensional regularization.
- For massless fermions, the fermion propagator counterterm Feynman rule translates into a factor $-\delta Z_\psi$ that must be multiplied to the tree level amplitude corresponding to the counterterm amplitude under consideration.

- Similarly, an amplitude with a photon propagator counterterm is obtained by multiplication of the corresponding tree level amplitude with $-\delta Z_A$.
- An amplitude with a QED vertex counterterm is obtained by multiplication of the corresponding tree level amplitude with δZ_e.

In conclusion, the counterterms for the QED initial state corrections to process (1.1) may be multiplicatively taken into account as it is done in equations (E.15) and (E.16).

Appendix C

Complex Logarithm and Polylogarithms

For the proper computation of many phase space and loop integrals, the definitions of the complex logarithm and the derived polylogarithms are needed. In this appendix, the necessary definitions are listed together with some useful relations. An exhaustive treatment of Polylogarithms is found in reference [103].

C.1 The Logarithm Function

Throughout this dissertation the logarithm is defined as the main branch of the inverse of the complex exponential function:

$$\begin{aligned} \ln z \;\equiv\; \ln\Big(|z|\cdot e^{\mathrm{i}\arg(z)}\Big) \;=\; \ln|z| + \mathrm{i}\arg(z) \quad , \qquad & z \in \mathbb{C}\setminus\mathbb{R}^- \\ & \arg(z) \;\in\;]-\pi,\pi[\end{aligned} \tag{C.1}$$

The logarithm of a product of two complex numbers a and b is given by [104]

$$\begin{aligned} \ln(a\cdot b) &= \ln a \;+\; \ln b \;+\; \eta(a,b) \qquad\qquad (C.2)\\ \eta(a,b) &= 2\pi\mathrm{i}\Big[\,\Theta(-\Im m\, a)\,\Theta(-\Im m\, b)\,\Theta(\Im m\, ab) \;-\; \Theta(\Im m\, a)\,\Theta(\Im m\, b)\,\Theta(-\Im m\, ab)\,\Big] \end{aligned}$$

with the Heavyside step function $\Theta(x)$. It can be concluded that

$$\begin{aligned} \ln(a\cdot b) &= \ln a \;+\; \ln b \qquad && \text{if } \Im m\, a \text{ and } \Im m\, b \text{ have different sign.} \\ \ln\frac{a}{b} &= \ln a \;-\; \ln b \qquad && \text{if } \Im m\, a \text{ and } \Im m\, b \text{ have equal sign.} \end{aligned}$$

From table C.1, where all possible sign combinations for $\eta(a,b)$ are listed, it can be seen that for real numbers x and y and infinitesimal ε

$$\ln(xy-\mathrm{i}\varepsilon) \;=\; \ln(x-\mathrm{i}\varepsilon) \;+\; \ln(y-\mathrm{i}\varepsilon/x) \quad . \tag{C.3}$$

$\mathrm{sgn}(\Im m\, a)$	$\mathrm{sgn}(\Im m\, b)$	$\mathrm{sgn}(\Im m\, ab)$	$\eta(a,b)$
$+$	$+$	$+$	0
$+$	$+$	$-$	$-2\pi\mathrm{i}$
$+$	$-$	$\pm$	0
$-$	$+$	$\pm$	0
$-$	$-$	$+$	$+2\pi\mathrm{i}$
$-$	$-$	$-$	0

Table C.1: *All possible values of* $\eta(a,b)$.

C.2 The Dilogarithm Function

The dilogarithm function is defined by the integral

$$\mathrm{Li}_2(z) \;\equiv\; -\int_0^1 \frac{\ln(1-tz)}{t}\,dt \quad , \qquad z \,\epsilon\, \mathbb{C}\backslash\{x \,\epsilon\, I\!R : x > 1\} \quad . \tag{C.4}$$

The following one parameter relations are valid for z being any complex number such that none of the involved arguments lie on the corresponding logarithmic or dilogarithmic cuts.

$$\mathrm{Li}_2(0) \;=\; 0\;, \qquad \mathrm{Li}_2(-1) \;=\; -\frac{\pi^2}{12}\;, \qquad \mathrm{Li}_2(1) \;=\; \frac{\pi^2}{6} \tag{C.5}$$

$$\mathrm{Li}_2(z) + \mathrm{Li}_2(-z) \;=\; \frac{1}{2}\,\mathrm{Li}_2(z^2) \tag{C.6}$$

$$\mathrm{Li}_2(z) + \mathrm{Li}_2(1/z) \;=\; -\frac{\pi^2}{6} \;-\; \frac{1}{2}\ln^2(-z) \tag{C.7}$$

$$\mathrm{Li}_2(z) + \mathrm{Li}_2(1-z) \;=\; \frac{\pi^2}{6} \;-\; \ln(z)\cdot\ln(1-z) \tag{C.8}$$

$$\mathrm{Li}_2(z) + \mathrm{Li}_2\left(\frac{1}{1-1/z}\right) \;=\; -\frac{1}{2}\,\ln^2(1-z) \tag{C.9}$$

$$\mathrm{Li}_2(1-z) + \mathrm{Li}_2(1-1/z) \;=\; -\frac{1}{2}\,\ln^2(z) \tag{C.10}$$

For an infinitesimal real number ε and $x \,\epsilon\, I\!R$ the dilogarithm satisfies

$$\Im m\,\{\mathrm{Li}_2(x+\mathrm{i}\varepsilon)\} \;=\; \mathrm{sgn}(\varepsilon)\cdot\Theta(x-1)\cdot\pi\,\ln|x| \quad . \tag{C.11}$$

Therefore, for $x \,\epsilon\, I\!R,\; x > 1$ one can easily deduce

$$\mathrm{Li}_2(x+\mathrm{i}\varepsilon) + \mathrm{Li}_2(x-\mathrm{i}\varepsilon) \;=\; \mathrm{sgn}(\varepsilon)\cdot 2\pi\mathrm{i}\cdot\ln x \quad .$$

A general two parameter relation for complex-valued dilogarithms which can be useful for special purposes and will not be repeated here is given in reference [86].

C.3 The Trilogarithm Function

Similar to the dilogarithm, the trilogarithm function is defined by an integral:

$$\mathrm{Li}_3(y) \equiv \int_0^y \frac{\mathrm{Li}_2(z)}{z}\,dz = \int_0^1 \frac{\mathrm{Li}_2(yz)}{z}\,dz = \int_0^1 \frac{\ln z \cdot \ln(1-yz)}{z}\,dz \quad , \qquad y \in \mathbb{C}\backslash\{x \in I\!R : x > 1\} \quad . \tag{C.12}$$

From this definition two integrals are easily derived:

$$\int_0^y \frac{\ln z \cdot \ln(1-z)}{z}\,dz = \mathrm{Li}_3(y) - \ln y \cdot \mathrm{Li}_2(y) \quad , \qquad y \in \mathbb{C}\backslash I\!R \cup [0,1] \tag{C.13}$$

$$\int_0^y \frac{\ln z \cdot \ln(1+az)}{z}\,dz = \mathrm{Li}_3(-ay) - \ln y \cdot \mathrm{Li}_2(-ay) \quad , \qquad y \in \mathbb{C}\backslash I\!R^- \quad , \quad ay \in \mathbb{C}\backslash\{x \in I\!R : x < -1\} \quad . \tag{C.14}$$

Some useful one parameter relations are given below. Again, it is understood that the arguments in each of all equations must not lie on any of the corresponding above-defined cuts:

$$\mathrm{Li}_3(0) = 0 \tag{C.15}$$

$$\mathrm{Li}_3(1) = \zeta(3) = 1.20205690... \quad , \qquad \mathrm{Li}_3(-1) = -\frac{3}{4}\,\mathrm{Li}_3(1) \tag{C.16}$$

$$\mathrm{Li}_3(z) + \mathrm{Li}_3(-z) = \frac{1}{4}\,\mathrm{Li}_3(z^2) \tag{C.17}$$

$$\mathrm{Li}_3(z) - \mathrm{Li}_3(1/z) = -\frac{\pi^2}{6}\ln(-z) - \frac{1}{6}\ln^3(-z) \tag{C.18}$$

Further, more complicated relations are found in chapter VI of reference [103]. Here, only some relations for real arguments x will be quoted in addition:

$$\mathrm{Li}_3(x) - \mathrm{Li}_3(1/x) = \frac{\pi^2}{3}\ln x - \frac{1}{6}\ln^3 x - \frac{1}{2}\,\mathrm{i}\pi \ln^2 x \quad , \qquad x > 1 \tag{C.19}$$

$$\mathrm{Li}_3\left(\frac{-x}{1-x}\right) + \mathrm{Li}_3(1-x) + \mathrm{Li}_3(x) = \mathrm{Li}_3(1) + \frac{\pi^2}{6}\ln(1-x) - \frac{1}{2}\,\ln x \cdot \ln^2(1-x) + \frac{1}{6}\ln^3(1-x) \quad , \quad 0 < x < 1 \tag{C.20}$$

$$\mathrm{Li}_3\left(\frac{-x}{1-x}\right) + \mathrm{Li}_3\left(\frac{1}{1-x}\right) + \mathrm{Li}_3(x) = \mathrm{Li}_3(1) - \frac{\pi^2}{6}\ln(1-x) - \frac{1}{2}\,\ln(-x) \cdot \ln^2(1-x) + \frac{1}{3}\ln^3(1-x) \quad , \quad x < 0 \ . \tag{C.21}$$

Appendix D

Description of the Phase Space

It is the intention of this appendix to familiarize the reader with the phase space parametrizations used throughout this thesis. For the Born case of process (1.1) and for the virtual initial state corrections, the $2 \to 4$ particle phase space is needed, whereas the $2 \to 5$ particle phase space parametrization is used to describe bremsstrahlung.

Figure D.1: *Graphical representation of a $2 \to 4$ particle reaction. In general, the vectors $\vec{p}_1, \vec{p}_2, \vec{p}_3$ and $\vec{p}_4$ do not lie in the plane of the picture.*

D.1 The $2 \to 4$ Particle Phase Space

A reaction of two particles to a four-particle final state has eight kinematical degrees of freedom which can be parametrized in many different ways. For semi-analytical calculations the following choice of kinematical variables has proven to be convenient [41, 42, 67]:

ϕ	:	Azimuth angle around the e^+ beam direction $\vec{k}_2$.
ϑ	:	Scattering angle of $\vec{v}_1$ with respect to the e^+ direction $\vec{k}_2$ in the center of mass frame.
ϕ_{12}	:	Azimuth angle around the $\vec{v}_1$ direction.
θ_{12}	:	Decay polar angle of $\vec{p}_1$ in the $\vec{v}_1$ rest frame with the z axis along $\vec{v}_1$.
ϕ_{34}	:	Azimuth angle around the $\vec{v}_2$ direction.
θ_{34}	:	Decay polar angle of $\vec{p}_3$ in the $\vec{v}_2$ rest frame with the z axis along $\vec{v}_2$.
s_{12}	:	Invariant mass of the final state fermion pair $f_1\bar{f}_1$: $s_{12} = -v_1^2 = -(p_1+p_2)^2$.
s_{34}	:	Invariant mass of the final state fermion pair $f_2\bar{f}_2$: $s_{34} = -v_2^2 = -(p_3+p_4)^2$.

Here, k_1 and k_2 are the momentum four-vectors of the initial state electron and positron, v_1 and v_2 denote the four-momenta of the intermediate bosons and p_1, p_2, p_3, and p_4 are the final state four-momenta. The corresponding three-momenta are given by superscript arrows. To illustrate the above kinematical variables, a graphical representation of a $2 \to 4$ particle reaction is shown in figure D.1. The center of mass energy squared is given by $s = -(k_1+k_2)^2 = -(p_1+p_2+p_3+p_4)^2$. The decomposition of the $2 \to n$ phase space into subsequently decaying compounds is, for example, worked out in chapter 4.2 of reference [105]. In terms of the above variables the four-particle Lorentz invariant phase space has the form

$$\begin{aligned} d\Gamma_4 &= \frac{1}{(2\pi)^{12}} \cdot \frac{d^3p_1}{2p_1^0}\,\frac{d^3p_2}{2p_2^0}\,\frac{d^3p_3}{2p_3^0}\,\frac{d^3p_4}{2p_4^0} \times \delta^{(4)}(k_1+k_2-\sum_{i=1}^{4} p_i) \\ &= \frac{1}{(2\pi)^{11}}\,\frac{\sqrt{\lambda(s,s_{12},s_{34})}}{8s}\,\frac{\sqrt{\lambda(s_{12},m_1^2,m_1^2)}}{8s_{12}}\,\frac{\sqrt{\lambda(s_{34},m_2^2,m_2^2)}}{8s_{34}} \times \\ &\qquad ds_{12}\,ds_{34}\,d\cos\vartheta\,d\phi_{12}\,d\cos\theta_{12}\,d\phi_{34}\,d\cos\theta_{34} \quad , \end{aligned} \tag{D.1}$$

with the usual definition of the λ function,

$$\lambda(a,b,c) = a^2+b^2+c^2-2ab-2ac-2bc$$

which is symmetric in all arguments and has the special cases

$$\begin{aligned} \lambda(a,b,b) &= a^2\cdot(1-4b/a) \quad , \\ \lambda(a,b,0) &= (a-b)^2 \quad , \\ \lambda(a,0,0) &= a^2 \quad . \end{aligned}$$

The limits of the phase space variables are:

$$\begin{array}{ccccc} 4\,m_1^2 & \le & s_{12} & \le & \left(\sqrt{s}-2\,m_2\right)^2 \\ 4\,m_2^2 & \le & s_{34} & \le & \left(\sqrt{s}-\sqrt{s_{12}}\right)^2 \\ -1 & \le & \cos\vartheta & \le & +1 \\ 0 & \le & \phi_{\{12,34\}} & \le & 2\pi \\ -1 & \le & \cos\theta_{\{12,34\}} & \le & +1 \end{array} \quad .$$

In the presented semi-analytical cross-section calculation, the integrations over the final state fermion decay angles $\phi_{12},\ \theta_{12}$ and $\phi_{34},\ \theta_{34}$ are separated from the other integrations and are carried out analytically with the help of invariant tensor integration (see appendix G.1). The remaining integrations over $\vartheta,\ s_{12}$, and s_{34} are non-trivial, especially, if virtual QED corrections are included. The angle ϑ is integrated analytically, s_{12} and s_{34} are integrated numerically. To perform integrations over the above variables, one must express the four-vectors of the four-particle final state in terms of the phase space parameters. All scalar products appearing in the cross-section calculation can then be expressed in terms of these integration variables. In the center of mass frame with a Cartesian coordinate system as drawn in figure D.1, the initial state vectors k_1 and k_2 are given by

$$\begin{aligned} k_1 &= (k^0,\ k\,\sin\vartheta,\ 0,\ -k\,\cos\vartheta) \\ k_2 &= (k^0,\ -k\,\sin\vartheta,\ 0,\ k\,\cos\vartheta) \end{aligned} \qquad \text{with} \qquad \begin{aligned} k^0 &= \tfrac{\sqrt{s}}{2} \\ k &= \tfrac{\sqrt{s}}{2}\,\beta \\ \beta &\equiv \sqrt{1-\tfrac{4m_e^2}{s}} \end{aligned} \tag{D.2}$$

and the electron mass m_e. Using the mass m_1 for f_1, and m_2 for f_2 one obtains further

$$\begin{aligned} p_1 &= \left(\gamma_{12}^0 p_{12}^{B,0} + \gamma_{12} p_{12}^B \cos\theta_{12},\ p_{12}^B \sin\theta_{12}\cos\phi_{12},\ p_{12}^B \sin\theta_{12}\sin\phi_{12},\ \gamma_{12}^0 p_{12}^B \cos\theta_{12} + \gamma_{12} p_{12}^{B,0}\right) \\ p_2 &= \left(\gamma_{12}^0 p_{12}^{B,0} - \gamma_{12} p_{12}^B \cos\theta_{12},\ -p_{12}^B \sin\theta_{12}\cos\phi_{12},\ -p_{12}^B \sin\theta_{12}\sin\phi_{12},\right. \\ &\qquad \left. -\gamma_{12}^0 p_{12}^B \cos\theta_{12} + \gamma_{12} p_{12}^{B,0}\right) \\ p_3 &= \left(\gamma_{34}^0 p_{34}^{B,0} - \gamma_{34} p_{34}^B \cos\theta_{34},\ p_{34}^B \sin\theta_{34}\cos\phi_{34},\ p_{34}^B \sin\theta_{34}\sin\phi_{34},\ \gamma_{34}^0 p_{34}^B \cos\theta_{34} - \gamma_{34} p_{34}^{B,0}\right) \\ p_4 &= \left(\gamma_{34}^0 p_{34}^{B,0} + \gamma_{34} p_{34}^B \cos\theta_{34},\ -p_{34}^B \sin\theta_{34}\cos\phi_{34},\ -p_{34}^B \sin\theta_{34}\sin\phi_{34},\right. \\ &\qquad \left. -\gamma_{34}^0 p_{34}^B \cos\theta_{34} - \gamma_{34} p_{34}^{B,0}\right) \end{aligned} \tag{D.3}$$

with

$$\begin{aligned} p_{12}^{B,0} &= \frac{\sqrt{s_{12}}}{2} & \qquad p_{34}^{B,0} &= \frac{\sqrt{s_{34}}}{2} \\ p_{12}^B &= \frac{\sqrt{\lambda(s_{12}, m_1^2, m_1^2)}}{2\sqrt{s_{12}}} & \qquad p_{34}^B &= \frac{\sqrt{\lambda(s_{34}, m_2^2, m_2^2)}}{2\sqrt{s_{34}}} \\ \gamma_{12}^0 &= \frac{s + s_{12} - s_{34}}{2\sqrt{s s_{12}}} & \qquad \gamma_{34}^0 &= \frac{s - s_{12} + s_{34}}{2\sqrt{s s_{34}}} \\ \gamma_{12} &= \frac{\sqrt{\lambda(s, s_{12}, s_{34})}}{2\sqrt{s s_{12}}} & \qquad \gamma_{34} &= \frac{\sqrt{\lambda(s, s_{12}, s_{34})}}{2\sqrt{s s_{34}}} \ . \end{aligned}$$

The superscript B hints at the relation of the corresponding quantities to the appropriate boson rest frame. The quantities $p_{ij}^{B,0},\ p_{ij}^B = \left|\vec{p}_{ij}^{\,B}\right|$, and γ_{ij}^0 are e.g. found in chapter IV, equations (3.4) and (3.6) of reference [106]. $\gamma_{ij} = |\vec{\gamma}_{ij}|$ may be derived from the equation

$\gamma_{ij}^{0\,2} - \vec{\gamma}_{ij}^{\,2} = 1$. For use in appendix D.2 vector components in the above equation (D.3) are rewritten in terms of the generic names

$$p_i \;=\; \Big(p_i^0(s),\; p_i^x(s),\; p_i^y(s),\; p_i^z(s)\Big) \quad . \tag{D.4}$$

All possible scalar products built from the four-vectors k_1, k_2, p_1, p_2, p_3, and p_4 can now be easily expressed in terms of the phase space parameters and the particle masses. Scalar products involving v_1 or v_2 are derived from $v_1 = p_1 + p_2$ and $v_2 = p_3 + p_4$:

$$\begin{aligned} v_1 &= \left(\frac{s + s_{12} - s_{34}}{2\sqrt{s}},\; 0,\; 0,\; \frac{\sqrt{\lambda(s, s_{12}, s_{34})}}{2\sqrt{s}} \right) \quad , \\ v_2 &= \left(\frac{s - s_{12} + s_{34}}{2\sqrt{s}},\; 0,\; 0,\; -\frac{\sqrt{\lambda(s, s_{12}, s_{34})}}{2\sqrt{s}} \right) \quad . \end{aligned} \tag{D.5}$$

Subsequently, the fermion masses m_1 and m_2 are neglected. The initial state electron mass m_e is neglected wherever reasonable which is called the "ultrarelativistic approximation" (URA). The following quantities are often used throughout the calculation:

$$\lambda \;\equiv\; \lambda(s, s_{12}, s_{34}) \quad , \qquad \sigma \;\equiv\; s_{12} + s_{34} \quad , \qquad \delta \;\equiv\; s_{12} - s_{34} \quad ,$$

$$t_{min} \;\equiv\; \frac{1}{2}\Big(s - \sigma - \sqrt{\lambda}\Big) \quad , \qquad t_{max} \;\equiv\; \frac{1}{2}\Big(s - \sigma + \sqrt{\lambda}\Big) \quad . \tag{D.6}$$

D.2 The $2 \to 5$ Particle Phase Space

In the case of initial state photon bremsstrahlung a fifth particle appears in the final state. The five-particle phase space has eleven kinematical degrees of freedom which are chosen as

ϕ	:	Azimuth angle around the e^+ beam direction $\vec{k}_2$.
θ	:	Polar (scattering) angle of the photon with respect to the e^+ direction $\vec{k}_2$ in the center of mass frame.
ϕ_R	:	Azimuth angle around the photon direction $\vec{p}$.
θ_R	:	Polar angle of $\vec{v}_1$ in the $(\vec{v}_1 + \vec{v}_2)$ rest frame with the z axis along $(\vec{v}_1 + \vec{v}_2)$.
ϕ_{12}	:	Azimuth angle around the $\vec{v}_1$ direction.
θ_{12}	:	Decay polar angle of $\vec{p}_1$ in the $\vec{v}_1$ rest frame with the z axis along $\vec{v}_1$.
ϕ_{34}	:	Azimuth angle around the $\vec{v}_2$ direction.
θ_{34}	:	Decay polar angle of $\vec{p}_3$ in the $\vec{v}_2$ rest frame with the z axis along $\vec{v}_2$.
s_{12}	:	Invariant mass of the final state fermion pair $f_1\bar{f}_1$: $s_{12} = -v_1^2 = -(p_1 + p_2)^2$.
s_{34}	:	Invariant mass of the final state fermion pair $f_2\bar{f}_2$: $s_{34} = -v_2^2 = -(p_3 + p_4)^2$.
s'	:	Reduced center of mass energy squared. This is equivalent to the invariant mass of the final state four-fermion system: $s' = -(v_1 + v_2)^2 = -(p_1 + p_2 + p_3 + p_4)^2$.

Figure D.2: *Graphical representation of a $2 \to 5$ particle reaction. In general, the vectors $\vec{v}_1, \vec{v}_2, \vec{p}_1, \vec{p}_2, \vec{p}_3$, and $\vec{p}_4$ do not lie in the plane of the picture. In the figure, the angle θ is called θ_γ to emphasize that it belongs to the direction of the radiated photon.*

The symbol p denotes the four-momentum of the photon radiated from the initial state. The kinematics of a $2 \to 5$ particle reaction is graphically illustrated in figure D.2. The center of mass energy squared is given by $s = -(k_1 + k_2)^2 = -(p + p_1 + p_2 + p_3 + p_4)^2$. The angle θ_R corresponds to the angle ϑ in the $2 \to 4$ phase space described in appendix D.1, where the two boson rest frame and the center of mass frame of the e^+e^- annihilation are identical. Due to the radiated photon, the two boson rest frame and the e^+e^- center of mass frame do not coincide for the $2 \to 5$ phase space. The five-particle Lorentz invariant phase space is parametrized by a decomposition into subsequently decaying compounds,

$$\begin{aligned} d\Gamma_5 \;=\; & \frac{1}{(2\pi)^{14}} \, \frac{s - s'}{8s} \, \frac{\sqrt{\lambda(s', s_{12}, s_{34})}}{8s'} \, \frac{\sqrt{\lambda(s_{12}, m_1^2, m_1^2)}}{8s_{12}} \, \frac{\sqrt{\lambda(s_{34}, m_2^2, m_2^2)}}{8s_{34}} \times \\ & ds' \, ds_{12} \, ds_{34} \, d\cos\theta \, d\phi_R \, d\cos\theta_R \, d\phi_{12} \, d\cos\theta_{12} \, d\phi_{34} \, d\cos\theta_{34} \end{aligned} \tag{D.7}$$

with phase space limits

$$
\begin{array}{ccccc}
(2\,m_1+2\,m_2)^2 & \leq & s' & \leq & s \\
4\,m_1^2 & \leq & s_{12} & \leq & \left(\sqrt{s'}-2\,m_2\right)^2 \\
4\,m_2^2 & \leq & s_{34} & \leq & \left(\sqrt{s'}-\sqrt{s_{12}}\right)^2 \\
-1 & \leq & \cos\theta & \leq & +1 \\
0 & \leq & \phi_{\{R,12,34\}} & \leq & 2\pi \\
-1 & \leq & \cos\theta_{\{R,12,34\}} & \leq & +1
\end{array} \quad , \tag{D.8}
$$

or alternatively

$$
\begin{array}{ccccc}
4\,m_1^2 & \leq & s_{12} & \leq & \left(\sqrt{s}-2\,m_2\right)^2 \\
4\,m_2^2 & \leq & s_{34} & \leq & \left(\sqrt{s}-\sqrt{s_{12}}\right)^2 \\
\left(\sqrt{s_{12}}+\sqrt{s_{34}}\right)^2 & \leq & s' & \leq & s \\
-1 & \leq & \cos\theta & \leq & +1 \\
0 & \leq & \phi_{\{R,12,34\}} & \leq & 2\pi \\
-1 & \leq & \cos\theta_{\{R,12,34\}} & \leq & +1
\end{array} \quad . \tag{D.9}
$$

In the semi-analytical bremsstrahlung cross-section calculation, after integrating over $\phi_{12},\ \theta_{12}$ and $\phi_{34},\ \theta_{34}$ with invariant tensor integration, the non-trivial angular integrations over $\phi_R,\ \theta_R$, and θ are performed analytically. The invariant masses $s_{12},\ s_{34}$, and s' are then integrated numerically, using the parametrization (D.9). Below, the four-vectors of the five-particle final state are expressed in terms of the variables of the phase space (D.7). Vectors are given for the center of mass frame with the Cartesian coordinate system of figure D.2. Similar to equation (D.2), k_1 and k_2 are represented by

$$
\begin{array}{rcl}
k_1 & = & (k^0,\ k\,\sin\theta,\ 0,\ -k\,\cos\theta) \\
k_2 & = & (k^0,\ -k\,\sin\theta,\ 0,\ k\,\cos\theta)
\end{array}
\qquad \text{with} \qquad
\begin{array}{rcl}
k^0 & = & \frac{\sqrt{s}}{2} \\
k & = & \frac{\sqrt{s}}{2}\,\beta \\
\beta & \equiv & \sqrt{1-\frac{4m_e^2}{s}}
\end{array} \quad . \tag{D.10}
$$

Secondly, one finds

$$
p \;=\; (p^0,\ 0,\ 0,\ p^0) \qquad \text{with} \qquad p^0 \;=\; \frac{s-s'}{2\sqrt{s}} \tag{D.11}
$$

for the four-momentum of the photon radiated along the z axis. The momenta of the final state fermions can be written down in terms of the expressions originally introduced for the four-particle final state in equation (D.4):

$$
p_i \;=\; \begin{pmatrix}
\gamma^{(0)}\,p_i^0(s') - \gamma\left(p_i^z(s')\,\cos\theta_R - p_i^x(s')\,\sin\theta_R\right) \\
\left(p_i^z(s')\,\sin\theta_R + p_i^x(s')\,\cos\theta_R\right)\cos\phi_R + p_i^y(s')\,\sin\phi_R \\
-\left(p_i^z(s')\,\sin\theta_R + p_i^x(s')\,\cos\theta_R\right)\sin\phi_R + p_i^y(s')\,\cos\phi_R \\
\gamma^{(0)}\left(p_i^z(s')\,\cos\theta_R - p_i^x(s')\,\sin\theta_R\right) - \gamma\,p_i^0(s')
\end{pmatrix} \tag{D.12}
$$

with

$$
\gamma^{(0)} \;=\; \frac{s+s'}{2\sqrt{ss'}} \quad , \qquad \gamma \;=\; \frac{s-s'}{2\sqrt{ss'}} \quad . \tag{D.13}
$$

In equation (D.12) the components of the momentum four-vector have been written in a column for reasons of clarity. Equation (D.12) is better understood, if one notes that, in the $p_1 + p_2 + p_3 + p_4 = v_1 + v_2$ rest frame, the fermion momenta are given by

$$p_i \;=\; \Big(p_i^0(s'),\; p_i^x(s'),\; p_i^y(s'),\; p_i^z(s')\Big) \quad , \tag{D.14}$$

where, compared to equation (D.4), only the center of mass energy had to be adjusted due to photon radiation. After rotating and boosting to the five-particle center of mass frame, equation (D.12) is obtained.

The intermediate boson momenta v_1 and v_2 are given by expressions similar to those in equation (D.3),

$$\begin{aligned} v_1 \;&=\; \Big(\gamma^{(0)}\, p_{12}^{R,0} - \gamma\mathcal{P}_R\cos\theta_R,\; \mathcal{P}_R\sin\theta_R\cos\phi_R,\; -\mathcal{P}_R\sin\theta_R\sin\phi_R, \\ &\qquad\qquad \gamma^{(0)}\mathcal{P}_R\cos\theta_R - \gamma\, p_{12}^{R,0}\Big) \quad , \\ v_2 \;&=\; \Big(\gamma^{(0)}\, p_{34}^{R,0} + \gamma\mathcal{P}_R\cos\theta_R,\; -\mathcal{P}_R\sin\theta_R\cos\phi_R,\; \mathcal{P}_R\sin\theta_R\sin\phi_R, \\ &\qquad\qquad -\gamma^{(0)}\mathcal{P}_R\cos\theta_R - \gamma\, p_{34}^{R,0}\Big) \;. \end{aligned} \tag{D.15}$$

with

$$\begin{aligned} \mathcal{P}_R \;&=\; \frac{\sqrt{\lambda(s', s_{12}, s_{34})}}{2\sqrt{s'}} \\ p_{12}^{R,0} \;&=\; \frac{s' + s_{12} - s_{34}}{2\sqrt{s'}} \quad , \qquad\qquad p_{34}^{R,0} \;=\; \frac{s' - s_{12} + s_{34}}{2\sqrt{s'}} \quad . \end{aligned} \tag{D.16}$$

The four-momentum of the two-boson system recoiling against the radiated photon is given by

$$(v_1 + v_2) \;=\; \Big(\gamma^{(0)}\sqrt{s'},\; 0,\; 0,\; -\gamma\sqrt{s'}\Big) \;=\; \left(\frac{s + s'}{2\sqrt{s}},\; 0,\; 0,\; \frac{s - s'}{2\sqrt{s}}\right) \tag{D.17}$$

Once more, some derived kinematical quantities are defined for use throughout the calculation:

$$\begin{aligned} s'_+ \;&\equiv\; s + s' \quad , \qquad\qquad s'_- \;\equiv\; s - s' \\ \lambda' \;&\equiv\; \lambda(s', s_{12}, s_{34}) \quad , \qquad \bar{\lambda} \;\equiv\; \lambda(s'_-, -s_{12}, -s_{34}) \;=\; {s'_-}^2 + 2s'_-\sigma + \delta^2 \quad . \end{aligned} \tag{D.18}$$

Finally, a short remark on the integration of phase space in the above $2 \to 4$ and $2 \to 5$ parametrizations is due: As all angular phase space variables are integrated analytically, and as the remaining invariant masses are integrated numerically without the use of Monte Carlo techniques, high precision numerical results can be obtained.

Appendix E

The Cross-Section: Matrix Elements, Details, and Techniques

In this appendix, matrix elements for process (1.1) will be presented. This includes the Born, the initial state bremsstrahlung, and the virtual initial state QED matrix elements. Together with the matrix elements, the analytical integrations of the angular variables are outlined. Results for the differential cross-sections obtained from these integrations are presented. Unless stated otherwise the ultrarelativistic approximation is used, that is the electron mass is neglected wherever possible. Correspondingly, final state masses are neglected too. A short account is given of the soft photon resummation technique which was applied to the $\mathcal{O}(\alpha)$ results. Generalization of the below results to process (4.2) means to add photonic Feynman diagrams with equal topology, as explained in chapter 4. The necessary changes to couplings and propagators are most efficiently implemented with equation (4.8).

E.1 Born Level Results

At Born level, the two Feynman diagrams given in figure 2.1 represent the amplitude for the Z^0 pair production process (1.1). According to the Feynman rules from appendix B.2, using the four-particle phase space parametrization as in appendix D.1, and neglecting the masses of the initial state electrons and final state fermions, the Born t-channel matrix element is

$$\mathcal{M}_t^B = \frac{g_{\beta\beta'}}{D_Z(s_{12})} \frac{g_{\alpha\alpha'}}{D_Z(s_{34})} \frac{1}{q_t^2 + m_e^2 - \mathrm{i}\varepsilon} M_{12}^{\beta'} M_{34}^{\alpha'} B_t^{\alpha\beta} \tag{E.1}$$

with

$$\begin{aligned} M_{ij}^{\mu} &= \bar{u}(p_i) \cdot \gamma^{\mu} \left[L_{f\bar{f}Z} \cdot (1+\gamma_5) + R_{f\bar{f}Z} \cdot (1-\gamma_5) \right] \cdot u(-p_j) \\ B_t^{\alpha\beta} &= \bar{u}(-k_2) \cdot \gamma^{\alpha} \left[L_{e^-e^+Z} \cdot (1+\gamma_5) + R_{e^-e^+Z} \cdot (1-\gamma_5) \right] \cdot \not{q}_t \times \\ &\qquad \gamma^{\beta} \left[L_{e^-e^+Z} \cdot (1+\gamma_5) + R_{e^-e^+Z} \cdot (1-\gamma_5) \right] \cdot u(k_1) \\ &= 2\, \bar{u}(-k_2) \cdot \gamma^{\alpha} \left[{L_{e^-e^+Z}}^2 \cdot (1+\gamma_5) + {R_{e^-e^+Z}}^2 \cdot (1-\gamma_5) \right] \cdot \not{q}_t \, \gamma^{\beta} \cdot u(k_1) \quad . \end{aligned} \tag{E.2}$$

Spin indices are suppressed. The electron couplings to the Z^0 boson are

$$\begin{aligned} L_{e^-e^+Z} &= -\frac{e}{4\,\sin\theta_w\,\cos\theta_w}\,\left(1-2\sin^2\theta_w\right) \\ R_{e^-e^+Z} &= \frac{e}{2\,\sin\theta_w\,\cos\theta_w}\,\sin^2\theta_w \quad , \end{aligned} \tag{E.3}$$

fermion couplings are derived from equation (B.28), and the t-channel electron momentum is given by

$$\begin{aligned} q_t &= k_1 - v_1 \;=\; -k_2 + v_2 \;=\; \frac{1}{2}\,(k_1 - k_2 - v_1 + v_2) \\ &= k_1 - p_1 - p_2 \;=\; -k_2 + p_3 + p_4 \;=\; \frac{1}{2}\,(k_1 - k_2 - p_1 - p_2 + p_3 + p_4) \quad . \end{aligned} \tag{E.4}$$

Using the representation of four-vectors in terms of phase space parameters from appendix D.1 and the ultrarelativistic approximation (URA) one arrives at

$$\begin{aligned} t &\equiv q_t^2 + m_e^2 \overset{\text{URA}}{=} \frac{1}{2}\,[A + B\cos\vartheta] \quad , \\ A &= s - s_{12} - s_{34} \quad , \\ B &= \sqrt{\lambda} \quad . \end{aligned} \tag{E.5}$$

The center of mass energy squared is given by s, the invariant Z^0 masses are s_{12} and s_{34}, ϑ is the Z^0 scattering angle, and $\lambda = \lambda(s, s_{12}, s_{34}) = s^2 + s_{12}^2 + s_{34}^2 - 2ss_{12} - 2ss_{34} - 2s_{12}s_{34}$. See appendix D.1 for further details. Finite boson widths are introduced into the Z^0 propagators $D_Z(s)$ from equation (E.2),

$$D_Z(s_{ij}) \;\equiv\; s_{ij} - M_Z^2 + \mathrm{i}\sqrt{s_{ij}}\,\Gamma_Z(s_{ij}) \quad , \tag{E.6}$$

where the Z^0 width is given by

$$\Gamma_Z(s_{ij}) = \frac{G_\mu\,M_Z^2}{24\pi\sqrt{2}}\,\sqrt{s_{ij}}\,\sum_f \left(g_{f\bar{f}Z}^{V}{}^2 + g_{f\bar{f}Z}^{A}{}^2\right)\cdot N_c(f) \quad . \tag{E.7}$$

with the color factor $N_c(f)$. For the Born u-channel amplitude one obtains

$$\begin{aligned} \mathcal{M}_u^B &= \frac{g_{\alpha\alpha'}}{D_Z(s_{12})}\,\frac{g_{\beta\beta'}}{D_Z(s_{34})}\,\frac{1}{q_u^2 + m_e^2 - \mathrm{i}\varepsilon}\,M_{34}^{\beta'}\,M_{12}^{\alpha'}\,B_u^{\alpha\beta} \quad , \\ B_u^{\alpha\beta} &= 2\,\bar{u}(-k_2)\cdot\gamma^\alpha\left[L_{e^-e^+Z}{}^2\cdot(1+\gamma_5) + R_{e^-e^+Z}{}^2\cdot(1-\gamma_5)\right]\cdot \not{q}_u\,\gamma^\beta\cdot u(k_1) \quad , \\ q_u &= k_1 - v_2 \;=\; -k_2 + v_1 \;=\; \frac{1}{2}\,(k_1 - k_2 + v_1 - v_2) \\ &= k_1 - p_3 - p_4 \;=\; -k_2 + p_1 + p_2 \;=\; \frac{1}{2}\,(k_1 - k_2 + p_1 + p_2 - p_3 - p_4) \\ u &= q_u^2 + m_e^2 \overset{\text{URA}}{=} \frac{1}{2}\,[A - B\cos\vartheta] \quad . \end{aligned} \tag{E.8}$$

It is appropriate to mention that the t-channel matrix element $\mathcal{M}_t^B$ and the u-channel matrix element $\mathcal{M}_u^B$ are obtained from each other by the interchanges

$$v_1 \leftrightarrow v_2 \quad , \qquad\qquad \mathcal{M}_{12}^\mu \leftrightarrow \mathcal{M}_{34}^\mu \quad . \tag{E.9}$$

After squaring the matrix element $\mathcal{M}^B = \mathcal{M}_t^B + \mathcal{M}_u^B$, application of Feynman rule 8 from appendix B.2, use of the phase space parametrization described in appendix D.1, and fivefold analytical integration over the angular degrees of freedom of the four-particle phase space with the help of the integrals listed in appendices G.1 and G.2 yields the unpolarized cross-section

$$\sigma^B(s) = \int_{4m_1^2}^{(\sqrt{s}-2m_2)^2} ds_{12}\, \rho_Z(s_{12}) \int_{4m_2^2}^{(\sqrt{s}-\sqrt{s_{12}})^2} ds_{34}\, \rho_Z(s_{34}) \times \sigma_4^B(s; s_{12}, s_{34}) \times 2 \cdot BR(1) \cdot BR(2) \qquad \text{(E.10)}$$

with branching ratios $BR(1)$ and $BR(2)$ of the Z^0 boson into the fermion-antifermion pairs $f_1\bar{f}_1$ and $f_2\bar{f}_2$ respectively, and with

$$\rho_Z(s_{ij}) = \frac{1}{\pi} \frac{\sqrt{s_{ij}}\,\Gamma_Z(s_{ij})}{|s_{ij} - M_Z^2 + i\sqrt{s_{ij}}\,\Gamma_Z(s_{ij})|^2} \xrightarrow{\Gamma_Z \to 0} \delta(s_{ij} - M_Z^2) \ .$$

A particularly convenient form for $\sigma_4^B(s; s_{12}, s_{34})$ is obtained by using $L_e \equiv L_{e^-e^+Z}/(g_Z g_2) = -(1 - 2\sin^2\theta_w)$ and $R_e \equiv R_{e^-e^+Z}/(g_Z g_2) = 2\sin^2\theta_w$:

$$\begin{aligned}
\sigma_4^B(s; s_{12}, s_{34}) &= \frac{\sqrt{\lambda}}{\pi\, s^2} \frac{\left(G_\mu M_Z^2\right)^2}{8} \left(L_e^4 + R_e^4\right) \mathcal{G}_4^{t+u}(s; s_{12}, s_{34}) \ , \\
\mathcal{G}_4^{t+u}(s; s_{12}, s_{34}) &= \frac{s^2 + (s_{12} + s_{34})^2}{s - s_{12} - s_{34}} \mathcal{L}_B - 2 \ , \\
\mathcal{L}_B &= \mathcal{L}(s; s_{12}, s_{34}) = \frac{1}{\sqrt{\lambda}} \ln \frac{s - s_{12} - s_{34} + \sqrt{\lambda}}{s - s_{12} - s_{34} - \sqrt{\lambda}} \ . \qquad \text{(E.11)}
\end{aligned}$$

$\mathcal{G}_4^{t+u}(s; s_{12}, s_{34})$ decomposes into three components stemming from the t-channel the u-channel and their interference:

$$\begin{aligned}
\mathcal{G}_4^{t+u}(s; s_{12}, s_{34}) &= \mathcal{G}_4^t + \mathcal{G}_4^u + \mathcal{G}_4^{tu} \\
\mathcal{G}_4^t = \mathcal{G}_4^u &= \frac{1}{8\, s_{12} s_{34}} \left[\frac{\lambda}{6} + 2s(s_{12} + s_{34}) - 8 s_{12} s_{34} + 4 s_{12} s_{34} (s - s_{12} - s_{34}) \mathcal{L}_B \right] \\
\mathcal{G}_4^{tu} &= -\frac{1}{8\, s_{12} s_{34}} \left[\frac{\lambda}{3} + 4s(s_{12} + s_{34}) + 16\, s\, s_{12} s_{34} \left(1 - \frac{s}{s - s_{12} - s_{34}} \right) \mathcal{L}_B \right] \ . \qquad \text{(E.12)}
\end{aligned}$$

To obtain the analytical result in equation (E.11), use was made of the representation of the processes Lorentz invariants in terms of phase space variables as outlined in appendix D.1. Throughout this thesis, algebraic manipulations were carried out with the help of SCHOONSCHIP [107], FORM [108], and Mathematica [109].

E.2 Virtual Initial State Corrections

Applying on-shell renormalization, the Feynman diagrams for the virtual initial state radiation to process (1.1) are shown in figure 3.2. The "amputated" diagrams presented there must be connected to both the t- and the u-channel, resulting in a total number of eight diagrams. For our calculation, it is sufficient to use the t-channel virtual matrix element and compute its interference with the t- and the u-channel Born matrix elements. The interferences of the virtual u-channel with the Born matrix elements are then obtained by symmetry arguments as outlined at the end of this section. The virtual t-channel matrix element is obtained by substituting $B_t^{\alpha\beta}/(q_t^2 + m_e^2 - \mathrm{i}\varepsilon) \to V_t^{\alpha\beta}$ in equation (E.1):

$$\mathcal{M}_t^V \;=\; \frac{g_{\beta\beta'}}{D_Z(s_{12})}\,\frac{g_{\alpha\alpha'}}{D_Z(s_{34})}\,M_{12}^{\beta'}\,M_{34}^{\alpha'}\,V_t^{\alpha\beta} \quad . \tag{E.13}$$

Using p as the loop photon momentum and applying dimensional regularization [110, 111], one finds

$$V_t^{\alpha\beta} \;=\; e^2 \cdot \left\{ \frac{V_{t,CT}^{\alpha\beta}}{16\pi^2} \;-\; \mathrm{i}\;\mu^{(4-n)} \int \frac{d^n p}{(2\pi)^n} \left(V_{t,v1}^{\alpha\beta} + V_{t,v2}^{\alpha\beta} + V_{t,self}^{\alpha\beta} + V_{t,box}^{\alpha\beta} \right) \Big|_{\mu=m_e} \right\} \quad . \tag{E.14}$$

The counterterm part $V_{t,CT}^{\alpha\beta}$ is given by

$$\begin{aligned} V_{t,CT}^{\alpha\beta} \;&=\; \frac{B_t^{\alpha\beta}}{q_t^2 + m_e^2 - \mathrm{i}\varepsilon} \left(C_{v1} + C_{v2} + C_{self} \right) \\ &=\; \frac{B_t^{\alpha\beta}}{q_t^2 + m_e^2 - \mathrm{i}\varepsilon} \left(2\mathrm{P} + 4\mathrm{P}^{\mathrm{IR}} - 4 \right) \quad . \end{aligned} \tag{E.15}$$

The counterterms C_{v1} and C_{v2} for the vertex corrections and C_{self} for the electron propagator self energy have been derived in appendix B.3.

$$\begin{aligned} C_{v1} \;&=\; C_{v2} \;=\; \tfrac{16\pi^2}{e^2}\,\delta Z_e \;=\; 2\mathrm{P} + 4\mathrm{P}^{\mathrm{IR}} - 4 \\ C_{self} \;&=\; -\tfrac{16\pi^2}{e^2}\,\delta Z_\psi \;=\; -2\mathrm{P} - 4\mathrm{P}^{\mathrm{IR}} + 4 \end{aligned} \tag{E.16}$$

The ultraviolet and infrared poles P and P^{IR} are given in equations (G.7) and (G.8) of appendix G.5. The matrix elements $V_{t,v1}^{\alpha\beta}$, $V_{t,v2}^{\alpha\beta}$, $V_{t,self}^{\alpha\beta}$, and $V_{t,box}^{\alpha\beta}$ belong to the positron and the electron vertex corrections, to the intermediate electron self energy, and to the box correction as depicted in figure 3.2. In the ultrarelativistic approximation one finds

$$\begin{aligned} V_{t,v1}^{\alpha\beta} \;&=\; \bar{u}(-k_2) \cdot \frac{(-2k_2^\mu - \gamma^\mu \not{p})\,\gamma^\alpha\,(\not{q}_t - \not{p})\,\gamma_\mu\,\not{q}_t\,\gamma^\beta}{\left[p^2 - \mathrm{i}\varepsilon\right]\left[(p-q_t)^2 + m_e^2 - \mathrm{i}\varepsilon\right]\,(p^2 + 2k_2 p)\,\left[q_t^2 + m_e^2 - \mathrm{i}\varepsilon\right]} \times \\ &\qquad 2\left[{L_{e^-e^+Z}}^2 \cdot (1+\gamma_5) + {R_{e^-e^+Z}}^2 \cdot (1-\gamma_5)\right] \cdot u(k_1) \quad , \\ V_{t,v2}^{\alpha\beta} \;&=\; \bar{u}(-k_2) \cdot \frac{\gamma^\alpha\,\not{q}_t\,\gamma^\mu\,(\not{q}_t - \not{p})\,\gamma^\beta\,(2k_{1,\mu} - \not{p}\,\gamma_\mu)}{\left[p^2 - \mathrm{i}\varepsilon\right]\left[(p-q_t)^2 + m_e^2 - \mathrm{i}\varepsilon\right]\,(p^2 - 2k_1 p)\,\left[q_t^2 + m_e^2 - \mathrm{i}\varepsilon\right]} \times \\ &\qquad 2\left[{L_{e^-e^+Z}}^2 \cdot (1+\gamma_5) + {R_{e^-e^+Z}}^2 \cdot (1-\gamma_5)\right] \cdot u(k_1) \quad , \end{aligned}$$

$$V^{\alpha\beta}_{t,self} = \bar{u}(-k_2)\cdot\frac{\gamma^\alpha \not{q}_t \gamma^\mu (\not{q}_t - \not{p}) \gamma_\mu \not{q}_t \gamma^\beta}{\Big[p^2-\mathrm{i}\varepsilon\Big]\Big[(p-q_t)^2+m_e^2-\mathrm{i}\varepsilon\Big]\Big[q_t^2+m_e^2-\mathrm{i}\varepsilon\Big]^2}\times$$
$$2\Big[{L_{e^-e^+Z}}^2\cdot(1+\gamma_5)+{R_{e^-e^+Z}}^2\cdot(1-\gamma_5)\Big]\cdot u(k_1) \quad ,$$

$$V^{\alpha\beta}_{t,box} = \bar{u}(-k_2)\cdot\frac{(-2k_2^\mu-\gamma^\mu\not{p})\gamma^\alpha(\not{q}_t-\not{p})\gamma^\beta(2k_{1,\mu}-\not{p}\gamma_\mu)}{\Big[p^2-\mathrm{i}\varepsilon\Big](p^2-2k_1p)(p^2+2k_2p)\Big[(p-q_t)^2+m_e^2-\mathrm{i}\varepsilon\Big]}\times$$
$$2\Big[{L_{e^-e^+Z}}^2\cdot(1+\gamma_5)+{R_{e^-e^+Z}}^2\cdot(1-\gamma_5)\Big]\cdot u(k_1) \quad .$$

Taking into account that the virtual u-channel matrix element $\mathcal{M}^V_u$ is obtained from $\mathcal{M}^V_t$ with the help of the symmetry relation (E.9) one can now write down the virtual $\mathcal{O}(\alpha)$ corrections to process (1.1) as the interference between the Born and the virtual matrix elements. Using the four-particle phase space parametrization from equation (D.1), appendix D.1, one arrives at

$$\sigma^V(s) = \frac{(2\pi)^4}{2\,s}\int d\Gamma_4\ \frac{1}{4}\sum_{spins} 2\,\Re\mathrm{e}\Big[\Big(\mathcal{M}^V_t+\mathcal{M}^V_u\Big)\Big(\mathcal{M}^{B*}_t+\mathcal{M}^{B*}_u\Big)\Big] \ . \tag{E.17}$$

The evaluation of equation (E.17) is carried out in four steps. First step: The final state fermion decay angles are integrated with the invariant tensor integration formula (G.1) from appendix G.1. Second step: The result of the first step is used as input for a computer algebra program written in FORM [108]. Inside the FORM program, steps three and four are carried out together with measures to simplify complicated intermediate expressions. Among the tools used to achieve simplifications, partial fraction decompositions played an important rôle. Third step: The photon loop momentum p is integrated over, making use of the integrals listed in appendix G.5. In the result of the third step, ultraviolet divergences from loop integrals and counterterms are explicitly cancelled. Fourth step: The integration over the boson scattering angle ϑ is performed with the help of the integrals given in appendix G.6. As a result of the above four steps, one can express the cross-section σ^V by a convolution similar to equation (E.10)

$$\sigma^V(s) \equiv \sigma^V_{uni} + \sigma^V_{nonuni}$$
$$= \frac{\alpha}{\pi}\cdot\delta^{\mathrm{IR}}_{virtual}\cdot\sigma^B(s) \quad +$$
$$\frac{\alpha}{\pi}\cdot\frac{(G_\mu M_Z^2)^2}{8\pi s}\Big(L_e^4+R_e^4\Big)\times 2\cdot BR(1)\cdot BR(2)\times$$
$$\int\limits_{4m_1^2}^{(\sqrt{s}-2m_2)^2} ds_{12}\,\rho_Z(s_{12}) \int\limits_{4m_2^2}^{(\sqrt{s}-\sqrt{s_{12}})^2} ds_{34}\,\rho_Z(s_{34})\,\sigma^V_{4,nonuni}(s;s_{12},s_{34})$$

$$\delta^{\mathrm{IR}}_{virtual} = \Re\mathrm{e}\left\{2\,\mathrm{P}^{\mathrm{IR}}(1-l_0)-\frac{l_0^2}{2}+\frac{3\,l_0}{2}+\frac{\pi^2}{6}-2\right\} \tag{E.18}$$

with $\alpha = e^2/(4\pi)$ and

$$l_0 = \ln(s/m_e^2)-\mathrm{i}\pi = l_\beta-\mathrm{i}\pi \ . \tag{E.19}$$

$\delta^{\rm IR}_{virtual}$ is identical to the $\mathcal{O}(\alpha)$ radiator obtained for the virtual initial state QED corrections in fermion pair production [56, 63]. $\delta^{\rm IR}_{virtual}$ contains all leading logarithms of the virtual cross-section. The infrared pole in $\delta^{\rm IR}_{virtual}$ is cancelled by the soft part of the $\mathcal{O}(\alpha)$ bremsstrahlung contribution. The $\mathcal{O}(\alpha)$ non-universal virtual cross-section does not contain leading logarithms l_β, but is rather complicated. It contains four parts corresponding to the four different matrix element products in equation (E.17),

$$\sigma^V_{4,nonuni}(s;s_{12},s_{34}) \;=\; \frac{1}{8s}\left(\sigma^{V,tt}_{4,nonuni} \;+\; \sigma^{V,tu}_{4,nonuni} \;+\; \sigma^{V,ut}_{4,nonuni} \;+\; \sigma^{V,uu}_{4,nonuni}\right)$$

with

$$\begin{aligned}
\sigma^{V,tt}_{4,nonuni} \;=\; \sigma^{V,uu}_{4,nonuni} \;=\;& \frac{3\,\mathcal{L}_{B3}}{2}\cdot\Big[s\,l_+ + \delta\,l_- - s\,(s-\sigma)\;I_{12Q}\Big] \;+\\
& \mathcal{L}_{B2}\cdot\left[(s-2\sigma)(s-\sigma)\,I_{12Q} + \frac{3\,\sigma\delta}{2\,s}\,l_- - (s-4\sigma)\,\frac{l_+}{2} + s - \sigma\right] \;+\\
& \mathcal{L}_B\cdot\left[-\left(\lambda+\sigma^2+s^2/2\right)\;I_{12Q} - \frac{5\,\delta}{2}\,l_- - 4\sigma\,l_+ + 8\sigma - 9s\right] \;+\\
& 8\,\sqrt{\lambda}\left(2-l_+\right) \;+\; \left(3s-\sigma\right)\cdot\left(2\mathcal{D}_+ - \mathcal{L}_-\,l_-\right)
\end{aligned}$$

$$\begin{aligned}
\sigma^{V,tu}_{4,nonuni} \;=\; \sigma^{V,ut}_{4,nonuni} \;=\;& \frac{3\,\mathcal{L}_{B3}}{2}\cdot\Big[s\,l_+ + \delta\,l_- - s(s-\sigma)\,I_{12Q}\Big] \;+\\
& \mathcal{L}_{B2}\cdot\left[(s-\sigma)\;\left(1+5\,s\,I_{12Q} + \frac{\delta}{2s}\,l_-\right) - \frac{9}{2}\left(s\,l_+ + \delta\,l_-\right)\right] \;+\\
& \mathcal{L}_B\cdot\left[\frac{s^2}{s-\sigma}\;\left\{-\frac{7}{3}\,\mathcal{L}_B^2 - 16\,\mathcal{D}_d + 4\,\mathcal{D}_{d+} - 4\,l_\sigma\left(l_\sigma - 2\,l_+ + 3/2\right) + \right.\right.\\
& \qquad\qquad \left.\left. 4\,l_-\,l_{d-} - 4\left(1-3\pi^2/2\right) - 3\,l_+\left(l_+-3\right)\right\}\right.\\
& \qquad + 2\,s^2\left\{\left(l_\sigma - 3\,l_+/4\right)\left(3\,h_{1+}+h_{2+}\right) + \frac{3}{4}\,l_-\;\left(3\,h_{1-}+h_{2-}\right) + 2\,h_{1+}\right\}\\
& \qquad + s\left\{2\,l_+ - 6\,l_\sigma - \frac{15}{2}\,s\,I_{12Q} - \frac{s_{12}}{s-s_{34}} - \frac{s_{34}}{s-s_{12}} - 3\right\}\\
& \qquad + \;\sigma\left(l_+ - 2\,l_\sigma\right) + \frac{\delta}{2}\,l_- \qquad\qquad\qquad\qquad\qquad\qquad\qquad\qquad \Bigg] \;+\\
& \frac{8\,s^2}{s-\sigma}\cdot\left[\mathcal{F}_{d-} - \mathcal{F}_{t-} - \mathcal{F}_\sigma + \left(3/4 - l_+/2\right)\mathcal{D}_\sigma + \frac{l_+}{2}\,\mathcal{D}_{d-}\right] \;+\\
& s^2\;\left(3\,h_{1+}+h_{2+}\right)\cdot\left[\mathcal{D}_+ - 2\,\mathcal{D}_\sigma - \frac{l_-}{2}\,\mathcal{L}_-\right] \;+\\
& s\;\cdot\left[2\,\mathcal{D}_+ + 6\,\mathcal{D}_\sigma + l_-\left(\sqrt{\lambda}\,h_{1-} - \mathcal{L}_-\right)\right] \quad + \quad 2\sigma\,\mathcal{D}_\sigma \;\;. \qquad\qquad \text{(E.20)}
\end{aligned}$$

In equation (E.20) the following notations are used:

$$
\begin{aligned}
d_{12} &= \frac{s - s_{34}}{s_{12}} && \text{(compare appendix G.6)} \\
d_{34} &= \frac{s - s_{12}}{s_{34}} && \text{(compare appendix G.6)} \\
h_{1\pm} &= \frac{1}{s - s_{12}} \pm \frac{1}{s - s_{34}} \\
h_{2\pm} &= \frac{s_{34}}{(s - s_{12})^2} \pm \frac{s_{12}}{(s - s_{34})^2} \\
l_+ &= \ln\frac{s_{12}}{s} + \ln\frac{s_{34}}{s} \\
l_- &= \ln\frac{s_{12}}{s} - \ln\frac{s_{34}}{s} = \ln\frac{s_{12}}{s_{34}} \\
l_\sigma &= \ln\frac{s - \sigma}{s} \\
l_{d-} &= \ln d_{12} - \ln d_{34} \\
\mathcal{L}_{B2} &= \frac{s\,(s - \sigma)}{\lambda}\left[\mathcal{L}_B - \frac{2\sqrt{\lambda}}{s - \sigma}\right] \\
\mathcal{L}_{B3} &= \frac{s\,(s - \sigma)^3}{\lambda^2}\left[\mathcal{L}_B - \frac{2\sqrt{\lambda}}{s - \sigma} - \frac{2}{3}\left(\frac{\sqrt{\lambda}}{s - \sigma}\right)^3\right] \\
\mathcal{L}_- &= \mathcal{L}_{12} - \mathcal{L}_{34} \\
\mathcal{D}_+ &= \mathrm{Li}_2\Big(-\frac{t_{max}}{s_{12}}\Big) - \mathrm{Li}_2\Big(-\frac{t_{min}}{s_{12}}\Big) + \mathrm{Li}_2\Big(-\frac{t_{max}}{s_{34}}\Big) - \mathrm{Li}_2\Big(-\frac{t_{min}}{s_{34}}\Big) \\
\mathcal{D}_\sigma &= \mathrm{Li}_2\Big(\frac{t_{max}}{s - \sigma}\Big) - \mathrm{Li}_2\Big(\frac{t_{min}}{s - \sigma}\Big) \\
\mathcal{D}_d &= \Re e\left[\mathrm{Li}_2(d_{12}) + \mathrm{Li}_2(d_{34})\right] \\
\mathcal{D}_{d+} &= \mathrm{Li}_2\Big(\frac{t_{max}}{s - s_{34}}\Big) + \mathrm{Li}_2\Big(\frac{t_{min}}{s - s_{34}}\Big) + \mathrm{Li}_2\Big(\frac{t_{max}}{s - s_{12}}\Big) + \mathrm{Li}_2\Big(\frac{t_{min}}{s - s_{12}}\Big) \\
\mathcal{D}_{d-} &= \mathrm{Li}_2\Big(\frac{t_{max}}{s - s_{34}}\Big) - \mathrm{Li}_2\Big(\frac{t_{min}}{s - s_{34}}\Big) - \mathrm{Li}_2\Big(\frac{t_{max}}{s - s_{12}}\Big) + \mathrm{Li}_2\Big(\frac{t_{min}}{s - s_{12}}\Big) \\
\mathcal{F}_\sigma &= \mathrm{Li}_3\Big(\frac{t_{max}}{s - \sigma}\Big) - \mathrm{Li}_3\Big(\frac{t_{min}}{s - \sigma}\Big)
\end{aligned}
$$

$$
\begin{aligned}
\mathcal{F}_{d-} &= \mathrm{Li}_3\Big(\frac{t_{max}}{s-s_{34}}\Big) - \mathrm{Li}_3\Big(\frac{t_{min}}{s-s_{34}}\Big) + \mathrm{Li}_3\Big(\frac{t_{max}}{s-s_{12}}\Big) - \mathrm{Li}_3\Big(\frac{t_{min}}{s-s_{12}}\Big) \\
\mathcal{F}_{t-} &= \mathrm{Li}_3\Big(-\frac{t_{max}}{d_{12}\,t_{min}}\Big) - \mathrm{Li}_3\Big(-\frac{t_{min}}{d_{12}\,t_{max}}\Big) \\
&\quad + \mathrm{Li}_3\Big(-\frac{t_{max}}{d_{34}\,t_{min}}\Big) - \mathrm{Li}_3\Big(-\frac{t_{min}}{d_{34}\,t_{max}}\Big)
\end{aligned}
\tag{E.21}
$$

See appendix G.6 for the definitions of $\mathcal{L}_B, \mathcal{L}_{12}$, and $\mathcal{L}_{34}$. I_{12Q} is found in integral 22.) of appendix G.5. It is noteworthy that the quantities $\mathcal{L}_{B2}$ and $\mathcal{L}_{B3}$ have zero limit for λ approaching zero. This is easily verified by expanding $\mathcal{L}_B$ in powers of $\sqrt{\lambda}/(s-\sigma)$. It is seen from equation (E.20), the cross-section parts stemming from identical channels are much simpler than those originating from different channels. More specifically, $\sigma^{V,tt}_{4,nonuni}$ and $\sigma^{V,uu}_{4,nonuni}$ do not contain trilogarithms whereas $\sigma^{V,tu}_{4,nonuni}$ and $\sigma^{V,ut}_{4,nonuni}$ do.

A word about the relations between the above twofold differential cross-sections is in order. From inspection of the virtual Feynman diagrams one finds

$$
\begin{aligned}
\sigma^{V,tt}_{4,nonuni}(s,s_{12},s_{34}) &= \sigma^{V,uu}_{4,nonuni}(s,s_{34},s_{12}) \\
\sigma^{V,tu}_{4,nonuni}(s,s_{12},s_{34}) &= \sigma^{V,ut}_{4,nonuni}(s,s_{34},s_{12}) \quad .
\end{aligned}
\tag{E.22}
$$

The equalities in equation (E.20) are due to the invariance of $\sigma^{V,tt}_{4,nonuni}$ and $\sigma^{V,tu}_{4,nonuni}$ under the interchange $s_{12} \leftrightarrow s_{34}$. This is not surprising, because final state masses are neglected in the matrix elements and $\sigma^{V,tt}_{4,nonuni}$ and $\sigma^{V,tu}_{4,nonuni}$ are kinematical functions, resulting in kinematically equivalent bosons. When adding the contributions given in equation (E.20) to obtain $\sigma^{V}_{4,nonuni}$, some minor simplifications of the overall expression are possible, but the representation (E.20) was chosen for reasons of transparency.

E.3 Initial State Bremsstrahlung

The amputated Feynman diagrams for initial state bremsstrahlung are presented in figure 3.1. They must be connected to both t-channel and u-channel. Once more, the symmetry of the problem simplifies the calculational task. It is sufficient to compute the square of the t-channel bremsstrahlung matrix element and the bremsstrahlung t-u interference. The u-channel contribution to the cross-section is obtained from the t-channel contribution by virtue of a symmetry operation similar to relation (E.22). The bremsstrahlung t-channel matrix element is derived from equation (E.1) via the substitution $B_t^{\alpha\beta}/(q_t^2 + m_e^2 - \mathrm{i}\varepsilon) \to e\, R_t^{\alpha\beta\mu}\, \varepsilon_\mu^\lambda$ with polarization index λ. Neglecting numerator electron masses, the Feynman rules in appendix B.2 yield

$$\mathcal{M}_t^{R,\lambda} \;=\; \frac{g_{\beta\beta'}}{D_Z(s_{12})}\,\frac{g_{\alpha\alpha'}}{D_Z(s_{34})}\, M_{12}^{\beta'}\, M_{34}^{\alpha'} \cdot e\, R_t^{\alpha\beta\mu}\, \varepsilon_\mu^\lambda \quad\equiv\quad \mathcal{M}_t^{R,\mu}\, \varepsilon_\mu^\lambda \tag{E.23}$$

with

$$\begin{aligned} R_t^{\alpha\beta\mu} \;=\; \bar{u}(-k_2)\cdot\Bigg\{ & \gamma^\alpha \frac{\not{v}_2 - \not{k}_2}{t_2}\,\gamma^\beta \frac{2k_1^\mu - \not{p}\,\gamma^\mu}{z_1} \;+\; \gamma^\alpha \frac{\not{v}_2 - \not{k}_2}{t_2}\,\gamma^\mu \frac{\not{k}_1 - \not{v}_1}{t_1}\,\gamma^\beta \\ & +\; \frac{\gamma^\mu \not{p} - 2k_2^\mu}{z_2}\,\gamma^\alpha \frac{\not{k}_1 - \not{v}_1}{t_1}\,\gamma^\beta \Bigg\} \times \\ & 2\left[{L_{e^-e^+Z}}^2 \cdot (1+\gamma_5) + {R_{e^-e^+Z}}^2 \cdot (1-\gamma_5) \right] \cdot u(k_1) \quad . \end{aligned} \tag{E.24}$$

The momentum of the radiated photon is called p. Similarly, one finds for the u-channel bremsstrahlung matrix element

$$\mathcal{M}_u^{B,\lambda} \;=\; \frac{g_{\alpha\alpha'}}{D_Z(s_{12})}\,\frac{g_{\beta\beta'}}{D_Z(s_{34})}\, M_{34}^{\beta'}\, M_{12}^{\alpha'} \cdot e\, R_u^{\alpha\beta\mu}\, \varepsilon_\mu^\lambda \quad , \quad\equiv\quad \mathcal{M}_u^{R,\mu}\, \varepsilon_\mu^\lambda$$

$$\begin{aligned} R_u^{\alpha\beta\mu} \;=\; \bar{u}(-k_2)\cdot\Bigg\{ & \gamma^\alpha \frac{\not{v}_1 - \not{k}_2}{u_2}\,\gamma^\beta \frac{2k_1^\mu - \not{p}\,\gamma^\mu}{z_1} \;+\; \gamma^\alpha \frac{\not{v}_1 - \not{k}_2}{u_2}\,\gamma^\mu \frac{\not{k}_1 - \not{v}_2}{u_1}\,\gamma^\beta \\ & +\; \frac{\gamma^\mu \not{p} - 2k_2^\mu}{z_2}\,\gamma^\alpha \frac{\not{k}_1 - \not{v}_2}{u_1}\,\gamma^\beta \Bigg\} \times \\ & 2\left[{L_{e^-e^+Z}}^2 \cdot (1+\gamma_5) + {R_{e^-e^+Z}}^2 \cdot (1-\gamma_5) \right] \cdot u(k_1) \quad . \end{aligned} \tag{E.25}$$

In the above matrix element the radiatively changed Mandelstam variables were introduced. In terms of the five-particle phase space parametrization from appendix D.2 they are given by

$$\begin{aligned} t_1 \;&=\; \left(k_1 - v_1\right)^2 + m_e^2 \;=\; a_1^t \;+\; b_1\,\cos\theta_R \;+\; c\,\sin\theta_R\cos\phi_R \\ t_2 \;&=\; \left(v_2 - k_2\right)^2 + m_e^2 \;=\; a_2^t \;+\; b_2\,\cos\theta_R \;+\; c\,\sin\theta_R\cos\phi_R \\ u_1 \;&=\; \left(k_1 - v_2\right)^2 + m_e^2 \;=\; a_1^u \;-\; b_1\,\cos\theta_R \;-\; c\,\sin\theta_R\cos\phi_R \\ u_2 \;&=\; \left(v_1 - k_2\right)^2 + m_e^2 \;=\; a_2^u \;-\; b_2\,\cos\theta_R \;-\; c\,\sin\theta_R\cos\phi_R \end{aligned}$$

$$
\begin{aligned}
z_1 &= -2\,k_1 p &&= \frac{s'_-}{2}\left(1+\beta\cos\theta\right) &&\equiv \frac{s'_-}{2}\cdot\bar{z}_1 \\
z_2 &= -2\,k_2 p &&= \frac{s'_-}{2}\left(1-\beta\cos\theta\right) &&\equiv \frac{s'_-}{2}\cdot\bar{z}_2
\end{aligned}
\tag{E.26}
$$

with the kinematical parameters

$$
\begin{aligned}
a_1^t &= -s_{12} + \frac{s'_+}{4\,s'}\left(s'+\delta\right) - \frac{s'_-}{4\,s'}\left(s'+\delta\right)\beta\,\cos\theta \\
a_2^t &= -s_{34} + \frac{s'_+}{4\,s'}\left(s'-\delta\right) + \frac{s'_-}{4\,s'}\left(s'-\delta\right)\beta\,\cos\theta \\
a_1^u &= -s_{34} + \frac{s'_+}{4\,s'}\left(s'-\delta\right) - \frac{s'_-}{4\,s'}\left(s'-\delta\right)\beta\,\cos\theta \\
a_2^u &= -s_{12} + \frac{s'_+}{4\,s'}\left(s'+\delta\right) + \frac{s'_-}{4\,s'}\left(s'+\delta\right)\beta\,\cos\theta
\end{aligned}
$$

$$
\begin{aligned}
b_1 &= \frac{\sqrt{\lambda'}}{4\,s'}\left(s'_+\,\beta\,\cos\theta - s'_-\right) \\
b_2 &= \frac{\sqrt{\lambda'}}{4\,s'}\left(s'_+\,\beta\,\cos\theta + s'_-\right)
\end{aligned}
$$

$$
c = -\frac{\sqrt{\lambda'}}{2}\sqrt{\frac{s}{s'}}\,\beta\,\sin\theta
\tag{E.27}
$$

derived from the representations (D.10) and (D.15) in appendix D.2. The Lorentz invariants satisfy the relations

$$
\begin{aligned}
t_1 + u_1 + z_1 &= s - \sigma \\
t_2 + u_2 + z_2 &= s - \sigma \\
z_1 + z_2 &= s'_- \quad .
\end{aligned}
\tag{E.28}
$$

The total bremsstrahlung cross-section is obtained by the integration

$$
\sigma^R(s) = \frac{(2\pi)^4}{2\,s}\int d\Gamma_5\;\frac{1}{4}\sum_{spins}\left(\mathcal{M}_t^{R,\mu}+\mathcal{M}_u^{R,\mu}\right)\left(\mathcal{M}_{t,\mu}^{R\;*}+\mathcal{M}_{u,\mu}^{R\;*}\right)
\tag{E.29}
$$

with the five-particle phase space $d\Gamma_5$ as parametrized in equation (D.9), appendix D.2. After invariant tensor integration over the boson decay degrees of freedom with formula (G.1) from appendix G.1, a FORM [108] computer algebra program is used to further evaluate equation (E.29). Inside the FORM code, partial fraction decomposition is used to simplify intermediate expressions, and the following non-trivial scalar products are needed:

$$
\begin{aligned}
k_1\cdot v_2 &= \left(t_1+z_1-s+s_{12}\right)/2 &&= -\left(u_1+s_{34}\right)/2 \\
k_2\cdot v_1 &= \left(t_2+z_2-s+s_{34}\right)/2 &&= -\left(u_2+s_{12}\right)/2 \\
k_1\cdot v_1 &= \left(u_1+z_1-s+s_{34}\right)/2 &&= -\left(t_1+s_{12}\right)/2 \\
k_2\cdot v_2 &= \left(u_2+z_2-s+s_{12}\right)/2 &&= -\left(t_2+s_{34}\right)/2 \\
p\cdot v_1 &= \left(t_2-t_1-z_1\right)/2 &&= \left(u_1-u_2-z_2\right)/2 \\
p\cdot v_2 &= \left(t_1-t_2-z_2\right)/2 &&= \left(u_2-u_1-z_1\right)/2 \quad .
\end{aligned}
\tag{E.30}
$$

The, after the tensor integration step, remaining three angles θ_R, ϕ_R, and finally θ (see appendix D.2) are integrated analytically with the help of the integrals listed in appendices G.3 and G.4. The complexity of this threefold analytical integration is due to the appearance of the angularly dependent Mandelstam variables $t_1,\ t_2,\ u_1,\ u_2,\ z_1$, and z_2 in the denominators of the matrix elements $\mathcal{M}_t^{R,\lambda}$ and $\mathcal{M}_u^{R,\lambda}$, equations (E.23) and (E.25). The result for the total bremsstrahlung cross-section splits into a universal, leading logarithm part with the Born cross-section factorizing and a non-universal part,

$$\begin{aligned}
\sigma^R(s) \;&\equiv\; \sigma^R_{uni} \;+\; \sigma^R_{nonuni} \\
&= \frac{\alpha}{\pi} \int\limits_{4m_1^2}^{(\sqrt{s}-2m_2)^2} ds_{12}\, \rho_Z(s_{12}) \int\limits_{4m_2^2}^{(\sqrt{s}-\sqrt{s_{12}})^2} ds_{34}\, \rho_Z(s_{34}) \int\limits_{(\sqrt{s_{12}}+\sqrt{s_{34}})^2}^{s} ds' \\
&\quad \left[\left(\ln\frac{s}{m_e^2} - 1 \right) \frac{s^2+s'^2}{s^2 s'_-}\, \sigma_4^B(s'; s_{12}, s_{34}) \;+ \right. \\
&\quad \left. \frac{(G_\mu M_Z^2)^2}{8\pi s^2} \left(L_e^4 + R_e^4 \right) \sigma^R_{4,nonuni}(s, s'; s_{12}, s_{34}) \right] \times 2 \cdot BR(1) \cdot BR(2) \quad .
\end{aligned} \tag{E.31}$$

The non-universal cross-section term $\sigma^R_{4,nonuni}$ is a sum of the t-channel, the u-channel and the t-channel/u-channel interference bremsstrahlung contributions,

$$\sigma^R_{4,nonuni}(s, s'; s_{12}, s_{34}) \;=\; \sigma^{R,t}_{4,nonuni} \;+\; \sigma^{R,tu}_{4,nonuni} \;+\; \sigma^{R,u}_{4,nonuni}$$

with

$$\begin{aligned}
\sigma^{R,t}_{4,nonuni} \;=\; \sigma^{R,u}_{4,nonuni} \;=\;& \sqrt{\lambda'} \left(\frac{1}{s'_-} - \frac{\sigma}{\bar{\lambda}} \right) \;+ \\
& \sqrt{\lambda'} \left(\frac{s}{4s'^2} + \frac{1}{4s'} + \frac{\sigma}{2\bar{\lambda}} + \frac{3\,\sigma s_{12} s_{34}}{\bar{\lambda}^2} \right) (L_{c3} + L_{c4}) \;+\; \frac{\sigma}{2} \left(\frac{s}{s'^2} - \frac{1}{s} \right) L_{c5} \;- \\
& \frac{D^t_{12}}{4\sqrt{\bar{\lambda}}} \left[2\sigma + s + s'_- + \frac{\sigma}{\bar{\lambda}} \left(s \left(s'_- + \sigma \right) - \sigma^2 + \delta^2 \right) + 12\, \frac{s\, s_{12}\, s_{34}\, \sigma \left(s'_- + \sigma \right)}{\bar{\lambda}^2} \right] \;+ \\
& \frac{s}{4s'} \left(\frac{\sigma}{s} + \frac{\sigma}{s'} - 1 \right) \left(D^t_1 + D^t_2 + D_{z1t2} + D_{z2t1} \right) \;-\; \frac{1}{4} \left(D^t_1 + D^t_2 - D_{z1t2} - D_{z2t1} \right) \;+ \\
& \frac{\delta}{4s'_-} (L_{c1} - L_{c2}) \cdot \left[2 - \frac{s'}{s} - \frac{s^2}{s'^2} + \frac{\sigma \left(3s - s'_- - \sigma \right)}{\bar{\lambda}} + \right. \\
& \qquad \left. \frac{s}{s'_-} \left(1 + \frac{\sigma^2}{\bar{\lambda}} \right) + 12\, \frac{s\, s_{12}\, s_{34}\, \sigma}{\bar{\lambda}^2} \right] \;+ \\
& \frac{1}{4} (L_{c1} + L_{c2}) \cdot \left[1 + \frac{\sigma}{s} + \frac{\sigma}{s'} - \frac{s - \sigma}{s'_-} - \frac{2s\sigma}{{s'_-}^2} \;+\; \frac{2\sigma}{\bar{\lambda}} \left(s'_+ - \sigma \right) \;+\; 24\, \frac{s\, s_{12}\, s_{34}\, \sigma}{\bar{\lambda}^2} \right],
\end{aligned}$$

$$
\begin{aligned}
\sigma^{R,tu}_{4,nonuni} \;=\; & \frac{2\,s'_-\sigma}{s'\,(s'-\sigma)}\cdot L_{c5} \;+\; \frac{s'_+}{s'}\left(D^t_1+D^t_2\right) \\
& -\frac{s^2+s'^2}{2\,s'_-\,(s'-\sigma)}\left(D_{z1t1}+D_{z2t2}\right) \;-\; \left(\frac{s}{s'}+\frac{s^2+s'^2}{2\,s'_-\,(s'-\sigma)}\right)\left(D_{z2t1}+D_{z1t2}\right) \\
& -\frac{s^2+s'^2-4\sigma\,(s'-\sigma)}{2\;(s'-\sigma)\,(s'_+-2\sigma)}\cdot\left[L_{c8}\left(L_{c6}+L_{c7}\right)+D^{tu}_{a1}+D^{tu}_{a2}\right] \\
& -\frac{s-2s_{12}}{\sqrt{s\,s_{12}}}\,D_{t1u2} \;-\; \frac{s-2s_{34}}{\sqrt{s\,s_{34}}}\,D_{t2u1} \;+\; \frac{s^2+s'^2}{4\,s'_-\,(s'-\sigma)}\left(D^z_{t1u2}+D^z_{t2u1}\right) \\
& +\frac{\sqrt{\lambda'}\left[s^2+s'^2-4\sigma(s'-\sigma)\right]\left[s(s'-\sigma)-s_{12}(s'_+-2\sigma)\right]}{2\,(s'_+-2\sigma)(s'-\sigma)}\cdot D^a_{t1u2} \\
& +\frac{\sqrt{\lambda'}\left[s^2+s'^2-4\sigma(s'-\sigma)\right]\left[s(s'-\sigma)-s_{34}(s'_+-2\sigma)\right]}{2\,(s'_+-2\sigma)(s'-\sigma)}\cdot D^a_{t2u1} \qquad . \qquad \text{(E.32)}
\end{aligned}
$$

The shorthand notations L_{c1}, L_{c2}, L_{c3}, L_{c4}, L_{c5}, L_{c6}, L_{c7}, L_{c8}, D^t_1, D^t_2, D^t_{12}, D_{z1t1}, D_{z1t2}, D_{z2t1}, D_{z2t2}, D^{tu}_{a1}, D^{tu}_{a2}, D_{t1u2}, D_{t2u1}, D^z_{t1u2}, D^z_{t2u1}, D^a_{t1u2}, and D^a_{t2u1} are introduced in appendix G.4. For easier reference, the number of the integral from appendix G.4 corresponding to each of these notations is given in table E.1. Together with $\sigma^V_{4,nonuni}$ from equation (E.20), $\sigma^R_{4,nonuni}$ from equation (E.32) represents a main result of this thesis.

Notation	L_{c1}	L_{c2}	L_{c3}	L_{c4}	L_{c5}	L_{c6}	L_{c7}	L_{c8}
Number from appendix G.4	10.)	13.)	30.)	31.)	10.)	26.)	27.)	26.)
Notation	D^t_1	D^t_2	D^t_{12}	D_{z1t1}	D_{z1t2}	D_{z2t1}	D_{z2t2}	D^{tu}_{a1}
Number from appendix G.4	18.)	19.)	46.)	10.)	11.)	12.)	13.)	26.)
Notation	D^{tu}_{a2}	D_{t1u2}	D_{t2u1}	D^z_{t1u2}	D^z_{t2u1}	D^a_{t1u2}	D^a_{t2u1}	
Number from appendix G.4	27.)	51.)	52.)	53.)	54.)	57.)	58.)	

Table E.1: *Shorthand notations from equation (E.32) together with the number of the integral from appendix G.4 where each notation is defined.*

The radiator $(s^2+s'^2)/(s^2 s'_-)$ obtained in equation (E.31) is known from e^+e^- annihilation into fermion pairs [112]. It is seen from equation (D.11) that the radiator's singularity in the factor $1/s'_- = 1/(s-s') \xrightarrow[s'\to s]{} \infty$ is related to the radiation of soft photons. This so-called infrared singularity is identically cancelled by the infrared singularity arising from the virtual corrections. The cancellation of infrared singularities is worked out in appendix E.4.

It is important that the non-universal contribution σ^R_{nonuni} is not infrared divergent. This was explicitly checked by taking the limit $s' \to s$ for all parts of $\sigma^R_{4,nonuni}$ that contain factors $1/s'_-$. In addition it was checked that all parts of $\sigma^R_{4,nonuni}$ have finite limits for $\sqrt{\lambda'} \to 0$. As a concluding remark it is mentioned that, similar to the case of virtual non-universal corrections, some simplifications are possible when terms are collected from the individual contributions in equation (E.32) to yield $\sigma^R_{4,nonuni}$. As these are not major, the expression for $\sigma^R_{4,nonuni}$ is not rewritten.

E.4 Treatment of Infrared Singularities

To show how the infrared divergences from the virtual and the real bremsstrahlung corrections cancel, a short derivation of this cancellation is worked out below. One starts from the bremsstrahlung matrix elements given in equations (E.23) to (E.25). The infrared divergence originates from the square of those parts of the matrix elements which contain the bremsstrahlung photon momentum p in the denominator. In equations (E.23) to (E.25) these are the parts containing $1/z_1$ and $1/z_2$ as is seen from equation (E.26). Denoting the matrix element parts yielding the divergence by $\mathcal{M}^{\rm IR}$, using very small p , i.e. neglecting numerator terms proportional to p, and applying the Dirac equation one gets

$$\mathcal{M}^{\rm IR} \;=\; \mathcal{M}^B \cdot e \cdot \left(\frac{k_1.\varepsilon}{k_1.p} - \frac{k_2.\varepsilon}{k_2.p} \right) \tag{E.33}$$

with the Born matrix element $\mathcal{M}^B = \mathcal{M}^B_t + \mathcal{M}^B_u$ taken from equations (E.1) and (E.8), and with the photon polarization vector ε. Evaluation of the fully differential bremsstrahlung cross-section from $\mathcal{M}^{\rm IR}$ and summation over photon polarizations yields the factorization

$$d\sigma^{\rm IR} \;=\; d\sigma^B \cdot \frac{\alpha}{\pi} \cdot \delta^{\rm IR} \tag{E.34}$$

$$\begin{aligned}
\delta^{\rm IR} \;&=\; \frac{1}{2\pi} \int \frac{d^3p}{2p^0} \left(\frac{k_1}{k_1.p} - \frac{k_2}{k_2.p} \right)^2 \\
&=\; \frac{1}{2\pi} \int \frac{d^3p}{2p^0} \Big[\Theta(\Delta - p^0) + \Theta(p^0 - \Delta) \Big] \left(\frac{k_1}{k_1.p} - \frac{k_2}{k_2.p} \right)^2 \\
&\equiv\; \delta^{\rm IR}_{soft} \;+\; \delta^{\rm IR}_{hard}
\end{aligned} \tag{E.35}$$

with the fully differential Born cross-section $d\sigma^B$, the photon energy p^0, the soft cutoff $\Delta > 0$, the Heavyside step function $\Theta(x)$, and the long known Low factor [113]

$$\mathcal{F}^{\rm IR} = \left(\frac{k_1}{k_1.p} - \frac{k_2}{k_2.p} \right)^2 \quad . \tag{E.36}$$

The infrared divergence is obviously contained in $\delta^{\rm IR}_{soft}$. Following a procedure of dimensional regularization similar to the one outlined in reference [110] and carried through in [114] one arrives at

$$\begin{aligned} \delta^{\rm IR}_{soft} &= 2 \left[{\rm P}^{\rm IR} + \ln\omega \right] \left(\ln\frac{s}{m_e^2} - 1 \right) + \frac{1}{2} \ln^2\frac{s}{m_e^2} - \frac{\pi^2}{3} \\ \omega &= \frac{2\Delta}{\sqrt{s}} \quad . \end{aligned} \tag{E.37}$$

A derivation of $\delta^{\rm IR}_{soft}$ is given at the end of this section. The result may be verified against reference [63] where regularization with a photon mass λ is used by the replacement

$${\rm P}^{\rm IR} \;\rightarrow\; -\frac{1}{2} \ln\frac{\lambda^2}{m_e^2} \quad . \tag{E.38}$$

The dependence of $\delta^{\rm IR}_{soft}$ on the cutoff ω is cancelled by a similar dependence in $\delta^{\rm IR}_{hard}$. Integration of equation (E.34) over the Born phase space yields the infrared divergent cross-section contribution with the factorized Born cross-section σ^B

$$\sigma^{\rm IR}_{soft} = \frac{\alpha}{\pi} \cdot \sigma^B(s) \cdot \delta^{\rm IR}_{soft} = \frac{\alpha}{\pi} \cdot \int\limits_{s'_{min}}^{s} \frac{ds'}{s} \; \delta\left(1 - \frac{s'}{s}\right) \cdot \delta^{\rm IR}_{soft} \cdot \sigma^B(s') \quad . \tag{E.39}$$

Next, the contributions from $\mathcal{O}(\alpha)$ virtual and bremsstrahlung corrections must be added to cancel the infrared divergence ${\rm P}^{\rm IR}$. As only universal cross-section parts are infrared divergent, it is sufficient to consider those. Non-universal contributions are therefore ignored for the remainder of this section. First, the universal cross-section contributions from equations (E.18) and (E.31) are rewritten using the definition $L \equiv \ln(s/m_e^2) - 1$:

$$\sigma^V_{uni} \equiv \frac{\alpha}{\pi} \cdot \delta^{\rm IR}_{virtual} \cdot \sigma^B(s) = \frac{\alpha}{\pi} \cdot \int\limits_{s'_{min}}^{s} \frac{ds'}{s} \; \delta\left(1 - \frac{s'}{s}\right) \cdot \delta^{\rm IR}_{virtual} \cdot \sigma^B(s') \tag{E.40}$$

$$\begin{aligned} \sigma^R_{uni} &= \frac{\alpha}{\pi} \cdot \int\limits_{s'_{min}}^{s} \frac{ds'}{s} \; \frac{s^2 + s'^2}{s\,(s - s')} \cdot L \cdot \sigma^B(s') \\ &= \frac{\alpha}{\pi} \cdot \int\limits_{s'_{min}}^{s\,(1-\omega)} \frac{ds'}{s} \; \frac{s^2 + s'^2}{s\,(s - s')} \cdot L \cdot \sigma^B(s') \\ &\qquad + \frac{\alpha}{\pi} \cdot \int\limits_{s\,(1-\omega)}^{s} \frac{ds'}{s} \left[\frac{2\,s}{s - s'} - \frac{s + s'}{s} \right] \cdot L \cdot \sigma^B(s') \quad . \end{aligned} \tag{E.41}$$

One observes that addition or subtraction of non-divergent terms in the second integrand of equation (E.41) yields negligible effects for sufficiently small infrared cutoff ω. Therefore

$$\sigma^R_{uni} \;=\; \frac{\alpha}{\pi}\cdot\int\limits_{s'_{min}}^{s\,(1-\omega)}\frac{ds'}{s}\;\frac{s^2+s'^2}{s\,(s-s')}\cdot L\cdot\sigma^B(s') \quad + \quad \frac{\alpha}{\pi}\cdot\int\limits_{s\,(1-\omega)}^{s}\frac{ds'}{s}\;\frac{2\,s}{s-s'}\cdot L\cdot\sigma^B(s') \;\;. \tag{E.42}$$

It is evident that the infrared divergence of the bremsstrahlung part is in the second term of equation (E.42). The infrared divergence is located at $s = s'$ and the corresponding cross-section is given by

$$\sigma^{\rm IR}_{soft} \;=\; \frac{\alpha}{\pi}\cdot\int\limits_{s\,(1-\omega)}^{s}\frac{ds'}{s}\;\frac{2\,s}{s-s'}\cdot L\cdot\sigma^B(s') \;\;. \tag{E.43}$$

Replacing this expression by the expression given in equation (E.39), one can rewrite equation (E.42):

$$\begin{aligned}\sigma^R_{uni} \;=\; \frac{\alpha}{\pi}\cdot\int\limits_{s'_{min}}^{s}\frac{ds'}{s}\;\sigma^B(s')\cdot\Bigg\{ & \quad\Theta\left(1-\frac{s'}{s}-\omega\right)\;\frac{s^2+s'^2}{s\,(s-s')}\cdot L \\ & +\;\delta\left(1-\frac{s'}{s}\right)\cdot\delta^{\rm IR}_{soft} \qquad\qquad\Bigg\} \;\;.\end{aligned} \tag{E.44}$$

The complete universal $\mathcal{O}(\alpha)$ cross-section is obtained by adding the virtual and the bremsstrahlung parts from equations (E.40) and (E.44). The result, also known from the literature on fermion pair production in e^+e^- annihilation [63, 112], reads

$$\begin{aligned}\sigma^{V+R}_{uni} \;&=\; \sigma^V_{uni} \;+\; \sigma^R_{uni} \\ &=\; \frac{\alpha}{\pi}\cdot\int\limits_{s'_{min}}^{s}\frac{ds'}{s}\;\sigma^B(s')\cdot\left\{\Theta\left(1-\frac{s'}{s}-\omega\right)H_e\left(\frac{s'}{s}\right)\;+\;\delta\left(1-\frac{s'}{s}\right)S_e(s)\right\}\end{aligned}$$

$$\begin{aligned}H_e(s'/s) \;&=\; \frac{s^2+s'^2}{s\,(s-s')}\cdot L \;=\; \frac{1+(s'/s)^2}{1-s'/s}\cdot L \\ S_e(s) \;&=\; \delta^{\rm IR}_{virtual}+\delta^{\rm IR}_{soft} \;=\; \left(2\ln\omega+\frac{3}{2}\right)\cdot L \;+\; \frac{\pi^2}{3} \;-\; \frac{1}{2}\end{aligned} \tag{E.45}$$

with $\delta^{\rm IR}_{virtual}$ from equation (E.18) and $\delta^{\rm IR}_{soft}$ from equation (E.37). The dependence on the infrared cutoff ω cancels if the integration is carried out. From the representation (E.45) of the universal $\mathcal{O}(\alpha)$ cross-section the cancellation of infrared divergences is obvious. As stated earlier, the non-universal $\mathcal{O}(\alpha)$ cross-section parts are infrared finite. One can therefore present a singularity-free full $\mathcal{O}(\alpha)$ cross-section by adding non-universal $\mathcal{O}(\alpha)$ virtual and bremsstrahlung contributions from equations (E.18) and (E.31) to the result (E.45).

Derivation of the soft bremsstrahlung infrared divergence $\delta_{soft}^{\rm IR}$

To derive the expression for $\delta_{soft}^{\rm IR}$ given in equation (E.37) on starts from equation (E.35). Introduction of a Feynman parameter α yields

$$\begin{aligned}\delta_{soft}^{\rm IR} &= \frac{1}{2\pi}\int\limits_0^1 d\alpha \int \frac{d^3p}{2p^0}\,\Theta(\Delta-p^0)\left\{\frac{s-2m_e^2}{(k_\alpha\cdot p)^2}\;-\;\frac{m_e^2}{(k_1\cdot p)^2}\;-\;\frac{m_e^2}{(k_2\cdot p)^2}\right\}\\ k_\alpha &= k_1\alpha + k_2\,(1-\alpha)\quad .\end{aligned} \tag{E.46}$$

Using the spatial angles $\theta_i,\ \ i=1,2,\alpha$ between the photon momentum $\vec{p}$ and the momenta $\vec{k}_i$, the above denominators are expressed as squares of

$$-\,k_i\cdot p \;=\; k_i^0 p^0\,(1-\beta_i\cos\theta_i) \qquad \text{with velocities} \qquad \beta_i \;=\; \frac{|\vec{k_i}|}{k_i^0}\quad . \tag{E.47}$$

To dimensionally regularize equation (E.46), the transition from 3-dimensional to $(n-1)$-dimensional space has to be performed. As all three terms in the integrand of equation (E.46) do not depend on the polar angle θ of the photon emission, one has the freedom to choose a coordinate system with $\theta=\theta_i$ for each of the three integrand terms in eq. (E.46). Physically this freedom of choice is equivalent to the isotropy of soft photon emission. With the mass scale μ to maintain the dimension of the expression, one gets

$$\begin{aligned}&\frac{(2\pi)^3}{2\pi}\int\limits_0^1 d\alpha\int\frac{d^3p}{(2\pi)^3}\frac{1}{2p^0}\,\theta(\Delta-p^0)\frac{1}{(k_i\cdot p)^2}\\ &\quad\to\;\frac{2\cdot(2\pi)^2}{\left(2\sqrt{\pi}\right)^n\Gamma\left(\frac{n}{2}-1\right)}\int\limits_0^1\frac{d\alpha}{\mu^{(n-4)}}\int\limits_0^\Delta dp^0\left(p^0\right)^{(n-5)}\int\limits_0^\pi\frac{\sin^{(n-3)}\theta_i\,d\theta_i}{(k_i^0)^2\,(1-\beta_i\cos\theta_i)^2}\;.\end{aligned} \tag{E.48}$$

Introducing the integrals

$$\begin{aligned}\frac{1}{\mu^{(n-4)}}\int\limits_0^\Delta dp^0\left(p^0\right)^{(n-5)} &= \frac{(\Delta/\mu)^{(n-4)}}{n-4} \;=\; \frac{1}{n-4}\cdot\left[1\;+\;(n-4)\ln\frac{\Delta}{\mu}\;+\;\mathcal{O}(n-4)\right]\\ \int\limits_0^\pi\frac{\sin^{(n-3)}\theta_i\,d\theta_i}{(1-\beta_i\cos\theta_i)^2} &= \int\limits_{-1}^{+1}\frac{(1-x^2)^{\frac{n-4}{2}}\,dx}{(1-\beta_i x)^2}\\ &= \int\limits_{-1}^{+1}\frac{dx}{(1-\beta_i x)^2}\left[1\;+\;\frac{n-4}{2}\ln(1-x^2)\;+\;\mathcal{O}(n-4)\right]\quad,\end{aligned} \tag{E.49}$$

neglecting terms of $\mathcal{O}(n-4)$, and taking into account that $\beta_1=\beta_2=\beta=\sqrt{1-4m_e^2/s}$, one finds

$$\begin{aligned}\delta_{soft}^{\rm IR} &= \frac{1}{2}\left[{\rm P}^{\rm IR}+\ln\frac{\Delta}{\mu}\right]\cdot\int\limits_0^1 d\alpha\int\limits_{-1}^{+1}dx\;\mathcal{F}(\alpha,x)\;+\;\frac{1}{4}\int\limits_0^1 d\alpha\int\limits_{-1}^{+1}dx\;\ln(1-x^2)\,\mathcal{F}(\alpha,x)\\ \mathcal{F}(\alpha,x) &= \frac{s-2m_e^2}{(k_\alpha^0)^2\,(1-\beta_\alpha x)^2}\;-\;\frac{4m_e^2}{s\;(1-\beta x)^2}\;-\;\frac{4m_e^2}{s\;(1-\beta x)^2}\quad.\end{aligned} \tag{E.50}$$

Using the two integrals

$$\int_{-1}^{+1} dx\ \frac{1}{(1-\beta_i x)^2} \;=\; \frac{2}{1-\beta_i^2}$$

$$\int_{-1}^{+1} dx\ \frac{\ln(1-x^2)}{(1-\beta_i x)^2} \;=\; \frac{2}{1-\beta_i^2}\left[\,2\ln 2\;-\;\frac{1}{\beta_i}\,\ln\frac{1+\beta_i}{1-\beta_i}\right] \tag{E.51}$$

results in

$$\begin{aligned}
\frac{1}{2}\int_0^1 d\alpha \int_{-1}^{+1} dx\ \mathcal{F}(\alpha,x) \;&=\; \left(s-2m_e^2\right)\cdot\int_0^1 \frac{d\alpha}{-k_\alpha^2} \;\;-\;\; 2 \\
\frac{1}{4}\int_0^1 d\alpha \int_{-1}^{+1} dx\ \ln(1-x^2)\,\mathcal{F}(\alpha,x) \;&=\; \ln 2\cdot\left[\,\left(s-2m_e^2\right)\cdot\int_0^1 \frac{d\alpha}{-k_\alpha^2} \;\;-\;\; 2\right] \\
&+\; \left(\frac{s-2m_e^2}{2}\right)\cdot\int_0^1 \frac{d\alpha}{-\beta_\alpha k_\alpha^2}\,\ln\frac{1-\beta_\alpha}{1+\beta_\alpha} \;\;-\;\; \frac{1}{\beta}\,\ln\frac{1-\beta}{1+\beta}
\end{aligned} \tag{E.52}$$

with the Feynman parameter integrals

$$\int_0^1 \frac{d\alpha}{-k_\alpha^2} \;=\; \int_0^1 \frac{d\alpha}{(s-4m_e^2)\,\alpha\,(1-\alpha)+m_e^2} \;=\; \frac{2}{s\beta}\,\ln\frac{1+\beta}{1-\beta}$$

$$\begin{aligned}
\int_0^1 \frac{d\alpha}{-\beta_\alpha k_\alpha^2}\,\ln\frac{1-\beta_\alpha}{1+\beta_\alpha} \;&=\; \int_0^1 \frac{d\alpha}{(s-4m_e^2)\,\alpha\,(1-\alpha)+m_e^2}\cdot\frac{1}{\beta\sqrt{(1-2\alpha)^2}}\cdot\ln\frac{1-\beta\sqrt{(1-2\alpha)^2}}{1+\beta\sqrt{(1-2\alpha)^2}} \\
&=\; \frac{4}{s\beta}\cdot\int_0^1 \frac{dx}{x\,(1-\beta x)\,(1+\beta x)}\cdot\ln\frac{1-\beta x}{1+\beta x} \\
&=\; \frac{2}{s\beta}\cdot\left[\,2\mathrm{Li}_2(-\beta)\;-\;2\mathrm{Li}_2(\beta)\;+\;\mathrm{Li}_2\!\left(\frac{1+\beta}{2}\right)\;-\;\mathrm{Li}_2\!\left(\frac{1-\beta}{2}\right)\right. \\
&\qquad\left.+\;\frac{1}{2}\ln^2\frac{1+\beta}{2}\;-\;\frac{1}{2}\ln^2\frac{1-\beta}{2}\,\right] \quad .
\end{aligned} \tag{E.53}$$

Introducing the results (E.52) and (E.53) into equation (E.50), using

$$\ln\frac{1+\beta}{1-\beta} \;\overset{URA}{=}\; \ln\frac{s}{m_e^2} \;=\; l_\beta \quad , \tag{E.54}$$

taking the result to the ultrarelativistic limit, and evaluating it at the scale $\mu=m_e^2$ yields exactly the result given in equation (E.37),

$$\begin{aligned}
\delta_{soft}^{\mathrm{IR}} \;&=\; 2\cdot\left[\mathrm{P}^{\mathrm{IR}}+\ln\frac{2\Delta}{\mu}\right]\cdot\left(\ln\frac{s}{m_e^2}\;-\;1\right)\;-\;\frac{\pi^2}{3}\;-\;\frac{1}{2}\,\ln^2\frac{s}{m_e^2}\;+\;\ln\frac{s}{m_e^2} \\
&=\; 2\,\left[\mathrm{P}^{\mathrm{IR}}+\ln\omega\right]\left(\ln\frac{s}{m_e^2}\;-\;1\right)\;+\;\frac{1}{2}\,\ln^2\frac{s}{m_e^2}\;-\;\frac{\pi^2}{3} \quad .
\end{aligned} \tag{E.55}$$

E.5 Soft Photon Exponentiation

The factor $\frac{1}{1-s'/s}$ in the universal part H_e (see equation (E.45)) yields large contributions at the phase space edge close to $s=s'$. Therefore resummation of higher order contributions is suggested to obtain reasonable precision. One can follow the derivation of the resummed cross-section given in reference [63], because its authors treat precisely the collinear leading logarithms that are found in the universal cross-section parts of the presented calculation. To connect to the formulae of ref. [63], one starts from equation (E.45) and introduces the notations

$$\begin{aligned} v &\equiv 1-\frac{s'}{s} \\ \beta_e &\equiv \frac{2\alpha}{\pi}\cdot L \\ \bar{S}_1 &\equiv \frac{\alpha}{\pi}\Big[S_e(s) - 2\ln\omega\cdot L\Big] &= \frac{\alpha}{\pi}\left[\frac{\pi^2}{3}-\frac{1}{2}\right] + \frac{3}{4}\beta_e \\ \bar{H}_1 &\equiv \frac{\alpha}{\pi}\left[H_e(s'/s) - \frac{2}{v}\cdot L\right] &= -\frac{1}{2}\Big[2-v\Big]\cdot\beta_e \ . \end{aligned} \tag{E.56}$$

From equation (E.45) one obtains the cross-section for process (1.1) with universal initial state QED corrections

$$\begin{aligned} \sigma^{ISR} = \int_0^{v_{max}} dv\ \sigma^B(s')\ \Bigg\{ & \delta(v)\left[1 + \beta_e\ln\omega + \bar{S}_1 + \frac{\beta_e^2}{2}\ln^2\omega + \beta_e\ln\omega\,\bar{S}_1 + \bar{S}_2\right] \\ & + \Theta(v-\omega)\left[\beta_e\frac{1}{v} + \bar{H}_1 + \beta_e^2\frac{\ln v}{v} + \beta_e\frac{1}{v}\bar{S}_1 + \bar{H}_2\right] \\ & + \mathcal{O}(\alpha^3) \Bigg\} \ , \end{aligned} \tag{E.57}$$

with the second order initial state radiation taken from reference [63] where expressions for the second order virtual+soft part $\bar{S}_2$ and the second order hard part $\bar{H}_2$ can be found. Before carrying on, it is worth mentioning that the infrared divergent second order soft initial state radiation part $\delta^{\rm IR}_{soft,soft}$ is given by

$$\delta^{\rm IR}_{soft,soft} = \frac{1}{2}\,{\delta^{\rm IR}_{soft}}^2 + c_2 \tag{E.58}$$

with infrared finite c_2. This remarkable property indicates the possibility to obtain higher order initial state soft-collinear divergences from an exponentiation of the lowest-order correction $\delta^{\rm IR}_{soft}$ apart from a finite correction factor c_n [63].

Equation (E.57) indicates that the cross-section will be enhanced by terms $\Big[\ln^{n-1} v\Big]/v$ which become especially important near the phase space boundary $v \to 0$, i.e. the enhancement is due to soft photon emission. It will be present in all orders n of perturbation theory, and therefore an appropriate resummation technique is needed. As the logarithms originate from infrared singularities they can be resummed [63], and, according to the

Bloch-Nordsieck theorem [115] and Yennie, Frautschi, and Suura [116], they indeed exponentiate to all orders of perturbation theory. Therefore equation (E.57) represents the truncated power series expansion of the universal cross-section to process (1.1) with soft photon exponentiation which reads

$$\sigma_{exp}^{ISR} \;=\; \int_0^{v_{max}} dv\;\; \sigma^B(s')\;\Big\{\delta(v)\cdot\bar{S}\cdot e^{\beta_e \ln\omega} \;+\; \Theta(v-\omega)\cdot H\Big\} \tag{E.59}$$

with the regular soft+virtual part $\bar{S}$ and the hard part H,

$$\bar{S} \;=\; \sum_{n=0}^{\infty}\bar{S}_n \qquad\qquad \text{with} \qquad\qquad \bar{S}_0 \;=\; 1 \quad \text{for the Born contribution} \quad ,$$

$$H \;=\; \sum_{n=1}^{\infty}\left[\frac{{\beta_e}^n}{(n-1)!}\cdot\frac{\ln^{n-1} v}{v}\cdot\bar{S} \;+\; \bar{H}_n\right] \quad . \tag{E.60}$$

All $\bar{H}_n$ are integrable in v, and the infrared divergent term in H is completely determined by the requirement that the $\ln\omega$ terms appearing in the v integration of H cancel all $\ln\omega$ terms in the virtual+soft part $\bar{S}\cdot e^{\beta_e \ln\omega}$. To rid equation (E.59) of the unphysical parameter ω one introduces $\bar{H} \equiv \sum_{n=1}^{\infty}\bar{H}_n$, uses the equality

$$\sum_{n=1}^{\infty}\frac{{\beta_e}^n}{(n-1)!}\cdot\frac{\ln^{n-1} v}{v} \;=\; \beta_e v^{\beta_e - 1} \tag{E.61}$$

and rewrites

$$\sigma_{exp}^{ISR} \;=\; \int_0^{v_{max}} dv\;\; \sigma^B(s')\;\Big\{\Big[\delta(v)\cdot e^{\beta_e \ln\omega} \;+\; \Theta(v-\omega)\cdot\beta_e v^{\beta_e-1}\Big]\cdot\bar{S} \;+\; \Theta(v-\omega)\cdot\bar{H}\Big\} \;. \tag{E.62}$$

For the three above integral terms one finds

$$\int_0^{v_{max}} dv\;\; \sigma^B(s')\cdot\delta(v)\cdot e^{\beta_e \ln\omega}\cdot\bar{S} \;=\; \sigma^B(s)\cdot\bar{S}\cdot\omega^{\beta_e} \;, \tag{E.63}$$

$$\begin{aligned}
&\int_0^{v_{max}} dv\;\; \sigma^B(s')\cdot\Theta(v-\omega)\cdot\beta_e v^{\beta_e-1}\cdot\bar{S} \\
&\qquad = \int_0^{v_{max}} dv\;\; \sigma^B(s')\cdot\beta_e v^{\beta_e-1}\cdot\bar{S} \;-\; \int_0^{\omega} dv\;\; \sigma^B(s')\cdot\beta_e v^{\beta_e-1}\cdot\bar{S} \\
&\qquad = \int_0^{v_{max}} dv\;\; \sigma^B(s')\cdot\beta_e v^{\beta_e-1}\cdot\bar{S} \;-\; \sigma^B(s)\cdot\bar{S}\cdot\omega^{\beta_e} \;,
\end{aligned} \tag{E.64}$$

and, because $\bar{H}$ is integrable and ω is sufficiently small,

$$\int_0^{v_{max}} dv\;\; \sigma^B(s')\cdot\Theta(v-\omega)\cdot\bar{H} \;=\; \int_0^{v_{max}} dv\;\; \sigma^B(s')\cdot\bar{H} \quad . \tag{E.65}$$

Adding the results of equations (E.63) to (E.65) one notices that the contributions from (E.63) and from the second term of (E.64) cancel each other. Thus a new and physical form of the initial state radiation corrected cross-section with soft photon exponentiation is obtained from equation (E.62):

$$\sigma_{exp}^{ISR} \;=\; \int\limits_{s'_{min}}^{s} \frac{ds'}{s}\; \sigma^B(s') \left\{ \beta_e v^{\beta_e - 1} \cdot \bar{S} + \bar{H} \right\} \quad . \tag{E.66}$$

A cross-section with $\mathcal{O}(\alpha^n)$ soft photon exponentiation is now obtained by replacing the terms $\bar{S}$ and $\bar{H}$ in (E.66) with corresponding truncated sums from equation (E.60). For an $\mathcal{O}(\alpha)$ ISR corrected cross-section with soft photon exponentiation the series' (E.60) are truncated after the first order term which means

$$\begin{aligned} \bar{S} &= 1 + \bar{S}_1 + \mathcal{O}(\alpha^2) \quad , \\ \bar{H} &= \quad\; \bar{H}_1 + \mathcal{O}(\alpha^2) \quad . \end{aligned}$$

Returning to process (1.1) and aiming at the $\mathcal{O}(\alpha)$ ISR cross-section with soft photon exponentiation, it is necessary to include non-universal cross-section parts. Since the virtual and the bremsstrahlung non-universal parts as derived in appendices E.2 and E.3 are both infrared finite and do not contain any singularity, they may be readily added to the regular first order expressions $\bar{S}_1$ and $\bar{H}_1$ without changing the argument leading to equation (E.66). Therefore accounting for $\mathcal{O}(\alpha)$ non-universal cross-section parts means to replace:

$$\begin{aligned} \sigma^B(s') \cdot \left(1 + \bar{S}_1\right) \;&\rightarrow\; \sigma^B(s') \cdot \left(1 + \bar{S}_1\right) \;+\; \sigma^V_{nonuni} \quad &\equiv\; \mathsf{S}_1 \\ \sigma^B(s') \cdot \bar{H}_1 \quad\quad &\rightarrow\; \sigma^B(s') \cdot \bar{H}_1 \quad\quad +\; s\, \frac{d\sigma^R_{nonuni}}{ds'} \quad &\equiv\; \mathsf{H}_1 \end{aligned} \tag{E.67}$$

with σ^V_{nonuni} from equation (E.18) and σ^R_{nonuni} taken from equation (E.31). Thus one obtains for the $\mathcal{O}(\alpha)$ ISR corrected cross-section with soft photon exponentiation for process (1.1)

$$\sigma_{exp}^{ISR,\mathcal{O}(\alpha)} \;=\; \int\limits_{s'_{min}}^{s} \frac{ds'}{s}\; \left\{ \beta_e v^{\beta_e - 1} \cdot \mathsf{S}_1 \;+\; \mathsf{H}_1 \right\} \quad . \tag{E.68}$$

Appendix F

Evaluation of Loop Integrals

Calculations of radiative corrections within the Electroweak Standard Model contain loop integrals as basic building blocks. For the one-loop case, loop integrals have been intensively studied by several authors [86, 104, 117, 118], and the literature also contains pedagogical treatments [26, 96]. It is noteworthy that scalar one-loop diagrams with five or more external lines can be reduced to the scalar 1-, 2-, 3-, and 4-point functions [104]. As tensor m-point functions are reducible to linear combinations of scalar k-point functions with $k \leq m$, it is sufficient to know all possible scalar 1-, 2-, 3-, and 4-point functions together with the appropriate tensor reduction rules. As it is not the intention of this appendix to repeat the results obtained and comprehensively presented earlier (see e.g. references [86, 118]), it will be restricted to the formulae relevant for this thesis. This means a restriction to the 1-, 2-, 3-point functions, because the only 4-point function that had to be dealt with could be easily evaluated by direct integration. It should be noted that, in special cases, the more general results obtained below may be subject to simplifications by virtue of the relations presented in appendix C. Such simplifications can often be more easily seen, if the specific loop integral is directly evaluated. In this case, however, the general result is still very useful for cross-checks. Subsequently, the following quantities will be investigated:

$$\begin{aligned} A_0(m_1^2) &\equiv \mu^{-(n-4)} \int \frac{d^n q}{(2\pi)^n} \frac{1}{D_1} \\ B_{(0,\mu,\mu\nu)}(p_1, m_1^2, m_2^2) &\equiv \mu^{-(n-4)} \int \frac{d^n q}{(2\pi)^n} \frac{\{1,\, q_\mu,\, q_\mu q_\nu\}}{D_1\, D_2} \\ C_{(0,\mu,\mu\nu,\mu\nu\rho)}(p_1, p_2, m_1^2, m_2^2, m_3^2) &\equiv \mu^{-(n-4)} \int \frac{d^n q}{(2\pi)^n} \frac{\{1,\, q_\mu,\, q_\mu q_\nu,\, q_\mu q_\nu q_\rho\}}{D_1\, D_2\, D_3} \quad . \end{aligned} \tag{F.1}$$

Dimensional regularization is applied to render all expressions well-defined. μ is an arbitrary mass scale. The following definitions are used:

$$\begin{aligned} D_1 &= q^2 + m_1^2 - \mathrm{i}\varepsilon \\ D_2 &= (q + p_1)^2 + m_2^2 - \mathrm{i}\varepsilon \\ D_3 &= (q + p_1 + p_2)^2 + m_3^2 - \mathrm{i}\varepsilon \quad . \end{aligned} \tag{F.2}$$

The n-dimensional Dirac algebra needed for the evaluation of loop expressions can be found in [96, 119] or in standard textbooks such as [57]. Care is required if γ_5 matrices

are involved. Note that the expressions in equation (F.1) are invariant under shifts of the loop momentum q. Before proceeding further a lemma will be presented that is going to be very useful in section F.1.

Lemma 1 *Let a be real. The numbers b,c and y_0 may be complex. Let further $-\varepsilon$ be an infinitesimal real number carrying the sign of $I = \Im m(ay^2+by+c)$, where I is supposed to not change sign for $y \in [0,1]$. Let the infinitesimal real number $-\delta$ carry the sign of $\Im m(ay_0^2+by_0+c)$. Let y_1 and y_2 be the roots of $ay^2+by+c=0$. Then the identity*

$$\begin{aligned}\int_0^1 \frac{dy}{y-y_0}\Big[\ln(ay^2+by+c)-\ln(ay_0^2+by_0+c)\Big] \;=\; \\ \ln\frac{y_0-1}{y_0}\cdot\Big[\eta(-y_1,-y_2) \;-\; \eta(y_0-y_1,y_0-y_2) \;-\; \eta(a-\mathrm{i}\varepsilon,a+\mathrm{i}\delta)\Big] \\ +\,\mathrm{R}(y_0,y_1) \;+\; \mathrm{R}(y_0,y_2) \qquad\qquad (\mathrm{F}.3)\end{aligned}$$

holds, if the two parameter function R is defined by

$$\begin{aligned}\mathrm{R}(y_0,y_i) \;&=\; \int_0^1 \frac{dy}{y-y_0}\Big[\ln(y-y_i)-\ln(y_0-y_i)\Big] \\ &=\; \mathrm{Li}_2\left(\frac{y_0}{y_0-y_i}\right) \;-\; \mathrm{Li}_2\left(\frac{y_0-1}{y_0-y_i}\right) \\ &\quad +\,\eta\left(-y_i,\frac{1}{y_0-y_i}\right)\cdot\ln\frac{y_0}{y_0-y_i} \;-\; \eta\left(1-y_i,\frac{1}{y_0-y_i}\right)\cdot\ln\frac{y_0-1}{y_0-y_i}\;. \qquad (\mathrm{F}.4)\end{aligned}$$

The proof of Lemma 1 can be found in appendix B of reference [104]. See appendix C.1 for the definition of $\eta(a,b)$.

F.1 Scalar m-Point Functions

The evaluation of scalar m-point functions in n dimensions is based on the representation of n-dimensional space in spherical coordinates as outlined in the appendix of reference [110]. For $m \geq 2$, the second important ingredient is Feynman parametrization. One arrives at expressions which become rather handy for $n = 4-\varepsilon,\ |\varepsilon| \ll 1$. Integrals converge for $\varepsilon > 0$ in the case of an ultraviolet (UV) divergence and for $\varepsilon < 0$ in the case of infrared divergences.

The scalar 1-point function is given by

$$\begin{aligned}A_0(m_1^2) \;&=\; \frac{\mathrm{i}}{16\,\pi^2}\,m_1^2\cdot\left[\Delta-1+\ln\frac{m_1^2-\mathrm{i}\varepsilon}{\mu^2}\right]\;, \\ \Delta \;&=\; \frac{2}{n-4}+\gamma_E-\ln(4\pi)\;, \qquad (\mathrm{F}.5)\end{aligned}$$

with Euler's constant $\gamma_E = 0.577216...$.

The scalar 2-point function is given by [104]

$$B_0(p_1,m_1^2,m_2^2) \;=\; -\frac{\mathrm{i}}{16\,\pi^2}\left\{\quad \Delta \;+\; \ln\frac{-p_1^2-\mathrm{i}\varepsilon}{\mu^2} \right.$$
$$\left. +\;\sum_{i=1}^{2}\left[\ln(1-x_i)-x_i\cdot\ln\frac{x_i-1}{x_i}-1\right]\right\} \quad , \tag{F.6}$$

where x_1 and x_2 are the roots of $-p_1^2x^2 \,+\, (p_1^2+m_2^2-m_1^2)x+m_1^2-\mathrm{i}\varepsilon \;=\; 0$. If $p_1^2=0$, there is only one root, and $\ln(-p_1^2-\mathrm{i}\varepsilon)$ should be replaced by $\ln(m_2^2-m_1^2-\mathrm{i}\varepsilon)$. If in addition $m_1^2=m_2^2=m^2$ one finds

$$B_0(0,m^2,m^2) \;=\; -\frac{\mathrm{i}}{16\,\pi^2}\left\{\Delta \;+\; \ln\frac{m^2-\mathrm{i}\varepsilon}{\mu^2}\right\} \quad . \tag{F.7}$$

The pathological case $p_1^2=m_1^2=m_2^2=0$ is infrared divergent and would require appropriate special treatment.

The scalar 3-point function has a more complicated structure, but is not ultraviolet divergent. It can be presented as

$$\begin{aligned} C_0(p_1,p_2,m_1^2,m_2^2,m_3^2) \;&=\; \frac{\mathrm{i}}{16\,\pi^2}\int\limits_0^1 dx\int\limits_0^x dy\,\Big[ax^2+by^2+cxy+dx+ey+f\Big]^{-1} \\ &\equiv\; \frac{\mathrm{i}}{16\,\pi^2}\,\tilde{C}_0 \end{aligned} \tag{F.8}$$

with

$$\begin{aligned} a=-p_2^2, \quad b=-p_1^2, \quad c=-2p_1p_2=p_1^2+p_2^2-(p_1+p_2)^2, \\ d=m_2^2-m_3^2+p_2^2, \quad e=m_1^2-m_2^2+p_1^2+2p_1p_2, \quad f=m_3^2-i\epsilon \quad . \end{aligned}$$

Defining α as one of the roots of $b\alpha^2+c\alpha+a=0$, the first integration yields:

$$\begin{aligned} \tilde{C}_0 \;=\; & \int\limits_0^1 dy\,\frac{\ln\Big[by^2+(c+e)y+a+d+f\Big] \;-\; \ln\Big[by_1^2+(c+e)y_1+a+d+f\Big]}{(c+2\alpha b)y+d+e\alpha+2a+c\alpha} \\ & -\int\limits_0^1 dy\,\frac{(1-\alpha)}{(c+2\alpha b)(1-\alpha)y+d+e\alpha}\times \\ & \qquad \Big\{\ln\Big[(a+b+c)y^2+(d+e)y+f\Big] \;-\; \ln\Big[(a+b+c)y_2^2+(d+e)y_2+f\Big]\Big\} \\ & +\int\limits_0^1 dy\,\frac{\alpha\cdot\Big\{\ln\Big[ay^2+dy+f\Big] \;-\; \ln\Big[ay_3^2+dy_3+f\Big]\Big\}}{(c+2\alpha b)\alpha y-(d+e\alpha)} \end{aligned} \tag{F.9}$$

with

$$\left.\begin{array}{rcl} y_1 &=& y_0 + \alpha \\ y_2 &=& \dfrac{y_0}{1-\alpha} \\ y_3 &=& -\dfrac{y_0}{\alpha} \end{array}\right\} \quad y_0 \;=\; -\,\frac{d+e\alpha}{c+2\alpha b} \quad .$$

Taking into account that for each term of equation (F.9) the non-logarithmic factor can be written as $(c+2\alpha b)\cdot[y-y_i]$ and using the identity (F.3) presented in Lemma 1 at the end of the previous section, it is straightforward to further integrate equation (F.9). This solution is valid for all physical cases, i.e. for physical four-momenta p_1 and p_2 and physical masses [104]. Physical four-momenta are real, masses may be complex but must have a positive real part.

For real roots α and stable particles, the 3-point function can be cast into a rather simple form:

$$\begin{aligned} &C_0(p_1,p_2,m_1^2,m_2^2,m_3^2) \quad \overset{\alpha, m_i \,\epsilon\, \mathbb{R}}{=} \\ &\quad \frac{\mathrm{i}}{16\pi^2(c+2\alpha b)} \sum_{l=1}^{3}\sum_{j=1}^{2} (-1)^{l+1} \left[\mathrm{Li}_2\!\left(\frac{x_l}{x_l - y_{lj}}\right) \;-\; \mathrm{Li}_2\!\left(\frac{x_l-1}{x_l-y_{lj}}\right)\right] \end{aligned} \tag{F.10}$$

with

$$\begin{aligned} x_1 &= -\,\frac{d+2a+(e+c)\alpha}{c+2\alpha b}\;, & y_{1j} &= \frac{-c-e\pm\sqrt{(c+e)^2-4b(a+d+f)}}{2b}\;, \\ x_2 &= -\,\frac{d+e\alpha}{(1-\alpha)(c+2\alpha b)}\;, & y_{2j} &= \frac{-d-e\pm\sqrt{(d+e)^2-4f(a+b+c)}}{2(a+b+c)}\;, \\ x_3 &= \;\;\frac{d+e\alpha}{\alpha(c+2\alpha b)}\;, & y_{3j} &= \frac{-d\pm\sqrt{d^2-4af}}{2a}\;. \end{aligned}$$

Among the special cases of the scalar 3-point function, one is rather interesting, namely the infrared divergent case which is encountered, if one propagator mass vanishes and the momenta p_1 and p_1+p_2 are on-shell. Without loss of generality one can choose

$$m_1 = 0\;, \qquad p_1^2 = -m_2^2\;, \qquad (p_1+p_2)^2 = -m_3^2\;. \tag{F.11}$$

The infrared divergent scalar 3-point function is then given by

$$\begin{aligned} &C_0^{\mathrm{IR}}(p_1,p_2,0,m_2^2,m_3^2) \;= \\ &\quad \mu^{-(n-4)} \int \frac{d^nq}{(2\pi)^n}\, \frac{1}{(q^2-\mathrm{i}\varepsilon)(q^2+2qp_1-\mathrm{i}\varepsilon)(q^2+2q(p_1+p_2)-\mathrm{i}\varepsilon)}\;. \end{aligned} \tag{F.12}$$

From power counting in equation (F.12) it is seen that C_0^{IR} is infrared divergent for $n=4$, but regularized by $n>4$. Expansion around $n=4$ yields

$$C_0^{\mathrm{IR}}(p_1,p_2,0,m_2^2,m_3^2) \;=\; \frac{\mathrm{i}}{16\,\pi^2}\cdot\frac{1}{2}\int_0^1 \frac{dy}{-p_y^2}\left[\Delta^{\mathrm{IR}} \;+\; \ln\left(\frac{-p_y^2}{\mu^2}\right)\right] \tag{F.13}$$

with $-p_y^2 = -p_2^2y^2+(p_2^2-m_2^2+m_3^2)y+m_2^2-\mathrm{i}\varepsilon$ and $\Delta^{\mathrm{IR}}=\Delta$, the superscript IR indicating its infrared origin. The case $p_2^2=0$ yields a simplified integral and will not be treated

here. In addition, the cases $m_2 = 0$ and $m_3 = 0$ are excluded from further consideration to ensure that the roots y_1 and y_2 of $-p_y^2 = 0$ do not coincide with the integration edges. Defining

$$\begin{aligned} -p_{y_1}^2 &\equiv -p_2^2 y_1^2 + (p_2^2 - m_2^2 + m_3^2) y_1 + m_2^2 - \mathrm{i}\varepsilon \\ -p_{y_2}^2 &\equiv -p_2^2 y_2^2 + (p_2^2 - m_2^2 + m_3^2) y_2 + m_2^2 - \mathrm{i}\varepsilon \end{aligned}$$

one can rewrite

$$\begin{aligned} &C_0^{\mathrm{IR}}(p_1, p_2, 0, m_2^2, m_3^2) \; = \\ &\quad \frac{\mathrm{i}}{16\,\pi^2} \cdot \frac{1}{2} \cdot \frac{1}{-p_2^2 \cdot (y_1 - y_2)} \left\{ \int_0^1 \frac{dy}{y - y_1} \left[\Delta^{\mathrm{IR}} + \ln \frac{-p_{y_1}^2}{\mu^2} + \ln(-p_y^2) - \ln(-p_{y_1}^2) \right] \right. \\ &\qquad \left. - \int_0^1 \frac{dy}{y - y_2} \left[\Delta^{\mathrm{IR}} + \ln \frac{-p_{y_2}^2}{\mu^2} + \ln(-p_y^2) - \ln(-p_{y_2}^2) \right] \right\} \end{aligned} \tag{F.14}$$

Using

$$\int_0^1 \frac{dy}{y - y_i} = \ln \frac{y_i - 1}{y_i} \tag{F.15}$$

and identity (F.3) from Lemma 1 further integration is straightforward. Despite the generality of this result direct integration of the R.H.S. of equation (F.13) is simpler in many practical cases.

F.2 Reduction of Tensor Integrals

Because of Lorentz covariance, tensor loop integrals can be decomposed into linear combinations of all possible tensors with identical rank that can be built from the involved external four-vectors and the metric tensor.

$$B_\mu = p_{1\mu}\, B_1 \tag{F.16}$$

$$B_{\mu\nu} = p_{1\mu} p_{1\nu}\, B_{21} \; + \; g_{\mu\nu} B_{22} \tag{F.17}$$

$$C_\mu = p_{1\mu}\, C_{11} \; + \; p_{2\mu}\, C_{12} \tag{F.18}$$

$$C_{\mu\nu} = p_{1\mu} p_{1\nu}\, C_{21} \; + \; p_{2\mu} p_{2\nu}\, C_{22} \; + \; \{p_1 p_2\}_{\mu\nu}\, C_{23} \; + \; g_{\mu\nu} C_{24} \tag{F.19}$$

$$\begin{aligned} C_{\mu\nu\rho} &= p_{1\mu} p_{1\nu} p_{1\rho}\, C_{31} \; + \; p_{2\mu} p_{2\nu} p_{2\rho}\, C_{32} \; + \; \{p_2 p_1 p_1\}_{\mu\nu\rho}\, C_{33} \\ &\quad + \{p_1 p_2 p_2\}_{\mu\nu\rho}\, C_{34} \; + \; \{p_1\, g\}_{\mu\nu\rho}\, C_{35} \; + \; \{p_2\, g\}_{\mu\nu\rho}\, C_{36} \end{aligned} \tag{F.20}$$

The linear factors $B_{i(j)}$ and C_{ij} are linear combinations of scalar loop integrals and depend on the Lorentz invariants that can be formed from the momenta p_i of the involved external four-vectors and on the propagator masses squared m_i^2. For the sake of simplicity, no arguments are exposed in equations (F.16) to (F.20). If nothing else is given, arguments are always assumed to be as exhibited in equation (F.1). The convenient shorthand prescriptions

$$\begin{aligned} \{p_1 p_2\}_{\mu\nu} &\equiv p_{1\mu}\, p_{2\nu} + p_{2\mu}\, p_{1\nu} \\ \{p_i p_j p_j\}_{\mu\nu\rho} &\equiv p_{i\mu}\, p_{j\nu}\, p_{j\rho} + p_{j\mu}\, p_{i\nu}\, p_{j\rho} + p_{j\mu}\, p_{j\nu}\, p_{i\rho} \\ \{p_i g\}_{\mu\nu\rho} &\equiv p_{i\mu}\, g_{\nu\rho} + p_{i\nu}\, g_{\mu\rho} + p_{i\rho}\, g_{\mu\nu} \end{aligned} \tag{F.21}$$

were taken from reference [118], the other notations are rather standard (see e.g. [86]). Now the computation of the linear factors $B_{i(j)}$ and C_{ij} is described. To evaluate B_1, both sides of (F.16) are multiplied by p_1^μ. This is followed by quadratic supplementation of the integrand's numerator on the L.H.S. Then division by p_1^2 yields the well-known result

$$B_1 = \frac{1}{2\,p_1^2}\Big[f_1 B_0 + A_0(m_1^2) - A_0(m_2^2)\Big] \tag{F.22}$$

with $f_1 = m_1^2 - m_2^2 - p_1^2$. Similarly, multiplication of both sides of (F.17) with $g^{\mu\nu}$ and $p_1^\mu p_1^\nu$ respectively yields a linear system of equations,

$$\begin{pmatrix} p_1^2 & n \\ p_1^2 & 1 \end{pmatrix} \begin{pmatrix} B_{21} \\ B_{22} \end{pmatrix} = \begin{pmatrix} A_0(m_2^2) - m_1^2\, B_0 \\ \frac{1}{2} A_0(m_2^2) + \frac{1}{2}\, f_1 B_1 \end{pmatrix} \quad , \tag{F.23}$$

which has the solution

$$\begin{aligned} B_{22} &= \frac{1}{n-1}\left[-\frac{1}{2}\, f_1 B_1 - m_1^2 B_0 + \frac{1}{2} A_0(m_2^2)\right] \\ B_{21} &= \frac{1}{p_1^2}\left[\frac{1}{2}\, f_1 B_1 + \frac{1}{2} A_0(m_2^2) - B_{22}\right] \quad . \end{aligned} \tag{F.24}$$

The above already reveals the algorithm for the reduction of tensor n-point functions. *Multiplication of both sides of the tensor integral's linear decomposition (see equations (F.16) to (F.20)) by the integral's tensor coefficients and subsequent evaluation of the resulting integrals with the help of quadratic supplementation of the integrand yields a linear system of equations for the linear factors $B_{i(j)}$ and C_{ij} in terms of scalar m-point functions.* This resulting system originally consists of k equations for the k linear factors to be evaluated. A more elegant way with reduced dimension of the system of equations to be evaluated is given in references [86, 118]. Subsequently, we shall follow their approach and present the solutions for the remaining linear factors C_{ij}. First define

$$B_{(0,\mu,\mu\nu)}(k,l) \equiv \mu^{-(n-4)} \int \frac{d^n q}{(2\pi)^n}\, \frac{\{1,\, q_\mu,\, q_\mu q_\nu\}}{D_k\, D_l}\bigg|_{Q_k=0} \tag{F.25}$$

with $Q_1 = 0$ and $Q_2 = p_1$. The denominators for this definition are found in equation (F.2). The arguments (k,l), $k<l$ will be correspondingly used for the linear factors $B_{i(j)}(k,l)$ which can be derived by virtue of equations (F.16) and (F.17). Using $f_2 \equiv m_2^2 - m_3^2 + p_1^2 - (p_1+p_2)^2$ and considering

$$X \;=\; \begin{pmatrix} p_1^2 & p_1p_2 \\ p_1p_2 & p_2^2 \end{pmatrix}$$

an invertible matrix (i.e. assuming $(p_1p_2)^2 - p_1^2p_2^2 \neq 0$), the linear factors C_{1j} for the R.H.S. of equation (F.18) are given by

$$\begin{aligned} \begin{pmatrix} C_{11} \\ C_{12} \end{pmatrix} &= X^{-1} \begin{pmatrix} R_1 \\ R_2 \end{pmatrix} \qquad\qquad (F.26) \\ R_1 \;\equiv\; p_1^\mu C_\mu &= \frac{1}{2}\Big[\, f_1 C_0 + B_0(1,3) - B_0(2,3)\Big] \\ R_2 \;\equiv\; p_2^\mu C_\mu &= \frac{1}{2}\Big[\, f_2 C_0 + B_0(1,2) - B_0(1,3)\Big] \quad . \end{aligned}$$

The linear factors C_{2j} on the R.H.S. of equation (F.19) are given by similar matrix relations, namely

$$\begin{pmatrix} C_{21} \\ C_{23} \end{pmatrix} = X^{-1} \begin{pmatrix} R_3 - C_{24} \\ R_4 \end{pmatrix} , \qquad \begin{pmatrix} C_{23} \\ C_{22} \end{pmatrix} = X^{-1} \begin{pmatrix} R_5 \\ R_6 - C_{24} \end{pmatrix} . \qquad (F.27)$$

The UV divergent linear factor

$$C_{24} \;=\; \frac{1}{n-2}\left[- m_1^2 C_0 - \frac{1}{2}\Big(f_1 C_{11} + f_2 C_{12} - B_0(2,3)\Big)\right]$$

is obtained from the original 5×5 system of linear equations and

$$\begin{aligned} R_3 \;\equiv\; \frac{1}{p_1p_2}\Big[\, p_1^\mu p_2^\nu\, C_{\mu\nu} - p_2^2\, R_5\Big] &= \frac{1}{2}\Big[\, f_1 C_{11} + B_1(1,3) + B_0(2,3)\Big] \quad , \\ R_4 \;\equiv\; \frac{(p_1p_2)\cdot p_2^\mu p_2^\nu - p_2^2 \cdot p_1^\mu p_2^\nu}{(p_1p_2)^2 - p_1^2p_2^2}\, C_{\mu\nu} &= \frac{1}{2}\Big[\, f_2 C_{11} + B_1(1,2) - B_1(1,3)\Big] \quad , \\ R_5 \;\equiv\; \frac{(p_1p_2)\cdot p_1^\mu p_1^\nu - p_1^2 \cdot p_1^\mu p_2^\nu}{(p_1p_2)^2 - p_1^2p_2^2}\, C_{\mu\nu} &= \frac{1}{2}\Big[\, f_1 C_{12} + B_1(1,3) - B_1(2,3)\Big] \quad , \\ R_6 \;\equiv\; \frac{1}{p_1p_2}\Big[\, p_1^\mu p_2^\nu\, C_{\mu\nu} - p_1^2\, R_4\Big] &= \frac{1}{2}\Big[\, f_2 C_{12} - B_1(1,3)\Big] \quad . \end{aligned}$$

Finally, the matrix relations for the linear factors C_{3j} are given by

$$\begin{aligned} \begin{pmatrix} C_{35} \\ C_{36} \end{pmatrix} &= X^{-1} \begin{pmatrix} R_{10} \\ R_{11} \end{pmatrix} , \\ \begin{pmatrix} C_{31} \\ C_{33} \end{pmatrix} &= X^{-1} \begin{pmatrix} R_{12} - 2\, C_{35} \\ R_{13} \end{pmatrix} , \qquad \begin{pmatrix} C_{34} \\ C_{32} \end{pmatrix} = X^{-1} \begin{pmatrix} R_{14} \\ R_{15} - 2\, C_{36} \end{pmatrix} . \qquad (F.28) \end{aligned}$$

In addition there is the redundant matrix relation

$$\begin{pmatrix} C_{33} \\ C_{34} \end{pmatrix} = X^{-1} \begin{pmatrix} R_{16} - C_{36} \\ R_{17} - C_{35} \end{pmatrix} . \qquad (F.29)$$

The scalar factors needed are

$$
\begin{aligned}
R_{10} &\equiv \frac{1}{2}\Big[\, f_1 C_{24} + B_{22}(1,3) - B_{22}(2,3)\Big] \quad , \\
R_{11} &\equiv \frac{1}{2}\Big[\, f_2 C_{24} + B_{22}(1,2) - B_{22}(1,3)\Big] \quad , \\
R_{12} &\equiv \frac{1}{2}\Big[\, f_1 C_{21} + B_{21}(1,3) - B_{0}(2,3)\Big] \quad , \\
R_{13} &\equiv \frac{1}{2}\Big[\, f_2 C_{21} + B_{21}(1,2) - B_{21}(1,3)\Big] \quad , \\
R_{14} &\equiv \frac{1}{2}\Big[\, f_1 C_{22} + B_{21}(1,3) - B_{21}(2,3)\Big] \quad , \\
R_{15} &\equiv \frac{1}{2}\Big[\, f_2 C_{22} - B_{21}(1,3)\Big] \quad , \\
R_{16} &\equiv \frac{1}{2}\Big[\, f_1 C_{23} + B_{21}(1,3) + B_{1}(2,3)\Big] \quad , \\
R_{17} &\equiv \frac{1}{2}\Big[\, f_2 C_{23} - B_{21}(1,3)\Big] \quad .
\end{aligned}
$$

This completes our outline of the reduction of tensor to scalar loop integrals and the appendix on loop integrals as a whole.

Appendix G

Table of Analytical Integrals

In this appendix the analytical solutions of the integrals needed for the semi-analytical cross-section calculation of process (1.1) are presented. These integrals are necessary to obtain the twofold differential cross-section $d^2\sigma/ds_{12}ds_{34}$ in the Born and virtual ISR cases and the threefold differential cross-section $d^3\sigma/ds'ds_{12}ds_{34}$ for initial state bremsstrahlung. This list is restricted to integrals needed for the t-channel contribution and the t-channel/u-channel interference, because the contributions from the u-channel and, in the virtual ISR case, from the u-channel/t-channel interference are obtained by symmetry arguments as detailed in appendix E. Integration of the azimuth around the beam axis is trivial. The integrals presented below have been numerically checked.

G.1 Fermion Decay Angle Tensor Integrals

Integrations over final state fermion decay angles are carried out with the help of invariant tensor integration. Using the decay matrix element M_{ij}^{μ} from equation (E.2) one obtains

$$\begin{aligned}\sum_{Spins\ i,j} \int d\Gamma_{ij}\, M_{ij}^{\mu} M_{ij}^{\nu} &\equiv \frac{\sqrt{\lambda(s_{ij}, m_{ij}^2, m_{ij}^2)}}{8\, s_{ij}} \sum_{Spins\ i,j} \int_{-1}^{+1} d\cos\theta_{ij} \int_0^{2\pi} d\phi_{ij}\, M_{ij}^{\mu} M_{ij}^{\nu} \\ &= \frac{\sqrt{\lambda(s_{ij}, m_{ij}^2, m_{ij}^2)}}{8\, s_{ij}} \frac{2\pi}{3} \left({g_{f\bar{f}B}^{V}}^2 + {g_{f\bar{f}B}^{A}}^2 \right) \times \\ &\qquad \left\{ s_{ij}\, g^{\mu\nu} + \left(p_i^{\mu} + p_j^{\mu}\right)\left(p_i^{\nu} + p_j^{\nu}\right) \right\} \end{aligned} \tag{G.1}$$

with $m_{12} \equiv m_1$ and $m_{34} \equiv m_2$. The vector and axial vector boson-fermion couplings $g_{f\bar{f}B}^{V}$ and $g_{f\bar{f}B}^{A}$ are found in appendix B.2. The result of the above decay phase space integral factorizes in the cross-section. Therefore one can use the above formula (G.1) to integrate the final state fermion decay angles for both the $2 \to 4$ and the initial state bremsstrahlung $2 \to 5$ particle phase space. The factor $\left({g_{f\bar{f}B}^{V}}^2 + {g_{f\bar{f}B}^{A}}^2 \right)$ enters the decay width $\Gamma_Z(s_{ij})$, equation (2.3), and thus the Breit-Wigner density $\rho_Z(s_{ij})$, equation (2.2).

G.2 Born Level Phase Space Integrals

For the calculation of the Born level cross-section of process (1.1) only a few integrals over the boson scattering angle ϑ are needed in addition to those over the final state fermion decay angles. They are listed below, making use of the phase space parametrization given in appendix D.1, the ultrarelativistic approximation (URA), and the notation

$$[A]_t \equiv \frac{1}{2}\int_{-1}^{+1} d\cos\vartheta \; A \quad . \tag{G.2}$$

1.) $[1]_t = 1$

2.) $[\cos\vartheta]_t = 0$

3.) $[\cos^2\vartheta]_t = 1/3$

4.) $\left[\frac{1}{t}\right]_t = \frac{1}{\sqrt{\lambda}} \ln\frac{s-\sigma+\sqrt{\lambda}}{s-\sigma-\sqrt{\lambda}}$

5.) $\left[\frac{1}{u}\right]_t = \frac{1}{\sqrt{\lambda}} \ln\frac{s-\sigma+\sqrt{\lambda}}{s-\sigma-\sqrt{\lambda}}$

6.) $\left[\frac{1}{t^2}\right]_t = \frac{1}{s_{12}s_{34}}$

G.3 Bremsstrahlung Integrals – First Series

For the calculation of the bremsstrahlung process (1.1), the phase space was parametrized as exposed in equation (D.9), appendix D.2. After integration over the final state fermion decay angles, the first series of bremsstrahlung integrals is over the scattering azimuth and polar angles ϕ_R and θ_R of the boson three-vector v_1 in the two-boson rest frame. Using the double integral notation

$$[A]_R \equiv \frac{1}{4\pi}\int_0^{2\pi} d\phi_R \int_{-1}^{+1} d\cos\theta_R \; A \tag{G.3}$$

and the ultrarelativistic approximation, i.e. neglecting the electron mass wherever possible, the bremsstrahlung integrals for the first series are listed below:

1.) $[1]_R = 1$

2.) $[\cos\phi_R \cdot f(\cos\theta_R)]_R = 0$

3.) $[\cos\theta_R]_R = 0$

4.) $[\cos^2\phi_R]_R = 1/2$

5.) $[\cos^2\theta_R]_R = 1/3$

6.) $[\cos^2\phi_R \cdot \cos^2\theta_R]_R = 1/6$

7.) $$\left[\frac{1}{t_1}\right]_R = \frac{2s'}{\sqrt{\lambda'}(s'_+ - s'_- \cos\theta)} \cdot \ln\left(\frac{s'_+(s'+\sqrt{\lambda'})-2s'\sigma+s'_-\,\delta-(s'+\delta+\sqrt{\lambda'})s'_-\,\cos\theta}{s'_+(s'-\sqrt{\lambda'})-2s'\sigma+s'_-\,\delta-(s'+\delta-\sqrt{\lambda'})s'_-\,\cos\theta}\right)^{\dagger}$$
$$\equiv \frac{2s'}{\sqrt{\lambda'}\,S_{d1}} \cdot l_{t1}$$

8.) $$\left[\frac{1}{t_2}\right]_R = \frac{2s'}{\sqrt{\lambda'}(s'_+ + s'_- \cos\theta)} \cdot \ln\left(\frac{s'_+(s'+\sqrt{\lambda'})-2s'\sigma-s'_-\,\delta+(s'-\delta+\sqrt{\lambda'})s'_-\,\cos\theta}{s'_+(s'-\sqrt{\lambda'})-2s'\sigma-s'_-\,\delta+(s'-\delta-\sqrt{\lambda'})s'_-\,\cos\theta}\right)$$
$$\equiv \frac{2s'}{\sqrt{\lambda'}\,S_{d2}} \cdot l_{t2}$$

9.) $$\left[\frac{1}{u_1}\right]_R = \frac{2s'}{\sqrt{\lambda'}(s'_+ - s'_- \cos\theta)} \cdot \ln\left(\frac{s'_+(s'+\sqrt{\lambda'})-2s'\sigma-s'_-\,\delta-(s'-\delta+\sqrt{\lambda'})s'_-\,\cos\theta}{s'_+(s'-\sqrt{\lambda'})-2s'\sigma-s'_-\,\delta-(s'-\delta-\sqrt{\lambda'})s'_-\,\cos\theta}\right)$$
$$= \mathcal{S}\left(\left[\frac{1}{t_2}\right]_R\right)^{\ddagger} \equiv \frac{2s'}{\sqrt{\lambda'}\,S_{d1}} \cdot l_{u1}$$

10.) $$\left[\frac{1}{u_2}\right]_R = \frac{2s'}{\sqrt{\lambda'}(s'_+ + s'_- \cos\theta)} \cdot \ln\left(\frac{s'_+(s'+\sqrt{\lambda'})-2s'\sigma+s'_-\,\delta+(s'+\delta+\sqrt{\lambda'})s'_-\,\cos\theta}{s'_+(s'-\sqrt{\lambda'})-2s'\sigma+s'_-\,\delta+(s'+\delta-\sqrt{\lambda'})s'_-\,\cos\theta}\right)$$
$$= \mathcal{S}\left(\left[\frac{1}{t_1}\right]_R\right) \equiv \frac{2s'}{\sqrt{\lambda'}\,S_{d2}} \cdot l_{u2}$$

11.) $$\left[\frac{\cos\theta_R}{t_1}\right]_R = \frac{16\ s'^2 b_1}{\lambda' \cdot {S_{d1}}^2} \cdot \left(1 - a_1^t \left[\frac{1}{t_1}\right]_R\right)$$

12.) $$\left[\frac{\cos\theta_R}{t_2}\right]_R = \frac{16\ s'^2 b_2}{\lambda' \cdot {S_{d2}}^2} \cdot \left(1 - a_2^t \left[\frac{1}{t_2}\right]_R\right)$$

---

†As used throughout the thesis, s (s') is the (reduced) center of mass energy squared, and s_{12}, s_{34} are the invariant masses of final state fermion pairs. The definitions of the derived quantities $t, u, t_1, t_2, u_1, u_2, z_1, z_2, \bar{z}_1, \bar{z}_2, s'_-, s'_+, \lambda, \lambda', \bar{\lambda}, \sigma, \delta, a_1^t, a_2^t, a_1^u, a_2^u, b_1, b_2$, and c are given in appendices D and E where details of the applied phase space parametrizations and the cross-section computation are worked out.

‡The symmetry operations $\mathcal{S}$ and $\mathcal{T}$ are defined by: $\mathcal{S}\left[f(\cos\theta)\right] \equiv f(-\cos\theta)$,
$\mathcal{T}\left[g(s_{12}, s_{34})\right] \equiv g(s_{34}, s_{12})$.

$$13.) \quad \left[\frac{1}{t_1^2}\right]_R = \frac{4s'}{s_{12}\cdot\left(s-\delta+\sqrt{\lambda'}-s'_-\cdot\cos\theta\right)\left(s-\delta-\sqrt{\lambda'}-s'_-\cdot\cos\theta\right)}$$

$$\equiv \frac{4s'}{s_{12}\cdot d_1^+\, d_1^-}$$

$$14.) \quad \left[\frac{1}{t_2^2}\right]_R = \frac{4s'}{s_{34}\cdot\left(s+\delta+\sqrt{\lambda'}+s'_-\cdot\cos\theta\right)\left(s+\delta-\sqrt{\lambda'}+s'_-\cdot\cos\theta\right)}$$

$$\equiv \frac{4s'}{s_{34}\cdot d_2^+\, d_2^-}$$

$$15.) \quad \left[\frac{1}{t_1 t_2}\right]_R = \frac{1}{2S_{t_1t_2}}\cdot\ln\left(\frac{A^t_{1-}\cdot A^t_{2+}}{A^t_{1+}\cdot A^t_{2-}}\right) \equiv \frac{1}{2S_{t_1t_2}}\cdot l_{t12}$$

$$S_{t_1t_2} = \frac{\sqrt{\lambda'}}{8s'}\cdot\left(\sqrt{\bar{\lambda}}+\delta+s'_-\cos\theta\right)\left(\sqrt{\bar{\lambda}}-\delta-s'_-\cos\theta\right)$$

$$\equiv \frac{\sqrt{\lambda'}}{8s'}\cdot S^t_{12+}\, S^t_{12-}$$

$$A^t_{1-} = a_{1-} + b_{1-}\cdot\cos\theta$$

$$A^t_{1+} = a_{1+} + b_{1+}\cdot\cos\theta$$

$$A^t_{2-} = a_{2-} + b_{2-}\cdot\cos\theta$$

$$A^t_{2+} = a_{2+} + b_{2+}\cdot\cos\theta$$

$$a_{1-} = s^2\sigma - s\delta^2 + \frac{s}{2}s'_-\left(s'+\delta-2\sigma\right) - \sqrt{\lambda'}\left(s\delta-\frac{s}{2}s'_-\right)$$

$$b_{1-} = -\left(\sqrt{\lambda'}+s'+\delta\right)\frac{s}{2}s'_-$$

$$a_{1+} = s^2\sigma - s\delta^2 + \frac{s}{2}s'_-\left(s'+\delta-2\sigma\right) + \sqrt{\lambda'}\left(s\delta-\frac{s}{2}s'_-\right)$$

$$b_{1+} = +\left(\sqrt{\lambda'}-s'-\delta\right)\frac{s}{2}s'_-$$

$$a_{2-} = s^2\sigma - s\delta^2 + \frac{s}{2}s'_-\left(s'-\delta-2\sigma\right) - \sqrt{\lambda'}\left(s\delta+\frac{s}{2}s'_-\right)$$

$$b_{2-} = -\left(\sqrt{\lambda'}-s'+\delta\right)\frac{s}{2}s'_-$$

$$a_{2+} = s^2\sigma - s\delta^2 + \frac{s}{2}s'_-\left(s'-\delta-2\sigma\right) + \sqrt{\lambda'}\left(s\delta+\frac{s}{2}s'_-\right)$$

$$b_{2+} = +\left(\sqrt{\lambda'}+s'-\delta\right)\frac{s}{2}s'_-$$

$$16.)\quad \left[\frac{1}{u_1u_2}\right]_R = \mathcal{S}\left(\left[\frac{1}{t_1t_2}\right]_R\right) = \frac{1}{2S_{u_1u_2}}\cdot\ln\left(\frac{A^u_{1-}\cdot A^u_{2+}}{A^u_{1+}\cdot A^u_{2-}}\right) \equiv \frac{1}{2S_{u_1u_2}}\cdot l_{u12}$$

$$\begin{aligned}
S_{u_1u_2} &= \frac{\sqrt{\lambda'}}{8s'}\cdot\left(\sqrt{\bar{\lambda}}+\delta-s'_-\cos\theta\right)\left(\sqrt{\bar{\lambda}}-\delta+s'_-\cos\theta\right)\\
&\equiv \frac{\sqrt{\lambda'}}{8s'}\cdot S^u_{12+}\,S^u_{12-}\\
A^u_{1-} &= a_{1-}\;-\;b_{1-}\cdot\cos\theta\\
A^u_{1+} &= a_{1+}\;-\;b_{1+}\cdot\cos\theta\\
A^u_{2-} &= a_{2-}\;-\;b_{2-}\cdot\cos\theta\\
A^u_{2+} &= a_{2+}\;-\;b_{2+}\cdot\cos\theta
\end{aligned}$$

$$17.)\quad \left[\frac{1}{t_1u_1}\right]_R = \frac{1}{a^{ut}_1}\left(\left[\frac{1}{t_1}\right]_R+\left[\frac{1}{u_1}\right]_R\right)$$

$$a^{ut}_1 = \frac{1}{2}\left(s'_+-s'_-\cos\theta\right)-\sigma \equiv \frac{a}{2}\left(1-b\cdot\cos\theta\right)$$

$$18.)\quad \left[\frac{1}{t_2u_2}\right]_R = \frac{1}{a^{ut}_2}\left(\left[\frac{1}{t_2}\right]_R+\left[\frac{1}{u_2}\right]_R\right)$$

$$a^{ut}_2 = \frac{1}{2}\left(s'_++s'_-\cos\theta\right)-\sigma \equiv \frac{a}{2}\left(1+b\cdot\cos\theta\right)$$

$$19.)\quad \left[\frac{1}{t_1u_2}\right]_R = \frac{1}{2\sqrt{C_{12}}}\cdot\left[\;\ln\left(\frac{A^-_1\cdot B^-_2}{A^+_1\cdot B^+_2}\right)+2\ln\left(\frac{a_{s1}+b_d}{a_{s1}-b_d}\right)\;\right] \equiv \frac{1}{2\sqrt{C_{12}}}\cdot l_{t_1u_2}$$

$$\begin{aligned}
A^-_1 &= \sqrt{C_{12}}\cdot b_d\cdot(a^t_1+b_1)+C_{12}+B^t_1\cdot(a_{s1}-b_d)/2\\
A^+_1 &= \sqrt{C_{12}}\cdot b_d\cdot(a^t_1-b_1)+C_{12}+B^t_1\cdot(a_{s1}+b_d)/2\\
B^-_2 &= \sqrt{C_{12}}\cdot b_d\cdot(a^u_2-b_2)+C_{12}+B^u_2\cdot(a_{s1}-b_d)/2\\
B^+_2 &= \sqrt{C_{12}}\cdot b_d\cdot(a^u_2+b_2)+C_{12}+B^u_2\cdot(a_{s1}+b_d)/2
\end{aligned}$$

$$\begin{aligned}
C_{12} &= \left(\frac{\sqrt{\lambda'}}{2s'}\right)^2\cdot\left(A_{12}\cdot\cos^2\theta+B_{12}\right)\\
A_{12} &= -s'^{\,2}_-\cdot s_{12}\cdot(s-s_{12})\\
B_{12} &= s'^{\,2}_-\cdot s\cdot(s-s_{12})-2ss'_-\,(s-\sigma)\,(s-s_{12})+s^2\,(s-\sigma)^2
\end{aligned}$$

$$
\begin{aligned}
B_1^t &= -2\left[b_1\left(a_1^t b_2 + a_2^u b_1\right) + a_{s1}c^2\right] \\
B_2^u &= -2\left[b_2\left(a_1^t b_2 + a_2^u b_1\right) + a_{s1}c^2\right] \\
a_{s1} &= a_1^t + a_2^u \;=\; \frac{s'_+}{2s'}\left(s' + \delta\right) - 2s_{12} \\
b_d &= b_2 - b_1 \;=\; \frac{\sqrt{\lambda'}}{2s'} s'_-
\end{aligned}
$$

20.)
$$
\begin{aligned}
\left[\frac{1}{t_2 u_1}\right]_R &= \mathcal{T}\left(\left[\frac{1}{t_1 u_2}\right]_R\right) \\
&= \frac{1}{2\sqrt{C_{21}}} \cdot \left[\; \ln\left(\frac{A_2^- \cdot B_1^-}{A_2^+ \cdot B_1^+}\right) + 2\ln\left(\frac{a_{s2} + b_d}{a_{s2} - b_d}\right) \;\right] \;\equiv\; \frac{1}{2\sqrt{C_{21}}} \cdot l_{t_2 u_1}
\end{aligned}
$$

$$
\begin{aligned}
A_2^- &= \sqrt{C_{21}} \cdot b_d \cdot \left(a_2^t - b_2\right) + C_{21} + B_2^t \cdot \left(a_{s2} - b_d\right)/2 \\
A_2^+ &= \sqrt{C_{21}} \cdot b_d \cdot \left(a_2^t + b_2\right) + C_{21} + B_2^t \cdot \left(a_{s2} + b_d\right)/2 \\
B_1^- &= \sqrt{C_{21}} \cdot b_d \cdot \left(a_1^u + b_1\right) + C_{21} + B_1^u \cdot \left(a_{s2} - b_d\right)/2 \\
B_1^+ &= \sqrt{C_{21}} \cdot b_d \cdot \left(a_1^u - b_1\right) + C_{21} + B_1^u \cdot \left(a_{s2} + b_d\right)/2 \\
C_{21} &= \left(\frac{\sqrt{\lambda'}}{2s'}\right)^2 \cdot \left(A_{34} \cdot \cos^2\theta + B_{34}\right) \\
A_{34} &= -{s'_-}^2 \cdot s_{34} \cdot \left(s - s_{34}\right) \\
B_{34} &= {s'_-}^2 \cdot s \cdot \left(s - s_{34}\right) - 2s s'_- \left(s - \sigma\right)\left(s - s_{34}\right) + s^2\left(s - \sigma\right)^2 \\
B_2^t &= -2\left[b_2\left(a_1^u b_2 + a_2^t b_1\right) + a_{s2}c^2\right] \\
B_1^u &= -2\left[b_1\left(a_1^u b_2 + a_2^t b_1\right) + a_{s2}c^2\right] \\
a_{s2} &= a_2^t + a_1^u \;=\; \frac{s'_+}{2s'}\left(s' - \delta\right) - 2s_{34}
\end{aligned}
$$

21.)
$$
\left[\frac{\cos\theta_R}{t_1^2}\right]_R = \frac{16\, {s'}^2\, b_1}{\lambda' {S_{d1}}^2} \cdot \left(\left[\frac{1}{t_1}\right]_R - a_1^t \left[\frac{1}{t_1^2}\right]_R\right)
$$

22.)
$$
\left[\frac{\cos\theta_R}{t_2^2}\right]_R = \frac{16\, {s'}^2\, b_2}{\lambda' {S_{d2}}^2} \cdot \left(\left[\frac{1}{t_2}\right]_R - a_2^t \left[\frac{1}{t_2^2}\right]_R\right)
$$

23.) $$\left[\frac{1}{t_1^2 t_2}\right]_R = \frac{1}{{S_{t_1 t_2}}^2}\left(-a_d^t + a_1^t\left(a_1^t\, a_d^t - b_1\, b_d\right)\left[\frac{1}{t_1^2}\right]_R + \left(b_2\left(a_1^t b_2 - a_2^t b_1\right) - a_d^t\, c^2\right)\left[\frac{1}{t_1 t_2}\right]_R\right)$$

$$a_d^t = a_2^t - a_1^t = -\frac{s'_-}{2\,s'}\left(\delta - s'\,\cos\theta\right)$$

24.) $$\left[\frac{1}{t_1 t_2^2}\right]_R = \frac{1}{{S_{t_1 t_2}}^2}\left(a_d^t - a_2^t\left(a_2^t\, a_d^t - b_2\, b_d\right)\left[\frac{1}{t_2^2}\right]_R - \left(b_1\left(a_1^t b_2 - a_2^t b_1\right) - a_d^t\, c^2\right)\left[\frac{1}{t_1 t_2}\right]_R\right)$$

25.) $$\left[\frac{1}{t_1 t_2 u_1}\right]_R = \frac{1}{a_1^{ut}}\left(\left[\frac{1}{t_1 t_2}\right]_R + \left[\frac{1}{t_2 u_1}\right]_R\right)$$

26.) $$\left[\frac{1}{t_1 t_2 u_2}\right]_R = \frac{1}{a_2^{ut}}\left(\left[\frac{1}{t_1 t_2}\right]_R + \left[\frac{1}{t_1 u_2}\right]_R\right)$$

27.) $$\left[\frac{1}{t_1 u_1 u_2}\right]_R = \frac{1}{a_1^{ut}}\left(\left[\frac{1}{u_1 u_2}\right]_R + \left[\frac{1}{t_1 u_2}\right]_R\right)$$

28.) $$\left[\frac{1}{t_2 u_1 u_2}\right]_R = \frac{1}{a_2^{ut}}\left(\left[\frac{1}{u_1 u_2}\right]_R + \left[\frac{1}{t_2 u_1}\right]_R\right)$$

29.) $$\left[\frac{1}{t_1 t_2 u_1 u_2}\right]_R = \frac{1}{a_1^{ut}}\cdot\frac{1}{a_2^{ut}}\left(\left[\frac{1}{t_1 t_2}\right]_R + \left[\frac{1}{u_1 u_2}\right]_R + \left[\frac{1}{t_1 u_2}\right]_R + \left[\frac{1}{t_2 u_1}\right]_R\right) \quad .$$

G.4 Bremsstrahlung Integrals – Second Series

Below, the integrals needed for the last analytical integration in the bremsstrahlung case are given. This integration is over the photon scattering angle θ. Using the electron mass m_e, the ultrarelativistic approximation[†], and the notation

$$[A]_\theta \equiv \frac{1}{2}\int_{-1}^{+1} d\cos\theta\ A \quad , \tag{G.4}$$

the following integrals are required for the "second series" of bremsstrahlung integrals:

1.) $\left[1\right]_\theta = 1$

2.) $\left[\frac{1}{\bar{z}_1}\right]_\theta = \frac{1}{2}\ln\left(\frac{s}{m_e^2}\right) \equiv \frac{1}{2}\,l_\beta$

3.) $\left[\frac{1}{\bar{z}_2}\right]_\theta = \frac{1}{2}\,l_\beta$

4.) $\left[\frac{m_e^2}{\bar{z}_1^2}\right]_\theta = \frac{s}{4}$

5.) $\left[\frac{m_e^2}{\bar{z}_2^2}\right]_\theta = \frac{s}{4}$

6.) $\left[\frac{1}{S_{d1}}\right]_\theta = \frac{1}{2s'_-}\ln\left(\frac{s}{s'}\right)$

7.) $\left[\frac{1}{S_{d2}}\right]_\theta = \frac{1}{2s'_-}\ln\left(\frac{s}{s'}\right)$

8.) $\left[\frac{1}{S_{d1}^2}\right]_\theta = \frac{1}{4\,ss'}$

9.) $\left[\frac{1}{S_{d2}^2}\right]_\theta = \frac{1}{4\,ss'}$

10.) $\left[\frac{1}{\bar{z}_1}\,l_{t1}\right]_\theta = \frac{1}{2}\left(\,l_\beta \cdot L_{t1} \;-\; D_{z1t1}\right)$

$$L_{t1} = L_{c5} - L_{c1}$$

$$L_{c1} = \ln\left(\frac{s'_-(s'+\sqrt{\lambda'}) + s'\sigma - s\delta}{s'_-(s'-\sqrt{\lambda'}) + s'\sigma - s\delta}\right)$$

$$L_{c5} = \ln\left(\frac{s'-\sigma+\sqrt{\lambda'}}{s'-\sigma-\sqrt{\lambda'}}\right)$$

$$D_{z1t1} = \mathrm{Li}_2\left(\frac{s'_-(s+s'_--\delta-\sqrt{\lambda'})}{2s(s'_--\delta)+s'(\sigma+\delta)}\right) - \mathrm{Li}_2\left(\frac{s'_-(s+s'_--\delta+\sqrt{\lambda'})}{2s(s'_--\delta)+s'(\sigma+\delta)}\right)$$

[†]To obtain the correct result, m_e must be retained in all integrals containing factors $1/z_i$. In addition, keeping m_e is sometimes suggested for the sake of stability of the numerical invariant mass integrations that follow the θ integration described in this section.

11.) $$\left[\frac{1}{\bar{z}_1}\, l_{t2}\right]_\theta = \frac{1}{2}\Big(\, l_\beta \cdot L_{c5} \;-\; D_{z1t2}\Big)$$

$$D_{z1t2} = \mathrm{Li}_2\left(\frac{-s'_{\_}(s'+\delta-\sqrt{\lambda'})}{s'(\sigma+\delta)}\right) - \mathrm{Li}_2\left(\frac{-s'_{\_}(s'+\delta+\sqrt{\lambda'})}{s'(\sigma+\delta)}\right)$$

12.) $$\left[\frac{1}{\bar{z}_2}\, l_{t1}\right]_\theta = \frac{1}{2}\Big(\, l_\beta \cdot L_{c5} \;-\; D_{z2t1}\Big)$$

$$D_{z2t1} = \mathrm{Li}_2\left(\frac{-s'_{\_}(s'-\delta-\sqrt{\lambda'})}{s'(\sigma-\delta)}\right) - \mathrm{Li}_2\left(\frac{-s'_{\_}(s'-\delta+\sqrt{\lambda'})}{s'(\sigma-\delta)}\right)$$

13.) $$\left[\frac{1}{\bar{z}_2}\, l_{t2}\right]_\theta = \frac{1}{2}\Big(\, l_\beta \cdot L_{t2} \;-\; D_{z2t2}\Big)$$

$$L_{t2} = L_{c5} - L_{c2}$$

$$L_{c2} = \ln\left(\frac{s'_{\_}(s'+\sqrt{\lambda'}) + s'\sigma + s\delta}{s'_{\_}(s'-\sqrt{\lambda'}) + s'\sigma + s\delta}\right)$$

$$D_{z2t2} = \mathrm{Li}_2\left(\frac{s'_{\_}(s+s'_{\_}+\delta-\sqrt{\lambda'})}{2s(s'_{\_}+\delta)+s'(\sigma-\delta)}\right) - \mathrm{Li}_2\left(\frac{s'_{\_}(s+s'_{\_}+\delta+\sqrt{\lambda'})}{2s(s'_{\_}+\delta)+s'(\sigma-\delta)}\right)$$

14.) $$\left[\frac{1}{\bar{z}_1}\, l_{u1}\right]_\theta = \left[\mathcal{S}\Big(\frac{1}{\bar{z}_2}\, l_{t2}\Big)\right]_\theta = \left[\frac{1}{\bar{z}_2}\, l_{t2}\right]_\theta$$

15.) $$\left[\frac{1}{\bar{z}_1}\, l_{u2}\right]_\theta = \left[\mathcal{S}\Big(\frac{1}{\bar{z}_2}\, l_{t1}\Big)\right]_\theta = \left[\frac{1}{\bar{z}_2}\, l_{t1}\right]_\theta$$

16.) $$\left[\frac{1}{\bar{z}_2}\, l_{u1}\right]_\theta = \left[\mathcal{S}\Big(\frac{1}{\bar{z}_1}\, l_{t2}\Big)\right]_\theta = \left[\frac{1}{\bar{z}_1}\, l_{t2}\right]_\theta$$

17.) $$\left[\frac{1}{\bar{z}_2}\, l_{u2}\right]_\theta = \left[\mathcal{S}\Big(\frac{1}{\bar{z}_1}\, l_{t1}\Big)\right]_\theta = \left[\frac{1}{\bar{z}_1}\, l_{t1}\right]_\theta$$

$$18.)\quad \left[\frac{1}{S_{d1}}\,l_{t1}\right]_\theta = \frac{1}{2s'_-}\,\Re e\Bigg[-\mathrm{Li}_2\left(\frac{s\,(s'+\delta+\sqrt{\lambda'})}{s'(\sigma+\delta)}\right) + \mathrm{Li}_2\left(\frac{s'+\delta+\sqrt{\lambda'}}{\sigma+\delta}\right) + \mathrm{Li}_2\left(\frac{s\,(s'+\delta-\sqrt{\lambda'})}{s'(\sigma+\delta)}\right) - \mathrm{Li}_2\left(\frac{s'+\delta-\sqrt{\lambda'}}{\sigma+\delta}\right)\Bigg]^{\dagger}$$

$$\equiv \frac{1}{2\,s'_-}\cdot D_1^t$$

$$19.)\quad \left[\frac{1}{S_{d2}}\,l_{t2}\right]_\theta = \left[\mathcal{S}\mathcal{T}\left(\frac{1}{S_{d1}}\,l_{t1}\right)\right]_\theta = \mathcal{T}\left(\left[\frac{1}{S_{d1}}\,l_{t1}\right]_\theta\right)$$

$$= \frac{1}{2s'_-}\,\Re e\Bigg[-\mathrm{Li}_2\left(\frac{s\,(s'-\delta+\sqrt{\lambda'})}{s'(\sigma-\delta)}\right) + \mathrm{Li}_2\left(\frac{s'-\delta+\sqrt{\lambda'}}{\sigma-\delta}\right) + \mathrm{Li}_2\left(\frac{s\,(s'-\delta-\sqrt{\lambda'})}{s'(\sigma-\delta)}\right) - \mathrm{Li}_2\left(\frac{s'-\delta-\sqrt{\lambda'}}{\sigma-\delta}\right)\Bigg]$$

$$\equiv \frac{1}{2\,s'_-}\cdot D_2^t$$

$$20.)\quad \left[\frac{1}{S_{d1}}\,l_{u1}\right]_\theta = \left[\mathcal{S}\left(\frac{1}{S_{d2}}\,l_{t2}\right)\right]_\theta = \left[\frac{1}{S_{d2}}\,l_{t2}\right]_\theta$$

$$21.)\quad \left[\frac{1}{S_{d2}}\,l_{u2}\right]_\theta = \left[\mathcal{S}\left(\frac{1}{S_{d1}}\,l_{t1}\right)\right]_\theta = \left[\frac{1}{S_{d1}}\,l_{t1}\right]_\theta$$

$$22.)\quad \left[\frac{1}{\bar{z}_1}\,l_{t12}\right]_\theta = \frac{1}{2}\left(\,l_\beta\cdot L_{c1} + D_{z1t1} + D_{z1t2}\right)$$

$$23.)\quad \left[\frac{1}{\bar{z}_2}\,l_{t12}\right]_\theta = \frac{1}{2}\left(\,l_\beta\cdot L_{c2} + D_{z2t1} + D_{z2t2}\right)$$

---

† A comment on the treatment of arguments of logarithms and dilogarithms is in order here. The logarithm is undefined for negative real values, the Dilogarithm has a cut for real numbers larger than 1 as is explained in appendix C. This means that, in principle, infinitesimal imaginary parts from the propagator denominators have to be carried along in the whole calculation. This, however, is an unnecessary nuisance, because all integrands are real and regular. If infinitesimal imaginary parts were needed, because logarithms or Dilogarithms lay on cuts in final results, they were attributed to the invariant masses s_{12} and s_{34}. As integrands are real and regular, this is a correct treatment, because it is then irrelevant for the integrand how an infinitesimal imaginary part is entered. This technique will be used in subsequent integrals without further notice.

24.) $\Big[\frac{1}{\bar{z}_1}\, l_{u12}\Big]_\theta \;=\; \Big[\mathcal{S}\Big(\frac{1}{\bar{z}_2}\, l_{t12}\Big)\Big]_\theta \;=\; \Big[\frac{1}{\bar{z}_2}\, l_{t12}\Big]_\theta$

25.) $\Big[\frac{1}{\bar{z}_2}\, l_{u12}\Big]_\theta \;=\; \Big[\mathcal{S}\Big(\frac{1}{\bar{z}_1}\, l_{t12}\Big)\Big]_\theta \;=\; \Big[\frac{1}{\bar{z}_1}\, l_{t12}\Big]_\theta$

26.) $$\Big[\frac{1}{a_1^{ut}} l_{t12}\Big]_\theta \;=\; \frac{1}{s'_-}\cdot \Re e\Big[\, L_{c8}\cdot L_{c6} \;+\; D_{a1}^{tu}\,\Big]$$

$$L_{c8} \;=\; \ln\Big(\frac{s-\sigma}{s'-\sigma}\Big)$$

$$L_{c6} \;=\; \ln\frac{(a_{1-}\,b+b_{1-})(a_{2+}\,b+b_{2+})}{(a_{1+}\,b+b_{1+})(a_{2-}\,b+b_{2-})} \qquad \Big(\text{see 15.) \& 17.) in app. G.3}\Big)$$

$$\begin{aligned} D_{a1}^{tu} \;=\; & -\,\mathrm{Li}_2\Big(\frac{b_{1-}(1+b)}{a_{1-}\,b+b_{1-}}\Big) \;+\; \mathrm{Li}_2\Big(\frac{b_{1-}(1-b)}{a_{1-}\,b+b_{1-}}\Big) \\ & -\,\mathrm{Li}_2\Big(\frac{b_{2+}(1+b)}{a_{2+}\,b+b_{2+}}\Big) \;+\; \mathrm{Li}_2\Big(\frac{b_{2+}(1-b)}{a_{2+}\,b+b_{2+}}\Big) \\ & +\,\mathrm{Li}_2\Big(\frac{b_{1+}(1+b)}{a_{1+}\,b+b_{1+}}\Big) \;-\; \mathrm{Li}_2\Big(\frac{b_{1+}(1-b)}{a_{1+}\,b+b_{1+}}\Big) \\ & +\,\mathrm{Li}_2\Big(\frac{b_{2-}(1+b)}{a_{2-}\,b+b_{2-}}\Big) \;-\; \mathrm{Li}_2\Big(\frac{b_{2-}(1-b)}{a_{2-}\,b+b_{2-}}\Big) \end{aligned}$$

27.) $$\Big[\frac{1}{a_2^{ut}} l_{t12}\Big]_\theta \;=\; \frac{1}{s'_-}\cdot \Re e\Big[\, L_{c8}\cdot L_{c7} \;+\; D_{a2}^{tu}\,\Big]$$

$$L_{c7} \;=\; \ln\frac{(a_{1-}\,b-b_{1-})(a_{2+}\,b-b_{2+})}{(a_{1+}\,b-b_{1+})(a_{2-}\,b-b_{2-})} \qquad \Big(\text{see 15.) \& 17.) in app. G.3}\Big)$$

$$\begin{aligned} D_{a2}^{tu} \;=\; & -\,\mathrm{Li}_2\Big(\frac{-b_{1-}(1+b)}{a_{1-}\,b-b_{1-}}\Big) \;+\; \mathrm{Li}_2\Big(\frac{-b_{1-}(1-b)}{a_{1-}\,b-b_{1-}}\Big) \\ & -\,\mathrm{Li}_2\Big(\frac{-b_{2+}(1+b)}{a_{2+}\,b-b_{2+}}\Big) \;+\; \mathrm{Li}_2\Big(\frac{-b_{2+}(1-b)}{a_{2+}\,b-b_{2+}}\Big) \\ & +\,\mathrm{Li}_2\Big(\frac{-b_{1+}(1+b)}{a_{1+}\,b-b_{1+}}\Big) \;-\; \mathrm{Li}_2\Big(\frac{-b_{1+}(1-b)}{a_{1+}\,b-b_{1+}}\Big) \\ & +\,\mathrm{Li}_2\Big(\frac{-b_{2-}(1+b)}{a_{2-}\,b-b_{2-}}\Big) \;-\; \mathrm{Li}_2\Big(\frac{-b_{2-}(1-b)}{a_{2-}\,b-b_{2-}}\Big) \end{aligned}$$

28.) $$\left[\frac{1}{a_1^{ut}} l_{u12}\right]_\theta = \left[\mathcal{S}\left(\frac{1}{a_2^{ut}} l_{t12}\right)\right]_\theta = \left[\frac{1}{a_2^{ut}} l_{t12}\right]_\theta$$

29.) $$\left[\frac{1}{a_2^{ut}} l_{u12}\right]_\theta = \left[\mathcal{S}\left(\frac{1}{a_1^{ut}} l_{t12}\right)\right]_\theta = \left[\frac{1}{a_1^{ut}} l_{t12}\right]_\theta$$

30.) $$\left[\frac{1}{{S_{d1}}^2}\, l_{t1}\right]_\theta = \frac{1}{4\, s'_- s' s_{12}} \left(\sqrt{\lambda'}\, \ln\frac{s'}{s} + \frac{\sqrt{\lambda'}}{2}\, L_{c3} - \frac{s'-\sigma}{2}\, L_{c5} + \frac{s(s'+\delta) - s'(\sigma+\delta)}{2s}\, L_{t1} \right)$$

$$L_{c3} = \ln\left(1 + \frac{s'_-(s-\delta)}{s' s_{34}}\right)$$

31.) $$\left[\frac{1}{{S_{d2}}^2}\, l_{t2}\right]_\theta = \frac{1}{4\, s'_- s' s_{34}} \left(\sqrt{\lambda'}\, \ln\frac{s'}{s} + \frac{\sqrt{\lambda'}}{2}\, L_{c4} - \frac{s'-\sigma}{2}\, L_{c5} + \frac{s(s'-\delta) - s'(\sigma-\delta)}{2s}\, L_{t2} \right)$$

$$L_{c4} = \ln\left(1 + \frac{s'_-(s+\delta)}{s' s_{12}}\right)$$

32.) $$\left[\frac{1}{{S_{d1}}^3}\, l_{t1}\right]_\theta = \frac{1}{16\, s'_-} \left[- \frac{s'_-\sqrt{\lambda'}}{s {s'}^2 s_{12}} + \frac{(s'+\delta)\sqrt{\lambda'}}{2\, {s'}^2 s_{12}^2}\, L_{c3} + \frac{\sigma^2 - \delta^2 + 2\sigma\delta + 2s'(\sigma-\delta) - 2{s'}^2}{4\, {s'}^2 s_{12}^2}\, L_{c5} + \frac{(s'+\delta)\sqrt{\lambda'}}{{s'}^2 s_{12}^2} \ln\frac{s'}{s} + \left(\frac{{s'}^2 - s'(\sigma-\delta) + \delta^2}{2\, {s'}^2 s_{12}^2} - \frac{1}{s^2}\right) L_{t1} \right]$$

33.) $$\left[\frac{1}{{S_{d2}}^3}\, l_{t2}\right]_\theta = \frac{1}{16\, s'_-} \left[- \frac{s'_-\sqrt{\lambda'}}{s {s'}^2 s_{34}} + \frac{(s'-\delta)\sqrt{\lambda'}}{2\, {s'}^2 s_{34}^2}\, L_{c4} + \frac{\sigma^2 - \delta^2 - 2\sigma\delta + 2s'(\sigma+\delta) - 2{s'}^2}{4\, {s'}^2 s_{34}^2}\, L_{c5} + \frac{(s'-\delta)\sqrt{\lambda'}}{{s'}^2 s_{34}^2} \ln\frac{s'}{s} + \left(\frac{{s'}^2 - s'(\sigma+\delta) + \delta^2}{2\, {s'}^2 s_{34}^2} - \frac{1}{s^2}\right) L_{t2} \right]$$

34.) $$\left[\frac{m_e^{\,2}}{\bar{z}_1^{\,2}}\,l_{t2}\right]_\theta \;=\; \frac{s}{4}\cdot L_{c5}$$

35.) $$\left[\frac{m_e^{\,2}}{\bar{z}_2^{\,2}}\,l_{t1}\right]_\theta \;=\; \frac{s}{4}\cdot L_{c5}$$

36.) $$\left[\frac{m_e^{\,2}}{\bar{z}_1^{\,2}}\,l_{u2}\right]_\theta \;=\; \left[\mathcal{S}\left(\frac{m_e^{\,2}}{\bar{z}_2^{\,2}}\,l_{t1}\right)\right]_\theta \;=\; \frac{s}{4}\cdot L_{c5}$$

37.) $$\left[\frac{m_e^{\,2}}{\bar{z}_2^{\,2}}\,l_{u1}\right]_\theta \;=\; \left[\mathcal{S}\left(\frac{m_e^{\,2}}{\bar{z}_1^{\,2}}\,l_{t2}\right)\right]_\theta \;=\; \frac{s}{4}\cdot L_{c5}$$

38.) $$\left[\frac{1}{d_1^+\,d_1^-}\right]_\theta \;=\; \frac{1}{4\,s'_-\sqrt{\lambda'}}\cdot L_{c1}$$

39.) $$\left[\frac{1}{d_2^+\,d_2^-}\right]_\theta \;=\; \frac{1}{4\,s'_-\sqrt{\lambda'}}\cdot L_{c2}$$

40.) $$\left[\frac{\cos\theta}{d_1^+\,d_1^-}\right]_\theta \;=\; \frac{1}{4\,s'^{\,2}_-}\left(\frac{s-\delta}{\sqrt{\lambda'}}\,L_{c1}\;-\;L_{c3}\right)$$

41.) $$\left[\frac{\cos\theta}{d_2^+\,d_2^-}\right]_\theta \;=\; -\,\frac{1}{4\,s'^{\,2}_-}\left(\frac{s+\delta}{\sqrt{\lambda'}}\,L_{c2}\;-\;L_{c4}\right)$$

42.) $$\left[\frac{1}{S^t_{12+}\,S^t_{12-}}\right]_\theta \;=\; \frac{1}{4\,s'_-\sqrt{\bar{\lambda}}}\cdot L_{\bar{\lambda}}$$

$$L_{\bar{\lambda}} \;=\; \ln\left(\frac{s'_- + \sigma + \sqrt{\bar{\lambda}}}{s'_- + \sigma - \sqrt{\bar{\lambda}}}\right)$$

43.) $$\left[\frac{\cos\theta}{S^t_{12+}\,S^t_{12-}}\right]_\theta \;=\; \frac{1}{4\,s'^{\,2}_-}\left(\ln\frac{s_{12}}{s_{34}}\;-\;\frac{\delta}{\sqrt{\bar{\lambda}}}\,L_{\bar{\lambda}}\right)$$

44.) $$\left[\frac{1}{{S^t_{12+}}^2\,{S^t_{12-}}^2}\right]_\theta = \frac{1}{8\,s'_-\bar{\lambda}}\left(\frac{1}{\sqrt{\bar{\lambda}}}\,L_{\bar{\lambda}} + \frac{s'_-\sigma+\delta^2}{2\,s'_-s_{12}s_{34}}\right)$$

45.) $$\left[\frac{\cos\theta}{{S^t_{12+}}^2\,{S^t_{12-}}^2}\right]_\theta = \frac{\delta}{8\,{s'_-}^2\bar{\lambda}}\left(-\frac{1}{\sqrt{\bar{\lambda}}}\,L_{\bar{\lambda}} + \frac{s'_-+\sigma}{2\,s_{12}s_{34}}\right)$$

46.) $$\begin{aligned}\left[\frac{l_{t12}}{S^t_{12+}\,S^t_{12-}}\right]_\theta &= \frac{1}{4\,s'_-\sqrt{\bar{\lambda}}}\,\Re e\Bigg[-\mathrm{Li}_2\Big(+\frac{c_{++}a_{--}e_+}{d}\Big)+\mathrm{Li}_2\Big(+\frac{c_{-+}a_{--}e_+}{d}\Big)\\ &\quad+\mathrm{Li}_2\Big(-\frac{c_{+-}a_{--}e_+}{d}\Big)-\mathrm{Li}_2\Big(-\frac{c_{--}a_{--}e_+}{d}\Big)\\ &\quad-\mathrm{Li}_2\Big(-\frac{c_{++}a_{-+}e_+}{d}\Big)+\mathrm{Li}_2\Big(-\frac{c_{-+}a_{-+}e_+}{d}\Big)\\ &\quad+\mathrm{Li}_2\Big(+\frac{c_{+-}a_{-+}e_+}{d}\Big)-\mathrm{Li}_2\Big(+\frac{c_{--}a_{-+}e_+}{d}\Big)\\ &\quad-\mathrm{Li}_2\Big(+\frac{c_{+-}a_{++}e_-}{d}\Big)+\mathrm{Li}_2\Big(+\frac{c_{--}a_{++}e_-}{d}\Big)\\ &\quad+\mathrm{Li}_2\Big(-\frac{c_{++}a_{++}e_-}{d}\Big)-\mathrm{Li}_2\Big(-\frac{c_{-+}a_{++}e_-}{d}\Big)\\ &\quad-\mathrm{Li}_2\Big(-\frac{c_{+-}a_{+-}e_-}{d}\Big)+\mathrm{Li}_2\Big(-\frac{c_{--}a_{+-}e_-}{d}\Big)\\ &\quad+\mathrm{Li}_2\Big(+\frac{c_{++}a_{+-}e_-}{d}\Big)-\mathrm{Li}_2\Big(+\frac{c_{-+}a_{+-}e_-}{d}\Big)\Bigg]\end{aligned}$$

$$\equiv \frac{1}{4\,s'_-\sqrt{\bar{\lambda}}}\cdot D^t_{12}$$

$$\begin{aligned}a_{\pm\pm} &= s\pm\sqrt{\lambda'}\pm\sqrt{\bar{\lambda}}\\ c_{\pm\pm} &= \delta\pm s'_-\pm\sqrt{\bar{\lambda}}\\ e_\pm &= s'-\sigma\pm\sqrt{\lambda'}\\ d &= 8\,s\,s_{12}\,s_{34}\end{aligned}$$

$$47.)\quad \left[\frac{l_{t12}}{{S^t_{12+}}^2\,{S^t_{12-}}^2}\right]_\theta = \frac{1}{2\,\bar\lambda}\left[\frac{l_{t12}}{S^t_{12+}\,S^t_{12-}}\right]_\theta + \frac{1}{8\,s'_-\bar\lambda}\Bigg[\frac{\sqrt{\lambda'}\sqrt{\bar\lambda}}{2\,ss_{12}s_{34}}\,L_{\bar\lambda} + \frac{s'_- - \delta}{2\,s'_-s_{12}}\,L_{c1} + \frac{s'_- + \delta}{2\,s'_-s_{34}}\,L_{c2} + \frac{\bar\lambda - s(s'_- + \sigma)}{4\,ss_{12}s_{34}}\,(L_{c1}+L_{c2}) - \frac{\sqrt{\lambda'}(s'_- + \sigma)}{4\,ss_{12}s_{34}}\,(L_{c3}+L_{c4})\Bigg]$$

$$48.)\quad \left[\frac{\cos\theta\ \cdot\ l_{t12}}{{S^t_{12+}}^2\,{S^t_{12-}}^2}\right]_\theta = -\frac{\delta}{s'_-}\left[\frac{l_{t12}}{{S^t_{12+}}^2\,{S^t_{12-}}^2}\right]_\theta + \frac{1}{8\,{s'_-}^2}\Bigg[\frac{\sqrt{\lambda'}}{2\,s's_{12}s_{34}}\ln\frac{s_{12}}{s_{34}} - \frac{1}{2\,s'_-s_{12}}\,L_{c1} + \frac{1}{2\,s'_-s_{34}}\,L_{c2} - \frac{s'-\sigma}{4\,ss_{12}s_{34}}\,(L_{c1}-L_{c2}) - \frac{\sqrt{\lambda'}}{4\,ss_{12}s_{34}}\,(L_{c3}-L_{c4})\Bigg]$$

$$49.)\quad \left[\frac{l_{t12}}{{S^t_{12+}}^3\,{S^t_{12-}}^3}\right]_\theta = \frac{3}{4\bar\lambda}\left[\frac{l_{t12}}{{S^t_{12+}}^2\,{S^t_{12-}}^2}\right]_\theta + \frac{1}{32\,s'_-\sqrt{\bar\lambda}^3}\times \Bigg[\frac{\sqrt{\bar\lambda}\,\sqrt{\lambda'}\,\left(s'_-\sigma + 2\delta^2\right)}{4\,ss'_-s_{12}^2s_{34}^2} + \frac{\sqrt{\bar\lambda}\,\delta}{4\,s_{12}^2s_{34}^2}\,L_{c12} + \frac{\sqrt{\bar\lambda}}{4\,s'_-s_{12}^2}\,L_{c1} + \frac{\sqrt{\bar\lambda}}{4\,s'_-s_{34}^2}\,L_{c2} - \frac{\sqrt{\lambda'}\left(2ss_{12}s_{34} + \bar\lambda(s'-\sigma)\right)}{4\,s^2s_{12}^2s_{34}^2}\,L_{\bar\lambda} - \frac{\sqrt{\bar\lambda}\left(6\,ss_{12}s_{34} - s^2(s'_- + \sigma) + \bar\lambda(s'_+ - \sigma)\right)}{8\,s^2s_{12}^2s_{34}^2}\,(L_{c1}+L_{c2}) + \frac{\sqrt{\bar\lambda}\,\sqrt{\lambda'}\,\left(s(s'_- + \sigma) - 2\,s_{12}s_{34} - \bar\lambda\right)}{8\,s^2s_{12}^2s_{34}^2}\,(L_{c3}+L_{c4})\Bigg]$$

$$L_{c12} = \frac{1}{s'_-}\cdot\left(\frac{s_{12}^2}{s'_-}\,L_{c2} - \frac{s_{34}^2}{s'_-}\,L_{c1} - \frac{\delta\sqrt{\lambda'}}{s}\right)$$

$$
\begin{aligned}
50.)\quad \left[\frac{\cos\theta\ \cdot\ l_{t12}}{{S^t_{12+}}^3\,{S^t_{12-}}^3}\right]_\theta \;=\;& \frac{1}{4\,\bar\lambda}\left[\frac{\cos\theta\ \cdot\ l_{t12}}{{S^t_{12+}}^2\,{S^t_{12-}}^2}\right]_\theta \;+\; \frac{\delta}{4\,s'_-\bar\lambda}\left[\frac{l_{t12}}{{S^t_{12+}}^2\,{S^t_{12-}}^2}\right]_\theta \\
& - \frac{\delta}{s'_-}\left[\frac{l_{t12}}{{S^t_{12+}}^3\,{S^t_{12-}}^3}\right]_\theta \\
& + \frac{1}{32\,{s'_-}^2\bar\lambda}\Bigg[\quad \frac{\sqrt{\lambda'}\,\bar\lambda\,\delta}{2\,s\,s'_-\,s_{12}^2 s_{34}^2} \;+\; \frac{\bar\lambda}{4\,s_{12}^2 s_{34}^2}\,L_{c12} \\
& \qquad + \frac{1}{2\,s'_-\,s_{12}}\,L_{c1} \;-\; \frac{1}{2\,s'_-\,s_{34}}\,L_{c2} \\
& \qquad - \frac{\sqrt{\lambda'}\left((s'-\sigma)\,\bar\lambda + 2\,s\,s_{12}s_{34}\right)}{8\,s^2 s_{12}^2 s_{34}^2}\times \\
& \qquad\qquad \left(2\ln\frac{s_{12}}{s_{34}} - L_{c3} + L_{c4}\right) \\
& \qquad + \frac{\bar\lambda\lambda' + 2\,s_{12}s_{34}\left(s\,(s'-\sigma) + \bar\lambda\right)}{8\,s^2 s_{12}^2 s_{34}^2}\,(L_{c1} - L_{c2})\quad\Bigg]
\end{aligned}
$$

$$
\begin{aligned}
51.)\quad \left[\frac{l_{t_1u_2}}{2\sqrt{C_{12}}}\right]_\theta \;=\;& \frac{\mathrm{i}\cdot c_{12}}{x_0}\cdot\Bigg[\quad \mathrm{Li}_2\!\left(\frac{\beta_{12}+\mathrm{i}x_0}{\tau_1}\right) \;+\; \mathrm{Li}_2\!\left(\frac{\beta_{12}+\mathrm{i}x_0}{\tau_2}\right) \\
& \qquad + \mathrm{Li}_2\!\left(\frac{\beta_{12}+\mathrm{i}x_0}{\tau_1^*}\right) \;+\; \mathrm{Li}_2\!\left(\frac{\beta_{12}+\mathrm{i}x_0}{\tau_2^*}\right) \\
& \qquad - \mathrm{Li}_2\!\left(-\frac{\beta_{12}+\mathrm{i}x_0}{\tau_1}\right) \;-\; \mathrm{Li}_2\!\left(-\frac{\beta_{12}+\mathrm{i}x_0}{\tau_2}\right) \\
& \qquad - \mathrm{Li}_2\!\left(-\frac{\beta_{12}+\mathrm{i}x_0}{\tau_1^*}\right) \;-\; \mathrm{Li}_2\!\left(-\frac{\beta_{12}+\mathrm{i}x_0}{\tau_2^*}\right)\quad\Bigg]^{\dagger} \\
\equiv\;& c_{12}\cdot D_{t1u2}
\end{aligned}
$$

$$
\begin{aligned}
c_{12} &= \frac{s'}{s'_-\sqrt{\lambda'\,s\,s_{12}}} \\
x_0 &= \sqrt{\frac{s-s_{12}}{s}} \\
\beta_{12} &= \sqrt{\frac{s_{12}-4m_e^2}{s}}
\end{aligned}
$$

$$
\begin{aligned}
\tau_1 &= \frac{+q_{12}-\mathrm{i}p_{12}}{b_{12}+\mathrm{i}r_{12}} \qquad & q_{12} &= (ss'-ss_{34}-s's_{12})\sqrt{\frac{s_{12}}{s}} \\
\tau_2 &= \frac{-q_{12}-\mathrm{i}p_{12}}{b_{12}+\mathrm{i}r_{12}} & p_{12} &= s'_-\,s_{12}\cdot x_0 \\
& & r_{12} &= \sqrt{\lambda'\,s\,s_{12}}\cdot x_0 \\
& & b_{12} &= s_{12}\,(s-\delta)
\end{aligned}
$$

[†]Integrals 51.) to 60.) were not directly calculated from the result of the Ω_R integration. Instead, a Feynman parametrization was used to "linearize" $1/t_1u_2$ and $1/t_2u_1$: $1/t_1u_2 = \int_0^1 d\alpha/\left[t_1\alpha + u_2(1-\alpha)\right]^2$. Then, Ω_R, θ, and finally the Feynman parameter α were integrated.

52.) $$\left[\frac{l_{t_2u_1}}{2\sqrt{C_{21}}}\right]_\theta \;=\; \mathcal{T}\left(\left[\frac{l_{t_1u_2}}{2\sqrt{C_{12}}}\right]_\theta\right)^{\dagger} \;\equiv\; c_{34}\cdot D_{t2u1}$$

53.) $$\left[\frac{l_{t_1u_2}}{\bar{z}_1\cdot 2\sqrt{C_{12}}}\right]_\theta \;=\; \frac{s'}{4\sqrt{\lambda'}\,(ss'-ss_{34}-s's_{12})}\times\Bigg\{\; 2\,l_\beta\cdot(2L_{c5}-L_{c1})$$

$$+\;\ln^2\!\left(\frac{2\,x_1}{x_1-1}\right)\;-\;\ln^2\!\left(\frac{2\,x_1}{x_1+1}\right)\;+\;\mathrm{Li}_2\!\left(-\frac{x_1+1}{x_1-1}\right)\;-\;\mathrm{Li}_2\!\left(-\frac{x_1-1}{x_1+1}\right)$$

$$-\;\ln^2\!\left(\frac{2\,x_2}{x_2-1}\right)\;+\;\ln^2\!\left(\frac{2\,x_2}{x_2+1}\right)\;-\;\mathrm{Li}_2\!\left(-\frac{x_2+1}{x_2-1}\right)\;+\;\mathrm{Li}_2\!\left(-\frac{x_2-1}{x_2+1}\right)$$

$$-\;\ln\frac{x_1-x_2}{x_1+x_2}\cdot\left(\ln\frac{x_2-1}{x_2+1}\;-\;\ln\frac{x_1-1}{x_1+1}\right)$$

$$+\;\ln\frac{x_1-1}{x_1-x_2}\cdot\ln\left|\frac{x_2-1}{x_1-x_2}\right|\;-\;\ln\frac{x_1+1}{x_1-x_2}\cdot\ln\left|\frac{x_2+1}{x_1-x_2}\right|$$

$$+\;\ln\frac{x_1+1}{x_1+x_2}\cdot\ln\left|\frac{x_2-1}{x_1+x_2}\right|\;-\;\ln\frac{x_1-1}{x_1+x_2}\cdot\ln\left|\frac{x_2+1}{x_1+x_2}\right|$$

$$+\;2\,\mathrm{Li}_2\!\left(-\frac{x_2-1}{x_1-x_2}\right)\;-\;2\,\mathrm{Li}_2\!\left(-\frac{x_2+1}{x_1-x_2}\right)$$

$$+\;\frac{s'_-\sqrt{s_{12}}}{\sqrt{s\lambda'}}\cdot\Re\mathrm{e}\left[\;\;\sum_{i=1}^{2}\frac{(-1)^{i+1}\cdot(x_i-a_{12})}{\sqrt{\beta^2\,x_i^2-x_0^2}}\times\right.$$

$$\sum_{k=1}^{8}(-1)^{k+1}\Bigg(\;\;\ln\frac{t^{(i)}_{k+}}{t^0_k}\cdot\Big(\ln\Big[u^{(i)}_+(+\beta)\Big]-\ln\Big[u^{(i)}_+(-\beta)\Big]-2\pi\mathrm{i}\cdot\Theta(x_i)\Big)$$

$$-\ln\frac{t^{(i)}_{k-}}{t^0_k}\cdot\Big(\ln\Big[u^{(i)}_-(+\beta)\Big]-\ln\Big[u^{(i)}_-(-\beta)\Big]-2\pi\mathrm{i}\cdot\Theta(-x_i)\Big)$$

$$-\,\mathrm{Li}_2\left[-\frac{u^{(i)}_+(+\beta)}{t^{(i)}_{k+}}\right]\;+\;\mathrm{Li}_2\left[-\frac{u^{(i)}_+(-\beta)}{t^{(i)}_{k+}}\right]$$

$$\left.\left.+\,\mathrm{Li}_2\left[-\frac{u^{(i)}_-(+\beta)}{t^{(i)}_{k-}}\right]\;-\;\mathrm{Li}_2\left[-\frac{u^{(i)}_-(-\beta)}{t^{(i)}_{k-}}\right]\;\;\right)\;\;\right]\;\;\Bigg\}$$

$$\equiv\;\frac{s'}{4\sqrt{\lambda'}\,(ss'-ss_{34}-s's_{12})}\cdot\Big\{2\,l_\beta\cdot(2L_{c5}-L_{c1})\;+\;D^z_{t1u2}\Big\}$$

[†]Here and in the remainder of this section the expressions obtained by the symmetry operation $\mathcal{T}$ will not be rewritten. The reader can easily do that by making the reciprocal replacement $s_{12}\leftrightarrow s_{34}$.

$$
\begin{aligned}
a_{12} &= \frac{s-\delta}{s'_-} \\
t_1^0 &= \tau_1 & t_2^0 &= -\tau_1 \\
t_3^0 &= \tau_2 & t_4^0 &= -\tau_2 \\
t_5^0 &= \tau_2^* & t_6^0 &= -\tau_2^* \\
t_7^0 &= \tau_1^* & t_8^0 &= -\tau_1^* \\
t_{k\pm}^{(i)} &= t_k^0 \; + \; t_\pm^{(i)} & u_\pm^{(i)}(x) &= t(x) \; - \; t_\pm^{(i)} \\
t_\pm^{(i)} &= \frac{\mathrm{i}x_0 \pm \sqrt{\beta^2 x_i^2 - {x_0}^2}}{x_i} & t(x) &= \frac{\mathrm{i}x_0 + \sqrt{x^2 - {x_0}^2}}{x} \\
x_{1/2} &= \frac{s'_-\, s_{12}(s-\delta) \pm \sqrt{\lambda'}\,(ss' - ss_{34} - s's_{12})}{{s'_-}^2 s_{12} - s\lambda'} \\
\beta &= \sqrt{1 - \frac{4\,m_e^2}{s}}
\end{aligned}
$$

54.) $$\left[\frac{l_{t_2u_1}}{\bar{z}_1 \cdot 2\sqrt{C_{21}}}\right]_\theta = \mathcal{T}\left(\left[\frac{l_{t_1u_2}}{\bar{z}_1 \cdot 2\sqrt{C_{12}}}\right]_\theta\right)$$
$$\equiv \frac{s'}{4\sqrt{\lambda'}\;(ss' - ss_{12} - s's_{34})} \cdot \left\{2\,l_\beta \cdot (2L_{c5} - L_{c2}) \; + \; D^z_{t2u1}\right\}$$

55.) $$\left[\frac{l_{t_1u_2}}{\bar{z}_2 \cdot 2\sqrt{C_{12}}}\right]_\theta = \left[\frac{l_{t_1u_2}}{\bar{z}_1 \cdot 2\sqrt{C_{12}}}\right]_\theta$$

56.) $$\left[\frac{l_{t_2u_1}}{\bar{z}_2 \cdot 2\sqrt{C_{21}}}\right]_\theta = \mathcal{T}\left(\left[\frac{l_{t_1u_2}}{\bar{z}_1 \cdot 2\sqrt{C_{12}}}\right]_\theta\right)$$

57.) $$\left[\frac{l_{t_1u_2}}{a_1^{ut}\cdot 2\sqrt{C_{12}}}\right]_\theta = \frac{s'}{s'_-}\cdot \Re e\left(X_0+X_1+X_2\right)$$

$$\equiv \frac{s'}{s'_-}\cdot D^a_{t1u2}$$

For the calculation of the integrals X_i the following quantities are needed:

$$\begin{aligned}
A_3 &= s_{12}\left(s'_+ - 2\sigma\right)^2 - \beta^2 s\lambda' \\
B_3 &= s_{12}\left(s'_+ - 2\sigma\right)(s-\delta) \\
\Delta_3 &= \lambda'\cdot\Big[\left\{ss' - ss_{34} - s's_{12} - 2s_{12}(s-\sigma)\right\}^2 \\
&\qquad - 4m_e^2\left\{s_{12}(s-\delta)^2 + \lambda'(s-s_{12})\right\}\Big] \\
x_{3/4} &= \beta\cdot\frac{-B_3 \pm \sqrt{\Delta_3}}{A_3}
\end{aligned}$$

In principle, depending on the values of x_3 and x_4, four cases have to be distinguished:

$$\begin{array}{lllllll}
(i) & x_{3/4}\,\epsilon\,I\!R; & |x_4| & \geq & |x_3| & > & \beta \\
(ii) & x_{3/4}\,\epsilon\,I\!R; & |x_4| & > & \beta & \geq & |x_3| \\
(iii) & x_{3/4}\,\epsilon\,I\!R; & \beta & \geq & |x_4| & \geq & |x_3| \\
(iv) & \Delta_3 \leq 0; & x_3 & = & x_4^* & \epsilon & \mathbb{C}
\end{array}$$

However, since the integrand is regular, it is sufficient to present the solution for case (i). The solutions for the other three cases are then obtained by analytical continuation. In case (iv), which is relevant for only a very small fraction of the phase space, the problem of a numerically correct treatment arises. This problem was solved by computing the integral's value for a very nearby phase space point so that the expression of case (i) could be used. Having in mind that the integral is regular, it is clear that thus only a negligible error is introduced. The expressions $X_0,\ X_1$, and X_2 for case (i) are presented below.

$$X_0 = \frac{2}{\sqrt{\Delta_3}}\cdot L_{c8}\cdot\left[\ln\left(\frac{\beta-x_3}{\beta+x_3}\right) - \ln\left(\frac{\beta-x_4}{\beta+x_4}\right)\right]$$

$$
\begin{aligned}
X_1 \;=\; & \frac{\sqrt{s_{12}}\cdot\left(s'_+ - \sigma\right)}{2\,\sqrt{s\,\lambda'\,\Delta_3}} \;\cdot\; \sum_{i=3}^{4} \frac{(-1)^{i+1}\cdot(x_i - a_{34})}{\sqrt{x_i^2 - x_0^2}} \;\times \\
& \sum_{k=1}^{8}(-1)^{k+1}\Bigg(\quad \ln\frac{t^{(i)}_{k+}}{t^0_k}\cdot\Big(\ln\Big[u^{(i)}_+(+\beta)\Big] - \ln\Big[u^{(i)}_+(-\beta)\Big] - 2\pi\mathrm{i}\cdot\Theta(x_i)\Big) \\
& \qquad - \ln\frac{t^{(i)}_{k-}}{t^0_k}\cdot\Big(\ln\Big[u^{(i)}_-(+\beta)\Big] - \ln\Big[u^{(i)}_-(-\beta)\Big] - 2\pi\mathrm{i}\cdot\Theta(-x_i)\Big) \\
& \qquad - \mathrm{Li}_2\left[-\frac{u^{(i)}_+(+\beta)}{t^{(i)}_{k+}}\right] \;+\; \mathrm{Li}_2\left[-\frac{u^{(i)}_+(-\beta)}{t^{(i)}_{k+}}\right] \\
& \qquad + \mathrm{Li}_2\left[-\frac{u^{(i)}_-(+\beta)}{t^{(i)}_{k-}}\right] \;-\; \mathrm{Li}_2\left[-\frac{u^{(i)}_-(-\beta)}{t^{(i)}_{k-}}\right] \quad \Bigg)
\end{aligned}
$$

$$
a_{34} \;=\; -\frac{s-\delta}{s'_+ - 2\sigma}
$$

$$
t^{(i)}_{\pm k} \;=\; t^0_k \;+\; t^{(i)}_\pm \qquad\qquad u^{(i)}_\pm(x) \;=\; t(x) \;-\; t^{(i)}_\pm
$$

$$
t^{(i)}_\pm \;=\; \frac{\mathrm{i}x_0 \pm \sqrt{x_i^2 - {x_0}^2}}{x_i} \qquad\qquad t(x) \;=\; \frac{\mathrm{i}x_0 + \sqrt{x^2 - {x_0}^2}}{x}
$$

$$
\begin{aligned}
X_2 \;=\; & -\frac{1}{2\,\sqrt{\Delta_3}} \;\times \\
& \sum_{i=1}^{2}\sum_{j=1}^{2}(-1)^{j+1}\Bigg(\quad \ln\frac{x_i - x_j - \mathrm{i}\varepsilon}{x_i + x_j - \mathrm{i}\varepsilon}\cdot\ln\frac{x_j - \beta}{x_j + \beta} \\
& \qquad - \mathrm{Li}_2\left[-\frac{x_j - \beta}{x_i - x_j - \mathrm{i}\varepsilon}\right] \;+\; \mathrm{Li}_2\left[-\frac{x_j + \beta}{x_i - x_j - \mathrm{i}\varepsilon}\right] \\
& \qquad + \mathrm{Li}_2\left[\frac{x_j - \beta}{x_i + x_j - \mathrm{i}\varepsilon}\right] \;-\; \mathrm{Li}_2\left[\frac{x_j + \beta}{x_i + x_j - \mathrm{i}\varepsilon}\right] \quad \Bigg)
\end{aligned}
$$

58.) $$\left[\frac{l_{t_2u_1}}{a_1^{ut}\cdot 2\sqrt{C_{21}}}\right]_\theta = \mathcal{T}\left(\left[\frac{l_{t_1u_2}}{a_1^{ut}\cdot 2\sqrt{C_{12}}}\right]_\theta\right) \equiv \frac{s'}{s'_-}\cdot D^a_{t2u1}$$

59.) $$\left[\frac{l_{t_1u_2}}{a_2^{ut}\cdot 2\sqrt{C_{12}}}\right]_\theta = \left[\frac{l_{t_1u_2}}{a_1^{ut}\cdot 2\sqrt{C_{12}}}\right]_\theta$$

60.) $$\left[\frac{l_{t_2u_1}}{a_2^{ut}\cdot 2\sqrt{C_{21}}}\right]_\theta = \mathcal{T}\left(\left[\frac{l_{t_1u_2}}{a_1^{ut}\cdot 2\sqrt{C_{12}}}\right]_\theta\right)$$

G.5 Loop Integrals

For the computation of the virtual initial state QED corrections to the studied process (1.1), apart from the integration over final state fermion decay angles, two sets of integrals are needed. The second set is given in section G.6. The first set is presented in this section and consists of the integration over the loop momentum p.

It is sufficient to present the integrals for the virtual t-channel graphs, because the interferences of the virtual u-channel graphs with the Born level t- and u-channel graphs equal the interferences of the virtual t-channel graphs with the Born level u-channel and t-channel graphs. This is easily verified by symmetry arguments. First, some definitions are introduced:

$$\begin{aligned}
\frac{1}{\Pi_0} &= \frac{1}{p^2-\mathrm{i}\varepsilon}\\
\frac{1}{\Pi_1} &= \frac{1}{(p-k_1)^2+m_e^2-\mathrm{i}\varepsilon} = \frac{1}{p^2-2pk_1-\mathrm{i}\varepsilon}\\
\frac{1}{\Pi_2} &= \frac{1}{(p+k_2)^2+m_e^2-\mathrm{i}\varepsilon} = \frac{1}{p^2+2pk_2-\mathrm{i}\varepsilon}\\
\frac{1}{\Pi_q} &= \frac{1}{(p-q_t)^2+m_e^2-\mathrm{i}\varepsilon} \quad .
\end{aligned} \tag{G.5}$$

The momenta k_1, k_2, and q_t are carried by the incoming electron, the incoming positron and the intermediate initial state electron. For brevity, $q\equiv q_t$ with $q^2=t$ (compare equation (E.5)) will be used subsequently. Dimensional regularization is used to consistently

treat divergent loop integrals. The following notations are employed:

$$[A]_n \equiv \mu^{(4-n)} \int \frac{d^n p}{(2\pi)^n}\, A \,\Big|_{\mu=m_e} \qquad \text{with} \quad |n-4| \ll 1\,, \tag{G.6}$$

$$\mathrm{P} \equiv \frac{1}{n-4} + \frac{1}{2}\,\gamma_E + \ln\frac{m_e}{\mu} - \ln\Big(2\sqrt{\pi}\Big)\,\Big|_{\mu=m_e} \qquad n = 4-\varepsilon\,, \tag{G.7}$$

$$\mathrm{P}^{\mathrm{IR}} \equiv \frac{1}{n-4} + \frac{1}{2}\,\gamma_E + \ln\frac{m_e}{\mu} - \ln\Big(2\sqrt{\pi}\Big)\,\Big|_{\mu=m_e} \qquad n = 4+\varepsilon\,, \tag{G.8}$$

and

$$\begin{aligned}
l_0 &\equiv \ln\left(-\frac{s}{m_e^2 - \mathrm{i}\varepsilon}\right) = \ln\frac{s}{m_e^2} - \mathrm{i}\pi = l_\beta - \mathrm{i}\pi \\
l_1 &\equiv \ln\left(-\frac{s_{12}}{m_e^2 - \mathrm{i}\varepsilon}\right) = \ln\frac{s_{12}}{m_e^2} - \mathrm{i}\pi \\
l_2 &\equiv \ln\left(-\frac{s_{34}}{m_e^2 - \mathrm{i}\varepsilon}\right) = \ln\frac{s_{34}}{m_e^2} - \mathrm{i}\pi \\
l_t &\equiv \ln\left(\frac{q^2 + m_e^2}{m_e^2}\right) \overset{\mathrm{URA}}{=} \ln\frac{q^2}{m_e^2} \qquad .
\end{aligned} \tag{G.9}$$

Euler's constant has the value $\gamma_E = 0.577216...$. The difference between the ultraviolet divergence P and the infrared divergence P^{IR} is that P is regularized by $n = 4-\varepsilon$ and P^{IR} by $n = 4+\varepsilon$ with $0 < \varepsilon \ll 1$. In the URA one obtains:

1.) $\left[\frac{1}{\Pi_0\Pi_1}\right]_n = \frac{\mathrm{i}}{16\,\pi^2}\Big(-2\mathrm{P}+2\Big)$ 2.) $\left[\frac{1}{\Pi_0\Pi_2}\right]_n = \frac{\mathrm{i}}{16\,\pi^2}\Big(-2\mathrm{P}+2\Big)$

3.) $\left[\frac{p^\mu}{\Pi_0\Pi_1}\right]_n = \frac{\mathrm{i}\cdot k_1^\mu}{16\,\pi^2}\left(-\mathrm{P}+\frac{1}{2}\right)$ 4.) $\left[\frac{p^\mu}{\Pi_0\Pi_2}\right]_n = -\frac{\mathrm{i}\cdot k_2^\mu}{16\,\pi^2}\left(-\mathrm{P}+\frac{1}{2}\right)$

5.) $\left[\frac{1}{\Pi_0\Pi_q}\right]_n = \frac{\mathrm{i}}{16\,\pi^2}\Big(-2\mathrm{P}-l_t+2\Big)$

6.) $\left[\frac{p^\mu}{\Pi_0\Pi_q}\right]_n = \frac{\mathrm{i}\cdot q^\mu}{16\,\pi^2}\left(-\mathrm{P}-\frac{l_t}{2}+1\right)$

7.) $\left[\frac{1}{\Pi_1\Pi_2}\right]_n = \frac{\mathrm{i}}{16\,\pi^2}\Big(-2\mathrm{P}-l_0+2\Big)$

8.) $\left[\frac{p^\mu}{\Pi_1\Pi_2}\right]_n = \frac{\mathrm{i}}{16\,\pi^2}\,(k_1-k_2)^\mu\left(-\mathrm{P}-\frac{l_0}{2}+1\right)$

9.) $$\left[\frac{1}{\Pi_1\Pi_q}\right]_n = \frac{\mathrm{i}}{16\,\pi^2}\Big(-2\mathrm{P}-l_1+2\Big)$$

10.) $$\left[\frac{1}{\Pi_2\Pi_q}\right]_n = \frac{\mathrm{i}}{16\,\pi^2}\Big(-2\mathrm{P}-l_2+2\Big)$$

11.) $$\left[\frac{p^\mu}{\Pi_1\Pi_q}\right]_n = \frac{\mathrm{i}}{16\,\pi^2}\,(q^\mu+k_1^\mu)\left(-\mathrm{P}-\frac{l_1}{2}+1\right)$$

12.) $$\left[\frac{p^\mu}{\Pi_2\Pi_q}\right]_n = \frac{\mathrm{i}}{16\,\pi^2}\,(q^\mu-k_2^\mu)\left(-\mathrm{P}-\frac{l_2}{2}+1\right)$$

13.) $$\left[\frac{1}{\Pi_0\Pi_1\Pi_2}\right]_n = \frac{\mathrm{i}}{16\,\pi^2}\left[-\frac{2\,l_0}{s}\cdot\mathrm{P}^{\mathrm{IR}}\;+\;\frac{1}{s}\left(\frac{\pi^2}{6}-\frac{l_0^2}{2}\right)\right]$$

14.) $$\left[\frac{p^\mu}{\Pi_0\Pi_1\Pi_2}\right]_n = -\frac{\mathrm{i}}{16\,\pi^2}\,(k_1-k_2)^\mu\cdot\frac{l_0}{s}$$

15.) $$\left[\frac{p^\mu p^\nu}{\Pi_0\Pi_1\Pi_2}\right]_n = \frac{\mathrm{i}}{16\,\pi^2}\left[\quad g^{\mu\nu}\cdot\left(-\frac{1}{2}\mathrm{P}-\frac{l_0}{4}+\frac{3}{4}\right)\right.$$
$$\left.+\;(k_1^\mu k_1^\nu+k_2^\mu k_2^\nu)\cdot\frac{1-l_0}{2s}\;+\;(k_1^\mu k_2^\nu+k_2^\mu k_1^\nu)\cdot\frac{1}{2s}\right]$$

16.) $$\left[\frac{1}{\Pi_0\Pi_1\Pi_q}\right]_n = \frac{\mathrm{i}}{16\,\pi^2}\cdot\frac{1}{t+s_{12}}\cdot\left[\frac{1}{2}\Big(l_t-l_1\Big)\Big(3l_1-l_t\Big)-2\,\mathrm{Li}_2\left(\frac{t+s_{12}-\mathrm{i}\varepsilon}{s_{12}}\right)\right]$$

17.) $$\left[\frac{1}{\Pi_0\Pi_2\Pi_q}\right]_n = \frac{\mathrm{i}}{16\,\pi^2}\cdot\frac{1}{t+s_{34}}\cdot\left[\frac{1}{2}\Big(l_t-l_2\Big)\Big(3l_2-l_t\Big)-2\,\mathrm{Li}_2\left(\frac{t+s_{34}-\mathrm{i}\varepsilon}{s_{34}}\right)\right]$$

18.) $$\left[\frac{p^\mu}{\Pi_0\Pi_1\Pi_q}\right]_n = \frac{\mathrm{i}}{16\,\pi^2}\cdot\frac{1}{t+s_{12}}\cdot\left\{q^\mu\Big(l_t-l_1\Big)\right.$$
$$\left.+\,k_1^\mu\left(-l_1\;+\;t\cdot\left[\frac{1}{\Pi_0\Pi_1\Pi_q}\right]_n-\;\frac{2t}{t+s_{12}}\Big(l_t-l_1\Big)\right)\right\}$$

19.) $$\left[\frac{p^\mu}{\Pi_0\Pi_2\Pi_q}\right]_n = \frac{\mathrm{i}}{16\,\pi^2}\cdot\frac{1}{t+s_{34}}\cdot\left\{q^\mu\Big(l_t-l_2\Big)\right.$$
$$\left.-\,k_2^\mu\left(-l_2\;+\;t\cdot\left[\frac{1}{\Pi_0\Pi_2\Pi_q}\right]_n-\;\frac{2t}{t+s_{34}}\Big(l_t-l_2\Big)\right)\right\}$$

$$20.)\quad \left[\frac{p^\mu p^\nu}{\Pi_0\Pi_1\Pi_q}\right]_n = \frac{\mathrm{i}}{16\,\pi^2}\cdot\left\{ g^{\mu\nu}\cdot\left(-\frac{\mathrm{P}}{2}+\frac{3}{4}-\frac{1}{4\,(t+s_{12})}\left(t\cdot l_t+s_{12}\cdot l_1\right)\right) + \frac{k_1^\mu k_1^\nu}{t+s_{12}}\cdot\left\{ \left(\frac{1}{2}+\frac{t}{t+s_{12}}\right)\left(1-l_1\right) - \frac{3\,t^2}{\left(t+s_{12}\right)^2}\left(l_t-l_1\right) + \frac{t^2}{t+s_{12}}\cdot\left[\frac{1}{\Pi_0\Pi_1\Pi_q}\right]_n \right\} + \frac{k_1^\mu q^\nu+k_1^\nu q^\mu}{2\,(t+s_{12})}\cdot\left\{\frac{t}{t+s_{12}}\left(l_t-l_1\right)-1\right\} + \frac{q^\mu q^\nu}{2\,(t+s_{12})}\cdot\left(l_t-l_1\right) \right\}$$

$$21.)\quad \left[\frac{p^\mu p^\nu}{\Pi_0\Pi_2\Pi_q}\right]_n = \frac{\mathrm{i}}{16\,\pi^2}\cdot\left\{ g^{\mu\nu}\cdot\left(-\frac{\mathrm{P}}{2}+\frac{3}{4}-\frac{1}{4\,(t+s_{34})}\left(t\cdot l_t+s_{34}\cdot l_2\right)\right) + \frac{k_2^\mu k_2^\nu}{t+s_{34}}\cdot\left\{ \left(\frac{1}{2}+\frac{t}{t+s_{34}}\right)\left(1-l_2\right) - \frac{3\,t^2}{\left(t+s_{34}\right)^2}\left(l_t-l_2\right) + \frac{t^2}{t+s_{34}}\cdot\left[\frac{1}{\Pi_0\Pi_2\Pi_q}\right]_n \right\} - \frac{k_2^\mu q^\nu+k_2^\nu q^\mu}{2\,(t+s_{34})}\cdot\left\{\frac{t}{t+s_{34}}\left(l_t-l_2\right)-1\right\} + \frac{q^\mu q^\nu}{2\,(t+s_{34})}\cdot\left(l_t-l_2\right) \right\}$$

22.) $$\left[\frac{1}{\Pi_1\Pi_2\Pi_q}\right]_n = \frac{\mathrm{i}}{16\,\pi^2\cdot\sqrt{\lambda}}\cdot\left\{2\,\mathrm{Li}_2(x_2)\;-\;2\,\mathrm{Li}_2(x_1)\;+\;\ln(x_1x_2)\cdot\ln\left(\frac{1-x_2}{1-x_1}\right)\right\}$$

$$\equiv \frac{\mathrm{i}}{16\,\pi^2}\cdot\mathrm{I}_{12\mathrm{q}}$$

$$x_{1/2} = \frac{s-\delta\pm\sqrt{\lambda}}{2\,s} \qquad \Rightarrow \qquad x_1\cdot x_2 \;=\; \frac{s_{34}}{s}$$

$$\frac{1-x_2}{1-x_1} \;=\; \frac{s+\delta+\sqrt{\lambda}}{s+\delta-\sqrt{\lambda}}$$

23.) $$\left[\frac{p^\mu}{\Pi_1\Pi_2\Pi_q}\right]_n = \frac{\mathrm{i}}{16\,\pi^2\cdot\lambda}\;\times$$

$$\left\{\quad q^\mu\left(s\left(s-\sigma\right)\mathrm{I}_{12\mathrm{q}}\;-\;(s+\delta)\ln\frac{s_{12}}{s}\;-\;(s-\delta)\ln\frac{s_{34}}{s}\right)\right.$$

$$+\,k_1^\mu\left(-\,s_{34}\left(s+\delta\right)\mathrm{I}_{12\mathrm{q}}\;+\;(s-\sigma)\ln\frac{s_{12}}{s}\;+\;2\,s_{34}\ln\frac{s_{34}}{s}\right)$$

$$\left.+\,k_2^\mu\left(s_{12}\left(s-\delta\right)\mathrm{I}_{12\mathrm{q}}\;-\;2\,s_{12}\ln\frac{s_{12}}{s}\;-\;(s-\sigma)\ln\frac{s_{34}}{s}\right)\quad\right\}$$

$$24.)\quad \left[\frac{p^\mu p^\nu}{\Pi_1\Pi_2\Pi_q}\right]_n = \frac{\mathrm{i}}{16\,\pi^2}\cdot\Big\{\quad g^{\mu\nu}\cdot F_{21} \;+\; q^\mu q^\nu\cdot F_{22} \;+\; k_1^\mu k_1^\nu\cdot F_{23} \;+\; k_2^\mu k_2^\nu\cdot F_{24}$$
$$+\;\Big(k_1^\mu k_2^\nu + k_1^\nu k_2^\mu\Big)\cdot F_{25} \;+\; \Big(k_1^\mu q^\nu + k_1^\nu q^\mu\Big)\cdot F_{26}$$
$$+\;\Big(k_2^\mu q^\nu + k_2^\nu q^\mu\Big)\cdot F_{27}\quad\Big\}$$

$$F_{21} = \frac{1}{4}\left\{\frac{1}{\lambda}\left[s_{12}\Big(s-\delta\Big)\ln\frac{s_{12}}{s} \;+\; s_{34}\Big(s+\delta\Big)\ln\frac{s_{34}}{s} \;-\; 2ss_{12}s_{34}\,\mathrm{I}_{12\mathrm{q}}\right]\right.$$
$$\left. -\,2\mathrm{P}+3-l_0\quad\right\}$$

$$F_{22} = \frac{1}{\lambda}\left\{-\,s \;-\; \frac{1}{2}\left[3s \;+\; \delta \;+\; \frac{6ss_{12}}{\lambda}\Big(s-\delta\Big)\right]\cdot\ln\frac{s_{12}}{s}\right.$$
$$+\;\frac{1}{2}\left[3s \;-\; \delta \;+\; \frac{6ss_{34}}{\lambda}\Big(s+\delta\Big)\right]\cdot\ln\frac{s_{34}}{s}$$
$$\left. +\,s^2\left[1 \;+\; \frac{6\,s_{12}s_{34}}{\lambda}\right]\cdot\mathrm{I}_{12\mathrm{q}}\qquad\right\}$$

$$F_{23} = \frac{1}{\lambda}\left\{-\,s_{34} \;+\; \frac{1}{2}\left[s \;-\; s_{12} \;-\; 3s_{34} \;-\; \frac{6\,s_{12}s_{34}}{\lambda}\Big(s-\delta\Big)\right]\cdot\ln\frac{s_{12}}{s}\right.$$
$$\left. -\,\frac{3\,s_{34}^2}{\lambda}\Big(s+\delta\Big)\ln\frac{s_{34}}{s} \;+\; s_{34}^2\left[1 \;+\; \frac{6\,ss_{12}}{\lambda}\right]\cdot\mathrm{I}_{12\mathrm{q}}\qquad\right\}$$

$$F_{24} = \frac{1}{\lambda}\left\{-\,s_{12} \;+\; \frac{1}{2}\left[s \;-\; s_{34} \;-\; 3s_{12} \;-\; \frac{6\,s_{34}s_{12}}{\lambda}\Big(s+\delta\Big)\right]\cdot\ln\frac{s_{34}}{s}\right.$$
$$\left. -\,\frac{3\,s_{12}^2}{\lambda}\Big(s-\delta\Big)\ln\frac{s_{12}}{s} \;+\; s_{12}^2\left[1 \;+\; \frac{6\,ss_{34}}{\lambda}\right]\cdot\mathrm{I}_{12\mathrm{q}}\qquad\right\}$$

$$F_{25} = \frac{1}{2\lambda}\left\{s-\sigma \;+\; s_{12}\left[1 \;+\; \frac{6\,s_{34}}{\lambda}\Big(s+\delta\Big)\right]\cdot\ln\frac{s_{12}}{s}\right.$$
$$+\;s_{34}\left[1 \;+\; \frac{6\,s_{12}}{\lambda}\Big(s-\delta\Big)\right]\cdot\ln\frac{s_{34}}{s}$$
$$\left. +\,2\,s_{12}s_{34}\left[1 \;-\; \frac{3\,s}{\lambda}\Big(s-\sigma\Big)\right]\cdot\mathrm{I}_{12\mathrm{q}}\qquad\right\}$$

$$
\begin{aligned}
F_{26} \;=\; \frac{1}{\lambda}\Bigg\{ & \frac{s-\delta}{2} + \left[\frac{s+s_{34}}{2} + \frac{6\,s s_{12} s_{34}}{\lambda}\right]\cdot \ln\frac{s_{12}}{s} \\
& - \left[\frac{s_{34}}{2} - \frac{3\,s s_{34}}{\lambda}\Big(s-\sigma\Big)\right]\cdot \ln\frac{s_{34}}{s} \\
& - s s_{34}\left[1 + \frac{3\,s_{12}}{\lambda}\Big(s-\delta\Big)\right]\cdot \mathrm{I}_{12\mathrm{q}} \Bigg\}
\end{aligned}
$$

$$
\begin{aligned}
F_{27} \;=\; -\frac{1}{\lambda}\Bigg\{ & \frac{s+\delta}{2} + \left[\frac{s+s_{12}}{2} + \frac{6\,s s_{12} s_{34}}{\lambda}\right]\cdot \ln\frac{s_{34}}{s} \\
& - \left[\frac{s_{12}}{2} - \frac{3\,s s_{12}}{\lambda}\Big(s-\sigma\Big)\right]\cdot \ln\frac{s_{12}}{s} \\
& - s s_{12}\left[1 + \frac{3\,s_{34}}{\lambda}\Big(s+\delta\Big)\right]\cdot \mathrm{I}_{12\mathrm{q}} \Bigg\}
\end{aligned}
$$

As mentioned in appendix E.2, a FORM computer algebra program was used to handle the many terms in the virtual corrections' calculation. Inspection of the FORM code at an intermediate level showed that, for the calculation of virtual QED corrections to process (1.1) (see appendix E.2), the four-point function is only needed in one specific Lorentz contraction. Precisely this Lorentz contraction is given below.

25.) $$\left[\frac{2\,p\cdot q}{\Pi_0\Pi_1\Pi_2\Pi_q}\right]_n \;=\; \frac{\mathrm{i}}{16\,\pi^2}\cdot\left\{\mathrm{I}_{12\mathrm{q}} + \frac{1}{s}\left[l_0\Big(l_1+l_2-2\,l_t\Big) + \frac{1}{2}\ln^2\frac{s_{12}}{s_{34}}\right]\right\}$$

G.6 Virtual Corrections' Phase Space Integrals

After the integration over the loop momentum, there is one non-trivial integration left when the virtual initial state corrections to process (1.1) are to be evaluated. This is the integration over the boson scattering angle ϑ in the center of mass system. It should be recalled that it is sufficient to present the integrals for the t-channel case and the t-channel/u-channel interference for reasons of symmetry. Making use of the URA and the notations

$$[A]_V \equiv \frac{\sqrt{\lambda}}{2}\int_{-1}^{+1} d\cos\vartheta\ A = \int_{t_{min}}^{t_{max}} dt\ A \tag{G.10}$$

$$\begin{aligned} t_{12} &= t + s_{12} \\ t_{34} &= t + s_{34} \end{aligned}$$

$$\begin{aligned} d_{12} &= \frac{s - s_{34}}{s_{12}} \qquad & t_{max} &= \frac{s - \sigma + \sqrt{\lambda}}{2} \\ d_{34} &= \frac{s - s_{12}}{s_{34}} \qquad & t_{min} &= \frac{s - \sigma - \sqrt{\lambda}}{2} \end{aligned}$$

the following list of integrals is obtained.

1.) $[\,1\,]_V = \sqrt{\lambda}$

2.) $[\,t\,]_V = \frac{\sqrt{\lambda}}{2}\cdot(s-\sigma)$

3.) $[\,t^2\,]_V = \frac{\sqrt{\lambda}}{3}\cdot\left\{(s-\sigma)^2 - s_{12}s_{34}\right\}$

4.) $\left[\frac{1}{t}\right]_V = \ln\frac{s-\sigma+\sqrt{\lambda}}{s-\sigma-\sqrt{\lambda}} \equiv \mathcal{L}_B$

5.) $\left[\frac{1}{u}\right]_V = \mathcal{L}_B$

6.) $\left[\frac{1}{t_{12}}\right]_V = \ln\frac{s+\delta+\sqrt{\lambda}}{s+\delta-\sqrt{\lambda}} \equiv \mathcal{L}_{12}$

7.) $\left[\frac{1}{t_{34}}\right]_V = \ln\frac{s-\delta+\sqrt{\lambda}}{s-\delta-\sqrt{\lambda}} \equiv \mathcal{L}_{34}$

8.) $\left[\frac{1}{t^2}\right]_V = \frac{\sqrt{\lambda}}{s_{12}s_{34}}$

9.) $\left[\frac{1}{t\cdot u}\right]_V = \frac{2}{s-\sigma}\cdot\mathcal{L}_B$

10.) $\left[\frac{1}{{t_{12}}^2}\right]_V = \frac{\sqrt{\lambda}}{ss_{12}}$

11.) $\left[\frac{1}{{t_{34}}^2}\right]_V = \frac{\sqrt{\lambda}}{ss_{34}}$

12.) $[\,l_t\,]_V = \frac{s-\sigma}{2}\cdot\mathcal{L}_B + \frac{\sqrt{\lambda}}{2}\cdot\mathcal{L}_S - \sqrt{\lambda}$

$$\mathcal{L}_S = \left(2\,l_\beta + \ln\frac{s_{12}}{s} + \ln\frac{s_{34}}{s}\right)$$

13.) $$\left[\frac{l_t}{t}\right]_V = \frac{1}{2}\,\mathcal{L}_B{\cdot}\mathcal{L}_S$$

14.) $$\left[\frac{l_t}{u}\right]_V = \ln\frac{s-\sigma}{m_e^2}{\cdot}\mathcal{L}_B \;-\; \mathrm{Li}_2\Big(\frac{t_{max}}{s-\sigma}\Big) \;+\; \mathrm{Li}_2\Big(\frac{t_{min}}{s-\sigma}\Big)$$

15.) $$\left[\frac{l_t}{t_{12}}\right]_V = \frac{\mathcal{L}_{12}{\cdot}\mathcal{L}_S}{2} \;-\; \frac{\mathcal{L}_B}{2}{\cdot}\ln\frac{s_{12}}{s} \;+\; \mathrm{Li}_2\Big(-\frac{t_{max}}{s_{12}}\Big) \;-\; \mathrm{Li}_2\Big(-\frac{t_{min}}{s_{12}}\Big)$$

16.) $$\left[\frac{l_t}{t_{34}}\right]_V = \frac{\mathcal{L}_{34}{\cdot}\mathcal{L}_S}{2} \;-\; \frac{\mathcal{L}_B}{2}{\cdot}\ln\frac{s_{34}}{s} \;+\; \mathrm{Li}_2\Big(-\frac{t_{max}}{s_{34}}\Big) \;-\; \mathrm{Li}_2\Big(-\frac{t_{min}}{s_{34}}\Big)$$

17.) $$\left[\frac{l_t}{t^2}\right]_V = \frac{1}{2\,s_{12}s_{34}}\Big(\sqrt{\lambda}{\cdot}(\mathcal{L}_S+2) \;-\; (s-\sigma){\cdot}\mathcal{L}_B\Big)$$

18.) $$\left[\frac{l_t}{{t_{12}}^2}\right]_V = \frac{1}{s_{12}}\left(\frac{s-\delta}{2s}{\cdot}\mathcal{L}_B \;-\; \mathcal{L}_{12} \;+\; \frac{\sqrt{\lambda}}{2s}{\cdot}\mathcal{L}_S\right)$$

19.) $$\left[\frac{l_t}{{t_{34}}^2}\right]_V = \frac{1}{s_{34}}\left(\frac{s+\delta}{2s}{\cdot}\mathcal{L}_B \;-\; \mathcal{L}_{34} \;+\; \frac{\sqrt{\lambda}}{2s}{\cdot}\mathcal{L}_S\right)$$

20.) $$\left[{l_t}^2\right]_V = \frac{s-\sigma}{2}{\cdot}\Big(\mathcal{L}_S-2\Big){\cdot}\mathcal{L}_B \;+\; \sqrt{\lambda}\,{\cdot}\left(\frac{{\mathcal{L}_B}^2}{4}+\frac{{\mathcal{L}_S}^2}{4}-\mathcal{L}_S+2\right)$$

21.) $$\left[\frac{{l_t}^2}{t}\right]_V = \mathcal{L}_B{\cdot}\left(\frac{{\mathcal{L}_B}^2}{12} \;+\; \frac{{\mathcal{L}_S}^2}{4}\right)$$

22.) $$\left[\frac{{l_t}^2}{t^2}\right]_V = \frac{1}{s_{12}s_{34}}\left[\sqrt{\lambda}\,{\cdot}\left(\frac{{\mathcal{L}_B}^2}{4}+\frac{{\mathcal{L}_S}^2}{4} \;+\; \mathcal{L}_S \;+\; 2\right) \;-\; \frac{s-\sigma}{2}{\cdot}\Big(\mathcal{L}_S+2\Big){\cdot}\mathcal{L}_B\right]$$

23.) $$\begin{aligned}\left[\frac{{l_t}^2}{u}\right]_V = &-\;\ln^2\left(\frac{t_{max}}{m_e^2}\right){\cdot}\ln\Big(\frac{t_{min}}{s-\sigma}\Big) \;+\; \ln^2\left(\frac{t_{min}}{m_e^2}\right){\cdot}\ln\Big(\frac{t_{max}}{s-\sigma}\Big)\\ &-\;2\,\ln\left(\frac{t_{max}}{m_e^2}\right){\cdot}\mathrm{Li}_2\Big(\frac{t_{max}}{s-\sigma}\Big) \;+\; 2\,\ln\left(\frac{t_{min}}{m_e^2}\right){\cdot}\mathrm{Li}_2\Big(\frac{t_{min}}{s-\sigma}\Big)\\ &+\;2\,\mathrm{Li}_3\Big(\frac{t_{max}}{s-\sigma}\Big) \;-\; 2\,\mathrm{Li}_3\Big(\frac{t_{min}}{s-\sigma}\Big)\end{aligned}$$

$$24.)\quad \left[\mathrm{Li}_2\Big(\frac{t_{12}-\mathrm{i}\varepsilon}{s_{12}}\Big)\right]_V \;=\; \frac{s-\sigma}{2}\cdot\mathcal{L}_B \;+\; \frac{\sqrt{\lambda}}{2}\cdot\Big(\mathcal{L}_S - 2\,l_1 - 2\Big)$$
$$+\;\Big(s_{12}+t_{max}\Big)\cdot\mathrm{Li}_2\Big(1+\frac{t_{max}-\mathrm{i}\varepsilon}{s_{12}}\Big)$$
$$-\;\Big(s_{12}+t_{min}\Big)\cdot\mathrm{Li}_2\Big(1+\frac{t_{min}-\mathrm{i}\varepsilon}{s_{12}}\Big)$$

$$25.)\quad \left[\mathrm{Li}_2\Big(\frac{t_{34}-\mathrm{i}\varepsilon}{s_{34}}\Big)\right]_V \;=\; \frac{s-\sigma}{2}\cdot\mathcal{L}_B \;+\; \frac{\sqrt{\lambda}}{2}\cdot\Big(\mathcal{L}_S - 2\,l_2 - 2\Big)$$
$$+\;\Big(s_{34}+t_{max}\Big)\cdot\mathrm{Li}_2\Big(1+\frac{t_{max}-\mathrm{i}\varepsilon}{s_{34}}\Big)$$
$$-\;\Big(s_{34}+t_{min}\Big)\cdot\mathrm{Li}_2\Big(1+\frac{t_{min}-\mathrm{i}\varepsilon}{s_{34}}\Big)$$

$$26.)\quad \left[\frac{1}{t}\cdot\mathrm{Li}_2\Big(\frac{t_{12}-\mathrm{i}\varepsilon}{s_{12}}\Big)\right]_V \;=\; \frac{\pi^2}{6}\cdot\mathcal{L}_B \;-\; 2\,\mathrm{Li}_3\Big(-\frac{t_{max}}{s_{12}}\Big) \;+\; 2\,\mathrm{Li}_3\Big(-\frac{t_{min}}{s_{12}}\Big)$$
$$+\;\left(\ln\frac{t_{max}}{m_e^2}-l_1\right)\cdot\mathrm{Li}_2\Big(-\frac{t_{max}}{s_{12}}\Big)$$
$$-\;\left(\ln\frac{t_{min}}{m_e^2}-l_1\right)\cdot\mathrm{Li}_2\Big(-\frac{t_{min}}{s_{12}}\Big)$$

$$27.)\quad \left[\frac{1}{t}\cdot\mathrm{Li}_2\Big(\frac{t_{34}-\mathrm{i}\varepsilon}{s_{34}}\Big)\right]_V \;=\; \frac{\pi^2}{6}\cdot\mathcal{L}_B \;-\; 2\,\mathrm{Li}_3\Big(-\frac{t_{max}}{s_{34}}\Big) \;+\; 2\,\mathrm{Li}_3\Big(-\frac{t_{min}}{s_{34}}\Big)$$
$$+\;\left(\ln\frac{t_{max}}{m_e^2}-l_2\right)\cdot\mathrm{Li}_2\Big(-\frac{t_{max}}{s_{34}}\Big)$$
$$-\;\left(\ln\frac{t_{min}}{m_e^2}-l_2\right)\cdot\mathrm{Li}_2\Big(-\frac{t_{min}}{s_{34}}\Big)$$

28.) $\Re\mathrm{e}\left(\left[\frac{1}{u}\cdot\mathrm{Li}_2\Big(\frac{t_{12}-\mathrm{i}\varepsilon}{s_{12}}\Big)\right]_V\right) \;=$

$$\begin{aligned}
&\mathcal{L}_B\cdot\Big[\quad\frac{{\mathcal{L}_B}^2}{6}\;-\;\frac{1}{2}\cdot\ln(d_{12})\cdot\ln\frac{s_{12}}{s_{34}}\;-\;\ln^2(d_{12})\;-\;2\,\mathrm{Li}_2\Big(\frac{1}{d_{12}}\Big)\;+\;\frac{2\pi^2}{3}\;\Big]\\
&-\;\ln\frac{t_{max}}{s_{12}}\cdot\mathrm{Li}_2\Big(\frac{t_{min}}{s-s_{34}}\Big)\;+\;\ln\frac{t_{min}}{s_{12}}\cdot\mathrm{Li}_2\Big(\frac{t_{max}}{s-s_{34}}\Big)\\
&+\;\mathrm{Li}_3\Big(-\frac{t_{max}}{s_{12}}\Big)\;-\;\mathrm{Li}_3\Big(-\frac{t_{min}}{s_{12}}\Big)\;-\;\mathrm{Li}_3\Big(\frac{t_{max}}{s-s_{34}}\Big)\;+\;\mathrm{Li}_3\Big(\frac{t_{min}}{s-s_{34}}\Big)\\
&+\;\mathrm{Li}_3\Big(-\frac{t_{max}}{d_{12}\,t_{min}}\Big)\;-\;\mathrm{Li}_3\Big(-\frac{t_{min}}{d_{12}\,t_{max}}\Big)
\end{aligned}$$

29.) $\Re\mathrm{e}\left(\left[\frac{1}{u}\cdot\mathrm{Li}_2\Big(\frac{t_{34}-\mathrm{i}\varepsilon}{s_{34}}\Big)\right]_V\right) \;=$

$$\begin{aligned}
&\mathcal{L}_B\cdot\Big[\quad\frac{{\mathcal{L}_B}^2}{6}\;+\;\frac{1}{2}\cdot\ln(d_{34})\cdot\ln\frac{s_{12}}{s_{34}}\;-\;\ln^2(d_{34})\;-\;2\,\mathrm{Li}_2\Big(\frac{1}{d_{34}}\Big)\;+\;\frac{2\pi^2}{3}\;\Big]\\
&-\;\ln\frac{t_{max}}{s_{34}}\cdot\mathrm{Li}_2\Big(\frac{t_{min}}{s-s_{12}}\Big)\;+\;\ln\frac{t_{min}}{s_{34}}\cdot\mathrm{Li}_2\Big(\frac{t_{max}}{s-s_{12}}\Big)\\
&+\;\mathrm{Li}_3\Big(-\frac{t_{max}}{s_{34}}\Big)\;-\;\mathrm{Li}_3\Big(-\frac{t_{min}}{s_{34}}\Big)\;-\;\mathrm{Li}_3\Big(\frac{t_{max}}{s-s_{12}}\Big)\;+\;\mathrm{Li}_3\Big(\frac{t_{min}}{s-s_{12}}\Big)\\
&+\;\mathrm{Li}_3\Big(-\frac{t_{max}}{d_{34}\,t_{min}}\Big)\;-\;\mathrm{Li}_3\Big(-\frac{t_{min}}{d_{34}\,t_{max}}\Big)
\end{aligned}$$

30.) $\left[\frac{1}{t^2}\cdot\mathrm{Li}_2\Big(\frac{t_{12}-\mathrm{i}\varepsilon}{s_{12}}\Big)\right]_V \;=$

$$\begin{aligned}
&-\;\frac{1}{t_{max}}\cdot\mathrm{Li}_2\Big(1+\frac{t_{max}-\mathrm{i}\varepsilon}{s_{12}}\Big)\;+\;\frac{1}{t_{min}}\cdot\mathrm{Li}_2\Big(1+\frac{t_{min}-\mathrm{i}\varepsilon}{s_{12}}\Big)\\
&+\;\frac{1}{s_{12}}\cdot\Big[\;\mathrm{Li}_2\Big(1+\frac{s_{12}}{t_{max}-\mathrm{i}\varepsilon}\Big)\;-\;\mathrm{Li}_2\Big(1+\frac{s_{12}}{t_{min}-\mathrm{i}\varepsilon}\Big)\;\Big]
\end{aligned}$$

31.) $$\left[\frac{1}{t^2}\cdot \mathrm{Li}_2\Big(\frac{t_{34}-\mathrm{i}\varepsilon}{s_{34}}\Big)\right]_V \;=$$

$$-\frac{1}{t_{max}}\cdot \mathrm{Li}_2\Big(1+\frac{t_{max}-\mathrm{i}\varepsilon}{s_{34}}\Big) \;+\; \frac{1}{t_{min}}\cdot \mathrm{Li}_2\Big(1+\frac{t_{min}-\mathrm{i}\varepsilon}{s_{34}}\Big)$$

$$+\frac{1}{s_{34}}\cdot\Big[\;\mathrm{Li}_2\Big(1+\frac{s_{34}}{t_{max}-\mathrm{i}\varepsilon}\Big) \;-\; \mathrm{Li}_2\Big(1+\frac{s_{34}}{t_{min}-\mathrm{i}\varepsilon}\Big)\;\Big]$$

Bibliography

[1] J.C. Maxwell, *"Treatise on Electricity and Magnetism"*, 3^{rd} edition (1891), 2 vols., reprint by Dover, New York (1964).

[2] A. Einstein, *Ann. Phys.* **17** (1905) 891.

[3] P.A.M. Dirac, *Proc. Roy. Soc.* **A114** (1927) 243.

[4] W. Heisenberg and W. Pauli, *Z. Phys.* **56** (1929) 1; *Z. Phys.* **59** (1930) 168.

[5] H. Weyl, *Z. Phys.* **56** (1929) 330.

[6] J. Schwinger, *Phys. Rev.* **74** (1948) 1439.

[7] R.P. Feynman, *Phys. Rev.* **76** (1949) 769.

[8] R.P. Feynman, *Phys. Rev.* **80** (1950) 440; *Phys. Rev.* **84** (1951) 108.

[9] T. Kinoshita and D.R. Yennie in:
T. Kinoshita (ed.), *"Quantum Electrodynamics", Advanced Series on Directions in High Energy Physics – Vol. 7*, World Scientific, Singapore, 1990, p.1.

[10] Particle Data Group (L. Montanet et al.), *"Review of Particle Properties"*, *Phys. Rev.* **D50** (1994).

[11] T. Kinoshita and W.J. Marciano in:
T. Kinoshita (ed.), *"Quantum Electrodynamics", Advanced Series on Directions in High Energy Physics – Vol. 7*, World Scientific, Singapore, 1990, p.420;
F.J.M. Farley and E. Picasso, ibid., p.474.

[12] F.M. Pipkin in:
T. Kinoshita (ed.), *"Quantum Electrodynamics", Advanced Series on Directions in High Energy Physics – Vol. 7*, World Scientific, Singapore, 1990, p.697.

[13] H. Becquerel, *C.R. Acad. Sci. (Paris)* **122** (1896) 501.

[14] E. Fermi, *Ricera Scient.* **2**, *issue 12* (1933); *Z. Phys.* **88** (1934) 161.

[15] T.D. Lee and C.N. Yang, *Phys. Rev.* **104** (1956) 254.

[16] C.S. Wu, E. Ambler, R. Hayward, D. Hoppes and R. Hudson,
Phys. Rev. **105** (1957) 1413.

[17] L.D. Landau, *JETP* **32** (1956) 405;
A. Salam, *Nuovo Cim.* **5** (1957) 299.

[18] H. Yukawa, *Proc. Phys. Math. Soc. Japan* **17** (1935) 48.

[19] C.N. Yang and R. Mills, *Phys. Rev.* **96** (1954) 191.

[20] F. Englert and R. Brout, *Phys. Rev. Lett.* **13** (1964) 321;
P.W. Higgs, *Phys. Rev. Lett.* **13** (1964) 508;
G.S. Guralnik, C.R. Hagen and T.W.B. Kibble, *Phys. Rev. Lett.* **13** (1964) 585;
P.W. Higgs, *Phys. Rev.* **145** (1966) 1156;
T.W.B. Kibble, *Phys. Rev.* **155** (1967) 1554.

[21] G. 't Hooft *Nucl. Phys.* **B35** (1971) 167.

[22] S.L. Glashow, *Nucl. Phys.* **22** (1961) 579;
S. Weinberg, *Phys. Rev. Lett.* **19** (1967) 1264;
A. Salam in:
N. Svartholm (ed.), *"Elementary Particle Theory", Proc. of the* 8^{th} *Nobel Symposium, Aspenäsgården, Lerum, Älvsborg, Sweden, May* $19^{th}-25^{th}$ *1968*, Almqvist & Wiksell, Stockholm, 1968, p.367.

[23] M. Gell-Mann, *Phys. Lett.* **8** (1964) 214.

[24] S.L. Glashow, J. Iliopoulos and L. Maiani, *Phys. Rev.* **D2** (1970) 1285.

[25] N. Cabbibo, *Phys. Rev. Lett.* **10** (1963) 531;
M. Kobayashi and T. Maskawa, *Prog. Th. Phys.* **49** (1973) 652.

[26] W. Hollik, *Fortschr. Phys* **38** (1990) 165; preprint MPI-Ph/93-21 (1993); and references therein.

[27] M. Gell-Mann, *Acta Phys. Austriaca,* Suppl. **9** (1972) 733;
H. Fritzsch and M. Gell-Mann in: *Proc. of the* XV^{th} *Intern. Conf. on High Energy Physics, Chicago-Batavia, 1973*;
D.J. Gross and F. Wilczek, *Phys. Rev.* **D8** (1973) 3633;
H. Fritzsch, M. Gell-Mann and H. Leutwyler, *Phys. Lett.* **B47** (1973) 365;
H. Politzer, *Phys. Rep.* **C14** (1974) 129.

[28] F.J. Hasert et al., *Phys. Lett.* **B46** (1973) 121 & 138; *Nucl. Phys.* **B73** (1974) 1.

[29] J.J. Aubert et al., *Phys. Rev. Lett.* **33** (1974) 1404;
J.E. Augustin et al., *Phys. Rev. Lett.* **33** (1974) 1406;
E.G. Cazzoli et al., *Phys. Rev. Lett.* **34** (1975) 1125;
G. Goldhaber et al., *Phys. Rev. Lett.* **37** (1976) 255.

[30] G. Arnison et al. (UA1 Collaboration), *Phys. Lett.* **B126** (1983) 398; *Phys. Lett.* **B129** (1983) 273;
P. Bagnaia et al. (UA2 Collaboration), *Phys. Lett.* **B129** (1983) 130.

[31] The LEP Electroweak Working Group, Internal Note LEPEWWG/95-01 (1995).

[32] S. Dittmaier, D. Schildknecht, K. Kołodziej and M. Kuroda, *Nucl. Phys.* **B426** (1994) 249;
D. Schildknecht, preprint BI-TP-95-03 (1995).

[33] F. Abe et al. (CDF Collaboration), *Phys. Rev.* **D50** (1994) 2966; *Phys. Rev. Lett.* **73** (1994) 225; FERMILAB-PUB-95/022-E (1995);
S. Abachi et al. (D0 Collaboration), FERMILAB-PUB-95/028-E (1995).

[34] G. Altarelli, informal proposal of simulation energies for LEP2 physics;
C. Wyss, *"LEP2 Programme – An Update"*, Talk presented at the First General Meeting of the LEP2 Workshop, CERN, Geneva, February 1995.

[35] K.R. Barger and M.H. Reno, *Phys. Rev.* **D51** (1995) 90;
K.J. Abraham, J. Kalinowski and P. Sciepko, *Phys. Lett.* **B339** (1994) 136;
D. Choudhury and F. Cuypers, *Nucl. Phys.* **B429** (1994) 33;
G. Abu Leil and W.J. Stirling, *Phys. Rev.* **D49** (1994) 3751;
M. Bilenky, J.L. Kneur, F.M. Renard and D. Schildknecht, *Nucl. Phys.* **B419** (1994) 240;
F. Jegerlehner, *"Search for Anomalous Gauge Boson Couplings", Proc. of the Zeuthen Workshop on Elementary Particle Theory "Physics at LEP200 and Beyond", Teupitz, Germany, April $10^{th}-15^{th}$ 1994*,
Nucl. Phys. **B** (Proc. Suppl.) 37B (1994), 129.

[36] U. Baur and D. Zeppenfeld, *Phys. Lett.* **B201** (1988) 383.

[37] M. Felcini, *"Prospects for Higgs detection at LEP2", Proc. of the Zeuthen Workshop on Elementary Particle Theory "Physics at LEP200 and Beyond", Teupitz, Germany, April $10^{th}-15^{th}$ 1994*,
Nucl. Phys. **B** (Proc. Suppl.) 37B (1994), 279.

[38] A. Sopczak, preprint CERN-PPE/95-46, to appear in the proceedings of the *IX^{th} International Workshop "High Energy Physics and Quantum Field Theory", Zvenigorod, Moscow Region, Russia, September $15^{th}-22^{nd}$ 1994.*

[39] D. Lehner, preprint MPI-PhE/93-02 (1993).

[40] D. Buskulic, ..., D. Lehner et al. (ALEPH Collaboration), *Z. Phys.* **C66** (1995) 3;
P. Abreu et al. (DELPHI Collaboration), *Nucl. Phys.* **B403** (1993) 299;
A. Adam et al. (L3 Collaboration), *Phys. Lett.* **B321** (1994) 283;
R. Akers et al. (OPAL Collaboration), preprint CERN–PPE/93–145 (1993);
and references therein.

[41] D. Lehner, *Mod. Phys. Lett.* **A9** (1994) 2937;
D. Bardin, D. Lehner and T. Riemann, preprint DESY 94-216, to appear in the proceedings of the *IX^{th} International Workshop "High Energy Physics and Quantum Field Theory", Zvenigorod, Moscow Region, Russia, September $15^{th}-22^{nd}$ 1994.*

[42] D. Bardin, M. Bilenky, A. Olchevski and T. Riemann, *Phys. Lett.* **B308** (1993) 403.

[43] D. Bardin, M. Bilenky, D. Lehner, A. Olchevski and T. Riemann, *"Semi-analytical approach to four-fermion production in e^+e^- annihilation", Proc. of the Zeuthen Workshop on Elementary Particle Theory "Physics at LEP200 and Beyond", Teupitz, Germany, April $10^{th}-15^{th}$ 1994*,
Nucl. Phys. **B** (Proc. Suppl.) 37B (1994), 148.

[44] R.W. Brown and K.O. Mikaelian, *Phys. Rev.* **D19** (1979) 922.

[45] A. Denner and T. Sack, *Nucl. Phys.* **B306** (1988) 221.

[46] A. Denner and T. Sack, *Z. Phys.* **C45** (1990) 439.

[47] F.A. Berends, R. Kleiss and R. Pittau, *Nucl. Phys.* **B424** (1994) 308; *Nucl. Phys.* **B426** (1994) 344; *Comp. Phys. Comm.* **85** (1995) 437.

[48] J. Hilgart, R. Kleiss and F. Le Diberder, *Comp. Phys. Comm.* **75** (1993) 191;
F.A. Berends, P.H. Daverveldt and R. Kleiss, *Nucl. Phys.* **B253** (1985) 441; *Comp. Phys. Comm.* **40** (1986) 285.

[49] G. Montagna, O. Nicrosini and F. Piccinini, *Phys. Lett.* **B348** (1995) 496;
E. Boos, M. Sachwitz, H.J. Schreiber and S. Shichanin, *Z. Phys.* **C61** (1994) 675;
preprint DESY 93-183.

[50] A. Leike, preprint LMU-11/95, to appear in the proceedings of the *Ringberg Workshop "Perspectives for electroweak interactions in e^+e^- collisions, Ringberg, Germany, February 1995.*

[51] H.E. Haber and G.L. Kane, *Phys. Rep.* **117** (1985) 75.

[52] H.P. Nilles, *Phys. Rep.* **110** (1984) 1.

[53] T. Mohaupt, private communication.

[54] J.L. Lopez, preprint CTP-TAMU-17/94 (1994).

[55] V. Baier, V. Fadin and V. Khoze, *Sov. Phys. JETP* **23** (1966) 104;
M. Cvetič and P. Langacker, *Phys. Rev.* **D46** (1992) 4943; E: ibid. **D48** (1993) 4484.

[56] B.A. Kniehl, M. Krawczyk, J.H. Kühn and R.G. Stuart, *Phys. Lett.* **B209** (1988) 337.

[57] C. Itzykson and J.-B. Zuber, *"Quantum Field Theory"*, McGraw-Hill, New York, 1980.

[58] W. Alles, Ch. Boyer and A.J. Buras, *Nucl. Phys* **B119** (1977) 125, and references therein.

[59] R. Brun, O. Couet, C. Vandoni and P. Zanarini, *PAW – Physics Analysis Workstation*, CERN Program Library Entry Q121, Version 2.05/22 (1994).

[60] D. Bardin, A. Leike, T. Riemann and M. Sachwitz, *Phys. Lett.* **B206** (1988) 539.

[61] U. Baur and D. Zeppenfeld, preprint MAD/PH/878 (1995).

[62] G. Passarino, Talk presented at the 3^{rd} meeting of the LEP2 working groups *"WW cross-sections and distributions"* and *"Event generators"*, CERN, Geneva, April 1995.

[63] F.A. Berends, G.J.H. Burgers and W.L. van Neerven, *Nucl. Phys.* **B297** (1987) 429, and references therein.

[64] G. Altarelli et al. in:
J. Ellis and R. Peccei (ed.), *"Physics at LEP", Vol. 1*, CERN Yellow Report 86–02 (1986) 3;
F.A. Berends et al. in:
G. Altarelli, R. Kleiss and C. Verzegnassi (ed.), *"Z Physics at LEP 1, Vol. 1: Standard Physics"*, CERN Yellow Report 89–08 (1989) 89.

[65] D. Bardin, A. Leike and T. Riemann, *Phys. Lett.* **B344** (1995) 383 and preprint DESY 95-057 (1995).

[66] R. Pittau, *Phys. Lett.* **B335** (1994) 490.

[67] T. Muta, R. Najima and S. Wakaizumi, *Mod. Phys. Lett.* **A1** (1986) 203.

[68] W. Beenakker, K. Kołodziej and T. Sack, *Phys. Letters* **B258** (1991) 469;
J. Fleischer, K. Kołodziej and F. Jegerlehner, *Phys. Rev.* **D47** (1993) 830.

[69] V.S. Fadin, V.A. Khoze and A.D. Martin, *Phys. Lett.* **B311** (1993) 311;
Yu.L. Dokshitzer, V.A. Khoze, L.H. Orr and W.J. Stirling, *Phys. Lett.* **B313** (1993) 171;
T. Sjöstrand and V.A. Khoze, *Z. Phys.* **C** (1994) 281.

[70] D. Bardin, W. Beenakker and A. Denner, *Phys. Lett.* **B317** (1993) 213;
V.S. Fadin, V.A. Khoze, A.D. Martin and A. Chapovskii, preprint DTP-94-116 (1994).

[71] W. Beenakker and A. Denner, *Int. J. Mod. Phys.* **A9** (1994) 4837.

[72] D. Bardin, D. Lehner and T. Riemann, in preparation.

[73] E.W.N. Glover, R. Kleiss and J.J. van der Bij, *Z. Phys.* **C47** (1990) 435.

[74] V.S. Fadin, V.A. Khoze and A.D. Martin, *Phys. Lett.* **B311** (1993), 311; *Phys. Lett.* **B320** (1994), 141; *Phys. Rev.* **D49** (1994), 2247.

[75] D. Bardin, A. Leike and T. Riemann, *"Semi-analytical Approach to Higgs Production at LEP 2", Proc. of the Zeuthen Workshop on Elementary Particle Theory "Physics at LEP200 and Beyond", Teupitz, Germany, April $10^{th}-15^{th}$ 1994*,
Nucl. Phys. **B** (Proc. Suppl.) 37B (1994), 274.

[76] E. Boos, M. Sachwitz, H.J. Schreiber and S. Shichanin, preprint DESY 95-002 (1995), to appear in *Z. Phys.* **C**.

[77] V.A. Khoze and T. Sjöstrand, *Phys. Rev. Lett.* **72** (1994) 28;
V.A. Khoze, preprint DTP-94-114 (1994).

[78] J. Fujimoto et al. (Minami-Tateya Collaboration), *"Non-resonant diagrams in radiative four-fermion processes", Proc. of the Zeuthen Workshop on Elementary Particle Theory "Physics at LEP200 and Beyond", Teupitz, Germany, April $10^{th}-15^{th}$ 1994*, *Nucl. Phys.* **B** (Proc. Suppl.) 37B (1994), 169;
Y. Kurihara, D. Perret-Gallix and Y. Shimizu, *Phys. Lett.* **B349** (1995) 367;
T. Ishikawa et al., KEK-Preprint-92-210 (1992).

[79] E. Boos, M. Sachwitz, H.J. Schreiber and S. Shichanin, preprint DESY 93-183 (1993), to appear in *Mod. Phys. Lett.* **A**; *Z. Phys.* **C64** (1994) 391;
E. Boos et al., *Phys. Lett.* **B326** (1994) 190;
M. Dubinin, V. Edneral, Y. Kurihara and Y. Shimizu, *Phys. Lett.* **B329** (1994) 379.

[80] H. Anlauf et al., *Comp. Phys. Comm.* **79** (1994) 487; preprint IKDA-95-14 (1995);
A. Borrelli, P.J. Franzini and G.J. van Oldenborgh, *Comp. Phys. Comm.* **83** (1994) 14.

[81] D. Bardin, M. Bilenky, A. Olchevski and T. Riemann, in preparation.

[82] U. Baur and E.L. Berger, *Phys. Rev.* **D47** (1993) 4889;
K. Hagiwara, R.D. Peccei and D. Zeppenfeld, *Nucl. Phys.* **B282** (1987) 253.

[83] G. Landsberg for the D0 Collaboration, preprint FERMILAB-Conf-95/061-E;
S. Abachi et al. (D0 Collaboration), preprint FERMILAB-Pub-95/042-E;
F. Abe at al. (CDF Collaboration), preprints FERMILAB-Pub-94/304-E and FERMILAB-Pub-94/244-E;
M. Acciari et al. (L3 Collaboration), preprint CERN-PPE/94-216.

[84] M. Gell-Mann, *Phys. Rev.* **92** (1953) 833;
K. Nishijima, *Prog. Theor. Phys.* **13** (1955) 285.

[85] I.J.R. Aitchison in:
K.J. Peach, L.L.J. Vick and P. Osborne (ed.), *Proc. of the forty second Scottish Universities Summer School in Physics: "High Energy Phenomenology", St. Andrews, Scotland, August 1993*, SUSSP Publications, Edinburgh & Institute of Physics Publishing, Bristol (UK), 1994, p.1.

[86] W.J.P. Beenakker, PhD thesis, Rijksuniversiteit Leiden, 1989.

[87] D. Ebert, *"Eichtheorien"*, VCH Verlagsgesellschaft, Weinheim, Germany, 1989.

[88] F. Mandl and G. Shaw, *"Quantum Field Theory"*, John Wiley & Sons, New York 1984.

[89] M. Böhm, H. Spiesberger and W. Hollik, *Fortschr. Phys.* **34** (1986) 687.

[90] J.D. Bjorken and S.D. Drell,
"Relativistic Quantum Mechanics", McGraw-Hill, New York 1964;
"Relativistic Quantum Fields", McGraw-Hill, New York 1965.

[91] M. Veltman, *"Diagrammatica"*, Cambridge Lecture Notes in Physics 4, Cambridge University press, Cambridge (UK), 1994.

[92] F. Jegerlehner, *Z. Phys.* **C32** (1986) 425; E: ibid. **C38** (1988) 519.

[93] A. Sirlin, *Phys. Rev.* **D22** (1980) 971;
W.J. Marciano and A. Sirlin, *Phys. Rev. Lett.* **46** (1981) 163;
Ch. Llewellyn-Smith and J.F. Wheater, *Nucl. Phys.* **B208** (1982) 27;
A. Sirlin, *Phys. Lett.* **B232** (1989) 123;
and references therein.

[94] G. Passarino and M. Veltman, *Phys. Lett.* **B237** (1990) 537.

[95] D. Kennedy and B. Lynn, *Nucl. Phys.* **B322** (1989) 1.

[96] F. Jegerlehner, preprint PSI-PR-91-08 (1991).

[97] D. Bardin et al. in:
D. Bardin, W. Hollik and G. Passarino (ed.), *"Reports of the Working Group on Precision Calculations for the Z Resonance"*, CERN Yellow Report 95–03 (1995) 7.

[98] D.A. Ross and J.C. Taylor, *Nucl. Phys.* **B51** (1973) 125;
G. Passarino and M. Veltman, *Nucl. Phys.* **B160** (1979) 151;
D.Yu. Bardin, P.Ch. Christova and O.M. Fedorenko, *Nucl. Phys.* **B175** (1980) 435;
Nucl. Phys. **B197** (1982) 1.

[99] D.Yu. Bardin, P.Ch. Christova and O.M. Fedorenko, *Nucl. Phys.* **B175** (1980) 435.

[100] F. Halzen and A.D. Martin, *"Quarks and Leptons: An Introductory Course in Modern Particle Physics"*, John Wiley & Sons, New York 1984.

[101] W.Hollik, preprint MPI-Ph/93-21 (1993).

[102] D.Yu. Bardin, P.Ch. Christova and O.M. Fedorenko, *Nucl. Phys.* **B197** (1982) 1.

[103] L. Lewin, *"Dilogarithms and Associated Functions"*, MacDonald, London (UK), 1958.

[104] G. 't Hooft and M. Veltman, *Nucl. Phys.* **B153** (1979) 365.

[105] Z. Wąs in:
N. Ellis and M.B. Gavela (ed.), *"1993 European School of High-Energy Physics"*, CERN Yellow Report 94–04 (1994) 307.

[106] E. Byckling and K. Kajantie, *"Particle Kinematics"*, John Wiley & Sons, London 1972.

[107] M. Veltman, *"*`SCHOONSCHIP` *– A Program for Symbol Handling"*, 1989;
H. Strubbe, *Comp. Phys. Comm.* **8** (1974) 1.

[108] J. Vermaseren, *"Symbolic Manipulations with* `FORM`*"*, Computer Algebra Nederland, Amsterdam, 1991.

[109] M.J. Abell and J.P. Braselton, *"The* `Mathematica` *Handbook"*, Academic Press, San Diego, CA, 1992;
N. Blachman, *"* `Mathematica`*: A Practical Approach"*, Prentice Hall, Englewood Cliffs, N. J., 1992.

[110] W.J. Marciano and A. Sirlin, *Nucl. Phys.* **B88** (1975) 86.

[111] G. 't Hooft and M. Veltman, *Nucl. Phys.* **B44** (1972) 189.

[112] G. Bonneau and F. Martin, *Nucl. Phys.* **B27** (1971) 381;
D. Bardin et al., *Phys. Lett.* **B229** (1989) 405, and references therein.

[113] F.E. Low, *Phys. Rev.* **110** (1958) 974.

[114] A. Akhundov, D. Bardin, L. Kalinovskaya and T. Riemann, preprint DESY 94-115.

[115] F. Bloch and A. Nordsieck, *Phys. Rev* **52** (1937) 54.

[116] D.R. Yennie, S.C. Frautschi and H. Suura, *Ann. Phys.* (*N.Y.*) **13** (1961) 379.

[117] G. 't Hooft and M. Veltman, *"Diagrammar"*, CERN Yellow Report 73–9 (1972).

[118] G. Passarino and M. Veltman, *Nucl. Phys.* **B160** (1979) 151.

[119] G. Leibbrandt, *Rev. Mod. Phys.* **47** (1975) 849.

Acknowledgments

I am very grateful to my thesis advisor Dr. T. Riemann whose guidance and teaching have been essential for the preparation of this thesis. I acknowledge many discussions with Dr. D. Bardin from whom I have learnt many things. It is a pleasure to thank the DESY directorate, and in particular to Prof. Dr. P. Söding, for giving me the opportunity to not only prepare this thesis at IfH Zeuthen, but also to attend conferences and a summer school which has considerably widened my horizon. I am very much indebted to Prof. Dr. M. Müller-Preußker for kindly acting as my official thesis supervisor.

I thank A. Leike for supplying me with his FORTRAN code `4fAN` (see reference [65]) which helped me to verify my Born results.

In addition I acknowledge scientific discussions with W. Beenakker, J. Blümlein, J. Botts, P. Christova, A. Denner, A. Leike, T. Mohaupt, U. Müller, and S. Riemann. I am indebted to the DESY-IfH Zeuthen computer center staff, especially to W. Friebel, A. Köhler, W. Niepraschk, and C. Rethfeld. I thank the Technical Support group at DESY-IfH for their permanent availability and M. Gohr for preparing the phase space illustrations in appendix D.

Careful reading of the manuscript by Dr. T. Riemann and J. Wegmann as well as comments on the presentation of the topic by Dr. D. Bardin and Prof. Dr. M. Müller-Preußker are acknowledged.

Thanks to Arnd, Christian, Denny, Dima, Jana, Jim, Lida, Penka, Sabine, Thomas, Tord, Uwe, and all the others for the wonderful time.

Curriculum Vitae

Name	Dietrich Lehner
2.11.1967	geboren in München als viertes Kind von Prof. Dr. rer. nat. Günther Lehner (geb. 1931) und dessen Ehefrau Dr. rer. nat. Lore Lehner (1932-1984), geborene Roßner.
1973–1975	Besuch der Toni-Pfülf-Grundschule in München.
1975	Umzug der Familie nach Böblingen.
1975–1977	Besuch der Eduard-Mörike-Grundschule in Böblingen.
1977–1986	Besuch des Otto-Hahn-Gymnasiums in Böblingen.
1983	Dreimonatiger Aufenthalt an den "University of Toronto Schools", Toronto, Ontario, Kanada als Austauschschüler.
10.6.1986	Abitur, Durchschnittsnote 1.3 .
Nov. 1986	Aufnahme des Physikstudiums an der Ludwig-Maximilians-Universität München.
3.11.1988	Vordiplom, Gesamturteil "sehr gut".
1989	Sommerstudent am Europäischen Laboratorium für Teilchenphysik CERN, Genf.
1989–1992	Stipendiat der Friedrich-Naumann-Stiftung, Berlin.
1990	Laborpraktikum am CERN.
April 1991	Beginn der Diplomarbeit "Messung der e^+e^-–Annihilation in die 4–leptonischen Endzustände $e^+e^-e^+e^-$, $e^+e^-\mu^+\mu^-$ und $\mu^+\mu^-\mu^+\mu^-$ an der Z^0–Resonanz" bei Priv. Doz. Dr. W. Blum am Max-Planck-Institut für Physik in München.
2.12.1992	Diplom, Gesamturteil "sehr gut".
Seit 1.2.1993	Doktorand bei Dr. T. Riemann am DESY-IfH Zeuthen.

List of Publications and Talks

Publications

[1] D. Lehner:
Messung der e^+e^-–Annihilation in die 4–leptonischen Endzustände $e^+e^-e^+e^-$, $e^+e^-\mu^+\mu^-$ und $\mu^+\mu^-\mu^+\mu^-$ an der Z^0–Resonanz.
MPI Munich preprint MPI–PhE/93–02;
Measurement of the 4–lepton final states $e^+e^-e^+e^-$, $e^+e^-\mu^+\mu^-$ and $\mu^+\mu^-\mu^+\mu^-$ in the 1990 and 1991 Data.
ALEPH collaboration internal note "ALEPH 93-019, PHYSIC 93-012".

[2] D. Bardin, M. Bilenky, D. Lehner, A. Olshevski, T. Riemann:
Semi-Analytical Approach to Four-Fermion Production in e^+e^- Annihilation.
Preprints CERN-TH.7295/94, DESY 94-093, Proceedings of the *Zeuthen Workshop on Elementary Particle Theory "Physics at LEP200 and Beyond", Teupitz, Germany, April* $10^{th} - 15^{th}$ *1994*,
Nucl. Phys. **B** (Proc. Suppl.) 37B (1994) 148–157.

[3] D. Lehner:
Initial State Radiation to Off-Shell Z^0 Pair Production in e^+e^- Annihilation.
Mod. Phys. Lett. **A9** (1994) 2937.

[4] The ALEPH collaboration (D. Buskulic, ... , D. Lehner et al.):
Study of the four-fermion final state at the Z^0 resonance.
Z. Phys. **C66** (1995) 3.

[5] D. Bardin, D. Lehner, T. Riemann:
Complete Initial State Radiation to Off-Shell Z^0 Pair Production in e^+e^- Annihilation.
Preprint DESY 94–216, to appear in the proceedings of the IX^{th} *International Workshop on "High Energy Physics and Quantum Field Theory", Zvenigorod, Moscow Region, Russia, September* $15^{th} - 22^{nd}$ *1994.*

Talks

1. *Measurement of the Final States $e^+e^-e^+e^-$, $e^+e^-\mu^+\mu^-$ and $\mu^+\mu^-\mu^+\mu^-$ in the ALEPH 1990 and 1991 Data*
   - → DESY–IfH Zeuthen, September 6^{th} 1992,
   - → Meeting of the ALEPH Searches group, CERN, March 1^{st} 1993,
   - → 1993 German Physical Society Spring Meeting, Mainz, Germany, March 1993.

2. *Initial State Radiation to Off-Shell Z^0 Pair Production in e^+e^- Annihilation*
   - → 1994 German Physical Society Spring Meeting, Dortmund, Germany, March 1994,
   - → Humboldt–University, Berlin, Germany, May 16^{th} 1994,
   - → $XVII^{th}$ Kazimierz Meeting on Elementary Particle Physics, Kazimierz, Poland, May 1994.

3. *Complete Initial State Radiation to Off-Shell Z^0 Pair Production in e^+e^- Annihilation*
   - → IX^{th} International Workshop on "High Energy Physics and Quantum Field Theory", Zvenigorod, Moscow Region, Russia, September 1994,
   - → DESY Theory Workshop, Hamburg, Germany, September 1994,
   - → 1995 German Physical Society Spring Meeting, Karlsruhe, Germany, March 1995.

4. *Semi-Analytical Approach to Standard Model Four-Fermion Production at LEP2 and Beyond*
   - → First Meeting of the LEP2 Working Group "Standard Model Processes", CERN, November 25^{th} 1994,
   - → 1995 German Physical Society Spring Meeting, Karlsruhe, Germany, March 1995,
   - → Meeting of the "L3-LEP2 Working Group", CERN, March 31^{st} 1995,
   - → Third Meeting of the LEP2 Working Group "Standard Model Processes", CERN, April 5^{th} 1995 (Update),
   - → Seminar at the "Centre de Physique des Particules de Marseille", Marseille, France, April 10^{th} 1995.

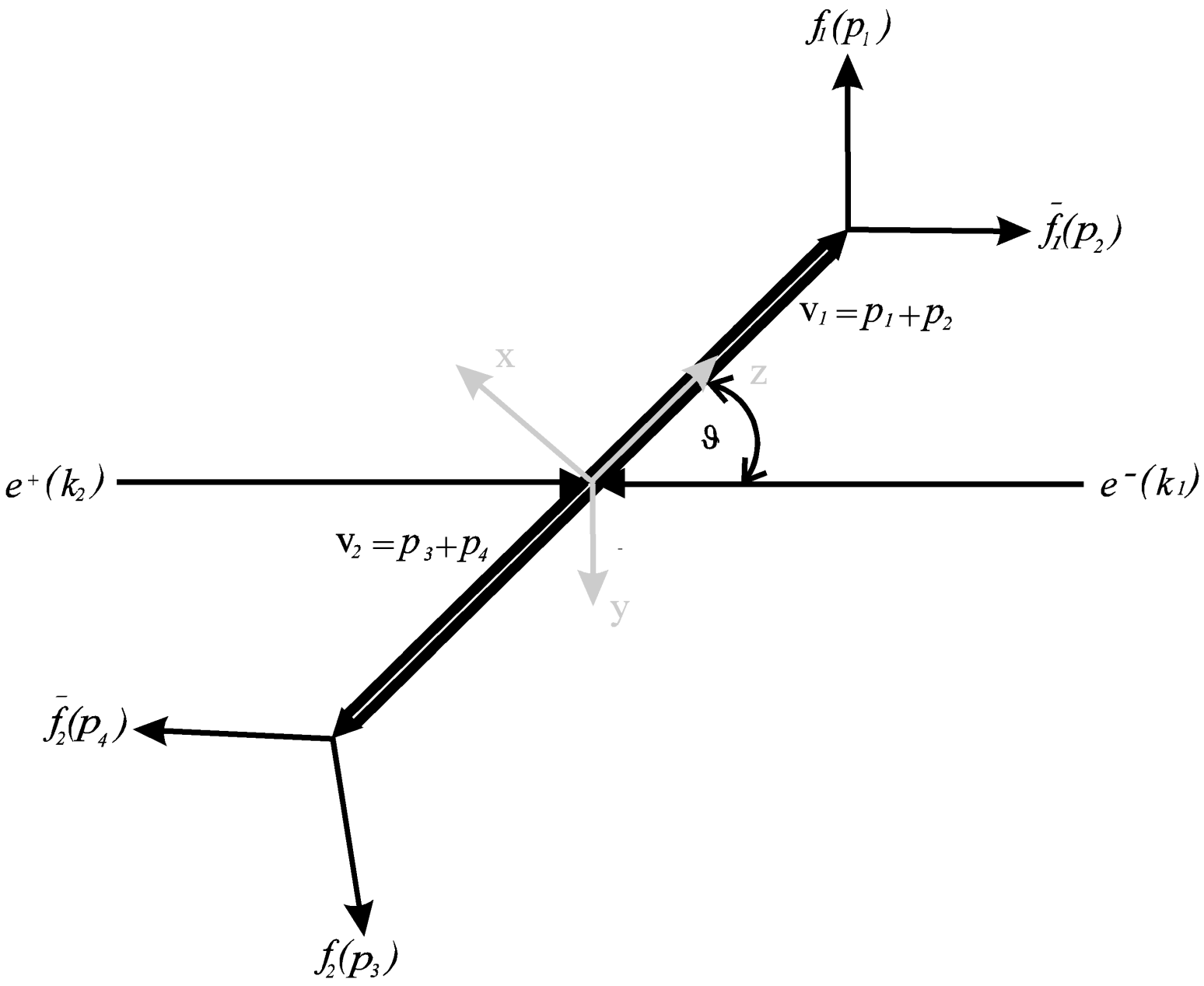
$f_1(p_1)$
$\bar{f}_1(p_2)$
$v_1 = p_1 + p_2$
x
z
ϑ
$e^+(k_2)$
$e^-(k_1)$
$v_2 = p_3 + p_4$
y
$\bar{f}_2(p_4)$
$f_2(p_3)$

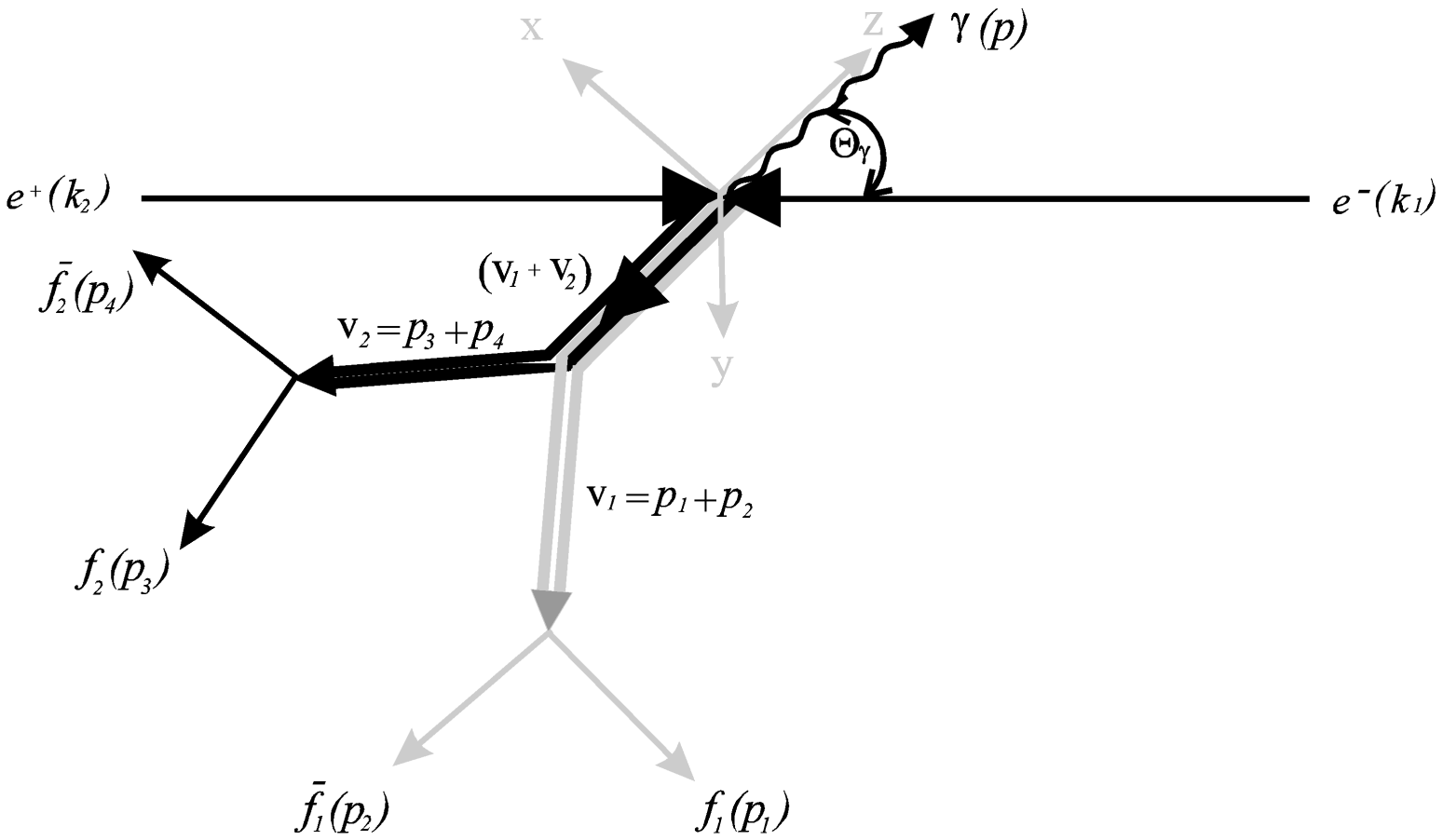
x
z
γ (p)
Θγ
e+ (k2)
e- (k1)
(v1 + v2)
f̄2 (p4)
v2 = p3 + p4
y
v1 = p1 + p2
f2 (p3)
f̄1 (p2)
f1 (p1)

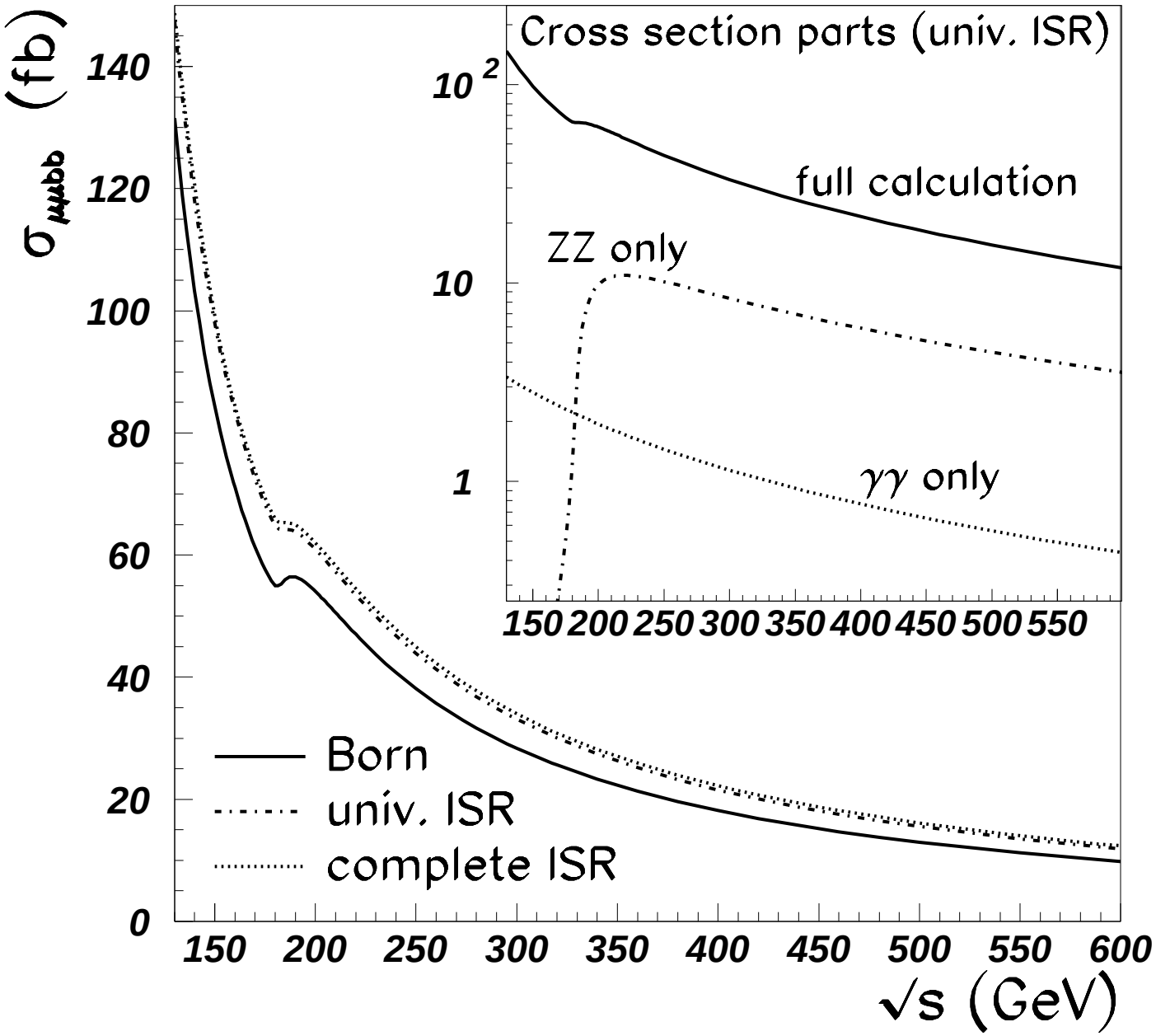
$\sigma_{\mu\mu bb}$ (fb)
140
120
100
80
60
40
20
0
150
200
250
300
350
400
450
500
550
600
√s (GeV)
Born
univ. ISR
complete ISR
Cross section parts (univ. ISR)
10^2
10
1
full calculation
ZZ only
$\gamma\gamma$ only
150 200 250 300 350 400 450 500 550

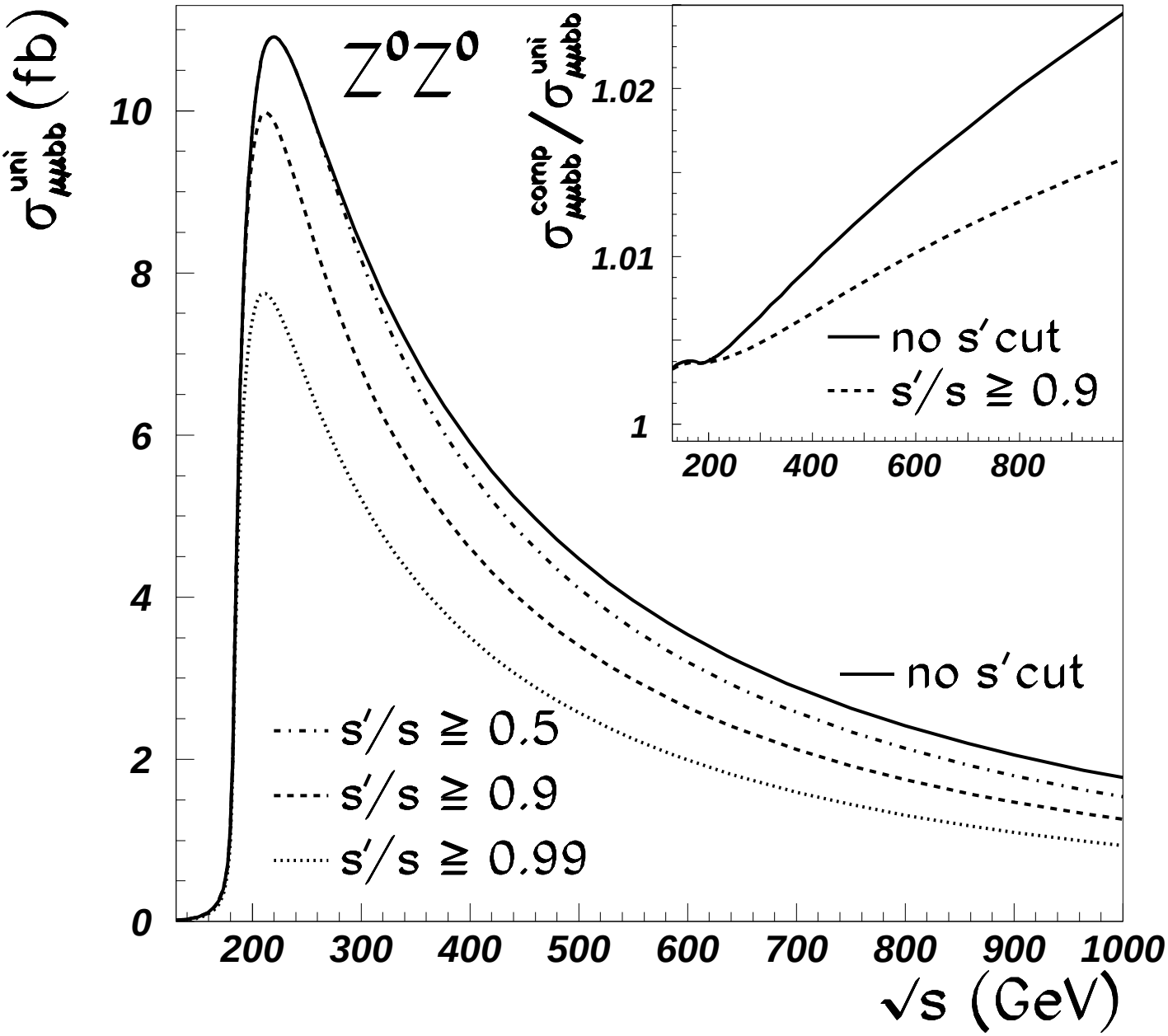
$\sigma^{uni}_{\mu\mu bb}$ (fb)
Z^0Z^0
$\sigma^{comp}_{\mu\mu bb} / \sigma^{uni}_{\mu\mu bb}$
1.02
1.01
1
no s′cut
s′/s ≧ 0.9
200
400
600
800
10
8
6
4
2
0
no s′cut
s′/s ≧ 0.5
s′/s ≧ 0.9
s′/s ≧ 0.99
200
300
400
500
600
700
800
900
1000
√s (GeV)

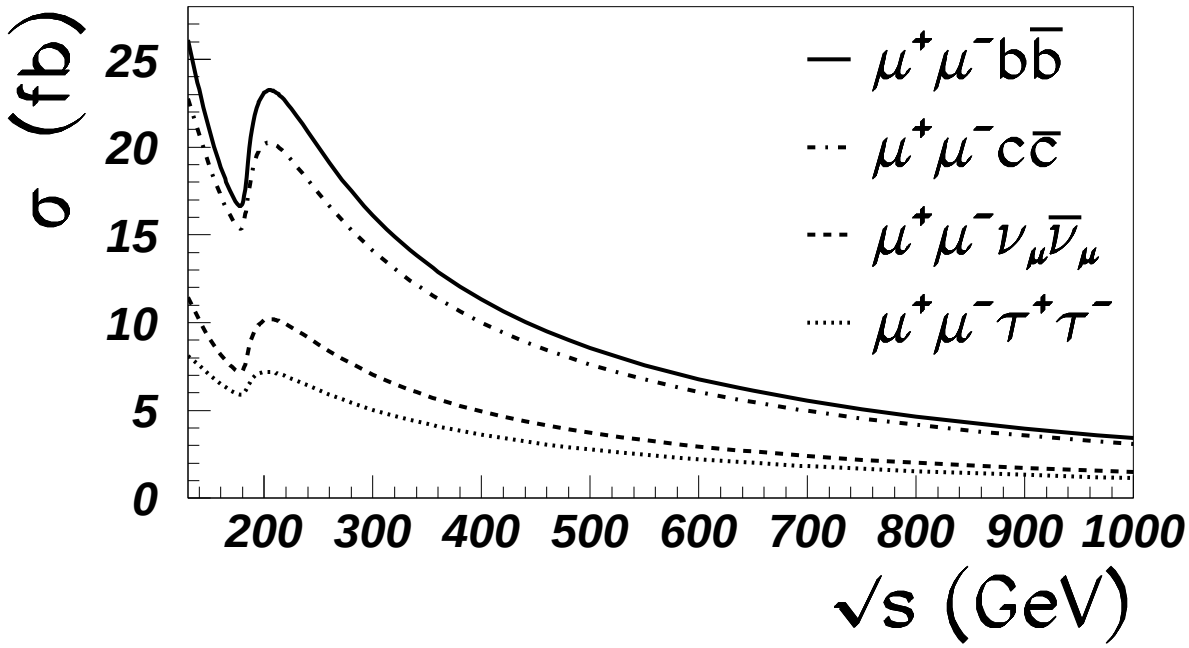
σ (fb)
25
20
15
10
5
0
200
300
400
500
600
700
800
900
1000
√s (GeV)
μ⁺μ⁻bb̄
μ⁺μ⁻cc̄
μ⁺μ⁻ν_μν̄_μ
μ⁺μ⁻τ⁺τ⁻

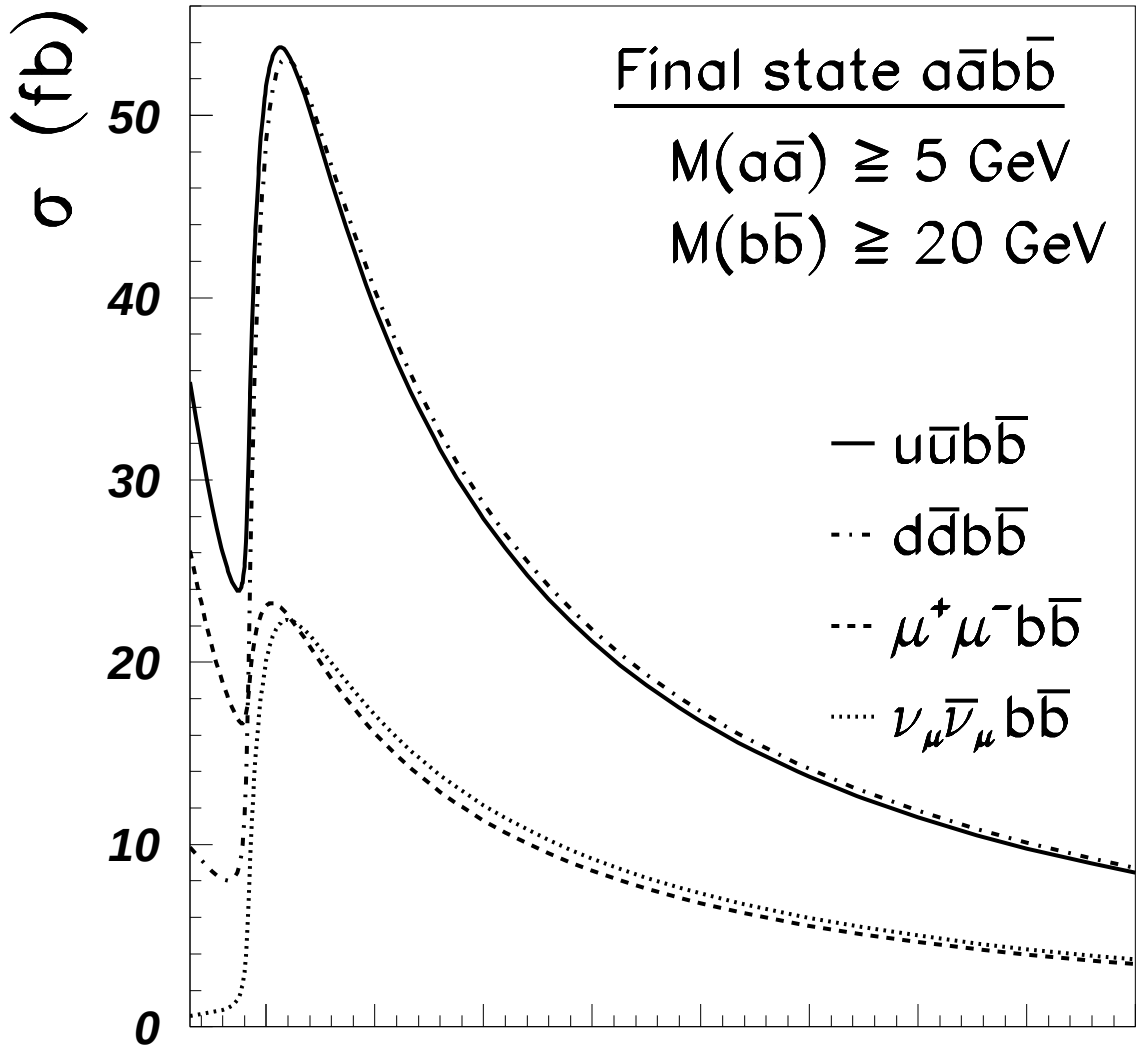
σ (fb)
50
40
30
20
10
0
Final state aāb̄b̄
M(aā) ≧ 5 GeV
M(b̄b̄) ≧ 20 GeV
— uūb̄b̄
··· dd̄b̄b̄
--- μ⁺μ⁻b̄b̄
····· ν_μν̄_μb̄b̄

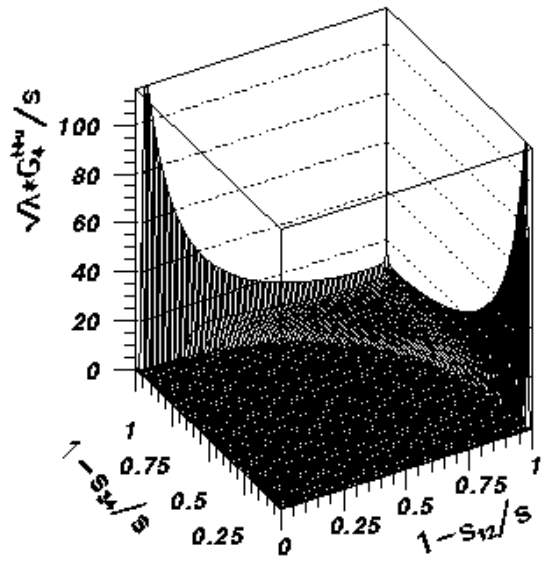
$\sqrt{\Lambda}*G_4^{tw}/s$
100
80
60
40
20
0
1
0.75
0.5
0.25
0
$1-s_{34}/s$
0.25
0.5
0.75
1
$1-s_{12}/s$

a)

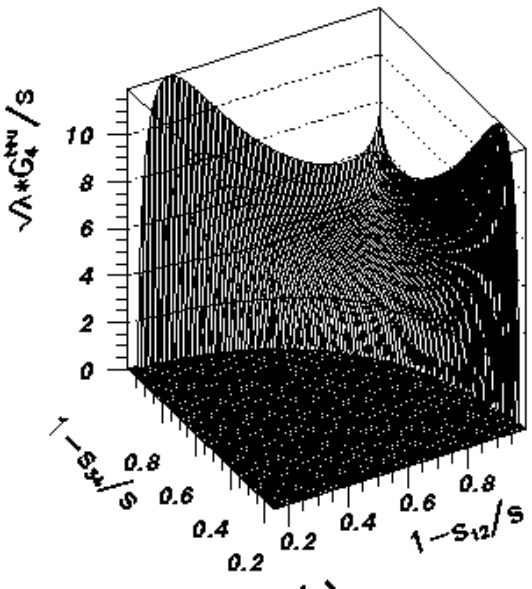
$\sqrt{\Lambda}*G_4^{tw}/s$
10
8
6
4
2
0
$1-s_{34}/s$
0.8
0.6
0.4
0.2
0.2
0.4
0.6
0.8
$1-s_{12}/s$

b)

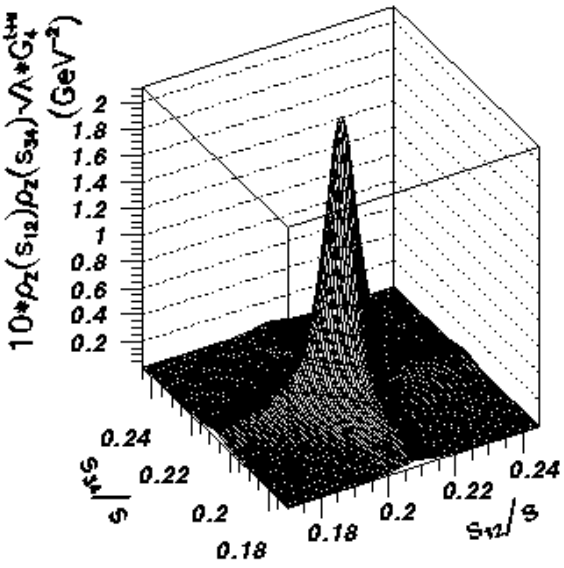
$10*\rho_2(s_{12})\rho_2(s_{34})\sqrt{\Lambda}*G_4^{tw}$ (GeV^{-2})
2
1.8
1.6
1.4
1.2
1
0.8
0.6
0.4
0.2
s_{34}/s
0.24
0.22
0.2
0.18
0.18
0.2
0.22
0.24
s_{12}/s

c)

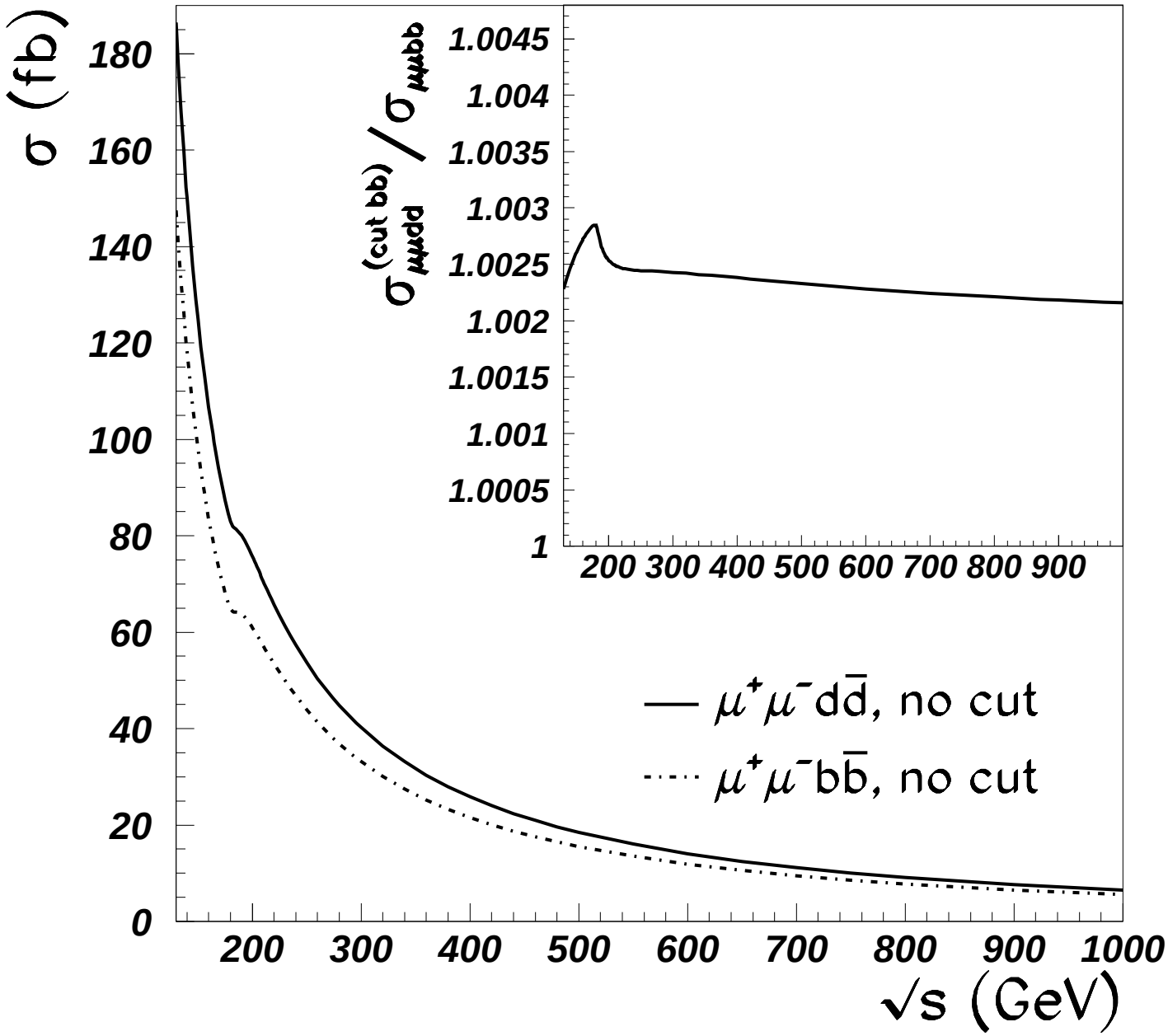
σ (fb)
180
160
140
120
100
80
60
40
20
0
200
300
400
500
600
700
800
900
1000
√s (GeV)
$\sigma^{(cut\ b\bar{b})}_{\mu\mu d\bar{d}} / \sigma_{\mu\mu b\bar{b}}$
1.0045
1.004
1.0035
1.003
1.0025
1.002
1.0015
1.001
1.0005
1
200 300 400 500 600 700 800 900
$\mu^+\mu^- d\bar{d}$, no cut
$\mu^+\mu^- b\bar{b}$, no cut

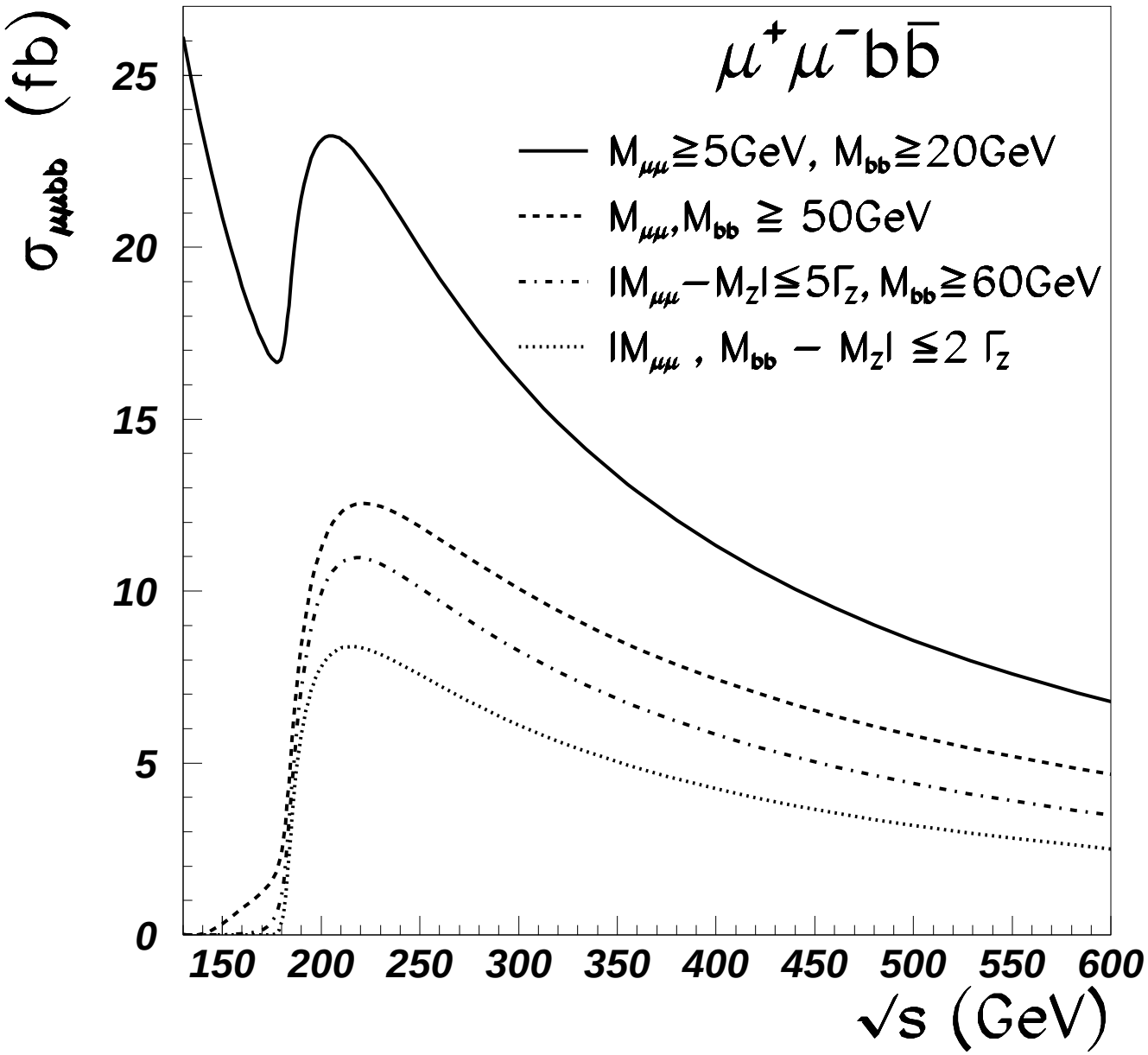
$\mu^+\mu^-b\bar{b}$
$M_{\mu\mu} \geqq 5$GeV, $M_{bb} \geqq 20$GeV
$M_{\mu\mu}, M_{bb} \geqq 50$GeV
$|M_{\mu\mu} - M_Z| \leqq 5\Gamma_Z$, $M_{bb} \geqq 60$GeV
$|M_{\mu\mu}, M_{bb} - M_Z| \leqq 2\Gamma_Z$
$\sigma_{\mu\mu bb}$ (fb)
0
5
10
15
20
25
150
200
250
300
350
400
450
500
550
600
$\sqrt{s}$ (GeV)

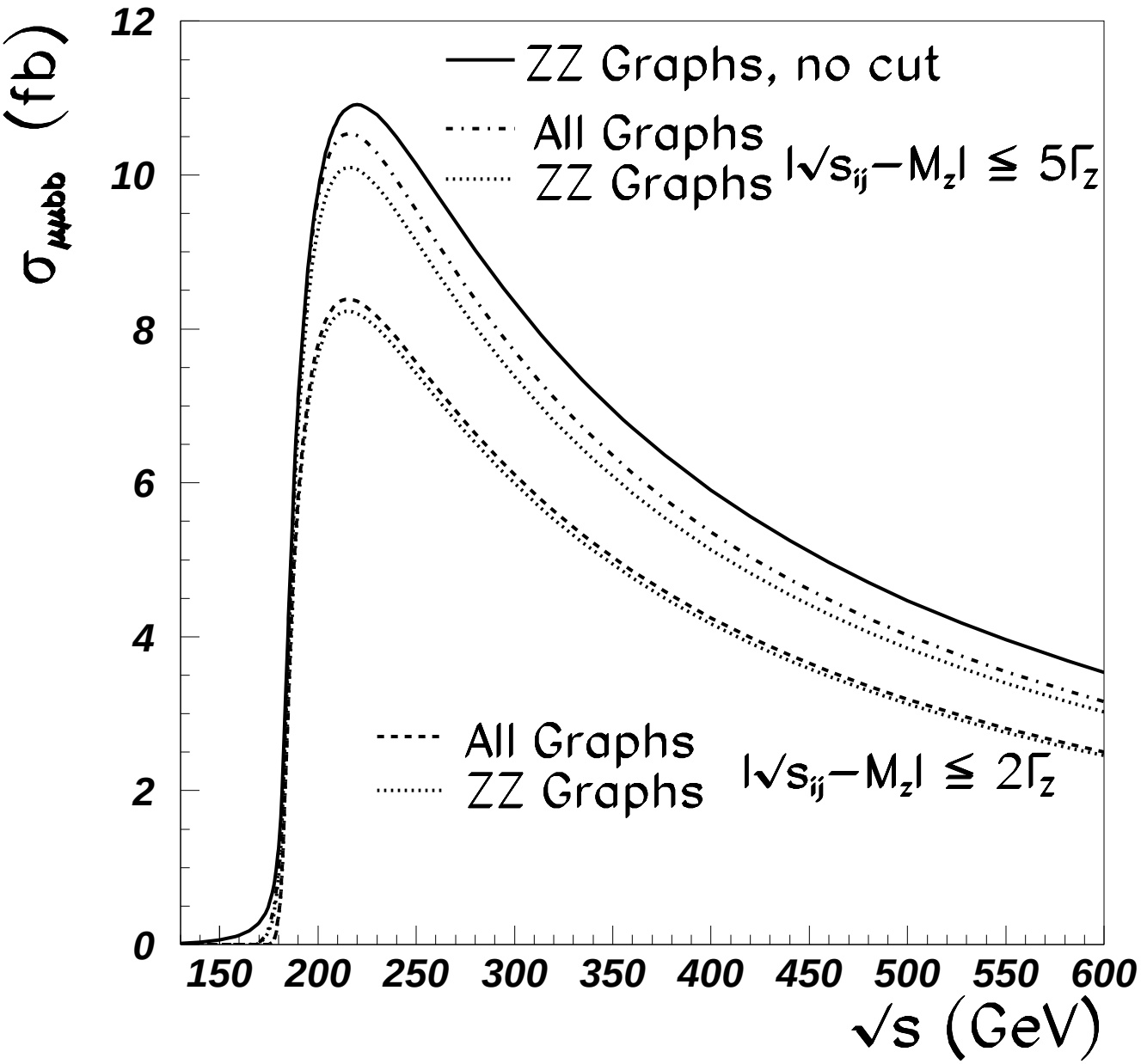
$\sigma_{\mu\mu bb}$ (fb)
12
10
8
6
4
2
0
150
200
250
300
350
400
450
500
550
600
√s (GeV)
ZZ Graphs, no cut
All Graphs
ZZ Graphs
$|\sqrt{s_{ij}} - M_z| \leqq 5\Gamma_z$
All Graphs
ZZ Graphs
$|\sqrt{s_{ij}} - M_z| \leqq 2\Gamma_z$

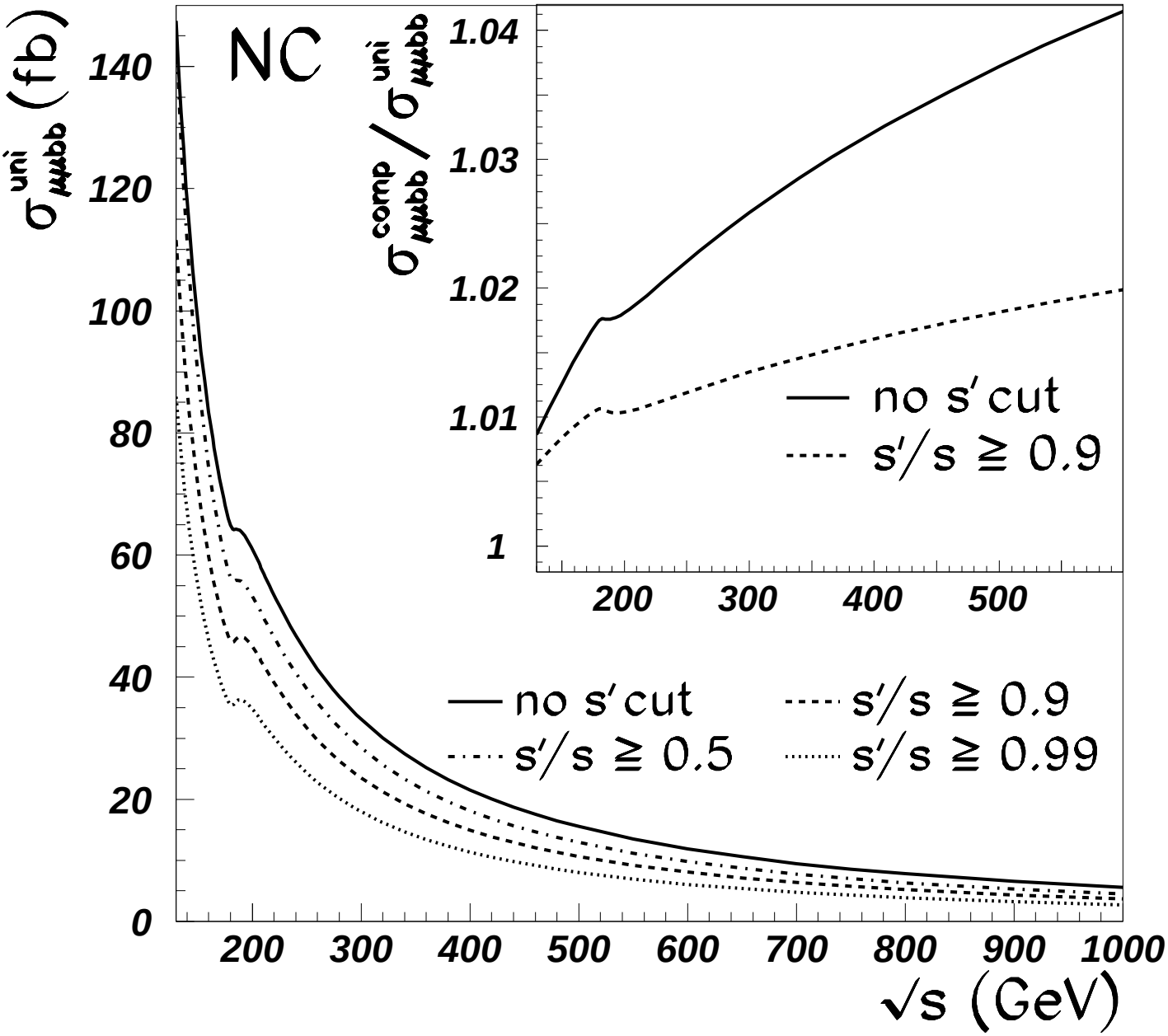
NC
$\sigma^{uni}_{\mu\mu bb}$ (fb)
$\sigma^{comp}_{\mu\mu bb} / \sigma^{uni}_{\mu\mu bb}$
no s′ cut
s′/s ≧ 0.9
s′/s ≧ 0.5
s′/s ≧ 0.99
√s (GeV)

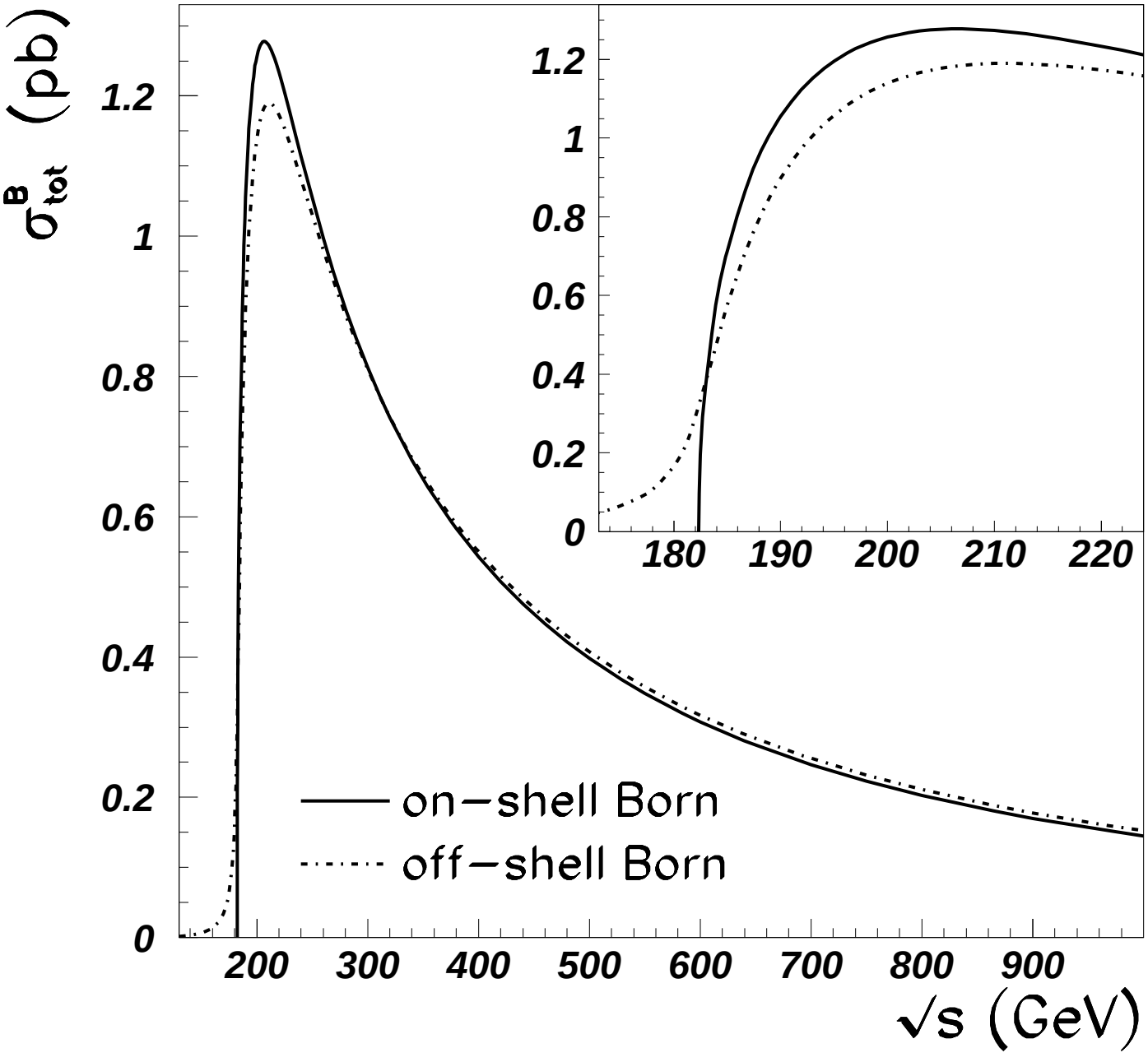
σ^{B}_{tot} (pb)
1.2
1
0.8
0.6
0.4
0.2
0
200
300
400
500
600
700
800
900
√s (GeV)
on−shell Born
off−shell Born
1.2
1
0.8
0.6
0.4
0.2
0
180
190
200
210
220

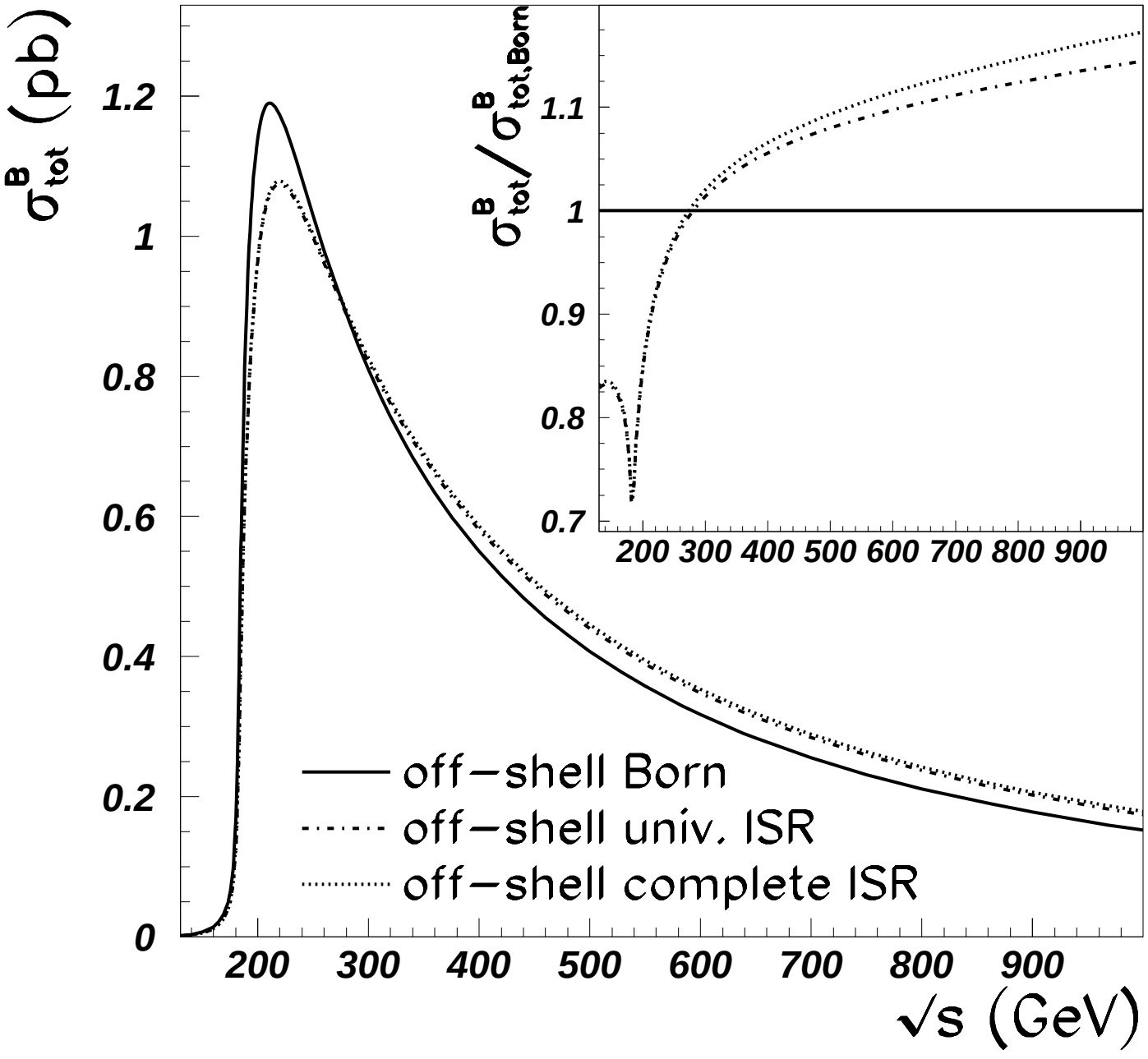
σ^B_{tot} (pb)
1.2
1
0.8
0.6
0.4
0.2
0
200
300
400
500
600
700
800
900
√s (GeV)
off−shell Born
off−shell univ. ISR
off−shell complete ISR
$\sigma^B_{tot}/\sigma^B_{tot,Born}$
1.1
1
0.9
0.8
0.7
200 300 400 500 600 700 800 900